PHYSICS REPORTS (Review Section of Physics Letters) 183, Nos. 5 & 6 (1989) 193–381. North-Holland, Amsterdam

LOW-ENERGY PHENOMENOLOGY OF SUPERSTRING-INSPIRED E_6 MODELS

JoAnne L. HEWETT

Department of Physics, University of Wisconsin, Madison, WI 53706, USA

and

Thomas G. RIZZO

Ames Laboratory and Department of Physics, Iowa State University, Ames, IA 50011, USA
and Department of Physics, University of Wisconsin, Madison, WI 53706, USA

Received March 1989

Contents:

Abstract:

In this report we survey the low-energy phenomenological implications of superstring-inspired E_6 models. The motivation for such models is reviewed. New particles including new gauge bosons, exotic fermions, Higgs bosons, and their superpartners are expected to exist in models of this type. We summarize the present experimental limits on these particles from both accelerator and non-accelerator data. Techniques for producing these new particles directly at existing and planned colliders as well as for searching for their indirect effects are examined in detail. Other phenomenological implications of such models are also reviewed.

0 370-1573/89/$66.15

LOW-ENERGY PHENOMENOLOGY OF SUPERSTRING-INSPIRED E_6 MODELS

JoAnne L. HEWETT

Department of Physics, University of Wisconsin, Madison, WI 53706, USA

and

Thomas G. RIZZO

Ames Laboratory and Department of Physics, Iowa State University, Ames, IA 50011, USA
and Department of Physics, University of Wisconsin, Madison, WI 53706, USA

NORTH-HOLLAND – AMSTERDAM

1. Introduction

1.1. Background

The standard model (SM), which combines the $SU(2)_L \times U(1)_Y$ Glashow–Weinberg–Salam electroweak theory [1.1] together with quantum chromodynamics (QCD) [1.2], the theory of the strong interactions, is in very good agreement with all experimental data (for a recent review of the status of the SM, see ref. [1.3]). Despite this great success, it has been believed for quite some time that the SM is inadequate since it fails to unify all of the forces, contains a large number of a priori unknown parameters, and has too many features (e.g., left-handed charged currents and the generation structure) which are put in by hand.

In order to deal with these difficulties there have been many attempts at physics beyond the SM. Among these attempts, grand unified theories (GUT), which unify strong and electroweak interactions within the context of a single gauge group, have been only partially successful (for an overview of the current status of GUTs, see ref. [1.4]). SU(5), which is the simplest GUT, still requires a large number of a priori unknown parameters and fails to deal with most of the theoretical difficulties of the SM. In addition, it is now clear that the predictions of ordinary SU(5) are inconsistent with data on both the proton lifetime (τ_p) and the electroweak mixing angle ($\sin^2\theta_w$) [1.5]. These failures of ordinary SU(5) (in addition to the difficulties associated with the hierarchy and fine-tuning problems) have led to the examination of supersymmetry (SUSY) (for an overview of SUSY phenomenology see in particular the second of refs. [1.6]) and larger GUT groups such as SO(10) [1.7]. E_6 as a group for grand unification was first discussed in this context over a decade ago [1.8]. In SU(5), the fifteen two-component fermion fields in each generation are distributed in the $\bar{\mathbf{5}}$ and **10** representations. In SO(10), the next simplest GUT, which is also automatically anomaly-free, a right-handed neutrino field [which is an SU(5) singlet] is added to each SM generation so that the sixteen fermion fields can now be placed in the **16** [$= \mathbf{1} + \bar{\mathbf{5}} + \mathbf{10}$ under SU(5)] dimensional representation. Note that in SO(10), as in the SM, the three (or more) copies of the generation structure are still put in by hand.

Greater interest in E_6 GUTs was first sparked in the late 1970's when it was noted that (i) E_6 was the next natural anomaly-free choice for a GUT group after SO(10), (ii) E_6 could have several intermediate mass breaking scales (see Robinett and Rosner in ref. [1.8]), and, most importantly, (iii) each generation of fermions was placed in the **27** dimensional representation. This meant that in addition to the sixteen fermions per generation in SO(10) there must exist eleven additional two-component fields for every generation. In terms of $SU(3)_C \times SU(2)_L \times U(1)_Y$ these additional fields consist of a vector-like, color singlet, weak isodoublet with electric charges $Q = 0, -1$; a vector-like, color triplet, weak isosinglet with $Q = -\frac{1}{3}$; plus an additional $Q = 0$, color singlet, weak isosinglet field. It was thus possible that the then newly discovered τ lepton and b quark could "fill-in" part of an already existing **27** representation so that a third generation would be unnecessary (the so-called "topless models"). (For a review of topless models based on E_6 and their comparison with data see in particular the first of refs. [1.9].) This was not to be, however, since later data [1.9] disproved the predictions of this model, which were that: (i) both b and τ have pure vector couplings to the Z and (ii) the final states of both b and τ decay involve a substantial fraction of flavor changing neutral current (FCNC) signatures, e.g., $b \to s\ell^+\ell^-$ and $\tau^+ \to e^+e^-e^+$. It is now well established that both b and τ belong to a new, third generation so that this model is clearly ruled out. If E_6 is relevant as a GUT group, these additional fermions cannot be identified with any of the known particles and cannot fit into the conventional family structure of the SM. Interest in E_6 thus declined until the revival of superstring theory and the

work of Green and Schwarz (GS) [1.10] in late 1984 (for a general introduction to string theory see the second of refs. [1.10]).

In their now classic paper, GS showed that string theory in ten dimensions is anomaly free (and thus potentially finite!) if the gauge group is either $E_8 \times E_8'$ or SO(32). $E_8 \times E_8'$ leads to chiral fermions (as exist in the SM), whereas SO(32) does not, so that $E_8 \times E_8'$ is the more phenomenologically attractive and has received the most attention. As will be further discussed in the latter part of this section, the compactification of the additional six dimensions (assuming unbroken $N = 1$ SUSY) can lead to E_6 as an "effective" GUT group [1.11]. It is this result which has inspired the recent interest in E_6 and its subgroups as sources of new physics beyond the SM. This is the subject of this review: the low-energy phenomenology of superstring-inspired E_6 models.

The outline of the rest of this review is as follows. In the remainder of section 1 we briefly review the origin of E_6 and its subgroups within the superstring framework, discuss the quantum numbers of the particles in the **27** supermultiplet and the resulting superpotential, and standardize the nomenclature for these fields. In section 2 we give an overview of the various strong–electroweak models of ranks 5 and 6 originating from E_6 and give the couplings of the matter fields in all cases of interest. We discuss the present limits on the existence of new neutral gauge bosons originating from these models and the bounds on their mixings with the SM Z from neutral current, collider, and other data. The properties of these new gauge bosons are discussed and signals for their production and decay are reviewed. Models which have new charged gauge bosons are also reviewed in this section.

In section 3, we review the phenomenology associated with the new fermion (and SUSY-partner boson) fields that lie in the **27** of E_6. We present an overview of the possible baryon and lepton number as well as R-parity assignments of the new fields. Limits on their masses and other properties implied by existing data are reviewed as are their production cross sections and signals at e^+e^-, ep, and hadron colliders. The effects of these new fields on rare processes is also summarized. The problem of neutrino mass generation within the E_6 model context is reviewed.

The phenomenology of the scalar sector of E_6 superstring-inspired models is reviewed in section 4. We present a theoretical overview of the properties of and constraints on the Higgs sector, concentrating on the rank 5 model. The physical Higgs mass spectrum is discussed and the fermionic and vector boson Higgs couplings are given. Signals for the production and decay of the Higgs bosons which are unique to E_6 (i.e., which are not present in the SM or in SUSY theories) are reviewed.

In section 5, we discuss some of the other implications and results from superstring-inspired models. This includes such topics as supersymmetry breaking in the E_8' hidden sector and the generation of scalar and gaugino masses in the observable sector. Problems associated with the generation and magnitude of an intermediate mass scale, which is necessary in many models of this type, are examined, and constraints on this mass scale are discussed. We present an overview of the Oxford superstring model, with three generations of fermions which leads to the SM as the electroweak group at low energies, as a prototype of the potential predictive power of string theories. Axion phenomenology and cosmology from the superstring point of view are discussed as well as the implications of renormalization group analyses for the top quark mass and a fourth generation of fermions. We also review a few technical aspects associated with extended electroweak models. Section 6 contains our summary and conclusions. The appendix contains a summary of some recent results on the production of new gauge bosons present in superstring-inspired E_6 models at high energy colliders.

1.2. Superstrings and E_6 overview

As mentioned in the discussion above, the current interest in E_6 and its subgroups, from a phenomenological standpoint, has its origin in the work of Green and Schwarz [1.10]. Within the

context of heterotic superstrings in ten dimensions, gauge and gravitational anomaly cancellation (which is necessary for a finite theory) was found to occur only for the gauge groups SO(32) or $E_8 \times E_8'$. $E_8 \times E_8'$ is phenomenologically interesting in that it allows for chiral fermions whereas SO(32) does not. Since the fermions of the SM form chiral representations (i.e., ones in which left and right-handed fermions transform differently under the gauge group), $E_8 \times E_8'$ can contain the SM in its usual form. To recover a more typical field theory one goes to the limit where the string tension is large and massive (of order the Planck mass, M_P) and string excitations are integrated out. One then recovers ten-dimensional supergravity coupled with an $E_8 \times E_8'$ gauge sector. To make connection with our four-dimensional world, the extra six dimensions must be compactified on some kind of manifold and several compactification scenarios are possible.

Compactification on a Calabi–Yau manifold [1.12] [with an SU(3) holonomy] results in the breaking $E_8 \to SU(3) \times E_6$ with the SU(3) gauge field becoming the spin connection on the compactified space. The remaining E_8' couples to the usual matter representations of the E_6 only by gravitational interactions and may provide the role of "the hidden sector" needed to break SUSY [1.13]; such "shadow" matter may also account for the missing mass problem in cosmology [1.14]. This all follows from the requirement that after compactification from ten to four dimensions there remains an unbroken $N = 1$ supersymmetry (in order to deal with the hierarchy and fine-tuning problems). In such models the matter superfields lie in the **27** and $\overline{\mathbf{27}}$ representations of E_6 with n_g **27**'s and δ ($\mathbf{27} + \overline{\mathbf{27}}$)'s ($E_6$ singlets are also possible). The coefficients n_g and δ are related to the topology of the compactified manifold, the Euler characteristics and Betti–Hodge number, respectively. Since all matter superfields lie in **27** and $\overline{\mathbf{27}}$'s of E_6, one cannot break E_6 in a conventional manner as the required Higgs fields are absent from the **27**. E_6 (and E_8' as well) groups can be broken by the Hosotani mechanism [1.15], which parallels the Aharonov–Bohm effect in the non-abelian case. Given a manifold which is not simply connected, due to the presence of non-abelian gauge fields, a field transported completely around a non-contractible Wilson loop picks up a phase $e^{i\phi}$. The set of all such phase factors forms a finite representation of a discrete group G operating on the matter fields representing the original gauge group. The subgroup S of E_6 which remains unbroken must have generators which commute with the elements of G. (It should be noted that the "trapped-flux" acts in some ways like a Higgs field in the adjoint representation of E_6, i.e., the **78**.) In the case where G is non-abelian, one arrives uniquely at a rank-5 group $[S = SU(3)_C \times SU(2)_L \times U(1)_Y \times U(1)_\eta]$; in the case of abelian G, several rank-6 groups result [1.16] (see also refs. [1.11, 1.13]): $SU(3)_C \times SU(2)_L \times U(1)^3$, $SU(3)_L \times SU(2)^2 \times U(1)^2$, $SU(3)^3$, $SU(4) \times SU(2) \times U(1)^2$, etc. Since the SM, $SU(3)_C \times SU(2)_L \times U(1)_Y$, has rank 4, it is obvious that at least one new neutral gauge boson must exist in these models and that in all cases (ranks 5 or 6) further symmetry breaking is required. As we will see below, the superfield content of the **27** is sufficient to provide us with effective Higgs fields so that the conventional spontaneous symmetry breaking mechanism will now go through as usual (for a recent review, see ref. [1.17]). The rank-5 or rank-6 groups can thus break to the SM and then to $U(1)_{em}$ in the conventional manner.

More recent work has shown, however, that there are alternative scenarios to Calabi–Yau compactification. There exist manifold compactifications (yielding Polyakov non-linear σ models) with different numbers of world sheet supersymmetries which lead to holonomy groups larger than SU(3) [1.18]. These do not leave as much residual four-dimensional symmetry as in the Calabi–Yau case, with $E_8 \to SO(6)$ [or SO(4)] $\times$ SO(10) or SU(5) $\times$ SU(5) leaving SO(10) or SU(5) as the effective GUT [1.19]. Thus the uniqueness of E_6 as a "prediction" from ten-dimensional string theory is lost. Furthermore, it has been shown to be possible [1.20], to directly obtain four-dimensional string theory, i.e., instead of compactifying subsequent to taking the field-theory limit one compactifies the string theory (on tori) directly down to four dimensions. Unfortunately (?) the allowed gauge symmetries in

such scenarios are not very well constrained and one finds that any of the large number of "simply based" groups of rank 22 [1.21] are allowed, e.g., SO(44). Such groups, as in the case of SO(44), generally do not contain $E_8 \times E_8'$ as a subgroup. In their original construction such four-dimensional string theories lead directly to $N = 4$ SUSY and do not contain chiral fermions. However, later work using "orbifolds" [1.22] has shown that chiral, $N = 1$ SUSY theories can indeed be obtained in such models. "Orbifold" compactifications were used earlier as an alternative to Calabi–Yau manifolds for the compactification of the ten-dimensional supergravity theory and also lead to extended strong–electroweak gauge groups at low energy [1.23].

Although the prediction of E_6 as "the" GUT arising from superstrings is no longer unique, most of the phenomenological efforts have concentrated on this group and thus we will make it the subject of this review. Since other schemes (such as four-dimensional strings) can also lead to extended strong–electroweak groups at low energy, much of the work done for E_6 models can be easily adapted to these models once more definite "predictions" are made. We will not discuss models which do not originate from E_6 theories, such as flipped SU(5) models.

It should be noted that in using E_6 as an "effective" GUT, the usual renormalization group analysis of the running coupling constants still holds, whereas relationships among the Yukawa couplings at the GUT level (associated with Clebsch–Gordan type factors) are to be relaxed (see Witten in ref. [1.11]).

1.3. Properties of matter supermultiplets

As discussed above, each chiral generation of matter must lie in the **27**-dimensional representation of E_6. Thus it is immediately clear that additional fields are needed beyond those expected in each generation of the SM in order to complete the **27**. In terms of the SO(10) and SU(5) subgroups of E_6, the **27** decomposes as

$$\mathbf{27} = (\mathbf{16}, \mathbf{10}) + (\mathbf{16}, \bar{\mathbf{5}}) + (\mathbf{16}, \mathbf{1}) + (\mathbf{10}, \mathbf{5}) + (\mathbf{10}, \bar{\mathbf{5}}) + (\mathbf{1}, \mathbf{1}) . \tag{1.1}$$

(For a review of the group theory involved in E_6 and its many subgroups see Slansky in ref. [1.8].) Since the "conventional" fields and the right-handed ν are usually assigned to the $\mathbf{10} + \bar{\mathbf{5}} + \mathbf{1}$ part of the **16** of SO(10), the additional fields that lie in the $\mathbf{10} + \mathbf{1}$ of SO(10) are called *exotics*. Table 1 shows the nomenclature we will follow in this review for all of the fields in the **27** including the exotics. In using the table, the reader should be aware that a fixed nomenclature for the exotics has yet to be settled upon (i.e., a variety of notations are in use in the literature), and that all fields are written as left-handed. Common alternatives to the notation used here include: D and g for h; ν_E and ν' for N; N^c for ν^c; N_E^c and N'^c for N^c; H^- for E; and n, ν'' and N for S^c. Table 1 also shows the color, weak-isospin (T_{3L}), hypercharge ($Y/2$), and electric charge (Q) for all of the fields in the **27**.

It should be noted that there is an ambiguity in the assignment of the various fields within the **27** of E_6. Although we usually place L and d^c into the $(\mathbf{16}, \bar{\mathbf{5}})$ and ν^c into the $(\mathbf{16}, \mathbf{1})$ we could instead place these same fields into the $(\mathbf{10}, \bar{\mathbf{5}})$ and $(\mathbf{1}, \mathbf{1})$. We see that at the SU(5) [or any SU(5) subgroup] level there exists a symmetry relating these two assignments,

$$\begin{pmatrix} L \\ d^c \end{pmatrix} \Leftrightarrow \begin{pmatrix} H \\ h^c \end{pmatrix}, \qquad \nu^c \Leftrightarrow S^c . \tag{1.2}$$

This symmetry, $SU(2)_I$, is most clearly apparent in the E_6 decomposition into $SU(6) \times SU(2)_I$ where

Table 1
Nomenclature and $SU(3)_C \times SU(2)_L \times U(1)_Y$ quantum numbers for the fields in the **27** representation of E_6

SO(10)	SU(5)		Color	T_{3L}	$Y/2$	Q
16	**10**	$Q \equiv \begin{pmatrix} u \\ d \end{pmatrix}_L$	**3**	$\begin{pmatrix} 1/2 \\ -1/2 \end{pmatrix}$	1/6	$\begin{pmatrix} 2/3 \\ 1/3 \end{pmatrix}$
		u_L^c	$\bar{\mathbf{3}}$	0	−2/3	−2/3
		e_L^c	**1**	0	1	1
	$\bar{\mathbf{5}}$	$L \equiv \begin{pmatrix} \nu \\ e \end{pmatrix}_L$	**1**	$\begin{pmatrix} 1/2 \\ -1/2 \end{pmatrix}$	−1/2	$\begin{pmatrix} 0 \\ -1 \end{pmatrix}$
		d_L^c	$\bar{\mathbf{3}}$	0	1/3	1/3
	1	ν_L^c	**1**	0	0	0
10	$\bar{\mathbf{5}}$	$H \equiv \begin{pmatrix} N \\ E \end{pmatrix}_L$	**1**	$\begin{pmatrix} 1/2 \\ -1/2 \end{pmatrix}$	−1/2	$\begin{pmatrix} 0 \\ -1 \end{pmatrix}$
		h_L^c	$\bar{\mathbf{3}}$	0	1/3	1/3
	5	$H^c \equiv \begin{pmatrix} E \\ N \end{pmatrix}_L^c$	**1**	$\begin{pmatrix} 1/2 \\ -1/2 \end{pmatrix}$	1/2	$\begin{pmatrix} 1 \\ 0 \end{pmatrix}$
		h_L	**3**	0	−1/3	−1/3
1	**1**	S_L^c	**1**	0	0	0

SU(6) contains the usual SM and where the **27** decomposes as

$$\mathbf{27} = (\mathbf{15}, \mathbf{1}) + (\bar{\mathbf{6}}, \mathbf{2}) . \tag{1.3}$$

Here the $\bar{\mathbf{6}}$ of SU(6) contains the $\bar{\mathbf{5}} + \mathbf{1}$ of SU(5) corresponding to the fields in eq. (1.2).

Although physics at the SM level is insensitive to this ambiguity in field assignments, if the effective low-energy group is larger than that of the SM, these new interactions *may* depend on how these assignments are chosen. As we will see in the next section, the greatest modification of physics expectations occurs when the electroweak group is extended by an SU(2) factor [as opposed to a U(1) or U(1) × U(1) factor].

Given the particle content in table 1, the most general $SU(3)_C \times SU(2)_L \times U(1)_Y$ invariant renormalizable superpotential that one can form from these fields alone is given by [1.11, 1.13]

$$\begin{aligned} W &= W_0 + W_1 + W_2 + W_3 , \\ W_0 &= \lambda_1 H^c Q u^c + \lambda_2 H Q d^c + \lambda_3 H L e^c + \lambda_4 H^c H S^c + \lambda_5 h h^c S^c , \\ W_1 &= \lambda_6 h u^c e^c + \lambda_7 L h^c Q + \lambda_8 \nu^c h d^c , \qquad W_2 = \lambda_9 h Q Q + \lambda_{10} h^c u^c d^c , \qquad W_3 = \lambda_{11} H^c L \nu^c . \end{aligned} \tag{1.4}$$

The superpotential, W, summarizes all of the gauge group and supersymmetry restrictions on couplings. To each term in W there correspond Yukawa couplings in which one identifies any two of the three fields with the fermion component of the superfield and the third field with the scalar component. Generation indices in W are suppressed but understood and intergenerational couplings can lead to new effects which will be discussed below. If there is more symmetry than that present in the SM, some of the terms in W may be absent and the number of independent λ_i is reduced.

Whereas the E_6 decomposition into $SU(3)_C \times SU(2)_L \times U(1)_Y$ dictates the color, isospin, and charge assignments of the exotic fields, their baryon (B) and lepton (L) numbers as well as their R-parities are not specified and several different assignments are possible. Note that for consistency we will assume for the moment that the usual L and B assignments for ν^c persist, but that in principle alternative assignments of these quantum numbers for this field are also possible, and are, in fact, necessary in rank-6 models. In order to make definite assignments of B and L for each of the exotics, not all of the terms in W can be allowed simultaneously without low-energy baryon and lepton number violation, e.g., the presence of W_1 would dictate $B(h) = \frac{1}{3}$, $L(h) = 1$ (leptoquark couplings), whereas W_2 leads instead to $B(h) = -\frac{2}{3}$ and $L(h) = 0$ (diquark couplings). Clearly terms in W_1 and W_2 cannot occur in the superpotential simultaneously without inducing $\Delta B \neq 0$ and $\Delta L \neq 0$ interactions. To avoid $\Delta B \neq 0$ and $\Delta L \neq 0$ terms, additional symmetries beyond $SU(3)_C \times SU(2)_L \times U(1)_Y$ must exist to eliminate certain couplings appearing in W. Such symmetries may be discrete (e.g., Z_n) or involve new gauge interactions such as an additional SU(2) group factor.

If there are no additional fields beyond those corresponding to the usual n_g generations of **27**'s then W_0 must lead to masses for the charged fermions. This can be accomplished by taking $B(H, H^c) = L(H, H^c) = 0$ and letting $\tilde{H}$ and $\tilde{H}^c$ (the superpartners of H and H^c, respectively) play the role of the pair of Higgs doublets in the usual SUSY version of the SM. $\langle \tilde{N} \rangle$ and $\langle \tilde{N}^c \rangle \neq 0$ (together with $\lambda_{1,2,3} \neq 0$) then produce masses for u, d, and e. To provide a mass for h, we must further assume $B(S^c) = L(S^c) = 0$ so that we can have $\langle \tilde{S}^c \rangle \neq 0$ and we must also assume $\lambda_{4,5} \neq 0$. Note that just as in the usual SUSY model we cannot take the Higgs doublet to be the superpartner of L since $\langle \tilde{\nu} \rangle \neq 0$ would violate lepton number (and R-parity). There are at least three generations of **27**'s containing Higgs fields. We can, however, always go to a basis where only one set of the fields obtain non-vanishing vacuum expectation values. The scalars not receiving vacuum expectation values are called "unHiggs". With $\tilde{H}$, $\tilde{H}^c$, and $\tilde{S}^c$ (and possibly $\tilde{\nu}^c$) playing the role of Higgs fields (case A) there are several possible assignments for the exotic field quantum numbers which correspond to the vanishing of subsets of the λ_i. If $L(\nu^c) = -1$, as is usually assumed in rank-5 models, three obvious sub-cases occur:

$$\begin{aligned}
&\text{(A1)} \quad \lambda_9 = \lambda_{10} = 0\,, && B(h) = \tfrac{1}{3},\ L(h) = 1 \quad \text{(leptoquark)}\,,\\
&\text{(A2)} \quad \lambda_6 = \lambda_7 = \lambda_8 = 0\,, && B(h) = -\tfrac{2}{3},\ L(h) = 0 \quad \text{(diquark)}\,,\\
&\text{(A3)} \quad \lambda_6 = \lambda_7 = \lambda_8 = \lambda_9 = \lambda_{10} = 0\,, && B(h) = \tfrac{1}{3},\ L(h) = 0 \quad \text{(quark)}\,.
\end{aligned} \tag{1.5}$$

In this case, λ_{11} induces a Dirac mass, m_D, for the neutrino and since $m_D \ll m_e$ we must unnaturally fine-tune ($\lambda_{11} \ll \lambda_3$) the parameters in W. In order to avoid this fine-tuning we must be able to set $\lambda_{11} = 0$ by a further symmetry. If $L(\nu^c) = 0$ then we must also have $\lambda_8 = \lambda_{11} = 0$ for case (A1) to prevent lepton number (and R-parity) violation. In this latter case it is then possible for $\langle \tilde{\nu}^c \rangle \neq 0$ without inducing mixing between L and H as well as h and d. For case (A3), $B(h)$ and $L(h)$ are not obviously constrained but for most assignments of these quantum numbers we would find h to be stable which is probably ruled out by cosmological considerations. If, for example $B(h) = \frac{1}{3}$ and $L(h) = 0$, then h is a conventional quark which can mix with d (via $\langle \tilde{\nu}^c \rangle \neq 0$ in rank-6 models) and then decay via flavor changing neutral currents (FCNC) or conventional charged currents (CC).

If flux breaking through the Hosotani mechanism leaves a rank-6 low energy group then both $\langle \tilde{S}^c \rangle$ and $\langle \tilde{\nu}^c \rangle \neq 0$ will be needed to break the symmetry down to the SM. For $\langle \tilde{\nu}^c \rangle \neq 0$ the λ_8 and λ_{11} terms must be eliminated from W in order to prevent ΔB and ΔL interactions at low energy. If on the other

hand, one is left with a rank-5 group only one of $\langle \tilde{S}^c \rangle$ and $\langle \tilde{\nu}^c \rangle$ needs to be non-zero and without any loss of generality one can take this to be $\langle \tilde{S}^c \rangle$. If $\langle \tilde{\nu}^c \rangle$ also obtains a vacuum expectation value (vev) in this case, then a Goldstone boson is generated and if $\lambda_8 \neq 0$ this leads to an inconsistent phenomenology [1.24]. Thus, in the rank-5 scenario, ν^c must have the usual $L = -1$ (R-parity positive) assignment so that $\langle \tilde{\nu}^c \rangle \neq 0$ is forbidden. Even in the rank-6 case, however, it may not always be easy to generate a non-zero vacuum expectation value for $\tilde{\nu}^c$.

A second possibility (case B), which is somewhat less economical, assigns the Higgs fields to a different **27** (or to a $\overline{\mathbf{27}}$) than those which contain the usual fermions. In this case one is free to treat the exotics as ordinary quarks and leptons (apart from their isospin properties), i.e.,

$$\text{(B)} \qquad B(h) = \tfrac{1}{3}\,, \quad L(h) = 0\,, \qquad B(H, H^c, \nu^c, S^c) = 0\,, \quad L(H, H^c, \nu^c, S^c) = \pm 1\,. \tag{1.6}$$

Additional doublet and singlet fields are introduced from another **27** (or $\overline{\mathbf{27}}$) of E_6 (with opposite R-parity) so that vev's can develop and transform under $SU(3)_C \times SU(2)_L \times U(1)_Y$ in a manner identical to the multiplets containing neutral fields in case (A),

$$H_1 \sim \tilde{L}\,, \qquad H_2 \sim \tilde{H} \quad (H_2^c \sim \tilde{H}^c)\,, \qquad H_3 \sim \tilde{\nu}^c\,, \qquad H_4 \sim \tilde{S}^c\,. \tag{1.7}$$

In this case we see that the B and L (and R-parity) conserving superpotential which leads to fermion masses takes the general form

$$\begin{aligned} W' = {} & \alpha_1 H_2^c Q u^c + \alpha_2 H_2 Q d^c + \alpha_3 H H_1^c e + \alpha_4 H_2 L e^c + \alpha_5 H^c H H_4 + \alpha_6 H_2^c H S^c \\ & + \alpha_7 H^c H_2 S^c + \alpha_8 h^c h H_4 + \alpha_9 H_1 h^c Q + \alpha_{10} H_3 h d^c + \alpha_{11} H_2^c L \nu^c + \cdots\,. \end{aligned} \tag{1.8}$$

W' not only leads to the usual mass terms but also to mixing between ordinary fermions and their exotic partners (e.g., e–E, d–h mixing). Additional terms beyond that explicitly displayed in (1.8) can also appear in W', however, these terms will not contribute to fermion masses and mixings. Family indices that can appear in eq. (1.8) are again suppressed. Mixings of this kind allow for the decay of exotic fermions via FCNC as well as CC and terms in W' in a manner similar to case (A3) above. Like case (A), further symmetries beyond $SU(3)_C \times SU(2)_L \times U(1)_Y$ can be used to eliminate several of the α_i in eq. (1.8).

There are several other possible assignments which can lead to interesting new physics beyond those discussed here which can result from using discrete symmetries [1.25]. The most common possibilities discussed in the literature are however (A1)–(A3) and (B) outlined above.

Note that independently of whether one has case (A) or (B), the effective Higgs fields are only doublets or singlets with respect to $SU(2)_L$. This will have important consequences for generating neutrino as well as gauge boson masses as we will discuss in the next few sections.

2. New gauge bosons in the low-energy electroweak sector

2.1. Overview of extended electroweak models

As discussed in the introduction, one of the possible hallmarks of superstring-inspired E_6 models at low energies is the existence of new gauge bosons which result from extensions of the usual SM

electroweak group, $SU(2)_L \times U(1)_Y$. Interest in extended electroweak models predates the superstring era by many years and much of the earlier work [2.1–2.3] can be adapted to the models of current interest.

Flux-breaking of E_6 leads directly to effective strong–electroweak groups of ranks 5 and 6 at low energies [1.11, 1.13]. So if the color group is chosen to be $SU(3)_C$ at these scales, then the rank-5 model is uniquely determined to be

$$SU(3)_C \times SU(2)_L \times U(1)_Y \times U(1)_\eta \,, \tag{2.1a}$$

with all the couplings of the additional $U(1)_\eta$ factor essentially fixed (as will be discussed below). In the rank-6 case, one finds the relevant groups to be

$$\begin{aligned} &\text{(a)} \quad SU(3)_C \times SU(2)_L \times U(1)_Y \times U(1)' \times U(1)'' \,, \\ &\text{(b)} \quad SU(3)_C \times SU(2)_L \times SU(2)' \times U(1)' \times U(1)'' \,, \end{aligned} \tag{2.1b}$$

where the primed group factors in (a) and (b) are in general unrelated. In case (a), the product $U(1)' \times U(1)''$ can be taken, without loss of generality [2.4] (see also Robinett and Rosner in ref. [1.8]), to be $U(1)_\psi \times U(1)_\chi$, where $U(1)_\psi$ and $U(1)_\chi$ are defined via the decomposition

$$\begin{array}{l} E_6 \to SO(10) \times U(1)_\psi \\ \qquad\quad \big\lfloor \to SU(5) \times U(1)_\chi \,, \end{array} \tag{2.2}$$

i.e., $U(1)_\psi$ and $U(1)_\chi$ form a basis for any pair of orthogonal abelian generators which are independent of the electric charge $Q\,(= T_{3L} + Y/2)$. Once the embeddings of the fields into SO(10) and SU(5) are given the couplings resulting in the covariant derivative for $U(1)_\psi$ and $U(1)_\chi$ are uniquely specified as will be discussed below. In case (b), there are several interesting possibilities depending on whether or not Q is orthogonal to the SU(2)′ generators. The two most frequently discussed sub-cases are

$$\begin{aligned} &\text{(b1)} \quad SU(3)_C \times SU(2)_L \times SU(2)_R \times U(1)_L \times U(1)_R \,, \\ &\text{(b2)} \quad SU(3)_C \times SU(2)_L \times U(1)_Y \times SU(2)_I \times U(1)' \,, \end{aligned} \tag{2.3}$$

the first of which is the rank-6 version of the left–right symmetric model (LRSM) (for a general survey of the left–right symmetric model and its basis in SO(10) see ref. [2.5]) and the second involves the $SU(2)_I$ symmetry discussed in the introduction.

For both cases (a) and (b) suitably large vev's could reduce the rank-6 low-energy model even further to an effective (!) rank-5 model (ER5M). For example, in model (a) we would obtain the reduction

$$U(1)_\psi \times U(1)_\chi \to U(1)_\theta \,, \tag{2.4}$$

with $U(1)_\theta$ being some linear combination of $U(1)_\psi$ and $U(1)_\chi$. For case (b) one can have, e.g.,

$$\text{(b1)} \quad U(1)_L \times U(1)_R \to U(1)_{V=L+R} \,, \qquad \text{(b2)} \quad SU(2)_I \times U(1)' \to SU(2)_I \,. \tag{2.5}$$

These (effective) rank-5 models together with the true rank-5 model, eq. (2.1a), are the ones which are most often discussed in the literature.

As is well known, additional U(1) factors beyond those of the SM lead to new neutral gauge bosons with flavor diagonal couplings (in the weak basis). However, new SU(2) factors lead to an additional pair of conjugate gauge bosons (with flavor-changing couplings) beyond the simple new neutral gauge boson of the U(1) case. If the SU(2) generators commute with Q, the conjugate gauge boson pair is neutral as in the case of $SU(2)_I$; otherwise the pair will be charged as is the case for $W_R^{\pm}$ within the $SU(2)_R$ example.

Table 2 shows the quantum number assignments for the various fields in terms of the normalized generators $Q_{\eta,\psi,\chi}$, their right-handed weak isospin and $U(1)_V$ within the LRSM (b1), and their corresponding T_{3I} for model (b2) with the additional $SU(2)_I$ factor. In writing down these values we have made the conventional assignments: in terms of eq. (1.1), $(L, d_L^c) = (\mathbf{16}, \bar{\mathbf{5}})$ and $\nu_L^c = (\mathbf{16}, \mathbf{1})$. If one instead assigns $\{L, d_L^c\} = (\mathbf{10}, \bar{\mathbf{5}})$ and $\nu_L^c = (\mathbf{1}, \mathbf{1})$ the quantum numbers of the fields $\{L, d_L^c, \nu_L^c\}$ must be interchanged with those of $\{H, h_L^c, S_L^c\}$. It is important to notice that this interchange does not alter the values of Q_η so that the rank-5 model is insensitive to this embedding ambiguity but all the rank-6 models are apparently modified.

In reading the table, it is important to remember that the corresponding couplings for right-handed fields are of *opposite sign* to those of the conjugate fields.

2.2. Specific models and Z–Z′ mixing

Consider the rank-6 models of type (a) discussed in the previous section. When the weak iso-singlet Higgs field(s) develop its (their) vev's, the gauge fields corresponding to $U(1)_\psi$ and $U(1)_\chi$ (Z_ψ and Z_χ) become massive but are not true mass eigenstates since these states can mix. Let us define the mass eigenstates at this point to be Z' and Z'' as given by

$$Z'(\theta) \equiv Z_\psi \cos\theta - Z_\chi \sin\theta\,, \qquad Z''(\theta) \equiv Z_\chi \cos\theta + Z_\psi \sin\theta\,, \tag{2.6}$$

Table 2
Quantum numbers for the fields in the **27** representation in E_6 under the groups $U(1)_\eta$, $U(1)_\psi$, $U(1)_\chi$, $SU(2)_R$, $U(1)_V$, and $SU(2)_I$ respectively

	$2\sqrt{15}\,Q_\eta$	$2\sqrt{6}\,Q_\psi$	$2\sqrt{10}\,Q_\chi$	T_{3R}	$V/2$	T_{3I}
$Q \equiv \begin{pmatrix} u \\ d \end{pmatrix}_L$	2	1	−1	0	$\frac{1}{6}$	0
$L \equiv \begin{pmatrix} \nu \\ e \end{pmatrix}_L$	−1	1	3	0	$-\frac{1}{2}$	$\frac{1}{2}$
u_L^c	2	1	−1	$-\frac{1}{2}$	$-\frac{1}{6}$	0
d_L^c	−1	1	3	$\frac{1}{2}$	$-\frac{1}{6}$	$\frac{1}{2}$
e_L^c	2	1	−1	$\frac{1}{2}$	$\frac{1}{2}$	0
ν_L^c	5	1	−5	$-\frac{1}{2}$	$\frac{1}{2}$	$\frac{1}{2}$
$H \equiv \begin{pmatrix} N \\ E \end{pmatrix}_L$	−1	−2	−2	$-\frac{1}{2}$	0	$-\frac{1}{2}$
$H^c \equiv \begin{pmatrix} E^c \\ N^c \end{pmatrix}_L$	−4	−2	2	$\frac{1}{2}$	0	0
h_L	−4	−2	2	0	$-\frac{1}{3}$	0
h_L^c	−1	−2	−2	0	$\frac{1}{3}$	$-\frac{1}{2}$
S_L^c	5	4	0	0	0	$-\frac{1}{2}$

with θ being dependent on the vev's and the gauge couplings, $g_{\psi,\chi}$, corresponding to $U(1)_{\psi,\chi}$. The reader should be aware that there exist many definitions of the mixing parameter (called θ here) in the literature and that great care is necessary in comparing the results of different authors. If $g_{\psi,\chi}$ and the corresponding hypercharge coupling, g_Y, break off from a larger group at a common scale and have identical renormalization group equations (which is the case with matter fields solely in the **27** of E_6) then Z' and Z'' have couplings of the form [2.4]

$$(g/c_w)(\tfrac{5}{3}x_w)^{1/2}[(Q_\psi \cos\theta - Q_\chi \sin\theta)Z' + (Q_\chi \cos\theta + Q_\psi \sin\theta)Z''], \tag{2.7}$$

with $Q_{\psi,\chi}$ given in table 2 and $x_w \equiv \sin^2\theta_w$ ($\simeq 0.23$). If, however, $U(1)_{\psi,\chi}$ break off from a larger group at a different scale than does $U(1)_Y$ or are still part of a larger group [e.g., an SU(2) factor] the couplings $g_{\psi,\chi}$ need to be calculated using their corresponding renormalization group equations. This would effectively rescale the overall couplings in eq. (2.7) by an additional factor: $g^2_{\psi,\chi} \to \lambda g^2_{\psi,\chi}$. We will assume that $\lambda = 1$ in the summary below. Although one could examine the three gauge boson system Z, Z', and Z'' it is much easier to first examine the rank-5 limit, eq. (2.4), in which Z'' becomes significantly more massive than Z'. This could either mean that Z'' is very heavy with a mass characteristic of a large intermediate mass scale ($M_I \sim 10^{10}$ GeV), the Planck scale, or perhaps relatively light ($\sim$10 TeV) but yet sufficiently heavy so that it effectively decouples from both Z and Z'. We will assume that only Z' is still relatively light enough to mix with the Z since one does not want to introduce a new hierarchy into the theory without any explanation or stability guaranteed by a symmetry. This leaves us with Z and $Z'(\theta)$ as the neutral gauge bosons within an effective rank-5 model (ER5M) with an a priori unknown parameter θ. This class of models has received a major fraction of the attention in the literature [2.4]. We will briefly return to a discussion of the full rank-6 situation below.

As θ is varied the identification $Z' = Z_\psi$ is recovered (model ψ) for $\theta = 0$ and $Z' = Z_\chi$ (model χ) for $\theta = -90°$. For $\theta = \sin^{-1}\sqrt{3/8}$ ($\simeq 37.76°$) the couplings of the rank-5 model (model η) are recovered. In addition, for $\theta = -\sin^{-1}\sqrt{5/8}$ ($\simeq -52.24°$), Z' can be identified as that which couples to the diagonal generator of $SU(2)_I$ in model (b2) in eq. (2.3) – called Z_I (and correspondingly, model I) in the literature. Note that Z_I is orthogonal to Z_η. The new neutral gauge bosons $Z_{\psi,\chi,\eta,I}$ are the ones most frequently discussed as being representative of those which can arise in low-energy superstring-inspired E_6 models.

As discussed above, the exchange of the assignments of the fields $\{L, d^c_L, \nu^c_L\}$ with those of the exotics $\{H, h^c_L, S^c_L\}$ leaves the couplings Q_η unaltered. For the $U(1)_\theta$ model, the couplings of $Z(\theta)$ are modified but in a rather simple way. Interchange of the two sets of fields corresponds to a mapping of $\theta \to \theta'$ given by

$$\theta' = \tan^{-1}(\sqrt{15}) - \theta\,, \tag{2.8}$$

and thus the general structure of the model is left unchanged. For the rank-6 model (b2) this interchange leaves the U(1)' couplings unaltered while flipping the isospin assignments within the $SU(2)_I$ group ($T_{3I} \to -T_{3I}$) for all the fields in the **27**. For the LRSM, as will be discussed below, this interchange will lead to new physics since, e.g., u^c and h^c now form a right-handed doublet instead of the usual combination u^c and d^c.

To further discuss the properties of the Z' in these models, we need to examine the possible mixing between the Z' and $Z \equiv Z_{SM}$, the neutral gauge boson of the SM. For the moment we restrict ourselves

to the case of the effective rank-5 models. We will return to the case involving an extra SU(2) group factor below. Let us write the coupling in eq. (2.7) in a slightly more general, but abbreviated, form and include the usual Z as well,

$$(g/c_w)[(T_3 - x_w Q)Z + (\tfrac{5}{3}x_w)^{1/2} Q' Z'] , \tag{2.9}$$

with, e.g., $Q' \equiv Q_\psi \cos\theta - Q_\chi \sin\theta$ in the effective rank-5 model resulting from (b1). We take the effective Higgs fields to be $\tilde{H}$, $\tilde{H}^c$, $\tilde{\nu}^c$ and $\tilde{S}^c$. It should be noted that although $\tilde{\nu}^c$ may be allowed by its quantum number assignments to get a vev (which would be necessary to break a rank-6 strong–electroweak group down to the SM) it may be difficult to generate such a vev in most classes of models so far considered [1.24]. A possible solution to this problem is to generate $\langle \tilde{\nu}^c \rangle$ by radiative corrections. We will assume that $\langle \tilde{\nu}^c \rangle$ can be non-zero in our general discussion below. In a generic model with two doublets and two singlets of Higgs fields we can label the representations, following ref. [2.6], as

$$\phi_1 = \begin{pmatrix} \phi_1^0 \\ \phi_1^- \end{pmatrix}, \qquad \phi_2 = \begin{pmatrix} \phi_2^+ \\ \phi_2^0 \end{pmatrix}, \qquad \phi_3 = \phi_3^0 , \qquad \phi_4 = \phi_4^0 , \tag{2.10}$$

with $\langle \phi_i^0 \rangle = v_i/\sqrt{2}$ and $Q'(\phi_i^0) = Q_i'$. In the absence of additional charged gauge bosons that can mix with the usual SM W boson (as are present in the LRSM), $M_W = gv/2$ is obtained with $v^2 = v_1^2 + v_2^2$ together with a Z–Z′ mass matrix

$$M^2 = \begin{pmatrix} M_Z^2 & \delta M^2 \\ \delta M^2 & M_{Z'}^2 \end{pmatrix}, \tag{2.11}$$

with M_Z being the usual SM Z mass in the absence of mixing and

$$\delta M^2/M_Z^2 = 2(\tfrac{5}{3}x_w)^{1/2}(Q_1' v_1^2 - Q_2' v_2^2)/v^2 , \qquad M_{Z'}^2/M_Z^2 = \tfrac{20}{3}x_w \frac{1}{v^2}\sum_{i=1}^{4} (Q_i' v_i)^2 . \tag{2.12}$$

The matrix in eq. (2.11) is diagonalized by an orthogonal transformation

$$\begin{pmatrix} Z_1 \\ Z_2 \end{pmatrix} = \begin{pmatrix} \cos\phi & \sin\phi \\ -\sin\phi & \cos\phi \end{pmatrix} \begin{pmatrix} Z \\ Z' \end{pmatrix}, \tag{2.13}$$

producing the mass eigenstates $Z_{1,2}$ with masses $M_{1,2}$ where ϕ is given by

$$\tan 2\phi \equiv 2\,\delta M^2/(M_Z^2 - M_{Z'}^2) . \tag{2.14}$$

In the large $v_{3,4}$ limit $M_{Z'} \to \infty$ and $\phi \to 0$ so that we recover $Z_1 = Z$. In addition to eq. (2.14) the following relations are obtained from the eigenvalue equation

$$\tan^2\phi = (M_Z^2 - M_1^2)/(M_2^2 - M_Z^2) , \qquad \delta M^2/M_2^2 = -(1 - M_1^2/M_Z^2)\cot\phi = -(M_2^2/M_Z^2 - 1)\tan\phi . \tag{2.15}$$

Note that eq. (2.15) places a Higgs sector (i.e., Q_i') independent constraint on the value ϕ for a fixed value of $\Delta M = M_Z - M_1 (\geq 0)$ as a function of M_2 (assuming M_1 is known),

$$|\phi| \leq \tan^{-1}(\{[2(\Delta M)M_1 + (\Delta M)^2]/[M_2^2 - (M_1 + \Delta M)^2]\}^{1/2}) . \tag{2.16}$$

Note that for $M_2 \to \infty$ and fixed ΔM, $\phi \sim M_2^{-1}$; this is called the *mass constraint* on the mixing angle ϕ. We can turn this constraint around and calculate the minimum value of ΔM for a given value of the mixing angle ϕ and a choice of M_2. One finds

$$\Delta M|_{\min} = -M_1 + [(M_1^2 + M_2^2 \tan^2\phi)/(1 + \tan^2\phi)]^{1/2} . \tag{2.17}$$

Figures 1a, b show $\Delta M|_{\min}$ versus M_2 for various choices of the angle ϕ. If we assume, for example, that $\Delta M|_{\min} = 1$ GeV and $|\phi| = 0.05$ then we are led to $M_2 \lesssim 300$ GeV. Data from the SLC and LEP should be able to probe values of ΔM as small as 30–50 MeV (see, for example, ref. [2.7]).

For a fixed Higgs sector (i.e., Q_i' are known) stronger limits on the mixing angle are possible by

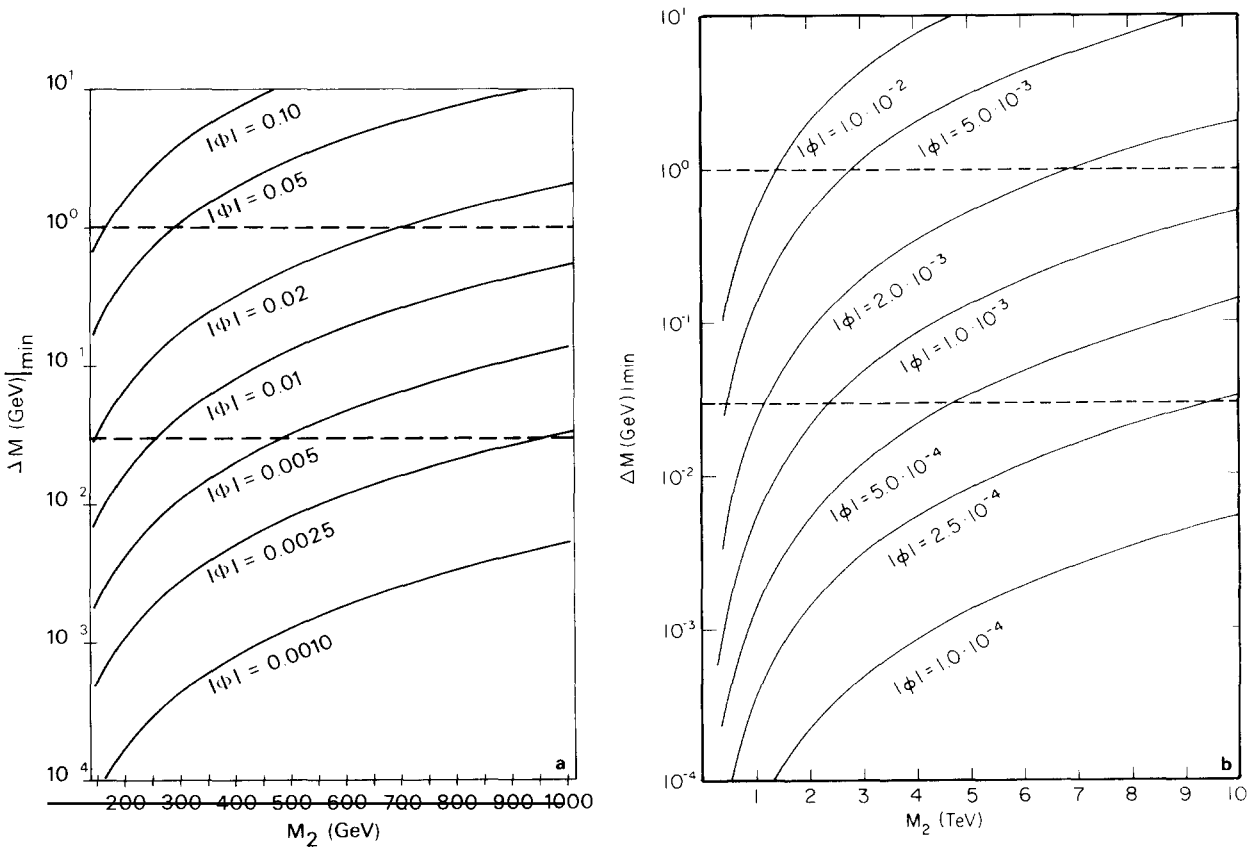

Fig. 1. The minimum value of the Z mass shift for different values of the Z–Z′ mixing angle $|\phi|$ as a function of M_2 in the ranges (a) $150 \leq M_2 \leq 1000$ GeV; (b) $0.5 \leq M_2 \leq 10$ TeV.

combining eqs. (2.12) and (2.15) and noting that $v_{1,2}^2/v^2 < 1$. One then obtains the so-called *Higgs constraint*,

$$2(\tfrac{5}{3}x_w)^{1/2}(Q')_{\min} \leq \tan\phi\,(M_2^2/M_Z^2 - 1) \leq 2(\tfrac{5}{3}x_w)^{1/2}(Q')_{\max}\,, \tag{2.18}$$

with $(Q')_{\min}$ and $(Q')_{\max}$ the smallest and largest of $-Q_1'$ and Q_2' respectively. In this case, for fixed ΔM, $\phi \sim 1/M_2^2$ so that this constraint is eventually stronger than the mass constraint for sufficiently large M_2. As will be discussed below, low-energy neutral current data (NC) can also be used to place limits on both ϕ and M_2 by looking for deviations from both the SM neutral current structure and overall strength (i.e., the ρ parameter). NC constraints on ϕ also scale like $\sim 1/M_2$ for large M_2 so that for sufficiently large M_2 the Higgs constraint is still dominant.

It should be noted that in some models of SUSY breaking, in particular no-scale models [2.8] (see also Ellis in ref. [1.17]), the ratio of the vev's of the Higgs doublets is somewhat limited: $\tan\beta = v_2/v_1 \simeq 2$. We will not assume this constraint in the analysis below but its assumption would provide further constraints on the size of Z–Z′ mixing and a limit on M_2.

Before ending this section we briefly review the full three neutral gauge boson sector of the rank-6 model, following the work presented in ref. [2.9]. Since this situation involves a large number of parameters it is sufficient to examine several limiting cases.

Case (1). $\langle \tilde{S}^c \rangle, \langle \tilde{\nu}^c \rangle \gg \langle \tilde{N}^c \rangle, \langle \tilde{N} \rangle$. Here $Z_2 (= Z')$ and $Z_3 (= Z'')$ decouple from the usual $Z (= Z_1)$ of the SM and the mixing angle θ is given by

$$\tan 2\theta = \sqrt{15}\langle \tilde{\nu}^c \rangle^2 / (7\langle \tilde{\nu}^c \rangle^2 - 8\langle \tilde{S}^c \rangle^2)\,, \tag{2.19}$$

and, via the eigenvalue equation, θ is restricted to the range $(M_2 \leq M_3)$

$$-\sqrt{15}/4 \leq \cos\theta \leq 0\,, \tag{2.20}$$

with $M_2^2/M_3^2 \leq 0.6$. The range of θ allowed by eq. (2.20) *excludes* the model η (rank-5) case where $\cos\theta = \sqrt{5/8}$ so that Z_2 can never be identified with Z_η. Note that if $\langle \tilde{\nu}^c \rangle^2 \gg \langle \tilde{S}^c \rangle^2$ then $\cos\theta = -\sqrt{15}/4$ but if $\langle \tilde{S}^c \rangle^2 \gg \langle \tilde{\nu}^c \rangle^2$ then $\cos\theta = 0$.

Case (2). $\langle \tilde{\nu}^c \rangle \gg \langle \tilde{S}^c \rangle, \langle \tilde{N}^c \rangle, \langle \tilde{N} \rangle$ leads to $\cos\theta = -\sqrt{15}/4$ with $Z_3 = Z''$. In this case Z and Z′ would have substantial mixing. This is one of the effective rank-5 models discussed above with a fixed value of θ.

Case (3). $\langle \tilde{S}^c \rangle \gg \langle \tilde{\nu}^c \rangle, \langle \tilde{N}^c \rangle, \langle \tilde{N} \rangle$ (with $Z_3 = Z''$) leads to $\cos\theta = 0$ which is essentially model χ already discussed above.

Case (4). All vev's comparable. In this case none of the new Z's can be extremely heavy and considerable mixing is possible, with three angles needed to describe the general mixing structure. This general case is difficult to analyze completely due to the large number of parameters.

It is clear from the above that if at least one vev is much larger than all the rest the resulting model (of the effective rank-5 type) will be easy to distinguish from the rank-5 model (η).

2.3. Constraints on Z–Z′ mixing and the Z_2 mass from existing data

The mass of the new gauge boson expected in effective rank-5 models and the amount of Z–Z′ mixing can be constrained in a number of ways some of which were briefly discussed in the previous section.

2.3.1.

The effects of a new neutral gauge boson (Z′) on low-energy neutral current (NC) phenomenology are well known [2.1–2.3]. With couplings normalized as

$$\mathscr{L} = (g/c_w)(J_\mu Z^\mu + J'_\mu Z'^\mu) , \tag{2.21}$$

and a mass matrix of the form given by eq. (2.11), the effective low-Q^2 ($Q^2 \ll M_i^2$) interaction is given by

$$\mathscr{L}_{NC}^{eff} = (4G_F/\sqrt{2})[\rho_1 J^2 + \rho_2 (J')^2 + \eta J J'] , \tag{2.22}$$

$$\rho_1 = M_{Z'}^2 M_Z^2 / D , \qquad \rho_2 = M_Z^4 / D , \qquad \eta = -2(\delta M^2) M_Z^2 / D , \tag{2.23}$$

and $D = M_Z^2 M_{Z'}^2 - (\delta M^2)^2$. In the mass eigenstate basis, $\mathscr{L}_{NC}^{eff}$ can be written as

$$\mathscr{L}_{NC}^{eff} = (4G_F/\sqrt{2})[(M_Z^2/M_1^2) J_1^2 + (M_Z^2/M_2^2) J_2^2] , \tag{2.24}$$

$$J_1 = J_Z \cos\phi + J_{Z'} \sin\phi , \qquad J_2 = J_{Z'} \cos\phi - J_Z \sin\phi . \tag{2.25}$$

By looking for deviations from the SM (i.e., $\rho_1 = 1$, $\rho_2 = \eta = 0$) and using the relations (2.23) one can constrain the model parameters $M_{1,2}$ and ϕ. These low-energy results can in turn be combined with direct measurements of the Z mass made by the UA1 and UA2 collaborations at the CERN $S\bar{p}pS$ collider [2.10]. Constraints on ϕ and M_2 from NC and Collider data have been examined by a large number of authors for different models [2.11, 2.12]. There have been two recent analyses [2.13, 2.14] which combine NC and Collider measurements to constrain M_2 and ϕ by following the analysis presented in the previous section. Figures 2a–c from Amaldi et al. show the bounds on the value of M_2 as a function of the mixing angle ϕ (denoted by either θ or θ_3 in the figures) for models ψ, χ, and η defined above. The "constrained" regions in the figures correspond to those allowed when $\rho = 1$, i.e., the *mass constraint* resulting from using Higgs doublets and singlets only. The "unconstrained" areas are allowed if $\rho \neq 1$ even in the limit of large M_2. This would correspond, for example, to models where triplet Higgs fields are present, which is not the case for the superstring-inspired E_6 models discussed

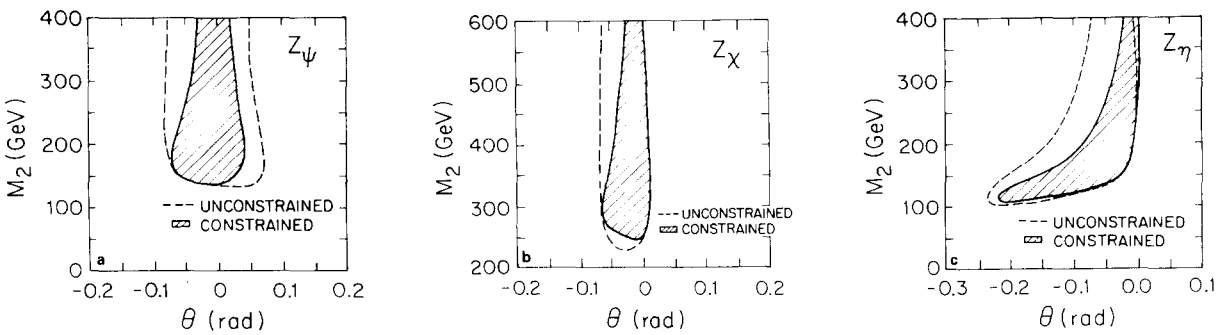

Fig. 2. Bounds from NC and collider data on M_2 as a function of the Z–Z′ mixing angle θ (called ϕ in the text) for constrained ($\rho = 1$) and unconstrained Higgs sectors: (a) model ψ; (b) model χ; (c) model η.

here. The figures from the analysis of Costa et al. [2.14] also show the result of adding the so-called *Higgs constraint* in which the quantum numbers of the Higgs fields under the new part of the gauge sector are completely specified (see figs. 3a–c). As one can easily see, bounds on M_2 and ϕ are quite sensitive to the choice of model (i.e., the value of θ). This is most clearly displayed in fig. 4 from the analysis of Amaldi et al. where bounds on ϕ (θ in their notation) and M_2 are shown as functions of cos β [where $\beta = \pi/2 + \theta$, θ being our Z′–Z″ mixing angle defined in eq. (2.6)].

In this analysis (which uses the limit on the shift of the Z boson mass as measured by the UA1 and UA2 collaborations to constrain both M_2 and ϕ) one needs to be somewhat careful in attributing any Z mass shift solely to Z–Z′ mixing. It is well known [2.15] that the existence of heavy fields (e.g., a fourth generation of ordinary fermions) may also induce a significant change in M_Z. As discussed above, low-energy E_6 models have a large number of new fields (h, N, E, S) which are reasonably massive and which (together with their superpartners as well as the usual fermions and charginos) could induce a shift in M_Z. Thus a shift in M_Z due to mixing may be enhanced or suppressed by an additional contribution due to radiative corrections from the new heavy particles we know to be present in the theory. The analyses above [2.13, 2.14] ignore these effects due to the large number of parameters (i.e., masses) involved but one must be aware that such effects may be important.

2.3.2.

New neutral (as well as charged) gauge bosons may make themselves known via radiative corrections, i.e., their appearance in loops. In particular, loop corrections to the Cabibbo–Kobayashi–Maskawa (CKM) [2.16] quark mixing matrix and unitarity can be used to place bounds on the Z_2 mass if one ignores other possible effects such as a fourth generation of fermions or new radiative corrections from other sources (such as the exotics h, N and E and SUSY partners). With a new Z′ boson interacting via

$$\mathcal{L}_{\text{int}} = -(3g/2\sqrt{10})C \sum_{\text{f}} (Q_{\text{f}_\text{L}} \bar{f}_\text{L} \gamma_\mu f_\text{L} + Q_{\text{f}_\text{R}} \bar{f}_\text{R} \gamma_\mu f_\text{R}) Z'^{\mu} , \tag{2.26}$$

one arrives at the following bound from the sum of the squares of the first row of the CKM matrix using unitarity:

$$\begin{aligned} &|V_{\text{ud}}|^2 + |V_{\text{us}}|^2 + |V_{\text{ub}}|^2 = 0.9984 \pm 0.0021 + \Delta , \\ &-0.0011 \leq \Delta \leq 0.0043 \ (90\% \text{ CL}) , \end{aligned} \tag{2.27}$$

where

$$\Delta = (-27\alpha/40\pi x_\text{w})|C|^2 Q_{\text{e}_\text{L}} (Q_{\text{e}_\text{L}} - Q_{\text{d}_\text{L}}) \frac{\ln x}{x-1} , \tag{2.28}$$

and $x \equiv M_\text{Z}^2/M_\text{W}^2$. Using (2.27) and (2.28) one now can place a bound on M_2 as a function of θ (if Z–Z′ mixing is ignored). These results are shown in fig. 5 from ref. [2.17] where their ϕ is given by $\theta + \pi/2$ (θ being the $Z_{\psi,\chi}$ mixing angle defined above). For some models, model χ ($\phi = 0$) in particular, this leads to a better limit than that from the NC analysis above, but for other models, such as model η (tan $\phi = -\sqrt{5/3}$), this bound is quite poor. Again, it is important to remember that this analysis ignores any possible contributions to Δ which may arise from the other new fields which we know to exist in these models.

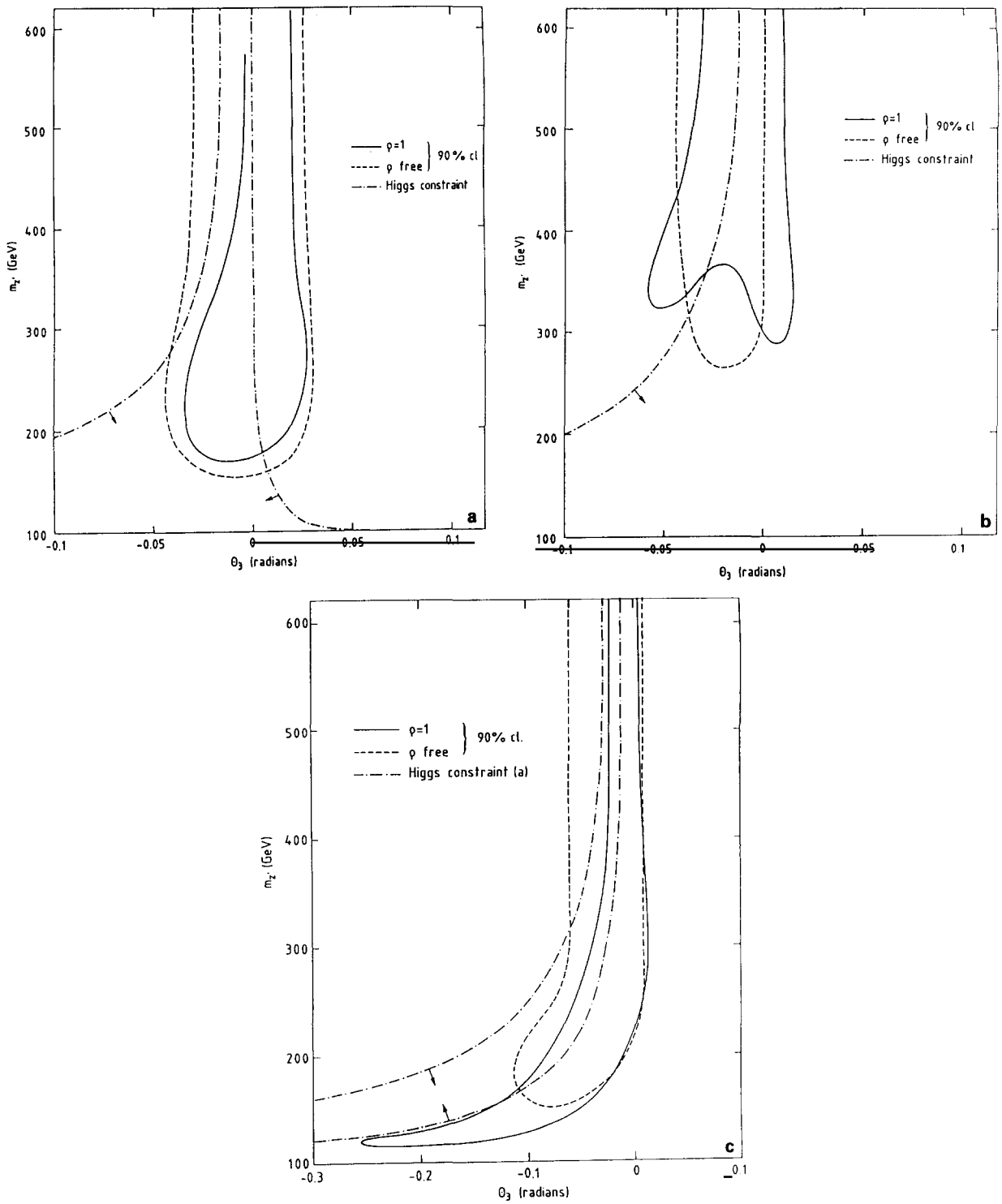

Fig. 3. Bounds on M_2 as a function of the Z–Z′ mixing angle θ_3 (called ϕ in the text) applying both mass and Higgs constraints as well as NC constraints: (a) model ψ; (b) model χ; (c) model η.

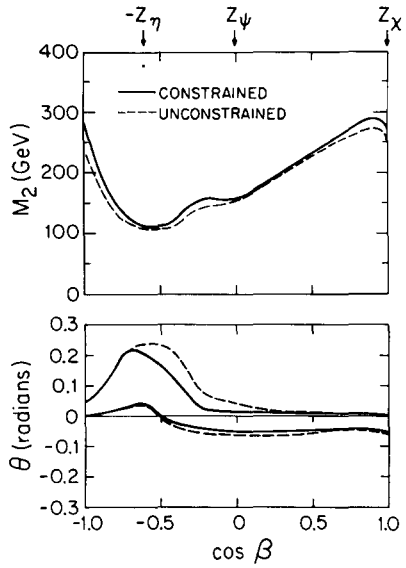

Fig. 4. Bounds from NC and collider data on M_2 and θ (i.e., ϕ) as a function of cos β for constrained ($\rho = 1$) and unconstrained Higgs sectors.

New neutral gauge bosons may also contribute to the anomalous magnetic moment of the muon even if its couplings are flavor diagonal. However, since $M_2^2 \gtrsim 4M_1^2$ and the Z_2 couplings are somewhat weaker than those of Z_1, these contributions are expected to be very small and unlikely to be observable any time soon.

2.3.3. *Direct search limits*

The UA1 and UA2 collaborations have performed a search for new neutral gauge bosons which decay to e^+e^- [2.18] with a null result: $\sigma \cdot B \lesssim 3$ pb. Since all of the Z′ couplings are known, one can use this data to place limits on Z's coming from E_6 with two caveats. (i) One must include QCD

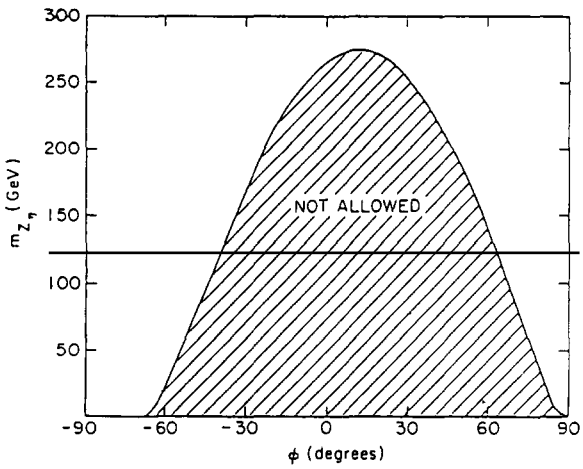

Fig. 5. Bounds on M_2 in model η as a function of ϕ (i.e., θ) from electroweak radiative corrections to the CKM matrix.

corrections to the production cross section in analogy with ordinary Drell–Yan ($q\bar{q} \to \gamma^*$) processes. (ii) One does not know if, e.g., the exotic fermions and/or superpartners make significant contributions to the Z′ width. These decay modes could drastically reduce the e^+e^- branching fraction for Z′ and weaken the resulting bound on M_2. Figure 6 from Barger et al. [2.19] shows the present limit on M_2 (with Z–Z′ mixing ignored) as a function of $\cos\alpha$ ($\alpha = -\theta$) for the case where no exotics contribute to $\Gamma(Z_2)$ ($n_g = 0$) or where three generations of exotics contribute to $\Gamma(Z_2)$ without phase space suppression ($n_g = 3$). A similar analysis by Ellis et al. [2.20] yields the limits

$$M(Z_\psi) > 158\,(118)\ \text{GeV}\,, \qquad M(Z_\chi) > 170\,(140)\ \text{GeV}\,, \qquad M(Z_\eta) > 167\,(115)\ \text{GeV}\,, \tag{2.29}$$

for $n_g = 0$ (3). It should be noted that these authors [2.20] use a bound of $\sigma \cdot B < 1.8\,\text{pb}$ from the combined UA1 and UA2 data sets. Note that Z–Z′ mixing is ignored in this second analysis as well. In all cases these limits are either comparable to or somewhat poorer than those resulting from the low-energy NC analysis. The results presented here (even in the $n_g = 3$ case) may be somewhat weaker if further exotic modes contribute to the Z_2 width.

We conclude this section by noting that significant limits exist on the mass of Z_2 from all three analyses (i)–(iii) but that these bounds are very model (i.e., θ *and* ϕ) dependent and that in all cases the existence of new particles may invalidate (or at least weaken) the conclusions obtained in each case.

2.4. *Decay modes and widths of new gauge bosons*

In order to search for new gauge bosons at colliders it is important to know as much as possible about their decay modes. Some modes (such as e^+e^- and $\mu^+\mu^-$) are used as production signals while others (such as W^+W^-) are very sensitive probes of Z–Z′ mixing. As discussed in the previous section, the existence of new Z_2 decay modes (beyond the usual fermions) leads to a lowering of the branching ratio into e^+e^- and, consequently, a weakening of the production signal. In addition, measurements of

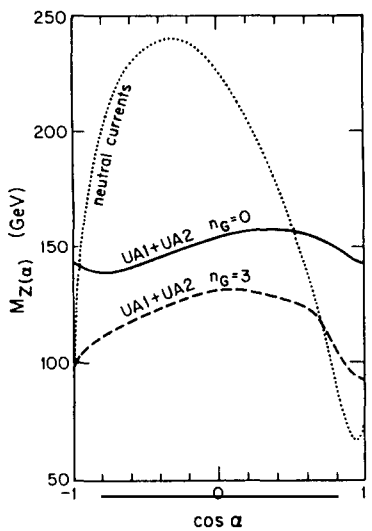

Fig. 6. Bounds on M_2 from direct searches for Z_2 at the CERN collider as a function of $\cos\alpha$ (i.e., $\cos\theta$).

certain relative branching ratios may lead to a complete determination of the Z_2 couplings within the E_6 context, as is discussed in the appendix.

2.4.1. Fermionic modes

Neglecting QCD radiative corrections the width $\Gamma(Z_2 \to \bar{f}f)$ is given by

$$\Gamma(Z_2 \to \bar{f}f) = C_f(g^2 M_2/12\pi)(1-4m_f^2/M_2^2)^{1/2}[v_f^2(1+2m_f^2/M_2^2) + a_f^2(1-4m_f^2/M_2^2)], \tag{2.30}$$

where C_f is a color factor [e.g., $C_f = 3$ (1) for quarks (leptons)] and the couplings are normalized to be

$$\mathcal{L} = g\bar{f}\gamma_\mu(v_f - a_f\gamma_5)fZ_2^\mu, \tag{2.31}$$

and can be read off directly from table 2 for the models of interest to us here. These fermionic modes are generally dominant and have been considered by a large number of authors [2.11, 2.19, 2.20]. If fermions are the only (or by far dominant) contributions to the Z_2 width, then fig. 7 from Barger et al. [2.19] best summarizes this situation (for the cases $n_g = 0$ and 3). For all values of the mixing angle θ, Γ_2^{tot}/M_2 is far smaller than what would be expected (for $n_g = 0$) by scaling up the same ratio for the SM Z boson. For the case $n_g = 3$, $\Gamma_2^{tot}/M_2 = 0.025$ and is θ independent but is still somewhat smaller than that expected from naive scaling.

2.4.2. SUSY partners

The SUSY partners ($\tilde{f}$) of the known fermions (as well as the exotics) may make a substantial contribution to the Z_2 width. Taking the normalization of the fermion couplings to be the same as that in (2.31), one obtains the width (assuming $\tilde{f}_L$ and $\tilde{f}_R$ are degenerate mass eigenstates)

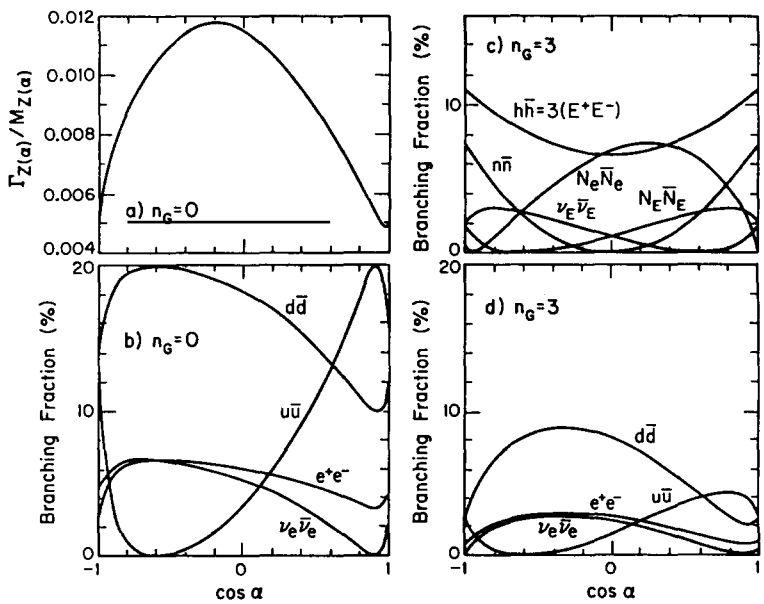

Fig. 7. Fermionic branching fractions for Z_2 decay as functions of cos α (i.e., cos θ).

$$\Gamma(Z_2 \to \bar{\tilde{f}}_{L,R} \tilde{f}_{LR}) = C_f (g^2 M_2/48\pi)(1 - 4m_{\tilde{f}}^2/M_2^2)^{3/2}(v_f \pm a_f)^2 \,. \tag{2.32}$$

Summing over all modes (and neglecting phase space effects) this could lead to as much as a 50% increase in Γ^{tot} for Z_2 which would then decrease the e^+e^- branching fraction (hence the production signal) by 1/3. These modes have not received much attention in the literature (see, however, ref. [2.21]).

2.4.3. $Z_2 \to W^+W^-$

This mode, if kinematically allowed, is extremely interesting in that it is very sensitive to Z–Z' mixing since in the $\phi = 0$ limit Z_2 does not couple to W^+W^-. The partial width is given by

$$\Gamma(Z_2 \to W^+W^-) = (g^2 M_2/192\pi c_w^2) \sin^2\phi \, (M_2/M_Z)^4 (1 - 4M_W^2/M_2^2)^{3/2} \times (1 + 20M_W^2/M_2^2 + 12M_W^4/M_2^4) \,, \tag{2.33}$$

and has been discussed by a large number of authors [2.22]. For large M_2, $\Gamma(Z_2 \to W^+W^-) \sim (M_2/M_Z)^4 \sin^2\phi$, but $\sin^2\phi \sim (M_Z/M_2)^4$ as well, leaving open the possibility for a reasonable branching fraction. For most models in the heavy ($\gtrsim$1 TeV) M_2 limit one finds that taking the largest allowed value of the mixing angle ϕ yields $\Gamma(Z_2 \to W^+W^-) \sim \Gamma(Z_2 \to e^+e^-)$ although for smaller values of M_2 larger rates may also occur depending on the "play-off" between the bounds on the angle ϕ and the factors appearing in eq. (2.33). For example, in model ψ with $\Delta M = 0.25$ (0.50, 1.0) GeV we find $R \equiv \Gamma(Z_2 \to W^+W^-)/\Gamma(Z_2 \to e^+e^-)$ can be as large as 1.33 (1.65, 2.15) for $M_2 = 650$ (450, 350) GeV. Similar situations can occur in other models.

For Z_2 masses below the W-pair threshold ($\simeq$163 GeV) the related process $Z_2 \to WW^* \to W\ell\bar{\nu}$ can still occur but with a small branching fraction [2.23]. This process occurs via W-boson bremsstrahlung as well as the mixing induced $Z_2W^+W^-$ coupling as shown in fig. 8. The two possible mechanisms do not interfere when E_6 model couplings are employed (since ν_L and e_L are in an isodoublet). Although this process has a small branching fraction (as shown in fig. 9 from ref. [2.23] for model η) it can be used to probe the $Z_2W^+W^-$ coupling at LEP II energies. It is important to remember that the bounds on the mixing angle ϕ are relatively poor for M_2 masses $\lesssim$163 GeV (see, e.g., figs. 1–4).

We will return to a discussion of the $Z_2W^+W^-$ coupling below in our discussion of Z_2 production signals at e^+e^- and hadron colliders.

2.4.4. $Z_2 \to$ gauginos and higgsinos

Such scenarios have generally been examined only within the rank-5 model context due to the complex structure of the mass matrices that need to be explored. For a neutralino coupling

$$\mathcal{L} = g k_{ij} \bar{\tilde{G}}_i \gamma^\mu \gamma_5 \tilde{G}_j Z_{2\mu} \tag{2.34}$$

(where $\tilde{G}_i$ is a generic higgsino or gaugino) one obtains [2.24]

$$\Gamma = (Z_2 \to \tilde{G}_i \tilde{G}_j) = \frac{g^2 M_2}{12\pi} k_{ij}^2 \left[1 - \frac{1}{2}\left(\frac{m_i^2 + m_j^2}{M_2^2}\right) - \frac{1}{2}\left(\frac{m_i^2 - m_j^2}{M_2^2}\right)^2 - \frac{3m_i m_j}{M_2^2}\right] \lambda^{1/2}(1, i, j) \,, \tag{2.35}$$

where k_{ij} are model dependent parameters of order unity and [with $(i, j) \equiv m_{i,j}^2/M_2^2$]

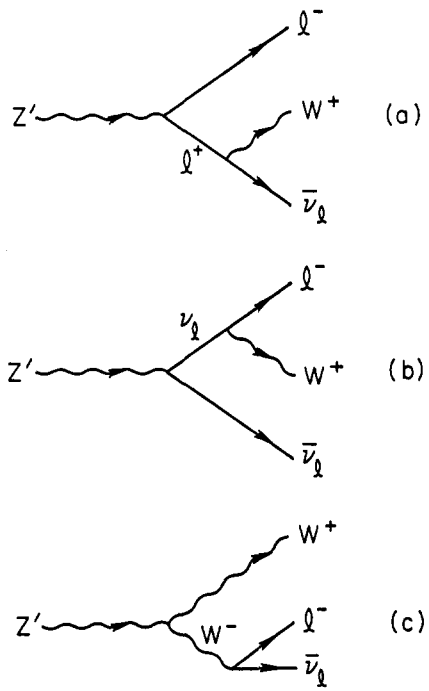

Fig. 8. Diagrams contributing to the process $Z_2 \to W\ell\bar{\nu}$.

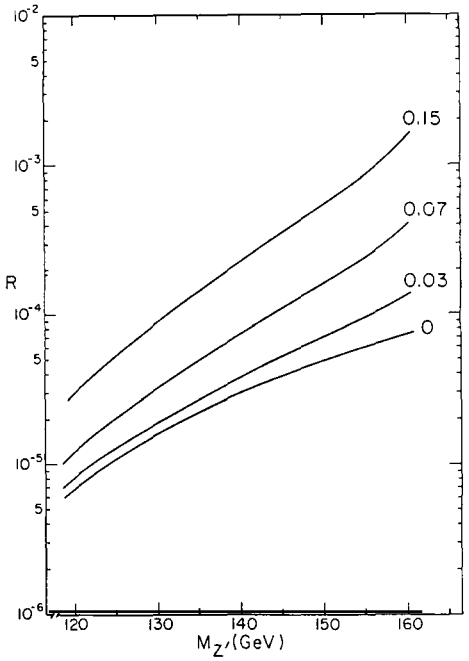

Fig. 9. Branching fraction for $Z_2 \to W\ell\bar{\nu}$ from model η as a function of $M_{Z'}$ for different values of ϕ.

$$\lambda(a, b, c) = a^2 + b^2 + c^2 - 2(ab + ac + bc) \tag{2.36}$$

is the usual triangle function. Summing over all modes (and neglecting possible phase space suppression) we see that gauginos may contribute as much as 10–20% to the total width of Z_2. These modes have mainly been studied as sources of multilepton events (and missing p_T) at hadron colliders such as the Tevatron and the SSC.

2.4.5. $Z_2 \to Z_1 H_i^0, H_i^0 H_j^0, W^{\pm} H^{\mp}$

These modes have only been studied in any detail within the framework of the rank-5 model [2.25] and in the limit of large M_2 values. The width for $Z_2 \to V + S$ (vector and scalar or pseudoscalar) is given by

$$\Gamma(Z_2 \to V + S) = \frac{f_{vs}^2 M_2}{192\pi} \lambda^{1/2}(1, v, s)[\lambda(1, v, s) + 12v], \tag{2.37}$$

where $v, s \equiv M_{v,s}^2 / M_2^2$ and f_{vs} is the coupling normalized as

$$\mathcal{L} = f_{vs} M_v Z_2^{\mu} V_{\mu} S . \tag{2.38}$$

In the rank-5 scenario, the Higgs sector in the mass eigenstate basis consists of three neutral scalar fields (H_i^0, $i = 1, 2, 3$), a neutral pseudoscalar (P^0) and a pair of charged scalars ($H^{\pm}$). In the large M_2 limit,

$M(H_3^0)$ is also large so that Z_2 decay final states involving H_3^0 are kinematically forbidden or suppressed. In the same limit (neglecting phase space corrections) one finds (over a reasonable range of parameter space)

$$\Gamma(Z_2 \to Z_1 H_1^0) = \Gamma(Z_2 \to W^+ W^-), \quad \Gamma(Z_2 \to P^0 H_2^0) = \Gamma(Z_2 \to H^+ H^-),$$
$$\Gamma(Z_2 \to Z_1 H_2^0) = \Gamma(Z_2 \to P^0 H_1^0) = \tfrac{1}{2}\Gamma(Z_2 \to W^{\pm} H^{\mp}). \tag{2.39}$$

Figure 10 shows the size of the above branching fractions as a function of $\tan\beta = v_2/v_1$ (the doublet vev's) for large M_2 with $n_g = 0$ for model η. Summing over all of the above modes one finds that their total contribution is

$$\Gamma = 34(g^2 x_w/36 \cdot 48\pi c_w^2) M_2, \tag{2.40}$$

which is of the order of a few percent of the total fermionic width when $n_g = 0$. One should expect that qualitatively similar results hold in other models as well, although since the parameter space is somewhat larger we would not expect relationships such as eq. (2.39) to remain valid. We will briefly discuss these modes as Z_2 production signals at hadron colliders below. These modes have recently been examined in the general effective rank-5 model by Deshpande and Trampetic [2.26].

2.4.6. *Loop order decays*

Rare decay modes for Z_2 induced at the one-loop level such as $Z_2 \to \gamma Z_1, 2Z_1$ have been considered [2.27] in the absence of Z–Z′ mixing (i.e., fermion loops only). The typical branching fractions for such processes are very small and probably unobservable: $\Gamma(Z_2 \to \gamma Z_1)/\Gamma(Z_2 \to e^+ e^-) \simeq 10^{-6}$ while $\Gamma(Z_2 \to 2Z_1)/\Gamma(Z_2 \to e^+ e^-) \simeq 10^{-5}$ for $M_2 \simeq 400$ GeV.

As can be seen from the above discussion, the decay modes of new Z_2 gauge bosons are quite model dependent with the fermionic modes and W^+W^- being the best understood. This problem will arise again when we discuss Z_2 production signatures below.

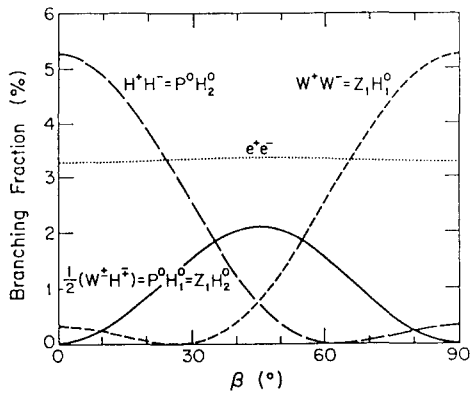

Fig. 10. Z_2 branching fractions as functions of β with $n_g = 0$ for model η.

2.5. Signals for new gauge bosons

Signals for new gauge bosons beyond those of the standard model (SM) may manifest themselves in many ways. As discussed in section 2.3, loop order processes involving Z_2 may lead to sizeable corrections to SM processes thus providing constraints on the Z_2 properties. However, in this section, we examine the signals for new gauge bosons at colliders only, since in rare processes other new particles appearing in the loops may interfere with or mask pure Z_2 contributions. Colliders certainly provide the cleanest way to search for new gauge bosons.

At colliders there are, in general, two ways to search for new gauge bosons: (i) indirect signals below production thresholds may indicate the presence of new gauge degrees of freedom and (ii) direct production. In what follows we will examine signals of both kinds at e^+e^-, ep, and $\overset{(-)}{p}p$ colliders separately and discuss how signals at the different colliders are related.

2.5.1. e^+e^- colliders

2.5.1.1. Indirect searches: asymmetries. Below the energies necessary for resonance production of Z_2 one could look for deviations away from the SM predictions in quantities such as the forward–backward asymmetry (A_{FB}) and various polarization asymmetries (such as the left–right and transverse polarization asymmetries, A_{LR} and A_ϕ respectively, to be defined below). The non-zero value of A_{FB} for muons clearly showed the existence of the SM Z long before its discovery at CERN. One could also examine the detailed properties of the Z_1 and look for small deviations from what is expected for the Z from the SM resulting from Z–Z′ mixing. Both these possibilities will be discussed in turn.

For a model with an arbitrary number of neutral gauge fields the differential cross section for the production of a pair of massless fermions ($F\bar{F}$) is given by (assuming s-channel exchange only!)

$$\frac{d\sigma}{dz} = C_F \frac{s}{32\pi} \sum_{ij} P_{ij}^{ss}[B_{ij}(1+z^2) + 2C_{ij}z], \tag{2.41}$$

where $z \equiv \cos\theta$, C_F is the usual color factor, and

$$P_{ij}^{ss} \equiv \frac{(s-M_i^2)(s-M_j^2) + (\Gamma_i M_i)(\Gamma_j M_j)}{[(s-M_i^2)^2 + (\Gamma_i M_i)^2][(s-M_j^2)^2 + (\Gamma_j M_j)^2]},$$
$$B_{ij} \equiv (v_i v_j + a_i a_j)_F (v_i v_j + a_i a_j)_e, \qquad C_{ij} \equiv (v_i a_j + a_i v_j)_F (v_i a_j + a_i v_j)_e, \tag{2.42}$$

with the couplings normalized as

$$\mathcal{L} = \sum_i [\bar{F}\gamma_\mu (v_{iF} - a_{iF}\gamma_5)F + \bar{e}\gamma_\mu (v_{ie} - a_{ie}\gamma_5)e]Z_i^\mu. \tag{2.43}$$

Here M_i (Γ_i) is the mass (width) of the ith gauge boson and $\sqrt{s}$ is the usual center of mass energy. To obtain the corresponding cross section for longitudinally polarized electrons in the initial state we make the replacements

$$v_{ie} \to V_{ie} = \tfrac{1}{2}(v_{ie} + \lambda a_{ie}), \qquad a_{ie} \to A_{ie} = \tfrac{1}{2}(a_{ie} + \lambda v_{ie}), \tag{2.44}$$

with $\lambda = +1\,(-1)$ corresponding to left (right) handed electrons. We now can form the asymmetries A_{FB} and $A_{LR}(z)$,

$$A_{FB} \equiv \frac{\int_0^1 (d\sigma/dz)\,dz - \int_{-1}^0 (d\sigma/dz)\,dz}{\int_{-1}^1 (d\sigma/dz)\,dz}\,, \qquad A_{LR}(z) \equiv \frac{d\sigma_L(z) - d\sigma_R(z)}{d\sigma_L(z) + d\sigma_R(z)}\,. \tag{2.45}$$

In what follows we will concentrate on $A_{LR}(z)$ at $\theta = 90°$, i.e., $A_{LR} = A_{LR}(0)$. Writing

$$G_{ij} = (v_i v_j + a_i a_j)_F (v_i v_j - a_i a_j)_e\,, \tag{2.46}$$

the azimuthally dependent (but θ integrated) cross section for $e^+e^- \to F\bar{F}$ for transversely polarized e^+e^- beams is

$$\frac{d\sigma}{d\phi} = \frac{s}{48\pi^2} \sum_{ij} P_{ij}^{ss} [2B_{ij} + (p_T)^2 G_{ij} \cos 2\phi]\,, \tag{2.47}$$

where p_T is the amount of e^+e^- beam polarization. The azimuthal asymmetry is defined as

$$A_\phi \equiv \left[\int^+ \left(\frac{d\sigma}{d\phi}\right) d\phi - \int^- \left(\frac{d\sigma}{d\phi}\right) d\phi\right] \sigma^{-1}\,, \tag{2.48}$$

where $\int^\pm$ implies integration over regions where $\cos 2\phi$ is positive or negative, respectively, and σ is the total cross section.

A large number of authors have examined these asymmetries to see how a Z′ would alter SM expectations, particularly for the process $e^+e^- \to \mu^+\mu^-$ [2.28–2.30]. The results of these calculations are shown in fig. 11 from ref. [2.29] and figs. 12 and 13 from ref. [2.30]. It is clear that significant deviations from the SM do not occur until one is outside the SLC and LEP I energy ranges (i.e., $\sqrt{s} \gtrsim$ 100–120 GeV) even for a relatively light ($\simeq$ 150 GeV) Z_2 so that indirect signals for the existence of a Z′ will not be easily obtainable unless very accurate measurements are made. Such analyses can also be extended for future planned colliders; see the appendix for further discussion of this possibility.

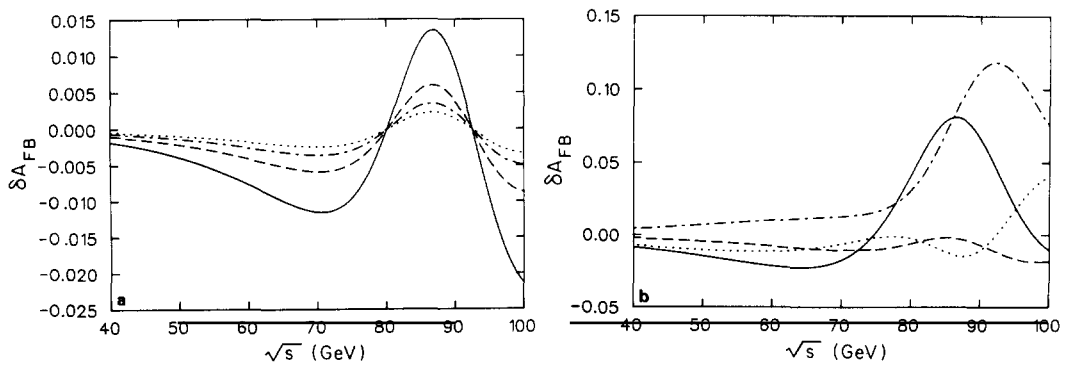

Fig. 11. Shift in A_{FB} (δA_{FB}) as a function of $\sqrt{s}$ for different E_6 models. (a) For model η with $\phi = 0$. The solid line is for $M_2 = 150$ GeV, the dashed line is for $M_2 = 200$ GeV, the dot-dashed line is for $M_2 = 250$ GeV and the dotted line is for $M_2 = 300$ GeV. (b) The solid line is for model χ with $M_2 = 260$ GeV and $\phi = -0.08$, the dot-dashed line is for model η with $M_2 = 120$ GeV and $\phi = -0.25$, the dashed line is for model η with $M_2 = 200$ GeV and $\phi = 0.04$ and the dotted line is for model ψ with $M_2 = 140$ GeV and $\phi = 0.06$.

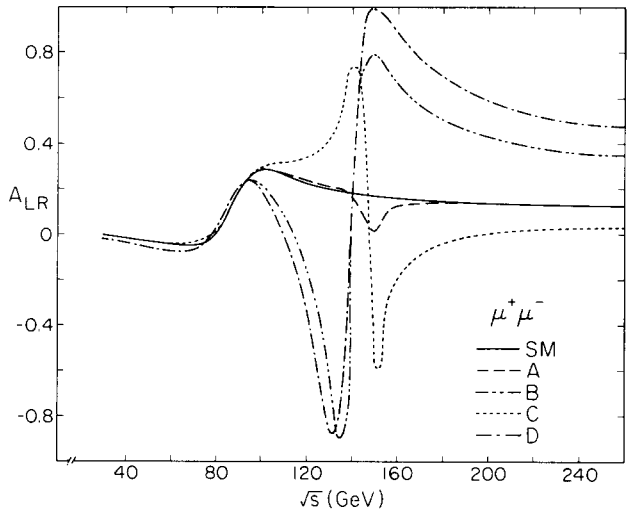

Fig. 12. A_{LR} as a function of $\sqrt{s}$ for models ψ (A), χ (B), η (C) and I (D) with $M_2 = 150$ GeV and $\phi = 0$.

Instead of purely s-channel processes such as $e^+e^- \to \mu^+\mu^-$, several groups have considered modifications in Bhabha and Møller scattering due to the existence of a Z′ [2.28–2.30]. For these reactions the differential cross sections are given by

$$\frac{d\sigma^B}{dz} = \frac{s}{32\pi}\sum_{ij}\{P_{ij}^{ss}[B_{ij}(1+z^2)+2C_{ij}z]+2P_{ij}^{tt}[B_{ij}(1+\tfrac{1}{4}(1+z)^2)-C_{ij}(1-\tfrac{1}{4}(1+z)^2)]$$
$$+P_{ij}^{st}(1+z)^2(B_{ij}+C_{ij})\},$$
$$\frac{d\sigma^M}{dz} = \frac{s}{32\pi}\sum_{ij}\{P_{ij}^{uu}[B_{ij}(1+\tfrac{1}{4}(1-z)^2)-C_{ij}(1-\tfrac{1}{4}(1-z)^2)] \tag{2.49}$$
$$+P_{ij}^{tt}[B_{ij}(1+\tfrac{1}{4}(1+z)^2)-C_{ij}(1-\tfrac{1}{4}(1+z)^2)]+2P_{ij}^{tu}(B_{ij}+C_{ij})\},$$

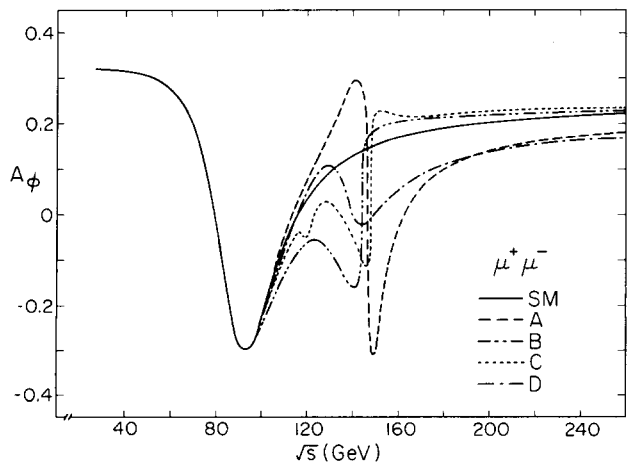

Fig. 13. Same as fig. 12 but for A_ϕ.

with $u, t = -\frac{1}{2}s(1 \pm z)$ and $P_{ij}^{tt}, P_{ij}^{tu}, \ldots$ can be obtained from P_{ij}^{ss} by substituting t and/or u for s as appropriate. For both Bhabha and Møller scattering one can form, e.g., the left–right asymmetry A_{LR} using the above prescription (2.44). The results of these calculations are shown in figs. 14 and 15 from ref. [2.30]. Clearly, with precise measurements it may be possible to see Z_2 signals for center of mass energies as much as 50–100 GeV below the Z_2 resonance depending on the couplings of the particular model. From the figures it appears that models χ and η produce the largest deviations from the SM.

2.5.1.2. Indirect searches: Z–Z′ mixing effects. We now turn our attention to the effects of Z–Z′ mixing on the properties of the SM Z. In addition to small mass shifts, the mixing of the Z and Z′ produces modifications in the couplings of the SM Z. In particular, one can look for changes in the SM Z total width, branching fractions and the values of the various asymmetries defined above on resonance. These possibilities have been considered by a number of authors for a wide spectrum of effective rank-5 models [2.31, 2.32]. Assuming $m_t \geq 46$ GeV (i.e. $M_Z/2$) in agreement with recent results from UA1 [2.33] and taking $n_g = 0$, fig. 16 shows the total width, Γ_Z, as a function of the mixing angle ϕ for the four generic effective rank-5 models discussed above. Note that the full range of ϕ shown may not be allowed for all of the models. It is clear from the figure that even a 1% change in Γ_Z requires values of ϕ which are substantially large so it is unlikely that Γ_Z will be a probe of Z–Z′ mixing.

In examining the influence of mixing on the various branching fractions one sees that, for the limited range of ϕ allowed by existing data, the $\nu\bar{\nu}$ and $\ell^+\ell^-$ modes are not very sensitive to $\phi \neq 0$ (see fig. 17 for the special cases of models χ and η). The most sensitive probes of mixing by this technique would be to measure the decay rates for $Z \to c\bar{c}$ and $b\bar{b}$ since such final states can be tagged, have stronger ϕ-dependent branching fractions, and yield higher event rates. However, even for model η (which has a relatively large allowed range for ϕ as well as particularly sensitive $c\bar{c}$ and $b\bar{b}$ branching fractions) one would still need $\phi \simeq -0.10$ to observe a $\simeq$10% decrease (increase) in the $c\bar{c}$ ($b\bar{b}$) decay rate. This would imply that the Z_2 in this model would have to be relatively light ($\lesssim$150 GeV or so), otherwise

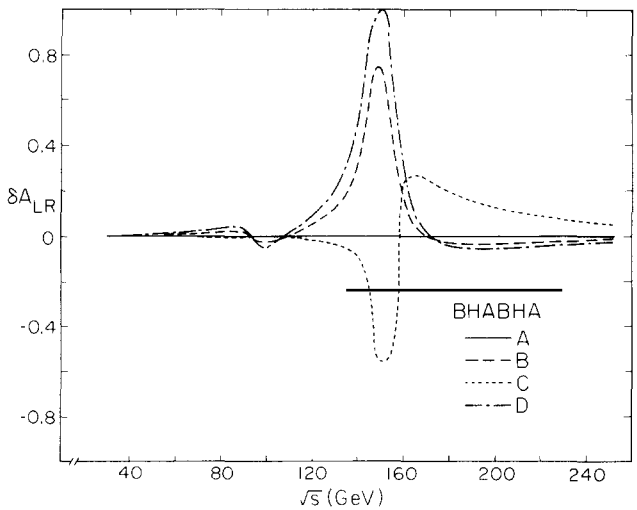

Fig. 14. Shift in A_{LR} (δA_{LR}) for Bhabha scattering as a function of $\sqrt{s}$ for models ψ (A), χ (B), η (c) and I (D) with $M_2 = 150$ GeV and $\phi = 0$.

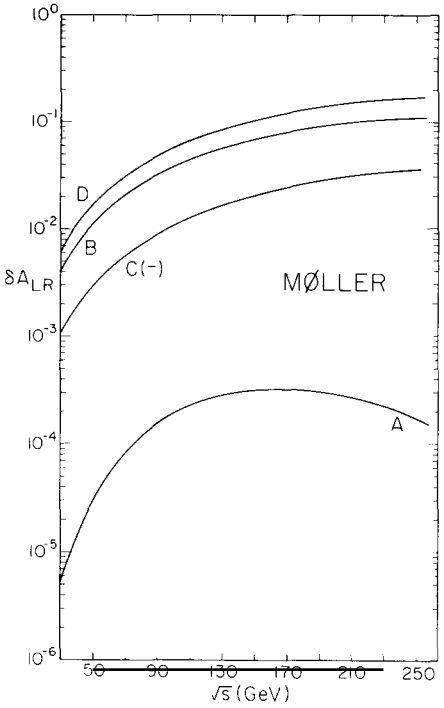

Fig. 15. Same as fig. 14 but for Møller scattering. For model η, $-\delta A_{LR}$ has been plotted.

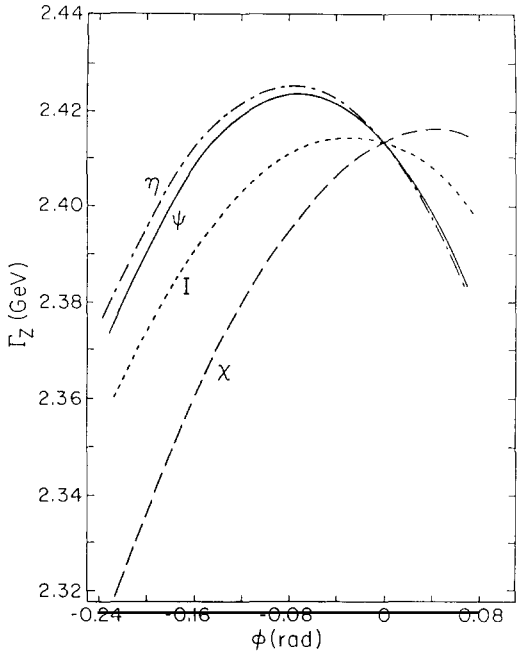

Fig. 16. Γ_Z as a function of the Z–Z′ mixing angle ϕ for models ψ, χ, η and I.

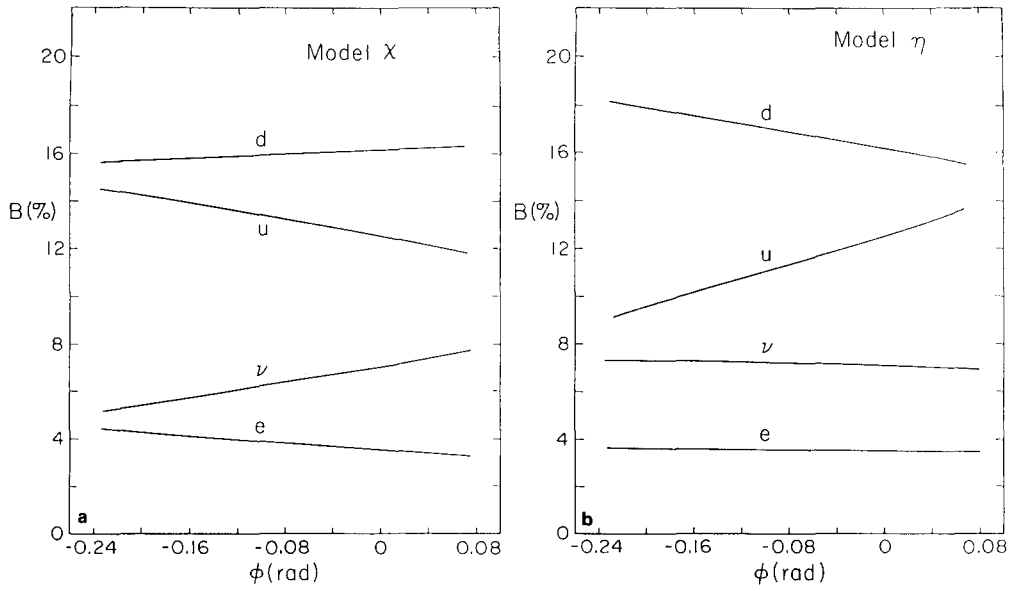

Fig. 17. Changes in the Z_1 branching fractions as a function of ϕ (a) for model χ and (b) for model η.

$\Delta M > 1$ GeV. This would be close to the present bounds on M_2 in this model from the direct searches by UA1 and UA2. Thus unless ϕ is reasonably large and Z_2 is light (in which case it would have already been seen by this time at the Tevatron) measuring changes in the Z branching fractions due to mixing will probably not yield any new evidence of the Z_2.

It is by now clear that the best way to look for the influence of Z–Z′ mixing by sitting on the Z pole is to measure various asymmetries, in particular, A_{FB}, A_{LR}, and A_ϕ. The expressions for these quantities simplify greatly on resonance and yield, for $e^+e^- \to Z \to \mu^+\mu^-$ (assuming e–μ universality)

$$A_{FB} = 3v_e^2 a_e^2/(v_e^2 + a_e^2)^2\,, \quad A_{LR} = 2v_e a_e/(v_e^2 + a_e^2)\,, \quad A_\phi = (1/\pi)(v_e^2 - a_e^2)/(v_e^2 + a_e^2)\,, \tag{2.50}$$

where v_e and a_e are the vector and axial vector couplings of the electron to Z_1. Since in the SM, $v_e \sim -\frac{1}{2} + 2x_w$ for x_w near 0.25 the value of v_e will be very sensitive to non-zero mixing between Z and Z′. Clearly then the forward–backward and left–right asymmetries will be far more sensitive to $\phi \neq 0$ than the azimuthal asymmetry. Figures 18a, b show A_{FB} and A_{LR} for the four models χ, ψ, η, and I as functions of ϕ. (Over this same range of ϕ, A_ϕ is found to vary by at most 5% which will be impossible to measure.) We see that A_{FB} can change from its SM value by as much as 50% even for values of $|\phi|$ as small as 0.03, except for the case of model ψ. In this model, the electron coupling to the Z′ is purely axial-vector that mixing leaves the value of v_e unaltered. The slight ϕ dependence in this case only enters through a modification of a_e. A_{LR} also shows a reasonably strong ϕ dependence, but since it is only linearly dependent on v_e the ϕ dependence is weaker than that for A_{FB}. Except for model ψ (for the reasons discussed above) substantial deviation from the SM prediction of A_{LR} is evident but much larger values of $|\phi|$ are necessary. Deviations from the SM of order ≃50% only occur for values of

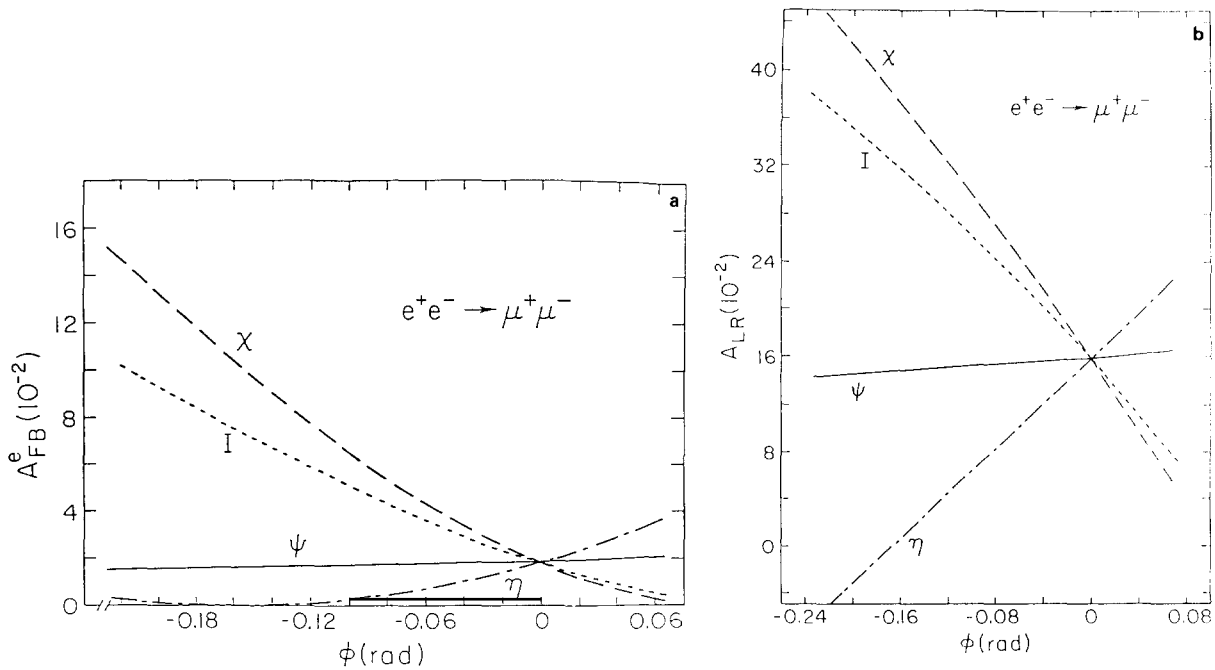

Fig. 18. (a) A^e_{FB} and (b) A_{LR} with $\sqrt{s} = M_{Z_1}$ for $e^+e^- \to \mu^+\mu^-$ for models ψ, χ, η, and I as functions of the Z–Z′ mixing angle ϕ.

$|\phi| \simeq 0.08$, thus far more sensitive measurements of A_{LR} will be necessary to probe small values of $|\phi| \lesssim 0.03$.

For both A_{FB} and A_{LR}, one must be careful to take into account radiative corrections to the SM predictions before one can actually claim deviations between experimental results and theoretical expectations. The radiative corrections to A_{FB} and A_{LR} are found to be substantial in the SM.

2.5.1.3. Indirect searches: neutrino counting. Three groups have considered the influence of additional neutral gauge bosons on attempts at neutrino counting in e^+e^- annihilation via $e^+e^- \to \nu\bar{\nu}\gamma$ [2.34]. The differential cross section for this process is ($x \equiv 2E_\gamma/\sqrt{s}$)

$$\frac{d\sigma}{dx} = \frac{2\alpha}{\pi} x^{-1}\left[[(1-\tfrac{1}{2}x)^2 + (\tfrac{1}{2}x)^2]\ln\left(\frac{1+\delta}{1-\delta}\right) - 2\delta(\tfrac{1}{2}x)^2\right]\sigma_M^{\nu\bar{\nu}}(x)\,, \tag{2.51}$$

where $\delta \equiv \cos\theta_{min}$ (θ_{min} being the minimum angle between e^- and γ allowed by the experimental cuts). With the couplings normalized as

$$\mathcal{L} = g\sum_i [C_i \bar{\nu}\gamma_\mu(1-\gamma_5)\nu + \bar{e}\gamma_\mu(v_i - a_i\gamma_5)e]Z_i^\mu\,, \tag{2.52}$$

and with $M^2 = s(1-x)$, $\sigma_M^{\nu\bar{\nu}}(x)$ is given by

$$\sigma_M^{\nu\bar{\nu}}(x) = \frac{G_F^2 M^2}{6\pi}\left(1 - \frac{\sqrt{2}g^2}{G_F}\sum_i \frac{C_i(v_i+a_i)(M^2-M_i^2)}{(M^2-M_i^2)^2 + (\Gamma_i M_i)^2}\right.$$
$$\left. + N_\nu \frac{g^4}{G_F^2}\sum_{ij} C_i C_j (v_i v_j + a_i a_j) P_{ij}^{ss}(s \to M^2)\right)\,, \tag{2.53}$$

where P_{ij}^{ss} is defined via eq. (2.42). To compare with experimental results, photon energy cuts ($E_\gamma \gtrsim 1$ GeV) need to be applied when integrating (2.51). Clearly if $\sqrt{s}$ is close to M_Z, the effect of new Z's is minimal and if $\sqrt{s}$ is small, weak interaction effects (such as this process) are again small. At $\sqrt{s} = 30$ GeV (corresponding to the PEP energy range) the effective additional number of neutrinos (ΔN_ν), in comparison to SM predictions, that one might measure from Z_2 exchange could be as large as $\simeq 0.4$. As $\sqrt{s}$ is increased through the PETRA and TRISTAN energy ranges the maximum value of ΔN_ν due to a new Z_2 drops significantly ($\lesssim 0.1$ for $\sqrt{s} = 60$ GeV). That this effect is small should not be surprising since $e^+e^- \to \nu\bar{\nu}$ is just the crossed process for $\nu e \to \nu e$ which has been used in the above NC analysis to constrain M_2 and ϕ. These results for $\sqrt{s} = 30$ GeV are best summarized by fig. 19 from Barger et al. [2.34].

2.5.1.4. Indirect searches: $e^+e^- \to W^+W^-$. The existence of new gauge bosons may significantly modify this process even below the Z_2 threshold since it is remarkably sensitive to small modifications in the various couplings (for a review of the couplings involved in the $e^+e^- \to W^+W^-$ process and how they can be probed at LEP II, see ref. [2.35]). In particular, since Z_2 only participates via Z–Z′ mixing, this process can be used as a sensitive probe of non-zero ϕ. The cross section for $e^+e^- \to W^+W^-$ in a general gauge model with an arbitrary number of neutral bosons is given by [$\beta \equiv (1 - 4M_W^2/s)^{1/2}$] [2.36]

$$\frac{d\sigma}{dz} = \frac{G_F^2 M_W^4}{8\pi s}\beta\left(\bar{\sigma}_{\nu\nu} + \bar{\sigma}_{\gamma\gamma} + \bar{\sigma}_{\gamma\nu} + \sum_i(\bar{\sigma}_{\gamma i} + \bar{\sigma}_{\nu i}) + \sum_{ij}\bar{\sigma}_{ij}\right)\,. \tag{2.54}$$

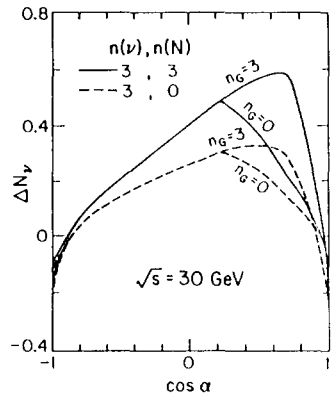

Fig. 19. ΔN_ν at $\sqrt{s} = 30$ GeV as a function of cos α (i.e. cos θ) for Z_2's with minimum allowed masses for $n_g = 0$ or 3 with or without contributions from right-handed neutrinos (N).

With the couplings normalized as

$$\mathcal{L} = \frac{g}{2c_w} \sum_i \bar{e}\gamma_\mu (v_i - a_i\gamma_5) e Z_i^\mu \,, \tag{2.55}$$

we find

$$\begin{aligned} &\bar{\sigma}_{\nu\nu} = F_1(z,s)\,, \qquad \bar{\sigma}_{\gamma\gamma} = x_w^2 F_2(z,s)\,, \qquad \bar{\sigma}_{\gamma\nu} = -x_w F_3(z,s)\,, \\ &\bar{\sigma}_{\gamma i} = x_w v_i R_i F_2(z,s)\,, \qquad \bar{\sigma}_{\nu i} = l_i R_i F_3(z,s)\,, \qquad \bar{\sigma}_{ij} = \tfrac{1}{4}(v_i v_j + a_i a_j) P_{ij}^{ss} F_2(z,s)\,, \end{aligned} \tag{2.56}$$

where $l_i = 1/2(v_i + a_i)$, P_{ij}^{ss} is defined above in eq. (2.42) and

$$R_i \equiv s(s - M_i^2)/[(s - M_i^2)^2 + (\Gamma_i M_i)^2]\,. \tag{2.57}$$

The functions $F_i(z, s)$ are given in ref. [2.37]. For $M_2 > \sqrt{s}$ one would expect that most of the deviation in the cross section occurs in the backward direction (i.e., $z < 0$) due to the dominance of the t-channel ν exchange diagram (and the corresponding t-channel pole). Figures 20a–d from ref. [2.36] show the deviations in the W^+W^- production cross section due to Z_2 for $\sqrt{s}$ values below the Z_2 resonance peak. Qualitatively, the various models (η, ψ, χ, and I) show very similar deviations with increasing $\sqrt{s}$ and mostly in the negative z region for fixed $\sqrt{s}$ as expected. Since the W-pair cross section at this energy is quite large ($\simeq$17 pb at $\sqrt{s} = 200$ GeV), implying very little background from other processes, it should be possible to make accurate cross section measurements as well as reliable determinations of the $W^\pm$ directions in order to determine the $W^\pm$ angular distributions [2.35].

2.5.1.5. Direct searches. Once a Z_2 resonance is found at an e^+e^- collider, by sitting on-resonance [2.22, 2.28, 2.31, 2.32, 2.38] one can measure the usual properties such as its width and leptonic branching fraction. Using polarized beams, the left–right asymmetry A_{LR} as well as the more conventional forward–backward asymmetry A_{FB} for $Z_2 \to \ell^+\ell^-$ can be determined. Combining these measurements with existing limits (and any improvements that are made by the time of the possible Z_2

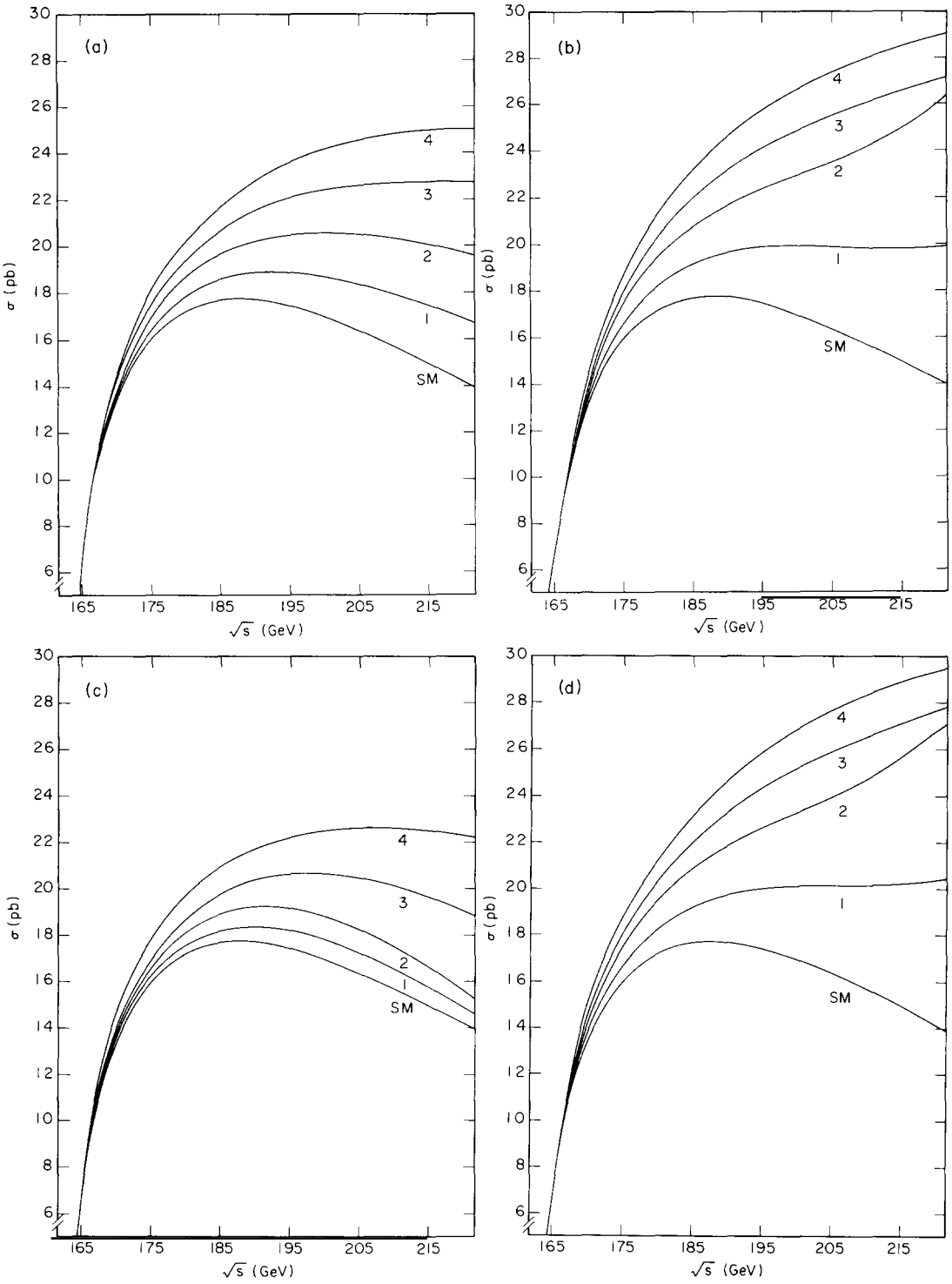

Fig. 20. Total cross sections for $e^+e^- \to W^+W^-$ in (a) model ψ, (b) model χ, (c) model η and (d) model I in comparison to the SM predictions. Curves labelled 1–4 correspond to different values of M_2 and ϕ. (1) $M_2 = 250$ GeV, $\phi = 0.025$; (2) $M_2 = 250$ GeV, $\phi = 0.05$; (3) $M_2 = 300$ GeV, $\phi = 0.075$ and (4) $M_2 = 500$ GeV, $\phi = 0.10$.

discovery) one should be able to determine the relevant values of θ and ϕ for this Z_2 (if any apply!). An interesting possibility would be that none of these models match the Z_2 observed in e^+e^- annihilation (and presumably at the Tevatron as well). This would not rule out E_6 as the origin of the Z_2 since this new gauge boson could arise from a new SU(2) factor (to be discussed below) or from a rank-6 model that does not look like an effective rank-5 model in the sense that it is not describable in terms of only three parameters: M_2, θ and ϕ (the rank-6 model could also involve another mass, M_3, and at least one further mixing parameter θ').

If $M_2 > 2M_W$ and/or $M_1 + M_H$ then the reactions $e^+e^- \to W^+W^-$ [2.22, 2.36] and Z_1H are substantially modified near the Z_2 resonance. In the case of W^+W^-, not only is there a substantial change in the total cross section but the W^+W^- angular distribution is substantially modified. The reason for this is easy to see; conventionally $e^+e^- \to W^+W^-$ is dominated by the t-channel ν exchange diagram, which results in a forward peaking of the $e^+e^- \to W^+W^-$ cross section away from the Z_2 resonance. On the Z_2 resonance, however, there is a substantially large additional contribution in the s-channel (controlled by the amount of Z–Z′ mixing) which causes a flattening of the W^+W^- angular distribution. Figure 21, from Kalyniak and Sundaresan [2.22], shows the modification of the W-pair total cross section as a function of $\sqrt{s}$ due to the Z_2 while fig. 22 from ref. [2.38] shows $d\sigma/d\cos\theta$ for $\sqrt{s} = M_2 = 200$ GeV for different values of ϕ. These figures indicate the behavior that is expected from the arguments made above.

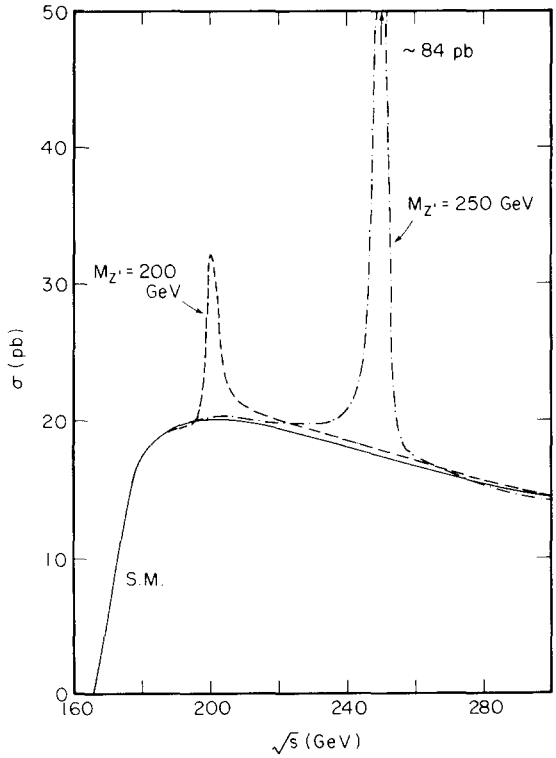

Fig. 21. $e^+e^- \to W^+W^-$ cross section versus $\sqrt{s}$ in model η. The solid line is the SM prediction, whereas the dashed curve is for $M_{Z'} = 200$ GeV and $\phi = 0.05$ and the dot–dashed curve is for $M_{Z'} = 250$ GeV with $\phi = 0.05$.

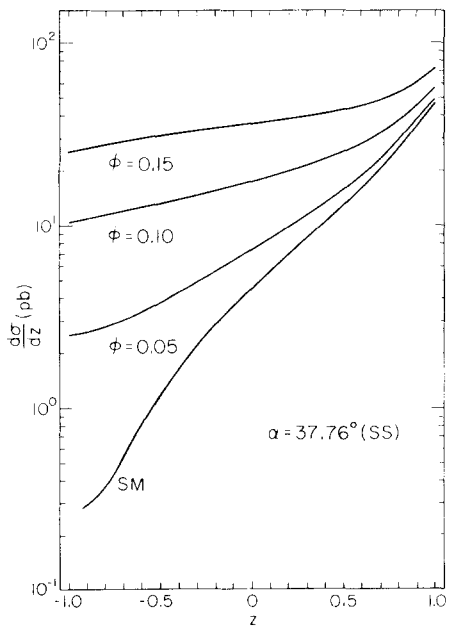

Fig. 22. Angular distribution ($d\sigma/d\cos\theta$) for $e^+e^- \to W^+W^-$ for different values of ϕ in model η ($\alpha = \theta = 37.76°$).

2.5.2. ep colliders

The effects of new Z′ gauge bosons may be indirectly observed at ep colliders. A number of authors have considered this possibility at HERA energies ($\sqrt{s} \simeq 314$ GeV) [2.39] and at a possible LEP × LHC collider ($\sqrt{s} \simeq 1.4$ TeV). Direct production and detection of a Z′ in the process $ep \to eZ'X$ seems to be very difficult even for a lighter mass Z′. This is easy to see since the production of the SM Z via the reaction $ep \to eZX$ is already small [2.40] and since the Z′ would be more weakly coupled and be more phase-space suppressed than the usual SM Z. Therefore, in ep collisions, the best way to look for a Z′ is by its indirect effects, i.e., modifications of the usual $e^{\pm}p \to e^{\pm}X$ neutral current reaction. Cross section measurements themselves are not very sensitive to Z′ exchange in the t-channel because of the large contribution from photon exchange and the weak Z′ couplings. The most sensitive tests for the existence of Z′ seem to be provided by measurements of various asymmetries one can form if polarized $e^{\pm}$ beams are available.

Writing the mass-eigenstate couplings of the fermions to the Z_i as

$$\mathscr{L} = \frac{e}{\sin\theta_w \cos\theta_w} \sum_i \sum_f \bar{f}\gamma^\mu (v_{if} - a_{if}\gamma_5) f Z_{i\mu} , \tag{2.58}$$

the inclusive differential cross section for incident $e^-_{L,R}$ is as follows:

$$\frac{d^2\sigma(e^-_{L,R})}{dx\,dy} = \frac{2\pi\alpha^2}{sx^2y^2}\left[(1+(1-y)^2)F_2^{L,R} + (1-(1-y)^2)xF_3^{L,R}\right], \tag{2.59}$$

where $x \equiv Q^2/2p\cdot q$, $y \equiv p\cdot q/p\cdot k$, $Q^2 = sxy$ [in these definitions $p(k)$ is the initial proton (electron) four-momentum and q is the momentum transfer: $q^2 = -Q^2$], and

$$F_2^{L,R} = \sum_q [xq(x,Q^2) + x\bar{q}(x,Q^2)]\tilde{F}_{2q}^{L,R}(Q^2), \qquad xF_3^{L,R} = \sum_q [xq(x,Q^2) - x\bar{q}(x,Q^2)]\tilde{F}_{3q}^{L,R}(Q^2). \tag{2.60}$$

Here $q(x,Q^2)$ and $\bar{q}(x,Q^2)$ are the relevant quark and anti-quark distribution functions of the proton and for the case of two Z bosons,

$$\begin{aligned}\tilde{F}_{2q}^{L,R}(Q^2) &= Q_q^2 + \sum_{i=1}^{2}\left[(v_{ie}\pm a_{ie})^2(v_{iq}^2 + a_{iq}^2)P_i^2 - 2Q_q(v_{ie}\pm a_{ie})v_{iq}P_i\right] \\ &\quad + 2(v_{ie}\pm a_{ie})(v_{2e}\pm a_{2e})(v_{1q}v_{2q} + a_{1q}a_{2q})P_1P_2 , \\ \tilde{F}_{3q}^{L,R}(Q^2) &= \pm 2\Big(\sum_{i=1}^{2}\left[(v_{ie}\pm a_{ie})^2 v_{iq}a_{iq}P_i^2 - Q_q(v_{ie}\pm a_{ie})a_{iq}P_i\right] \\ &\quad + (v_{ie}\pm a_{ie})(v_{2e}\pm a_{2e})(v_{1q}a_{2q} + v_{2q}a_{1q})P_1P_2\Big) ,\end{aligned} \tag{2.61}$$

$$P_i \equiv \frac{1}{x_w(1-x_w)}\,\frac{Q^2}{Q^2+M_i^2} . \tag{2.62}$$

The corresponding expressions for $e^+_{L,R}p$ scattering are obtainable from the above with the replacement $F_2^{R,L} \to F_2^{R,L}$, $F_3^{L,R} \to -F_3^{L,R}$. The expressions given above are easily generalized to the situation of an arbitrary number of neutral gauge bosons.

From the above cross section expressions one can form six asymmetries of the type

$$A(e_1\text{–}e_2) \equiv [d\sigma(e_1) - d\sigma(e_2)]/[d\sigma(e_1) + d\sigma(e_2)]\,, \tag{2.63}$$

with $e_{1,2} = e^{\pm}_{L,R}$. There are polarization asymmetries, $A(e^{\pm}_L\text{–}e^{\pm}_R)$, charge asymmetries, $A(e^{-}_{L,R}\text{–}e^{+}_{L,R})$, and mixed asymmetries, $A(e^{-}_L\text{–}e^{+}_R)$ and $A(e^{-}_R\text{–}e^{+}_L)$. Figure 23 from Capstick and Godfrey [2.39] shows the results of integrating the above asymmetries over x and y ($0.1 \le x, y \le 1$) and subtracting off the SM result for different values of the angle θ with $\phi = 0$. Figure 24 from the same reference shows the region probed in the M_2–θ plane (with $\phi = 0$) by ep asymmetry measurements in comparison with existing data and new measurements which can be performed at TRISTAN and LEP/SLC. (Note the difference between the value of θ used in these figures and that used in this paper.) Clearly, for certain ranges of the angle θ, ep asymmetry measurements at HERA will be able to probe larger values of M_2. Figure 25 from Cornet and Rückl [2.39] displays the limits one can set on M_2 as a function of ϕ (θ in the figure) for two models (corresponding to our η and χ) assuming a sensitivity of $\delta A = 0.02$ in the asymmetry measurements with $Q^2 \ge 6 \times 10^4$ GeV^2 at a $\sqrt{s} = 1.4$ TeV ep collider assuming an integrated luminosity of 1 pb^{-1} shared equally among $e^{\pm}_{L,R}$ initial states. These are substantially better than one can do at HERA or at LEP/SLC (but, of course, inferior to new e^+e^- or hadron colliders).

2.5.3. *Hadron colliders*

A very large number of authors have considered the production of a new neutral gauge boson at pp and $\bar{p}p$ colliders with its subsequent decay to lepton pairs ($\ell^+\ell^-$) [2.41]. This is clearly the most important though not the only production signal possible for new Z's as we will see below. The relevant quantity to examine is $\sigma \cdot B$: the production cross section times branching fraction of Z_2 into lepton

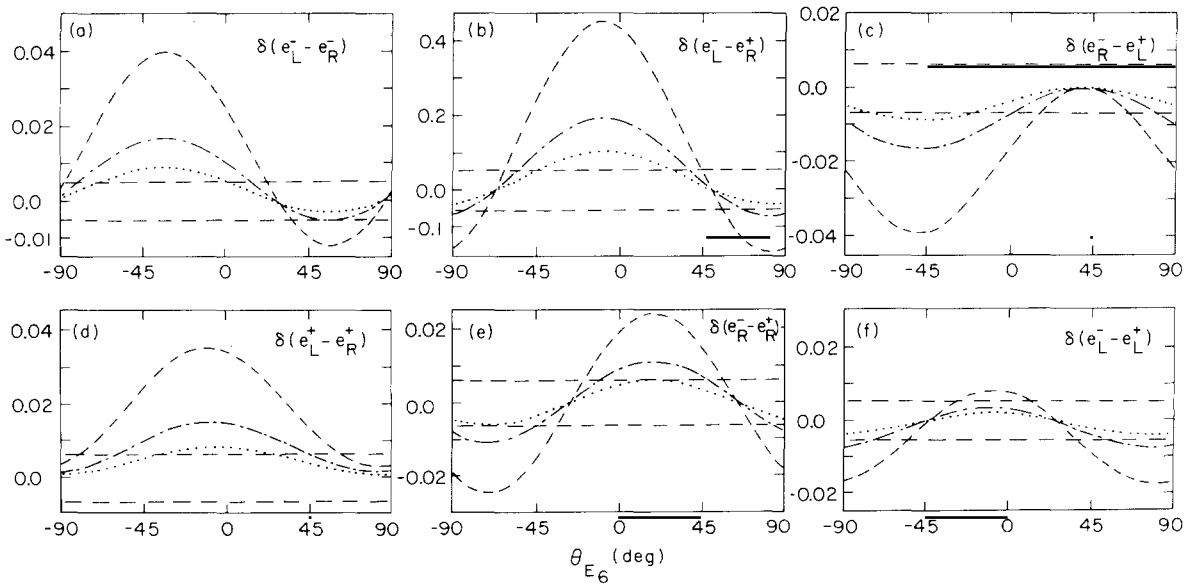

Fig. 23. Deviations from the SM for various ep asymmetries as functions of θ_{E_6} ($= -\theta$) with $\phi = 0$ and $s = 64\,000$ GeV^2 found by integrating $d\sigma/dx\,dy$ over the ranges $0.1 \le x, y \le 1$. The short dashed line is for $M_2 = 150$ GeV, the dot-dashed line is for $M_2 = 250$ GeV, and the dotted line is for $M_2 = 350$ GeV. The long dashed lines represent 1 σ deviations from the SM for an integrated luminosity of 600 pb^{-1} per polarization.

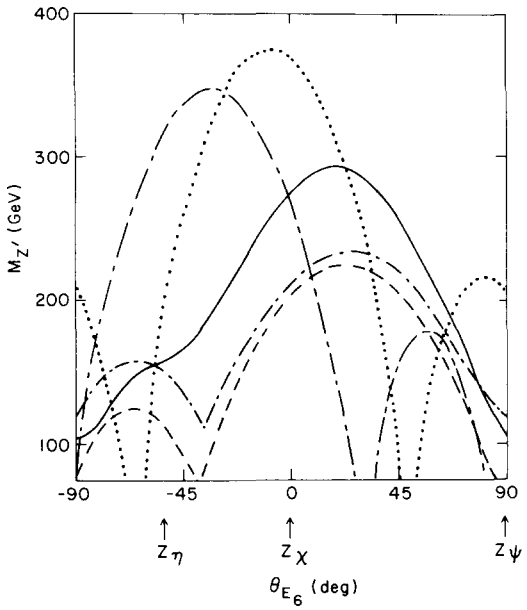

Fig. 24. 95% confidence level bounds on M_2 with $\phi = 0$ as a function of θ_{E_6} ($= -\theta$). Solid curve: present NC data; dashed curve: region that can be probed by TRISTAN; dot–dashed curve: region that can be probed by LEP/SLC with $\sqrt{s} = 110$ GeV; the dotted curve: region that can be explored by HERA using the ep asymmetry in $\sigma(e_L^-) - \sigma(e_R^-)$ and also (the short-dashed long-dashed curve) the $\sigma(e_L^-) - \sigma(e_R^-)$ asymmetry.

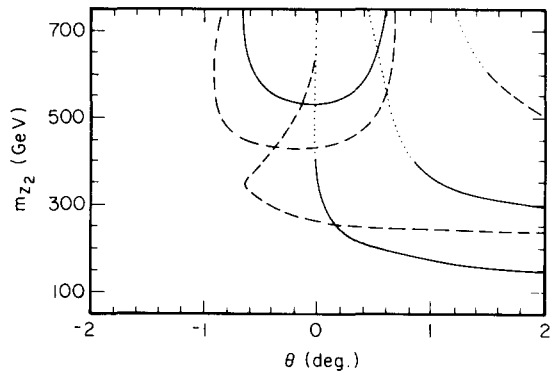

Fig. 25. Detection limits for model η (full) and model χ (dashed) expected from asymmetry measurements at a $\sqrt{s} = 1.4$ TeV ep collider with an integrated luminosity of $1\,\text{fb}^{-1}$ essentially by using $A(e_L^- - e_R^-)$. The thin full (model η) and dashed (model χ) lines show limits from Amaldi et al. Dotted lines are extrapolations assuming θ (i.e., ϕ) scales like $\sim 1/M_2$.

pairs with the model dependence (e.g., θ and ϕ dependence) entering in both quantities. Calculation of $\sigma \cdot B$ for CERN S$\bar{\text{p}}$pS collider energies and comparison with limits from UA1 and UA2 has already led to the bounds on M_2 discussed earlier. Production of Z_2's at the Tevatron, LHC, and SSC has also been calculated; fig. 26 from Barger et al. [2.41] shows $\sigma \cdot B$ as a function of the M_2 mass for both $n_g = 0$ (no exotics contributing to the Z_2 width) and $n_g = 3$ (three generations of exotics contributing fully to the Z_2 width) cases when ϕ is set to zero. With an integrated luminosity of $1\,\text{pb}^{-1}$ the Tevatron will be sensitive to Z_2 masses in the 200–250 GeV range, whereas the SSC with an integrated luminosity of $10^4\,\text{pb}^{-1}$ should be able to probe Z_2 masses as high as 5 TeV. Figure 27 from the same reference shows Z_2 production at the SSC while fig. 28 from Ellis [2.41] compares Z_2 production at the SSC and LHC. See the appendix for a further discussion of these points.

Once a Z′ is discovered at a hadron collider a measurement of the forward–backward asymmetry of the outgoing lepton pair could yield valuable information about the Z′ couplings. The parton-level differential cross section for $q\bar{q} \to \ell^+\ell^- + X$ can be written as

$$\frac{d\hat{\sigma}_q}{d\cos\theta^*} = \frac{\pi\alpha^2}{8M^2}\left[S_q(1+\cos^2\theta^*) + 2A_q\cos\theta^*\right], \tag{2.64}$$

where

$$S_q, A_q = \sum_{i,j}\left(\frac{g_i}{e}\right)^2\left(\frac{g_j}{e}\right)^2 M^4 P_{ij}^{ss}(s \to M^2)(C_{Li}^q C_{Lj}^q \pm C_{Ri}^q C_{Rj}^q)(C_{Li}^\ell C_{Lj}^\ell \pm C_{Ri}^\ell C_{Rj}^\ell), \tag{2.65}$$

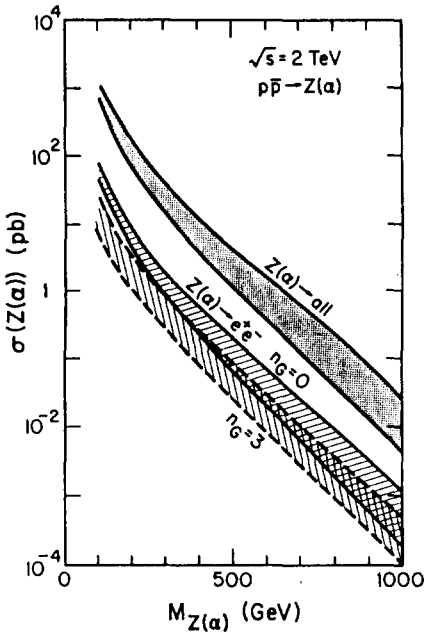

Fig. 26. $\sigma \cdot B$ for Z_2 production at the Tevatron ($\sqrt{s} = 2$ TeV) with $n_g = 0$ or 3. The shaded areas correspond to variations in θ (labeled as α in the figure).

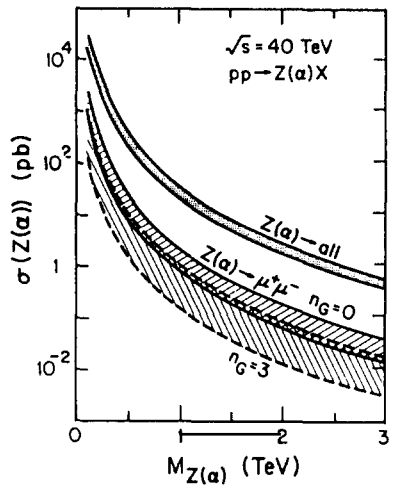

Fig. 27. Same as fig. 26 but for the SSC ($\sqrt{s} = 40$ TeV).

with P_{ij}^{ss} defined in eq. (2.42), θ^* being the $\ell^+\ell^-$ center-of-mass scattering angle, and $C_{L,R}$ are the couplings of the neutral gauge bosons to the fermions q and ℓ. Folding in distribution functions, this yields the cross section for $A + B \to \ell^+\ell^- + X$,

$$\frac{d\sigma}{dy\, dM\, d\cos\theta^*} = K \frac{2\pi\alpha^2}{3M^3} x_A x_B \sum_q [S_q G_q^+ (1 + \cos^2\theta^*) + 2A_q G_q^- \cos\theta^*] , \tag{2.66}$$

where K is a QCD correction factor,

$$G_q^{\pm} \equiv q_A(x_A)\bar{q}_B(x_B) \pm \bar{q}_A(x_A) q_B(x_B) , \tag{2.67}$$

and $x_{A,B} = (M/\sqrt{s})\, e^{\pm y}$. Integrating over θ^* with the following definition:

$$\frac{d\sigma^{\pm}}{dy\, dM} = \left(\int_0^1 \pm \int_{-1}^0 \right) d\cos\theta^* \frac{d\sigma}{dy\, dM\, d\cos\theta^*} , \tag{2.68}$$

and sitting on the Z_2 peak (integrating over dM using the narrow width approximation) one obtains

$$\begin{aligned} \frac{d\sigma^+}{dy} &= \frac{\pi^2\alpha^2 x_A x_B}{9 M_2 \Gamma_2} \left(\frac{g_2}{e}\right)^4 [(C_L^\ell)^2 + (C_R^\ell)^2] \sum_q [(C_L^q)^2 + (C_R^q)^2] G_q^+ , \\ \frac{d\sigma^-}{dy} &= \frac{\pi^2\alpha^2 x_A x_B}{12 M_2 \Gamma_2} \left(\frac{g_2}{e}\right)^4 [(C_L^\ell)^2 - (C_R^\ell)^2] \sum_q [(C_L^q)^2 - (C_R^q)^2] G_q^- , \end{aligned} \tag{2.69}$$

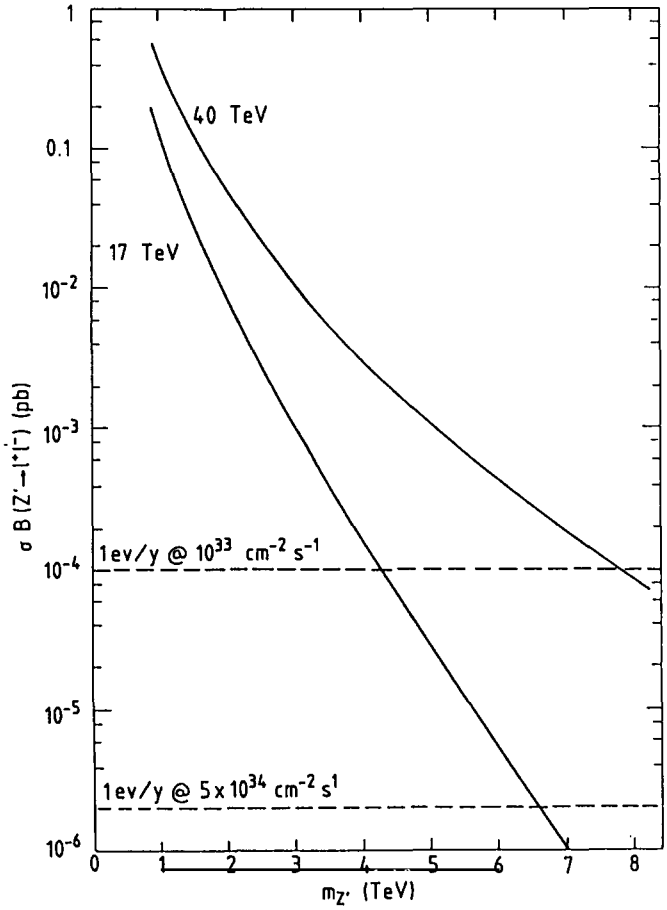

Fig. 28. A comparison of $\sigma \cdot B$ for Z_η production at the LHC and SSC for different values of M_{Z_η}.

so that, on resonance, the production cross section for lepton pairs is simply

$$\sigma = \int_{-\ln \sqrt{s}/M_2}^{\ln \sqrt{s}/M_2} \left(\frac{d\sigma^+}{dy}\right) dy \,, \tag{2.70}$$

and the forward–backward asymmetry, A_{FB}^h, is

$$A_{FB}^h = \frac{1}{\sigma}\left(\int_0^{\ln \sqrt{s}/M_2} \pm \int_{-\ln \sqrt{s}/M_2}^{0} \right)\left(\frac{d\sigma^-}{dy}\right) dy \,, \tag{2.71}$$

with the + (−) sign relevant for $\bar{p}p$ (pp) collisions. It should be noted that for three special values of θ ($\cos\theta = \sqrt{3/8}, \pm 1$) A_{FB}^h vanishes identically since for those values of θ, $(C_L^\ell)^2 - (C_R^\ell)^2$ and $(C_L^d)^2 - (C_R^d)^2 = 0$, and the u-quark, which is always coupled in an axial-vector manner to Z_2 (in the $\phi = 0$ limit), does not contribute to the sum in $d\sigma^-/dy$. Figure 29 from Barger et al. [2.41] shows the

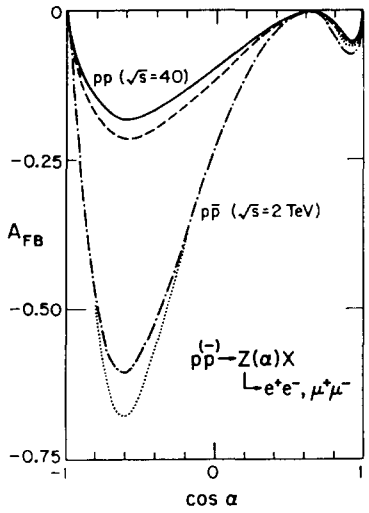

Fig. 29. A_{FB}^h for lepton pairs from Z_2 produced at the Tevatron ($\sqrt{s} = 2$ TeV) and the SSC ($\sqrt{s} = 40$ TeV) as a function of $\cos\alpha$ (i.e., $\cos\theta$). Solid curve: $M_2 = 200$ GeV; dashed curve: $M_2 = 300$ GeV; dot-dashed curve: $M_2 = 0.5$ TeV; dotted curve: $M_2 = 1$ TeV.

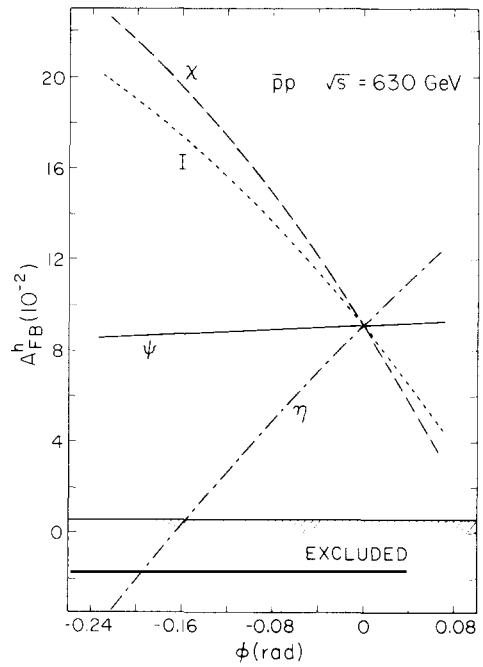

Fig. 30. A_{FB}^h for lepton pairs from Z_1 at the CERN collider for different E_6 models as functions of ϕ. The region excluded by UA1 data at 95% confidence level is shown.

prediction of A_{FB}^h for new Z's at Tevatron and SSC energies over a range of $\cos\theta$ ($\alpha = -\theta$ here!). Note that A_{FB}^h is generally quite small at SSC energies but is significant over a reasonable range of parameter space at the Tevatron.

A measurement of the A_{FB}^h for the Z_1 may also show indications of Z–Z′ mixing if sufficiently precise data were available. The current value of $A_{FB}^h = 0.30 \pm 0.15$ from the UA1 collaboration is compared in fig. 30 [2.32] to the SM value as well as models χ, ψ, η, and I with non-zero Z–Z′ mixing. The shaded area is excluded at the 95% CL limit and, if confirmed, would constrain ϕ in model η to be > -0.16. It is apparent that the other models (except for model ψ) agree with the data somewhat better than the SM, although more data is needed in order to draw any concrete conclusions.

Since at SSC energies for a wide range of θ, A_{FB}^h is quite small (due to the reasons discussed above) one could try to measure A_{FB}^h off the Z_2 peak by integrating over some bin in M. Rosner [2.42] has shown that integrating over a range of M from 50 to 250 GeV below the Z_2 mass, yields asymmetries that are statistically significant even for cases where on-resonance asymmetries (such as in models ψ and η) are small or zero. Although rates are smaller off-peak, the asymmetries are significantly enhanced over a wide range of θ due to interference with the γ and Z_1 amplitudes.

In order to probe the nature of any new Z found at a hadron collider one may also want to look for the final states from the decay $Z' \to W^+W^-$ (which can have a branching fraction similar to that for lepton pairs as discussed above). The mode which appears most promising for W^+W^- reconstruction is the lepton–jet–jet–missing p_T final state [2.43]. A judicious choice of cuts can be used to significantly reduce the QCD (i.e., W + two jets) as well as the SM W^+W^- continuum backgrounds. For a 1 TeV

Z_2, these cuts would optimistically leave ~500 signal events while the background would contain ~100 events at SSC energies with an integrated luminosity of $10^4\,\mathrm{pb}^{-1}$. A full Monte Carlo simulation may lower the ratio of signal to background down to the level of approximately one to one.

Other possible Z_2 signals discussed in the literature include like-sign dileptons from the decay of heavy Majorana neutrinos (e.g., $Z_2 \to NN^c \to \ell^\pm \ell^\pm X$) [2.44] and multilepton signals from the decay of neutralinos (e.g., $Z_2 \to \tilde{Z}_1 \tilde{Z}_1 \to \ell^+\ell^-\ell^+\ell^- + \tilde{\gamma}$). These modes may be useful in probing the nature of Z_2 decay products but not as signals for Z_2 production itself since they are relatively rare and depend on the detailed nature of the final state.

2.5.4. ve scattering

Future precision measurements of the cross section for elastic neutrino–electron scattering may yield strong new constraints on M_2 and ϕ. These processes have the particular advantage that they are free from QCD corrections as well as quark structure function uncertainties and have been discussed by two groups [2.45]. If we write

$$\mathcal{L} = \frac{g}{c_w} \sum_i C_i J^i_\mu Z^{i\mu} , \tag{2.72}$$

with

$$J^i_\mu = \sum_f (Q^i_{f_R} \bar{f}_R \gamma_\mu f_R + Q^i_{f_L} \bar{f}_L \gamma_\mu f_L) , \tag{2.73}$$

and $f_{R,L} = \frac{1}{2}(1 \pm \gamma_5) f$ we obtain the cross sections

$$\begin{aligned}
&\sigma(\nu_\mu e \to \nu_\mu e) = (2G_F^2 m_e E^\nu/\pi)(\varepsilon_-^2 + \tfrac{1}{3}\varepsilon_+^2) , \qquad \sigma(\bar{\nu}_\mu e \to \bar{\nu}_\mu e) = (2G_F^2 m_e E^\nu/\pi)(\tfrac{1}{3}\varepsilon_-^2 + \varepsilon_+^2) , \\
&\sigma(\nu_e e \to \nu_e e) = (2G_F^2 m_e E^\nu/\pi)[(\varepsilon_- - 1)^2 + \tfrac{1}{3}\varepsilon_+^2] , \\
&\sigma(\bar{\nu}_e e \to \bar{\nu}_e e) = (2G_F^2 m_e E^\nu/\pi)[\tfrac{1}{3}(\varepsilon_- - 1)^2 + \varepsilon_+^2] ,
\end{aligned} \tag{2.74}$$

where

$$\varepsilon_{+,-} = -2 \sum_i |C_i|^2 (M_Z^2/M_i^2) Q^i_{\nu_L} Q^i_{e_{R,L}} . \tag{2.75}$$

Note the additional charge-current contribution for both $\nu_e e$ and $\bar{\nu}_e e$ processes. From the review presented in Godfrey and Marciano [2.45] we see that the ratio

$$R \equiv \sigma(\nu_\mu e \to \nu_\mu e)/\sigma(\bar{\nu}_\mu e \to \bar{\nu}_\mu e) = 1.29 \pm 0.22 , \tag{2.76}$$

is relatively free of systematic uncertainties and is included in the NC data discussed in that reference. The CHARM II experiment at CERN is capable of improving the determination of R by about a factor of 4 (statistically). In addition, a newly proposed experiment at LAMPF [2.46] would measure the ratio

$$R' \equiv \sigma(\nu_\mu e \to \nu_\mu e)/[\sigma(\nu_e e \to \nu_e e) + \sigma(\bar{\nu}_\mu e \to \bar{\nu}_\mu e)] , \tag{2.77}$$

to the level of ±1.7%. If one still observed agreement with the SM prediction for these cross sections, substantially improved limits on Z_2 could be obtained. This is best displayed by fig. 31 from Godfrey

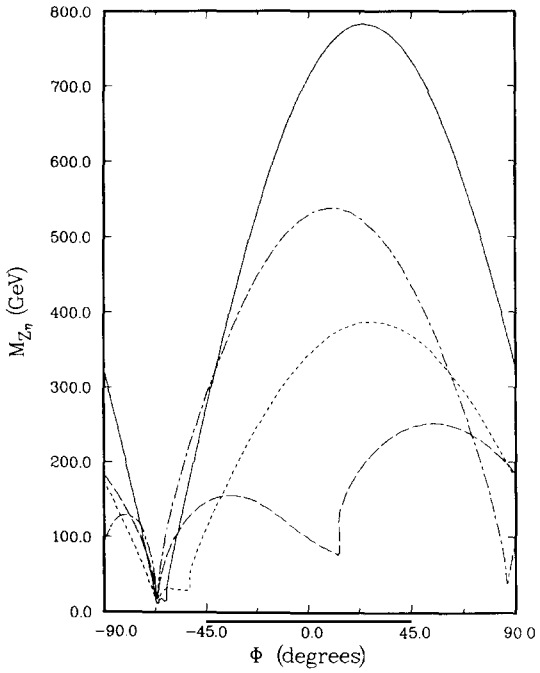

Fig. 31. Expected bounds (90% CL) on M_2 in the effective rank-5 model as a function of Φ from νe scattering. The dotted line gives the bound from a 5% measurement of $\sigma(\nu_\mu e)$, the dashed line gives the bounds from a 5% measurement of $\sigma(\bar{\nu}_\mu e)$, the dot-dashed line gives the bounds from a 2% measurement of R, and the solid line gives the bounds from a 1.7% measurement of R'. $\Phi = \theta + \pi/2$.

and Marciano [2.45], which shows the bounds on M_2 for various improved measurements of the neutrino cross sections (in the limit of zero Z–Z′ mixing). The angle Φ displayed in the figure is related to the angle θ used in our discussion above to describe $Z_{\psi,\chi}$ mixing via: $\Phi = \theta + \pi/2$. It is clear from the figure that for most values of Φ a precise measurement of R' would yield the strongest bound on the Z_2 mass. The work of London et al. [2.45] shows that the above cross sections are also quite sensitive to small amounts of Z–Z′ mixing. Clearly new ν_e, ν_μ data will be able to put rather stringent bounds on ϕ and M_2 for a wide range of the parameter θ over a range of masses comparable to that which can be probed by the Tevatron.

2.5.5. *Search limit summary*

In comparing the discovery limits for new neutral gauge bosons at existing and planned accelerators one finds a few surprises [2.47]. By the early 1990's new data from high precision neutral current experiments (e.g. $\overset{(-)}{\nu}_\mu e$ elastic scattering) and data from existing colliders (HERA, SLC, LEP I and LEP II, as well as the Tevatron) will be probing similar Z_2 mass scales of order 400–500 GeV. Different machines using various techniques (e.g., asymmetry measurements) will probe some regions in θ and ϕ space better than others, of course. To push Z_2 searches into the TeV region will require a $\sqrt{s} = 1$–2 TeV e^+e^- collider or new hadron colliders such as the LHC and/or the SSC which can probe Z_2 masses as high as ~5 TeV. Further discussion of these possibilities is given in the appendix.

2.6. $SU(2)_L \times SU(2) \times U(1)$ *models*

In the previous three sections (which discussed present limits, production signals and decay modes of new gauge bosons) we concentrated mainly on the general rank-5 models of the $U(1)_\theta$ type [of which

the actual rank-5 $U(1)_\eta$ model is a subcase]. We now turn to the case where the electroweak group is augmented by an additional SU(2) factor. As discussed in section 2.1, the two rank-5 models of this kind are

$$\begin{aligned} &\text{(A)}\quad SU(3)_C \times SU(2)_L \times SU(2)_R \times U(1)_V\,, \\ &\text{(B)}\quad SU(3)_C \times SU(2)_L \times U(1)_Y \times SU(2)_I\,, \end{aligned} \tag{2.78}$$

and we will review the situation of each in turn in this section. We remind the reader that in case (A) the conventional assignment of quantum numbers, as shown in table 2, leads to an augmented version of the left–right symmetric model which has been discussed at some length elsewhere and is not a subject for this review [2.5]. However, alternative assignments of quantum numbers are possible due to the E_6 origin of this group and can lead to new and interesting physics as will be discussed below.

2.6.1. Alternative $SU(2)_L \times SU(2)_R \times U(1)_V$ model

As discussed earlier in section 2.1, the rank-5 and effective rank-5 models of the $U(1)_\theta$ type are unaffected by the ambiguity of fermion assignments, [e.g., $\{L, d_L^c\} = (\mathbf{16}, \bar{\mathbf{5}})$ versus $(\mathbf{10}, \bar{\mathbf{5}})$] except by a possible redefinition of the angle θ (eq. 2.8). As we will see, this is no longer true when the SM is augmented by an additional SU(2) factor.

In the alternative left–right symmetric model (ALRM) proposed by Ma [2.48] the $SU(2)_L$ doublets are (u, d) and (N, E), the $SU(2)_R$ doublets are (u^c, h^c) and (e^c, S^c), and the states (E^c, N^c, ν, e) form a mixed doublet under both $SU(2)_L$ and $SU(2)_R$. The remaining fields (h, d^c and ν^c) are singlets with respect to both SU(2) groups. The existence of the $SU(2)_R$ symmetry and this assignment of fields has several immediate and important consequences [2.49].

(i) The complexity of the superpotential (1.4) is greatly reduced; neglecting generation labels we now have

$$\begin{aligned} W = {} & \lambda_1(uu^cN^c - du^cE^c - uh^ce + dh^c\nu) + \lambda_2(ud^cE - dd^cN) + \lambda_3(hu^ce^c - hh^cS^c) \\ & + \lambda_4 hd^c\nu^c + \lambda_5(ee^cN + EE^cS^c - Ee^c\nu - NN^cS^c) + \lambda_6(\nu\nu^cN^c - eE^c\nu^c)\,, \end{aligned} \tag{2.79}$$

with 5 fewer parameters λ_i. With the usual R-parity assignments for the SM fermions, W leads to an *almost unique* assignment of R, B, and L for all exotic fermions which automatically guarantees proton stability. One obtains for h: $R = -1$, $B = \frac{1}{3}$, $L = 1$ (i.e., h is a leptoquark); (N, E): $R = -1$, $B = L = 0$; S^c: $R = -1$, $B = L = 0$; and two possible assignments for ν^c: $R = +1$, $B = 0$, $L = -1$ or $R = -1$, $B = L = 0$. In the last case, R-parity conservation would demand that $\lambda_4 = \lambda_6 = 0$ in the superpotential (2.79).

(ii) W_R, the right-handed charged gauge boson, has negative R-parity and non-zero lepton number, and thus cannot mix with W_L.

(iii) The mass limits on W_R coming from the K_L–K_S mass difference (see, for example, ref. [2.50]) and polarized μ-decay [2.51] are evaded since W_R couples u^c to h^c (and not d^c) and e^c to S^c (and not ν^c). S^c is expected to have a mass of order a few GeV.

(iv) W_R and Z_R [the neutral gauge boson arising from $SU(2)_R$] as well as the exotics h and E obtain masses from the same scale.

(v) The couplings of Z_R will differ from that of other Z's which arise in rank-5 or effective rank-5 models and so this new neutral gauge boson must have its properties separately analyzed.

The phenomenology of this model has been explored by several authors [2.49]. In what follows we concentrate our discussion on the gauge bosons ($W_R^{\pm}, Z_R$) appearing in this model. The $W_{L,R}$ masses are given by

$$M_{W_L}^2 = \tfrac{1}{4} g_L^2(\langle \tilde{N} \rangle^2 + \langle \tilde{N}^c \rangle^2), \qquad M_{W_R}^2 = \tfrac{1}{4} g_R^2(\langle \tilde{S}^c \rangle^2 + \langle \tilde{N}^c \rangle^2), \tag{2.80}$$

with $v^2 = \langle \tilde{N} \rangle^2 + \langle \tilde{N}^c \rangle^2$ fixed by the SM and we will for convenience define the ratio

$$\tan\beta \equiv \langle \tilde{N}^c \rangle / \langle \tilde{N} \rangle . \tag{2.81}$$

In the weak-interaction basis, Z and Z_R are found to couple via ($g_L = g_R$)

$$\mathcal{L} = (g_L/c_w)(J_Z Z + J_R Z_R), \tag{2.82}$$

with

$$J_R = (1-2x_w)^{-1/2}[x_w T_{3L} + (1-x_w) T_{3R} - x_w Q] . \tag{2.83}$$

Equation (2.83) can be written differently by noting that $Q = T_{3L} + T_{3R} + V/2$. Neutral current data can be used to bound M_2 as a function of ϕ in this model as in the other effective rank-5 models described above. The mass constraint (i.e., Higgs doublets and singlets together with only a small shift allowed for the SM Z mass) is the same as described above. The Higgs constraint (2.18) now gives

$$-x_w \le \tan\phi\,(1-2x_w)^{1/2}(M_2^2 - M_Z^2)/M_Z^2 \le 1 - 2x_w , \tag{2.84}$$

while the ratio of W_L and W_R masses is linked to the values of M_2 and M_Z by

$$\frac{M_{W_L}^2}{M_{W_R}^2} = (1-x_w)^2\left((1-x_w^2)\sin^4\beta - [x_w - \sin^2\beta\,(1-x_w)]^2\,\frac{M_2^2}{M_2^2 - M_Z^2} + (1-2x_w)\,\frac{M_2^2}{M_Z^2}\right)^{-1} . \tag{2.85}$$

At 90% CL one then finds the bounds $M_{W_R} \ge 210$ GeV, $M_2 \ge 250$ GeV and the more general bounds on ϕ and M_2 presented in figs. 32a, b from Barger and Whisnant [2.49]. For large M_2, M_{W_R} we obtain (in the $\phi \to 0$ limit)

$$M_2 = [(1-x_w)/(1-2x_w)]^{1/2} M_{W_R} , \tag{2.86}$$

and the W_R coupling to fermions is given by

$$\mathcal{L} = (g_R/2\sqrt{2}) W_R^{\mu}[\bar{h}^c \gamma_\mu (1-\gamma_5) u^c + \bar{E}^c \gamma_\mu (1-\gamma_5)\nu + \bar{N}^c \gamma_\mu (1-\gamma_5) e + \bar{e}^c \gamma_\mu (1-\gamma_5) S^c] + \text{h.c.} \tag{2.87}$$

2.6.1.1. Z_2 properties. Figure 33 from Barger and Whisnant [2.49] displays the production cross section for Z_2 in the ALRM at the Tevatron and the SSC; note they are somewhat larger than those for the neutral gauge bosons predicted by the other effective rank-5 E_6 models due to the stronger

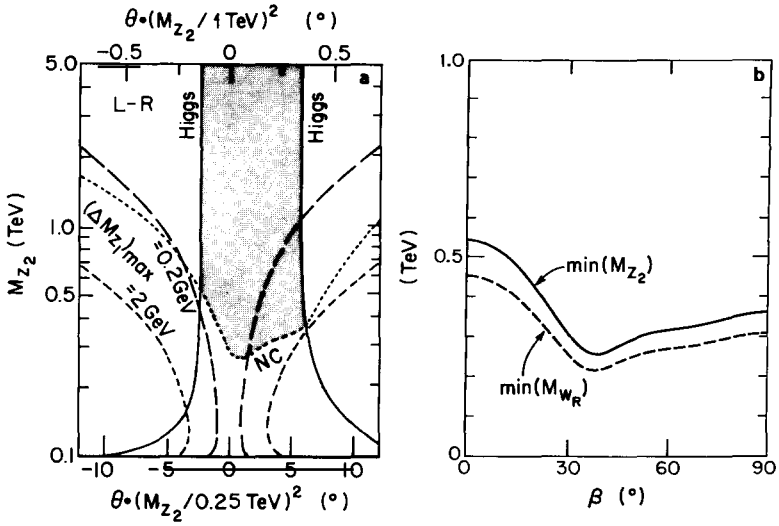

Fig. 32. (a) Constraints on M_2 and Z–Z′ mixing angle θ (called ϕ in the text) in the ALRM. Solid curves: Higgs constraint; mass constraints for $\Delta M_1 \leq 2$ GeV (short dashed curves) and $\Delta M_1 \leq 0.2$ GeV (long dashed curves) are also shown together with present limits from NC data. (b) Lower bound on Z_2 (solid curve) and W_R (dashed curve) masses as a function of β from NC data.

couplings which are present in this case. Figure 34 from the same reference shows a comparison of the asymmetry A_{FB}^{h} for the Z_2 of the ALRM with that of a Z_2 from the effective rank-5 $U(1)_\theta$ model discussed above. The Z_2 in the ALRM is quite distinct. Sitting on the Z_1 at an e^+e^- collider, the values of A_{FB} and A_{LR} will be altered via Z–Z_R mixing as shown in fig. 35 from Barger and Whisnant in comparison to model η. (Note A_{LR} in this figure is opposite in sign to that defined above.) The total fermionic width of Z_2 is given by

$$\Gamma(Z_2 \to \text{fermions}) = (1.9 + 0.6n_g)\ \text{GeV} \times M_2/M_Z \tag{2.88}$$

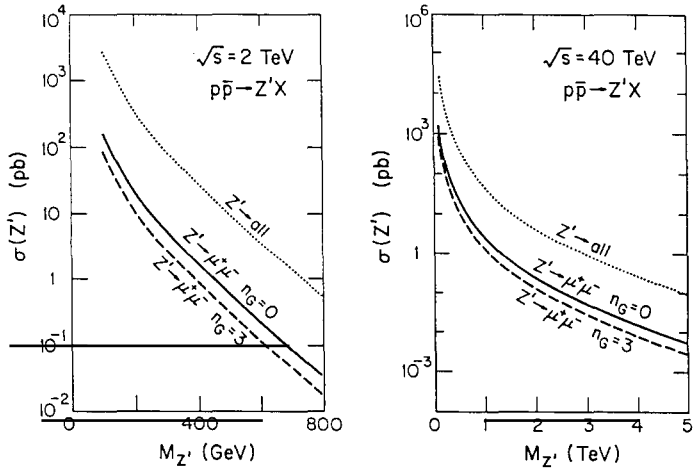

Fig. 33. Production cross section for Z_2 in the ALRM at the Tevatron ($\sqrt{s} = 2$ TeV) and the SSC ($\sqrt{s} = 40$ TeV).

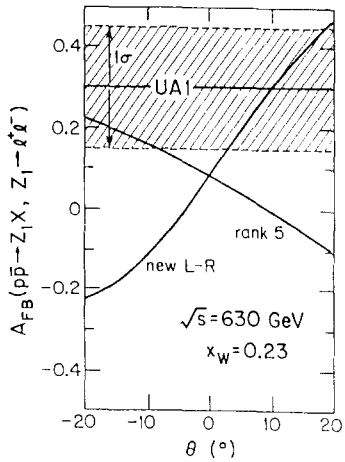

Fig. 34. A_{FB}^{h} for the Z_1 at CERN collider energies in model η (rank 5) and the ALRM (L–R) as a function of θ (i.e. ϕ) and the range allowed by the UA1 data.

(n_g being the number of generations of heavy exotic fermions h, E and N contributing) while the gauge boson and/or Higgs final states could contribute as much as 0.21 GeV $\times M_2/M_Z$ and the SUSY partners (*not* counting those used as Higgs) as much as 1.55 GeV $\times M_2/M_Z$. These numbers are somewhat larger than those obtained in $U(1)_\theta$ models. The leptonic branching ratio for $Z_2 \to e^+e^-$ is also larger than that seen in other E_6 models.. It should be noted that $M_2 < 2M_{W_R}$ so that the decay $Z_2 \to W_R^+ W_R^-$ is always forbidden.

2.6.1.2. W_R properties. As discussed above W_R has negative R-parity and carries lepton number so that it cannot be produced in the usual manner in hadronic collisions via $u\bar{d} \to W_R$ and the h, $\bar{h}$ sea is sufficiently tiny to suppress $u\bar{h} \to W_R$. Since $Z_2 \not\to W_R^+ W_R^-$ we cannot use this resonance to produce W_R

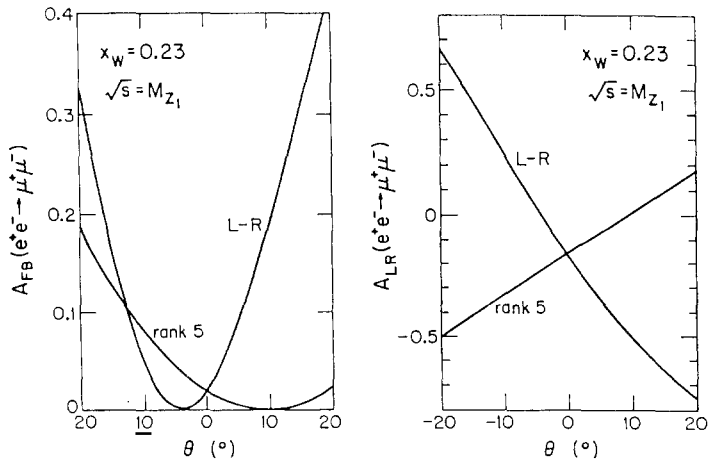

Fig. 35. A comparison of A_{FB} and A_{LR} for $e^+e^- \to \mu^+\mu^-$ with $\sqrt{s} = M_1$ in model η (rank 5) and the ALRM (L–R) as a function of θ (i.e., ϕ).

pairs. Thus the best way to produce W_R is in association with an exotic fermion: $gu \to W_R^+ h$ via the diagrams in fig. 36 from Gunion et al. [2.49]. The spin and color-averaged matrix element for this process is given by

$$|\bar{M}|^2 = \frac{\pi G_F M_W^2}{3\sqrt{2}}\,\alpha_s\left(\frac{|A|^2}{s^2} + \frac{|B|^2}{t'^2} + \frac{2AB^*}{st'}\right), \tag{2.89}$$

with $t' = t - M_h^2$ and $|A|^2$, $|B|^2$, and AB^* given in detail in ref. [2.49]. Figures 37a and b from Gunion et al. [2.49] show $W_R^{\pm(-)} h$ production at the SSC and Tevatron, respectively. Since (2.87) shows that W_R kinematically prefers to decay into eS^c (since they are both light) the production signal depends on the S^c decay modes. If S^c is the lightest SUSY particle (LSP) then R-parity conservation demands its stability so that W_R decay would leave $e\not{p}_T$ as a signal. If S^c is not the LSP, it may decay into $\tilde{\gamma}\gamma$ via loop diagrams and produce a $e\gamma\not{p}_T$ signal if the lifetime is short enough. (Note that S^c could mix with other neutral fermions and gauginos and complicate this simple picture of W_R decay.) The additional h decay (as a leptoquark) on the side opposite to the W_R will lead to a production signal for W_R which is quite unique. (h decay will be discussed in the next chapter.) The W_R width to fermions is

$$\Gamma(W_R \to \text{fermions}) = (0.69 + 1.15 n_g)\ \text{GeV} \times M_{W_R}/M_{W_L}\,, \tag{2.90}$$

with an additional amount of 0.23 (1.74) GeV $\times M_{W_R}/M_{W_L}$ coming from possible decays into gauge bosons and Higgs (SUSY partners) which are possible if phase space effects are neglected.

W_R may also be seen indirectly in ep interactions through the process $ep \to \bar{h}S^c$ via t-channel W_R exchange [2.52]. Figures 38a, b from this reference show the production cross section for $h + S^c$ (assuming S^c has a mass of only a few GeV) as a function of M_h for different values of M_{W_R} at HERA ($\sqrt{s} = 314$ GeV) and a proposed $\sqrt{s} = 1.5$ TeV ep collider. The cross sections are quite reasonable over a wide range of M_{W_R} and M_h values and the production signal (from h decay and $\not{p}_T$ or $\gamma\not{p}_T$ from S^c) is spectacular.

Pair production of W_R gauge bosons at high-energy e^+e^- colliders has not been considered and further analysis of this model may prove quite interesting.

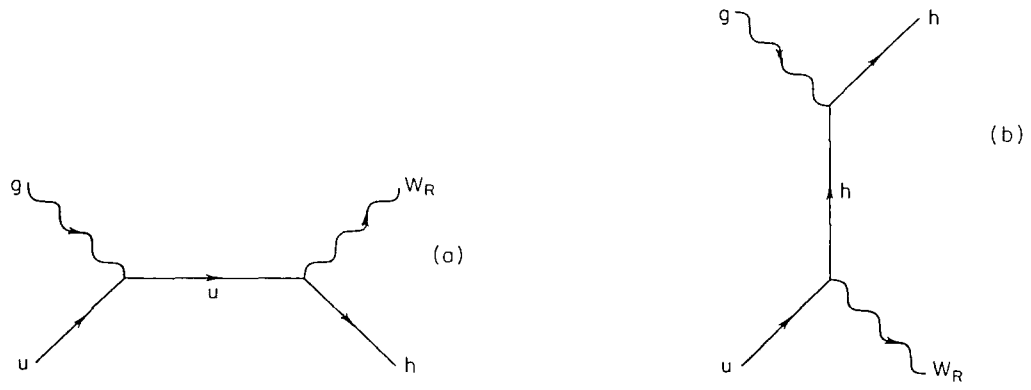

Fig. 36. Diagrams responsible for the subprocess $gu \to W_R h$.

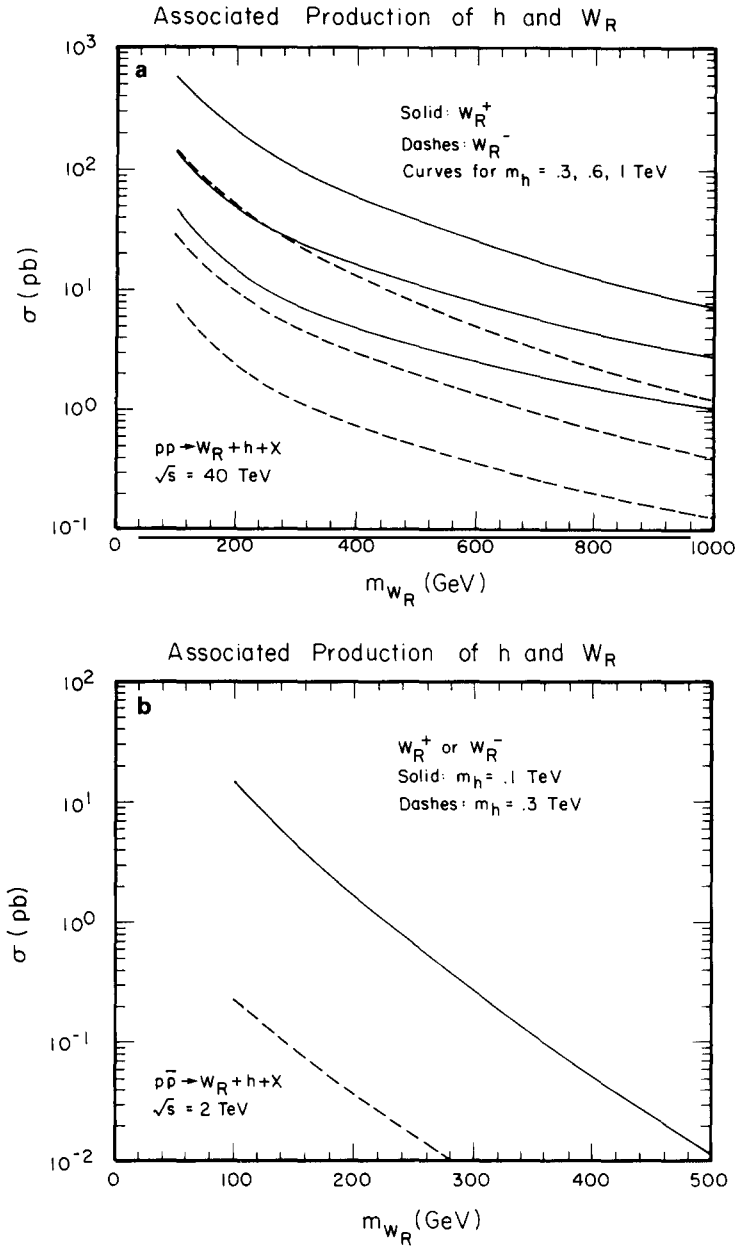

Fig. 37. $\overset{(-)}{p}p \to W_R h + X$ production cross sections at the (a) SSC and (b) the Tevatron.

2.6.2. $SU(2)_L \times U(1)_Y \times SU(2)_I$ model

Within the context of E_6, there are several possible ways to arrive at an extra SU(2) group whose generators commute with the electric charge [2.53], which is generally denoted by $SU(2)_I$. In addition to the neutral gauge boson, Z_I, corresponding to the diagonal generator of $SU(2)_I$ there corresponds a pair of conjugate non-hermitian gauge bosons (W_I and W_I^+). Z_I has already been discussed since it corresponds to a particular value of $\theta (= -\sin^{-1}\sqrt{5/8})$ within the context of the effective rank-5 $U(1)_\theta$

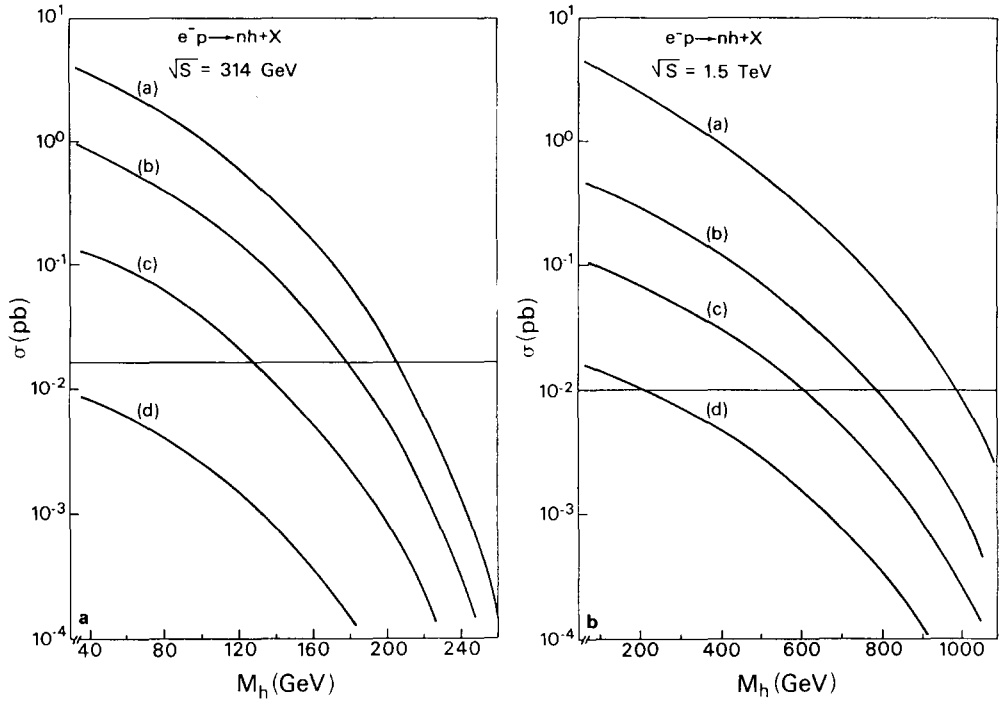

Fig. 38. $h + S^c$ production in ep collisions at (a) HERA ($\sqrt{s} = 314$ GeV) and (b) at a 1.5 TeV ep collider.

models in the analysis above. The only difference, however, is that since Z_I is now a part of the $SU(2)_I$ group [and does not originate from $U(1)_I$] the Z_I couplings in the $SU(2)_I$ case are larger by a factor of

$$[5x_w/3(1-x_w)]^{-1/2} \simeq \sqrt{2}\,, \tag{2.91}$$

due to differences in the RG evolution equations. This would roughly scale limits obtained on Z_2 from the $U(1)_I$ analysis by a factor $\simeq(\sqrt{2})^2 = 2$.

Under the action of $SU(2)_L \times U(1)_Y \times SU(2)_I$ the fermions can be grouped as

$$\begin{pmatrix} \nu & N \\ e & E \end{pmatrix}_L, \quad \begin{pmatrix} u \\ d \end{pmatrix}_L, \quad \begin{pmatrix} E^c \\ N^c \end{pmatrix}_L, \quad (d^c, h^c)_L, \quad (\nu^c, S^c)_L, \quad h_L, \quad e^c_L, \quad u^c_L, \tag{2.92}$$

with $SU(2)_I$ acting in the horizontal direction. The coupling of W_I to fermions is given symbolically as $[(\bar{f}_1 f_2)_{L,R} \equiv \bar{f}_1 \gamma_\mu (\frac{1}{2})(1 \mp \gamma_5) f_2]$

$$\mathcal{L} = (g_I/\sqrt{2})[(\bar{\nu}N)_L + (\bar{e}E)_L + (\bar{h}d)_R + (\bar{\nu}^c S^c)_L]W_I + \text{h.c.}\,, \tag{2.93}$$

with $g_I = g$ if both SU(2)'s have a common scale of origin (which we assume in what follows). Note that since $\langle \tilde{S}^c \rangle$ is responsible for $SU(2)_I$ breaking, as we will discuss below, Z_I and W_I are degenerate in mass before mixing (i.e., before $Z_I \to Z_2$) and thus Z_I (or Z_2) $\to W_I W_I^+$ is kinematically forbidden.

The constraint of $SU(2)_I$ invariance on the superpotential (1.4) reduces the number of independent Yukawa couplings, as in the case of $SU(2)_R$ discussed above, and leaves (neglecting generation indices) [2.54]

$$W = \lambda_1(\nu\nu^c N^c + eE^c\nu^c + NN^cS^c + EE^cS^c) + \lambda_2(d^c\nu^c h + hh^cS^c) + \lambda_3 u^c e^c h$$
$$+ \lambda_4(uu^cN^c + u^cdE^c) + \lambda_5(\nu e^cE + ee^cN) + \lambda_6(ud^cE + dd^cN + uh^ce + dh^c\nu)\,. \tag{2.94}$$

Note that W forces h to be a leptoquark while N, E, and S^c carry $B = L = 0$ and ν^c has $B = 0$, $L = -1$. These assignments insure proton stability. Since W also forces N, N^c, and S^c to have negative R-parity only the scalar partners of these fields can obtain non-zero vev's. W_I has negative R-parity and non-zero lepton number $L = -1$.

W_I production signals have been examined at hadron–hadron [2.54], e^+e^- [2.54], and ep colliders [2.55]. At a hadron collider, single W_I production can only proceed via associated production $g + d \to h + W_I$ in a manner similar to the production of W_R in the ALRM above. One finds the differential cross section

$$\frac{d\sigma}{dt'} = \frac{G_F M_W^2}{48\sqrt{2}}\,\frac{\alpha_s}{\hat{s}^2}\left(-\left(\frac{t'}{\hat{s}} + \frac{\hat{s}}{t'}\right)\left(2 + \frac{m^2}{M_I^2}\right) - \frac{2m^2}{M_I^2} + 2\left(2M_I^2 - m^2 - \frac{m^4}{M_I^2}\right)\left(\frac{1}{\hat{s}} + \frac{1}{t'}\right)\right.$$
$$\left. + 2\left(3m^2M_I^2 - 2M_I^4 - \frac{m^6}{M_I^2}\right)\frac{1}{\hat{s}t'} + 2\left(sM_I^2 - m^2 - \frac{m^4}{M_I^2}\right)\frac{m^2}{t'^2}\right), \tag{2.95}$$

with $m = m_h$, $t' = \hat{t} - m^2$ and $(\hat{s}, \hat{t})$ are the usual Mandelstam variables. $M_2 = M_{W_I} = M_I$ has been assumed in (2.95). Figures 39a, b from ref. [2.54] show W_I and W_I^+ production at hadron colliders.

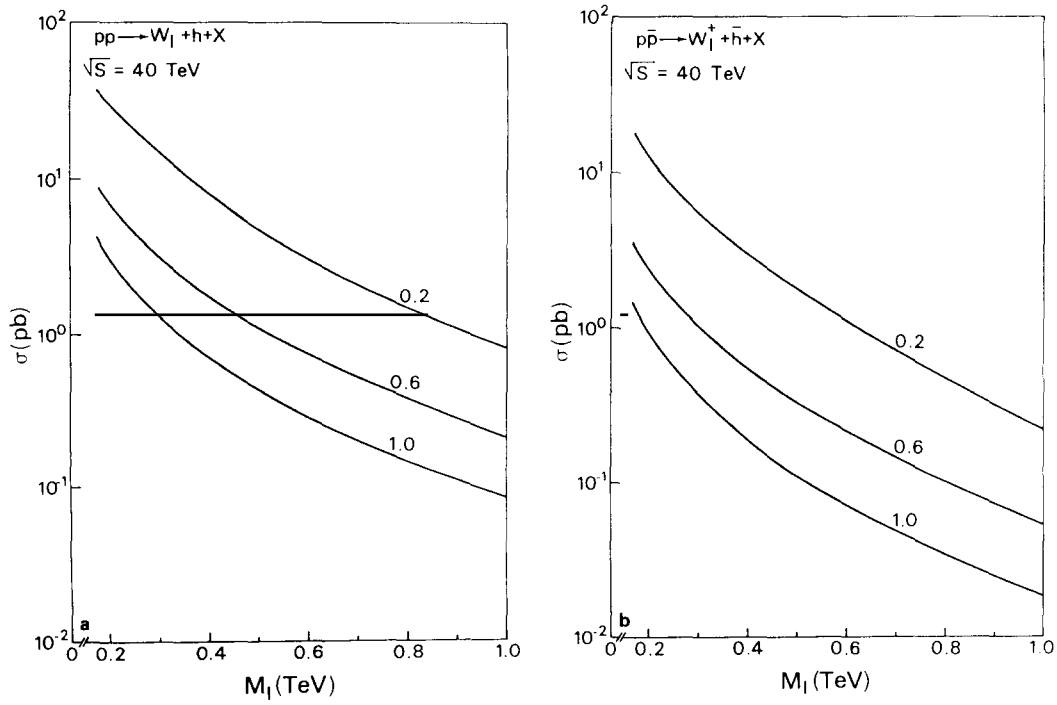

Fig. 39. Cross sections for (a) $pp \to W_I h + X$ and (b) $p\bar{p} \to W_I^+ \bar{h} + X$ at the SSC ($\sqrt{s} = 40$ TeV).

At high energy e^+e^- colliders [2.54] $W_IW_I^+$ production occurs via s-channel Z_I exchange as well as t-channel E exchange. As in the case of $W^\pm$ pair production, this process is particularly sensitive to gauge cancellations between the amplitudes. Figures 40a–d from ref. [2.54] show $W_IW_I^+$ production in e^+e^- collisions for various values of $\sqrt{s}$, M_E, and M_I. In most cases the cross section is quite substantial for such large $\sqrt{s}$ values. For certain mass combinations the cross section is not as forwardly peaked as in the case of $e^+e^- \to W^+W^-$.

In ep collisions [2.55], W_I exchange in the t-channel can produce exotic fermion final states via the sub-process $ed \to Eh$ with a very clean signature. The cross sections for such a process involving two heavy fermions in the final state are not large.

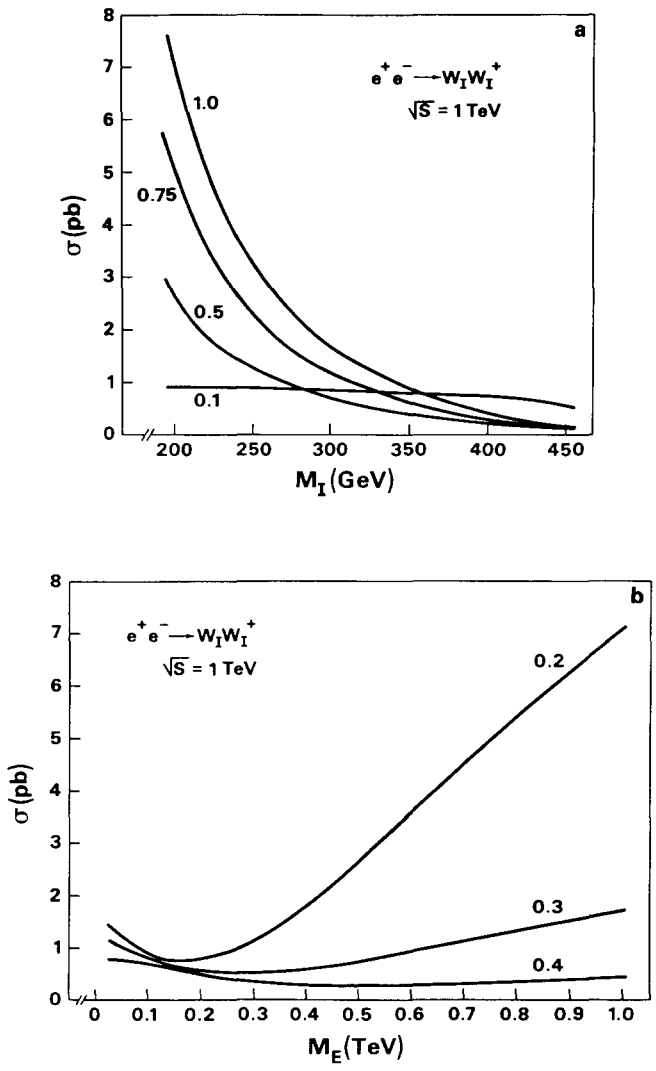

Fig. 40. Production cross sections for $e^+e^- \to W_IW_I^+$ (a) as a function of M_I for $M_E = 0.1$, 0.5, 0.75 and 1 TeV at $\sqrt{s} = 1$ TeV; (b) as a function of M_E for $M_I = 0.2$, 0.3, and 0.4 TeV at $\sqrt{s} = 1$ TeV.

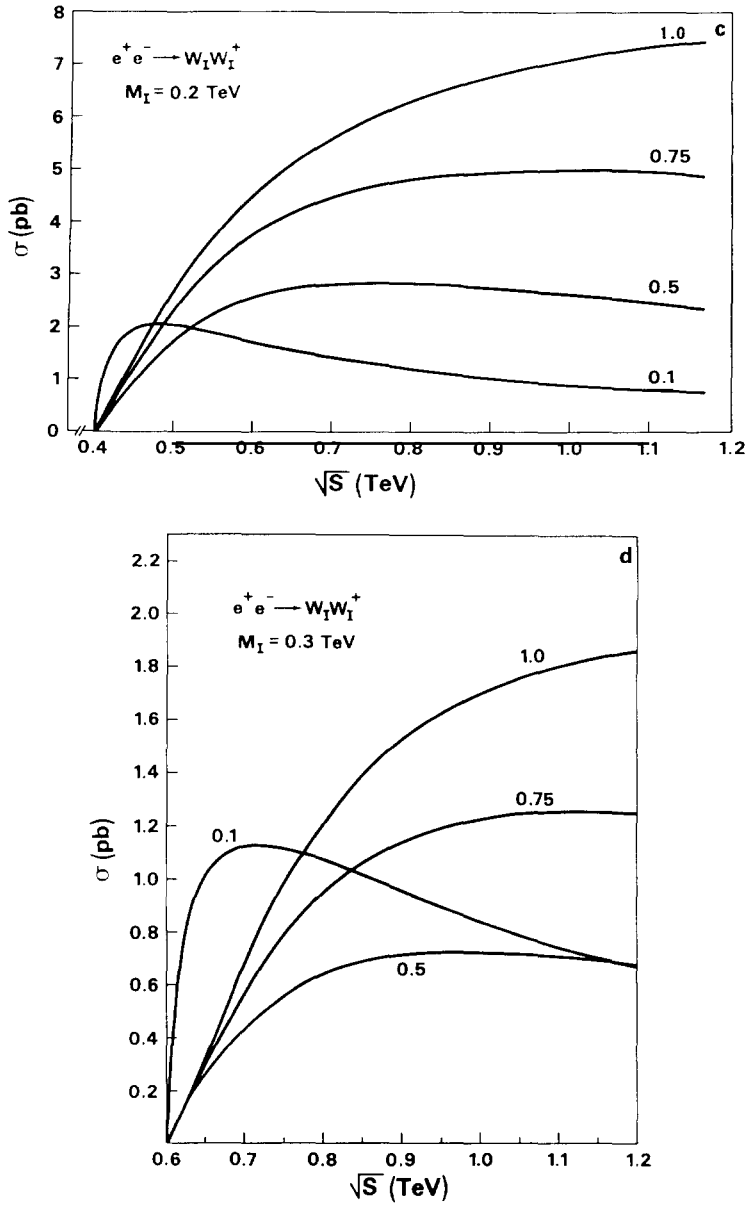

Fig. 40. Production cross sections for $e^+e^- \rightarrow W_I W_I^+$ (c) as a function of $\sqrt{s}$ for $M_I = 0.2$ TeV and $M_E = 0.1$, 0.5, 0.75 and 1 TeV; (d) same as (c) but for $M_I = 0.3$ TeV.

Pair production of W_I at hadron colliders and single W_I production in e^+e^- collisions has recently been considered (see, however, ref. [2.56]). In e^+e^- collisions, single W_I production occurs via the subprocess $\gamma e \rightarrow W_I E$ so that search limits for W_I also depend on the mass of the E. At a $\sqrt{s} = 1(2)$ TeV collider with an integrated luminosity of 30 fb^{-1} (and assuming 10 events establishes a search limit) one finds that masses as large as $M_E + M_I \lesssim 950$ (1950) GeV can be probed. Certainly more work needs to be done on this model.

3. Exotic fermions

The fermions which complete the **27**-representation of E_6 and which are not present in the SM, are called exotic fermions and are the true hallmark of E_6 theories. These new fermions (sometimes simply called exotics) have several possible quantum number assignments (which were discussed in section 1.3 and will be reviewed below), many of which are indigenous to E_6 theories, and if discovered, their presence would pinpoint E_6 as the underlying GUT group. In this chapter we review their phenomenology, including their expected mass spectrum and current mass limits as well as their direct and indirect production and signals, for each of the possible quantum number assignments.

3.1. Overview of exotic fermion properties and decay modes

The fermions which lie in the **27** and the values of their strong and electroweak quantum numbers are listed in table 1. The exotics (excluding the right-handed ν) are contained in the $\mathbf{10}+\mathbf{1}$ representations of SO(10) [the $\mathbf{5}+\bar{\mathbf{5}}$ and **1** of SU(5)] and consist of h, a color triplet, weak iso-singlet, $Q=-\frac{1}{3}$ fermion; N and E, which are color singlet, weak iso-doublet, $Q=0$ and -1 fermions, respectively; and S^c, a color singlet, weak iso-singlet, neutral fermion. The nomenclature for the exotics is quite varied in the literature; other popular notations are listed in section 1.3. Since the superstring-inspired E_6 models possess an $N=1$ SUSY, the corresponding scalar super-partners of all the exotic fermions are also present.

The interactions of the exotic fermions are governed by the superpotential W, which is given in eq. (1.4) for the class of superstring-inspired models where the Higgs fields are contained along with the matter fields in the **27**. In this case, the role of the Higgs fields is played by $\tilde{N}$, $\tilde{N}^c$, and $\tilde{S}^c$ for rank-5 models, and also by $\tilde{\nu}^c$ in rank-6 models. It is then clear that all the terms in W cannot simultaneously exist, otherwise low-energy baryon and lepton number violation will occur. In rank-5 models, if one assumes the lepton number assignment $L(\nu^c)=-1$, then three possible cases of baryon number, lepton number, and R-parity assignments for h may occur:

$$\begin{aligned}
&\text{(i)}\quad \text{h-quarks}\quad \lambda_6=\lambda_7=\lambda_8=\lambda_9=\lambda_{10}=0\,, && B(h)=\tfrac{1}{3}\,,\quad L(h)=0\,,\quad R=+1\,,\\
&\text{(ii)}\quad \text{h-leptoquarks}\quad \lambda_9=\lambda_{10}=0\,, && B(h)=\tfrac{1}{3}\,,\quad L(h)=1\,,\quad R=-1\,,\\
&\text{(iii)}\quad \text{h-diquarks}\quad \lambda_6=\lambda_7=\lambda_8=0\,, && B(h)=-\tfrac{2}{3}\,,\quad L(h)=0\,,\quad R=-1\,.
\end{aligned} \tag{3.1}$$

The vanishing of the various Yukawa couplings, λ_i, may be achieved by topological properties of the compactification manifold or by the use of certain discrete symmetries. It has been shown [3.1] that only two types of Z_2 symmetries as well as certain Z_3 symmetries can naturally simultaneously suppress proton decay, neutrino masses, and flavor-changing neutral currents. Both Z_2 solutions require an operator which distinguishes between generations and introduce a multiplicatively conserved quantity called "exoticness parity". For case (i), the superpotential does not obviously constrain B and L for h, however all other possible assignments would leave h stable. If $L(\nu^c)=0$ and $\tilde{\nu}^c$ acquires a vev, as in the case of rank-6 models, then λ_8 need not necessarily be set to zero, and it will then induce mixing between h and d. However, due to the apparent absence of FCNC, λ_8 must be tuned to be small, which may be somewhat problematic [1.24] without the use of discrete symmetries. For case (ii), $\lambda_8=0$ is also required in rank-6 models as ν^c must acquire a vev. We note that in the ALRM [2.48] (discussed in the previous chapter) the quantum number assignments are uniquely determined to be those of case (ii),

i.e., h's are leptoquarks. The exotic fields N and E have either (1) conventional lepton and baryon number assignments ($L = 1$, $B = 0$), or (2) $L = B = 0$, and are the superpartners of the Higgs fields. In the former case, their phenomenology is interesting and has received much attention in the literature and thus will be surveyed in this chapter. In the latter case the situation is more intricate since E and N mix, in general, with the other charginos and neutralinos present in the theory; this situation has not been thoroughly analyzed. In the models where the Higgs fields are assigned to a different **27** (or to a $\overline{\mathbf{27}}$) than those which contain the usual fermions, the superpotential is given in eq. (1.8). Here, the exotics h and E, N may have the quantum number assignments of ordinary quarks and leptons, respectively, as shown in eq. (1.6).

Notice that, regardless of the particular baryon and lepton number attributes that the exotics may have, h, N, and E are always vector-like, i.e., they only possess vector couplings to the SM Z. Axial-vector couplings to the Z_1 can then only be produced via Z–Z′ mixing and hence will be constrained to be small. This property has some interesting phenomenological consequences.

Although other quantum number assignments for the exotics are possible, those outlined above are the most fashionable in the literature, and will be all that we will discuss here. We will now review the specific properties and decay modes of the exotics for each of these three assignments. The phenomenology of the neutral exotics is more complex due to the possibility of mixing between the five neutral fields in the **27** and will be discussed separately in section 3.6.

3.1.1. E-leptons and h-quarks

If the exotic fermions have conventional baryon and lepton number assignments, then the superpotential can induce mixing between these new fields and the ordinary fermions with the same electric and color charges. As we will see below, this mixing can lead to flavor changing neutral current (FCNC) type couplings of ordinary fermions to the neutral gauge and Higgs bosons when several generations of **27**'s are present. In addition, we also need to address the flavor changing couplings of the exotic to the ordinary fermions since this same mixing allows the exotic fermions to decay and provides signatures for their production. For simplicity we will first consider the case of a single generation of fermions in the **27** and return to the case of n generations later. We will also limit ourselves to fermion couplings to the gauge bosons $W^{\pm}$, Z, and Z′ and extend this analysis to the more complex Higgs sector later. We will follow the discussion in refs. [3.2–3.4]. (For an early discussion of mixing with heavy isosinglet quarks outside of the E_6 context see the second of refs. [3.4].)

Let us label the ordinary and exotic fermion weak interaction eigenstates by f^0 and F^0, respectively. Then the superpotential can produce, in general, a 2×2 mass matrix for fermions with $Q = -1, -\frac{1}{3}$ as well as a 5×5 matrix for the $Q = 0$ fermions, which will be discussed later in section 3.6 in greater detail. In order to diagonalize these matrices, bi-unitary transformations of the fermion fields are in general necessary,

$$\mathscr{L}_{\text{mass}} = \sum_i (\bar{f}^0, \bar{F}^0)^i_{\text{L}} M_i \begin{pmatrix} f^0 \\ F^0 \end{pmatrix}^i_{\text{R}} + \text{h.c.} \;\rightarrow\; \sum_i (\bar{f}, \bar{F})^i_{\text{L}} M^{\text{D}}_i \begin{pmatrix} f \\ F \end{pmatrix}^i_{\text{R}} + \text{h.c.}\,, \tag{3.2}$$

where M^{D}_i is diagonal and

$$M^{\text{D}}_i = U^i_{\text{L}} M_i (U^i_{\text{R}})^+\,, \qquad \begin{pmatrix} f \\ F \end{pmatrix}^i_{\text{L,R}} = U^i_{\text{L,R}} \begin{pmatrix} f^0 \\ F^0 \end{pmatrix}^i_{\text{L,R}}\,, \tag{3.3}$$

with i being a charge labeling index. For n generations, the fields f and F become n-component column vectors and the mass matrix is $2n \times 2n$ dimensional. Let us first consider the charged currents (CC) for the $Q = \frac{2}{3}, -\frac{1}{3}$ sector of the theory. The coupling of these fermions to the W are given by

$$\mathscr{L}^{CC} = \frac{g}{\sqrt{2}} (\bar{u}^0, 0)_L \gamma_\mu T_+^L \begin{pmatrix} d^0 \\ h^0 \end{pmatrix}_L W^\mu + \text{h.c.}\,, \quad T_+^L = \begin{pmatrix} 1 & 0 \\ 0 & 0 \end{pmatrix}, \tag{3.4}$$

where T_+^L is the left-handed weak isospin raising operator. In the mass eigenstate basis for a single generation this becomes

$$\begin{aligned} \mathscr{L}^{CC} &= \frac{g}{\sqrt{2}} (\bar{u}, 0)_L \gamma_\mu \begin{pmatrix} 1 & 0 \\ 0 & 0 \end{pmatrix} (U_L^d)^+ \begin{pmatrix} d \\ h \end{pmatrix}_L W^\mu + \text{h.c.} \\ &= (g/2\sqrt{2}) \bar{u} \gamma_\mu (1 - \gamma_5)(d \cos\theta_d - h \sin\theta_d) W^\mu + \text{h.c.}\,, \end{aligned} \tag{3.5}$$

with θ_d being the d–h mixing angle and where we have neglected the possibility that U_L^d contains non-trivial phases. For several generations, u^0 represents the vector $(u_1^0, u_2^0, \ldots, u_n^0)^T$ etc., and we obtain instead

$$\mathscr{L}^{CC} = \frac{g}{\sqrt{2}} (\bar{u}, 0) \begin{pmatrix} U_L^u & 0 \\ 0 & 0 \end{pmatrix} \begin{pmatrix} I & 0 \\ 0 & 0 \end{pmatrix} (U_L^d)^+ \gamma_\mu (1 - \gamma_5) \begin{pmatrix} d \\ h \end{pmatrix} W^\mu + \text{h.c.}\,, \tag{3.6}$$

with U_L^u and I being $n \times n$ matrices, and U_L^d being a $2n \times 2n$ matrix. Thus the generalized $2n \times 2n$ KM matrix is given by

$$V_{KM} = \begin{pmatrix} U_L^u & 0 \\ 0 & 0 \end{pmatrix} (U_L^d)^+, \tag{3.7}$$

and is not unitary as we will now see. If we write U_L^d in block form,

$$U_L^d = \begin{pmatrix} A & B \\ C & D \end{pmatrix}, \tag{3.8}$$

V_{KM} then becomes

$$V_{KM} = \begin{pmatrix} U_L^u A^+ & U_L^u C^+ \\ 0 & 0 \end{pmatrix}. \tag{3.9}$$

Note that the $n \times n$ submatrix $V_0 = U_L^u A^+$ only involves the couplings of the ordinary quarks to themselves and is what may usually be defined as the KM matrix; however, it is also, in general, not unitary: $V_0^+ V_0 = AA^+ \neq I$. In fact, $V_{KM}^+ V_{KM} \neq V_{KM} V_{KM}^+$,

$$V_{KM} V_{KM}^+ = \begin{pmatrix} I & 0 \\ 0 & 0 \end{pmatrix}, \quad V_{KM}^+ V_{KM} = \begin{pmatrix} AA^+ & AC^+ \\ CA^+ & CC^+ \end{pmatrix}, \tag{3.10}$$

whereas the unitarity of U_L^d only demands that

$$AA^+ + BB^+ = A^+A + C^+C = CC^+ + DD^+ = B^+B + D^+D = I\,,$$
$$CA^+ + DB^+ = A^+B + C^+D = 0\,, \tag{3.11}$$

so that V_0 is unitary if and only if $BB^+ = C^+C = 0$. V_{KM} is *never* unitary.

The CC for the $Q = 0, -1$ sector is even more complex. Let us consider the following simple scenario for purposes of demonstration. We will assume that both ν and N are Dirac fields and that S^c decouples in such a way that it remains unmixed. In this simple case the effective $Q = 0$ fermion mass matrix is also $2n \times 2n$ dimensional. Then

$$\mathscr{L}^{CC} = \frac{g}{\sqrt{2}}\left[(\bar{\nu}^0, \bar{N}^0)_L \gamma_\mu T_+^L \begin{pmatrix} e^0 \\ E^0 \end{pmatrix}_L + (\bar{\nu}^0, \bar{N}^0)_R \gamma_\mu T_+^R \begin{pmatrix} e^0 \\ E^0 \end{pmatrix}_R\right] W^\mu + \text{h.c.}\,, \tag{3.12}$$

with (for n generations),

$$T_+^L = \begin{pmatrix} I & 0 \\ 0 & I \end{pmatrix}, \qquad T_+^R = \begin{pmatrix} 0 & 0 \\ 0 & I \end{pmatrix} \tag{3.13}$$

so that we now have

$$\begin{aligned}\mathscr{L}^{CC} &= \frac{g}{\sqrt{2}}\left[(\bar{\nu}, \bar{N})_L \gamma_\mu U_L^\nu (U_L^e)^+ \begin{pmatrix} e \\ E \end{pmatrix}_L + (\bar{\nu}, \bar{N})_R \gamma_\mu U_R^\nu \begin{pmatrix} 0 & 0 \\ 0 & I \end{pmatrix} (U_R^e)^+ \begin{pmatrix} e \\ E \end{pmatrix}_R\right] W^\mu + \text{h.c.} \\ &\equiv \frac{g}{2\sqrt{2}}(\bar{\nu}, \bar{N})\gamma_\mu (V - A\gamma_5)\begin{pmatrix} e \\ E \end{pmatrix} W^\mu + \text{h.c.}\,,\end{aligned} \tag{3.14}$$

with the definitions

$$V \equiv V_L + V_R\,, \qquad A \equiv V_L - V_R\,, \qquad V_L = U_L^\nu (U_L^e)^+\,, \qquad V_R = U_R^\nu \begin{pmatrix} 0 & 0 \\ 0 & I \end{pmatrix} (U_R^e)^+\,. \tag{3.15}$$

Note V_L is unitary, whereas V_R is not. $V_R \neq 0$ implies in this example that right-handed leptons experience CC interactions. This is clearly seen in the case of a single generation for which we find explicitly (ignoring possible phases)

$$V_L = \begin{pmatrix} \cos\delta & \sin\delta \\ -\sin\delta & \cos\delta \end{pmatrix}, \quad \delta \equiv \theta_\nu^L - \theta_e^L\,, \qquad V_R = \begin{pmatrix} \sin\theta_e^R \sin\theta_\nu^R & \cos\theta_e^R \sin\theta_\nu^R \\ \sin\theta_e^R \cos\theta_\nu^R & \cos\theta_e^R \cos\theta_\nu^R \end{pmatrix}, \tag{3.16}$$

which leads to the coupling of right-handed electrons and neutrinos

$$(g/2\sqrt{2})\bar{\nu}\gamma_\mu(1 + \gamma_5) e \sin\theta_e^R \sin\theta_\nu^R\, W^\mu + \text{h.c.} \tag{3.17}$$

Clearly, the angles δ, θ_e^R, and θ_ν^R must be rather severely constrained in order to comply with bounds from existing data, as will be discussed below. Note that the CC couplings allow, e.g., for the decays h$\to$uW and E$\to\nu$W, with the W being real or virtual depending on the mass of E and h.

The fermionic coupling to the neutral gauge bosons, Z_a^μ, is given by (where f_i is now a vector containing *all* fermions of a given charge)

$$\begin{aligned}\mathscr{L}^{\mathrm{NC}} &= \sum_{i,a} (\bar{f}^0_{\mathrm{L},i}\gamma_\mu P^{i,a}_{\mathrm{L}} f^0_{\mathrm{L},i} + \mathrm{L}\leftrightarrow\mathrm{R}) Z^\mu_a \\ &= \sum_{i,a} [\bar{f}_{\mathrm{L},i}\gamma_\mu U^i_{\mathrm{L}} P^{i,a}_{\mathrm{L}} (U^i_{\mathrm{L}})^+ f_{\mathrm{L},i} + \mathrm{L}\leftrightarrow\mathrm{R}] Z^\mu_a ,\end{aligned} \tag{3.18}$$

with $P^{i,a}_{\mathrm{L,R}}$ being the coupling matrices for fermions of charge i to Z^μ_a. Defining

$$C^{i,a}_{\mathrm{L,R}} \equiv U^i_{\mathrm{L,R}} P^{i,a}_{\mathrm{L,R}} (U^i_{\mathrm{L,R}})^+ , \tag{3.19}$$

$\mathscr{L}^{\mathrm{NC}}$ becomes

$$\mathscr{L}^{\mathrm{NC}} = \sum_{i,a} (\bar{f}_{\mathrm{L},i}\gamma_\mu C^{i,a}_{\mathrm{L}} f_{\mathrm{L},i} + \mathrm{L}\leftrightarrow\mathrm{R}) Z^\mu_a . \tag{3.20}$$

Here $C^{i,a}_{\mathrm{L,R}}$ are the coupling matrices in the mass eigenstate basis. Unless the P's are proportional to the identity, the C's will have off-diagonal terms. Consider the couplings of the $Q=-1$ fermions to the SM Z. In this case $P^{-1}_{\mathrm{L}} = (g/c_{\mathrm{w}})(-\frac{1}{2} + x_{\mathrm{w}})I$, so that the left-handed couplings in the mass eigenstate basis are diagonal: $C^{-1}_{\mathrm{L}} = P^{-1}_{\mathrm{L}}$. However, in the right-handed sector one finds

$$C^{-1}_{\mathrm{R}} = \frac{g}{c_{\mathrm{w}}}\left[x_{\mathrm{w}} I - \tfrac{1}{2} U^{\mathrm{e}}_{\mathrm{R}} \begin{pmatrix} 0 & 0 \\ 0 & I \end{pmatrix} (U^{\mathrm{e}}_{\mathrm{R}})^+\right]. \tag{3.21}$$

Similarly, for the $Q=-\frac{1}{3}$ sector, one has $C^{-1/3}_{\mathrm{R}} = P^{-1/3}_{\mathrm{R}}$, whereas

$$C^{-1/3}_{\mathrm{L}} = \frac{g}{c_{\mathrm{w}}}\left[\tfrac{1}{3} x_{\mathrm{w}} I - \tfrac{1}{2} U^{\mathrm{d}}_{\mathrm{L}} \begin{pmatrix} I & 0 \\ 0 & 0 \end{pmatrix} (U^{\mathrm{d}}_{\mathrm{L}})^+\right]. \tag{3.22}$$

Writing $C^{-1/3}_{\mathrm{L}}$ in the (d, h) basis, one finds using (3.8)

$$C^{-1/3}_{\mathrm{L}} = \frac{g}{c_{\mathrm{w}}}\left[(-\tfrac{1}{2} + \tfrac{1}{3} x_{\mathrm{w}}) \begin{pmatrix} I & 0 \\ 0 & I \end{pmatrix} + \tfrac{1}{2} \begin{pmatrix} AA^+ & AC^+ \\ CA^+ & CC^+ \end{pmatrix}\right], \tag{3.23}$$

where the non-diagonal matrix is observed to be $V^+_{\mathrm{KM}} V_{\mathrm{KM}}$ (3.10). This shows that the non-unitarity of the KM matrix is intimately linked to the presence of FCNC couplings. In the single generation limit, C^{-1}_{R} and $C^{-1/3}_{\mathrm{L}}$ lead to the couplings

$$\frac{g}{2c_{\mathrm{w}}}\left[-\tfrac{1}{2} \sin\theta^{\mathrm{R}}_{\mathrm{e}} \cos\theta^{\mathrm{R}}_{\mathrm{e}}\, \bar{e}\gamma_\mu(1+\gamma_5)E + \tfrac{1}{2} \sin\theta^{\mathrm{L}}_{\mathrm{d}} \cos\theta^{\mathrm{L}}_{\mathrm{d}}\, \bar{d}\gamma_\mu(1-\gamma_5)h\right] Z^\mu + \mathrm{h.c.} , \tag{3.24}$$

which allows for the decay $\mathrm{h}\to\mathrm{dZ}$ and $\mathrm{E}\to\mathrm{eZ}$ with the Z being real or virtual depending on the masses of h and E.

As we will see below, ordinary–exotic fermion mixing can lead to a variety of new phenomena (in addition to the FCNC and leptonic right-handed currents discussed above) which stem from the non-unitarity of the KM matrix. For example, the usual GIM suppression of loop amplitudes relies on the unitarity of V_{KM} which is now, at best, only approximate. In addition, helicity suppression of leptonic loop amplitudes also fails since the CC is no longer purely left-handed. This subject will be discussed further below.

What kind of mass matrices should one expect to be generated by the superpotential in eq. (1.8)? Using the notation of eq. (3.2) the d–h and e–E mass matrices take the form (i.e., for $Q = -\frac{1}{3}$ and -1 respectively)

$$M_{-1/3} \sim \begin{pmatrix} D & D \\ S & S \end{pmatrix}, \qquad M_{-1} \sim \begin{pmatrix} D & S \\ D & S \end{pmatrix}, \tag{3.25}$$

where D (S) signifies an entry arising from an iso-doublet (iso-singlet) Higgs vev multiplied by a Yukawa coupling. (The mixing in the $Q = 0$ sector will be discussed in section 3.6.) Then the appropriate mixing matrices can be calculated from

$$\begin{aligned} (M^{\mathrm{D}}_{-1/3})^2 &= U^{\mathrm{d}}_{\mathrm{L}}(M_{-1/3}M^{+}_{-1/3})(U^{\mathrm{d}}_{\mathrm{L}})^{+} = U^{\mathrm{d}}_{\mathrm{R}}(M^{+}_{-1/3}M_{-1/3})(U^{\mathrm{d}}_{\mathrm{R}})^{+}, \\ (M^{\mathrm{D}}_{-1})^2 &= U^{\mathrm{e}}_{\mathrm{L}}(M_{-1}M^{+}_{-1})(U^{\mathrm{e}}_{\mathrm{L}})^{+} = U^{\mathrm{e}}_{\mathrm{R}}(M^{+}_{-1}M_{-1})(U^{\mathrm{e}}_{\mathrm{R}})^{+}. \end{aligned} \tag{3.26}$$

Note that

$$M^{+}_{-1/3}M_{-1/3}, M_{-1}M^{+}_{-1} \sim \begin{pmatrix} D^2+S^2 & D^2+S^2 \\ D^2+S^2 & D^2+S^2 \end{pmatrix}, \qquad M_{-1/3}M^{+}_{-1/3}, M^{+}_{-1}M_{-1} \sim \begin{pmatrix} D^2 & DS \\ DS & S^2 \end{pmatrix}. \tag{3.27}$$

If doublet vev's are much smaller than singlet vev's (i.e., $D \ll S$) this suggests that $\theta^{\mathrm{d}}_{\mathrm{L}} \sim \theta^{\mathrm{e}}_{\mathrm{R}} \sim D/S \ll 1$, while $\theta^{\mathrm{d}}_{\mathrm{R}} \sim \theta^{\mathrm{e}}_{\mathrm{L}} \sim 1$ apart from Yukawa couplings. Since it is, in fact, $\theta^{\mathrm{d}}_{\mathrm{L}}$ and $\theta^{\mathrm{e}}_{\mathrm{R}}$ which control FCNC couplings to the Z, it is fortunate that this suppression occurs naturally. Large $\theta^{\mathrm{d}}_{\mathrm{R}}$ has no effect on the W and Z couplings while $\theta^{\mathrm{e}}_{\mathrm{L}}$ can be large so long as the difference $\theta^{\nu}_{\mathrm{L}} - \theta^{\mathrm{e}}_{\mathrm{L}}$ is small. The low-energy FCNC Z′ couplings *are* sensitive to both $\theta^{\mathrm{d}}_{\mathrm{R}}$ and $\theta^{\mathrm{e}}_{\mathrm{L}}$, but these effects are suppressed due to the relatively large Z′ mass.

Other similar analyses of the fermion mass matrices exist in the literature [3.5].

The mixing of the d and h quarks may resolve one of the old problems involving the quark mass hierarchy; this being the question of why m_{u} is so small. For both the second and third generations $m_{2/3} > m_{-1/3}$, but this relation is inverted for the first generation. In the Wolfenstein parameterization [3.6] one sees that the masses scale approximately as ($\lambda \simeq \sin\theta_{\mathrm{c}}$)

$$m_{\mathrm{t}} : m_{\mathrm{c}} : m_{\mathrm{u}} \simeq 1 : \lambda^2 : \lambda^6, \qquad m_{\mathrm{b}} : m_{\mathrm{s}} : m_{\mathrm{d}} \simeq 1 : \lambda^2 : \lambda^4, \tag{3.28}$$

so that the pattern is broken by the first generation masses. Directly related to this is the usual explanation [3.7] for the smallness of the KM angles which is that the $M_{2/3}$ and $M_{-1/3}$ mass matrices are nearly proportional, i.e., $M_{2/3}/m_{\mathrm{t}} = M_{-1/3}/m_{\mathrm{b}} + \Delta$, where Δ is a small correction. The $\Delta = 0$ limit implies two relations: (i) $m_{\mathrm{t}}/m_{\mathrm{b}} = m_{\mathrm{c}}/m_{\mathrm{s}}$ and (ii) $m_{\mathrm{c}}/m_{\mathrm{s}} = m_{\mathrm{u}}/m_{\mathrm{d}}$, the first of which may be satisfied if m_{t} is not much larger than 50 GeV, while the second apparently never holds true. From this we would conclude that $\Delta \neq 0$ must significantly modify (ii). The connection with the KM matrix is easily seen in the Fritzsch scheme [3.8], which for $m_{\mathrm{u}} \ll m_{\mathrm{c}} \ll m_{\mathrm{t}}$ and $m_{\mathrm{d}} \ll m_{\mathrm{s}} \ll m_{\mathrm{b}}$ predicts, for example,

$$V_{\mathrm{us}} = (m_{\mathrm{d}}/m_{\mathrm{s}})^{1/2} - (m_{\mathrm{u}}/m_{\mathrm{c}})^{1/2}, \qquad V_{\mathrm{cb}} = (m_{\mathrm{s}}/m_{\mathrm{b}})^{1/2} - (m_{\mathrm{c}}/m_{\mathrm{t}})^{1/2}. \tag{3.29}$$

V_{cb} is small since (i) is nearly satisfied, while since (ii) is not satisfied, V_{us} is large (in fact, anomalously so).

Perhaps, instead of m_u being too small, one might imagine that it is m_d which is too big and Δ is somehow responsible for raising the d-quark mass. To see that this scenario may be realized, consider SU(5), where one expects (a) $m_b/m_s \simeq m_\tau/m_\mu$, which is reasonably well satisfied, whereas one also finds (b) $m_d/m_s \simeq m_e/m_\mu$, which *would* hold if m_d were much lighter. In fact, if $m_d \simeq 0.5$–1 MeV, both (ii) *and* (b) would be satisfied. However, m_d is found instead to be 7–9 MeV. What physics could lead to Δ and raise m_d, and render the above mass relations invalid? One proposal [3.9] is that d–h mixing can be used to induce a shift of this magnitude in m_d for a reasonable choice of model parameters, while leaving m_u unaltered. This scenario would also predict small values ($= 0.01$–0.10) for the mixing angle θ_L^d. Although a successful model of this kind has been discussed for the case of a single generation, a realistic model of this kind for two or more generations of quarks has yet to be worked out. It should be noted that if the shift Δ in the $Q = -\frac{1}{3}$ quark masses was generation independent, it would only make its presence known for the first generation, as $\Delta \ll m_s, m_b$. Clearly, more work needs to be done to explore this area.

We now turn to a discussion of the decay modes of the exotic fermions. Let us first consider the decays of the h-quark. If h is lighter than the W or Z, then as mentioned above, h decays into virtual W's and Z's (i.e., $h \to uW^*, dZ^*$) which then subsequently decay to a pair of fermions. The three-body decay rate for $h \to ab\bar{c}$ through the exchange of a set of gauge bosons X_i of mass M_i and width Γ_i is given by ref. [3.2]

$$\Gamma(h \to ab\bar{c}) = N_c \frac{M_h^5}{48\pi^3} \int_0^{1/2} x^2 \, dx \sum_{ij} A_{ij}[B_{ij}(9 - 16x) + C_{ij}(-3 + 8x)] , \tag{3.30}$$

where $x = E_a/M_h$ and $A_{ij} = P_{ij}(s \to q^2)$ is the propagator function from section 2 with $q^2 = M_h^2(1 - 2x)$. B_{ij} and C_{ij} are defined via

$$B_{ij} = (v_i v_j + a_i a_j)(v_i' v_j' + a_i' a_j') , \qquad C_{ij} = (v_i a_j + v_j a_i)(v_i' a_j' + v_j' a_i') . \tag{3.31}$$

Our normalization is such that for ordinary μ decay we would have $v = v' = a = a' = g/(2\sqrt{2})$. Note that the above formula does not apply to the decay $h \to dd\bar{d}$ due to the additional diagrams present in the case of identical particles. If $M_h^2 \ll M_{W,Z}^2$ and the h–d mixing is small we have [3.3]

$$\begin{aligned} &B(h \to \text{hadrons}) \simeq 66\% , \qquad B(h \to u\ell^- \bar{\nu}_\ell) \simeq 8\% , \qquad B(h \to d\nu_\ell \bar{\nu}_\ell) \simeq 2\% , \\ &B(h \to d\ell^+ \ell^-) \simeq 1\% . \end{aligned} \tag{3.32}$$

As M_h increases, the relative proportion of W* and Z* final states also increases due to the finite effect of the propagators. It should be noted that the $h \to d\ell^+\ell^-$ mode is the one which most clearly signals the production of h-quarks (as will be further discussed below), but unfortunately the corresponding branching fraction is relatively small.

Since the partial widths for the above decay modes are mixing angle suppressed, it is possible that the h-quark may have sizeable flavor-changing second-order decays. One such promising process is $h \to dg$, which proceeds through a class of one-loop penguin-type diagrams, and has been examined in

ref. [3.10]. Clearly, this process may be important only for $M_h < M_W$. It is shown in this reference that in the limit of small h–d mixing, the ratio $\Gamma(h \to dg)/\Gamma(h \to u\ell\bar{\nu}_\ell)$ is independent of the mixing, and is of order a few percent for the mass range $26 < M_h < 82$ GeV. This result changes only slightly for different E_6 models (i.e., different values of θ) and for varying values of M_{Z_2}. This is in contrast to the SM, where loop-order decays have much smaller relative branching fractions. The signature for $h \to dg$ is two jets and since the process should occur at a larger rate than is expected for a SM rare decay, it should provide a good signal for h production.

If the h-quark is sufficiently massive, it decays into real W's and Z's. The width for $h \to fX$ is given by (neglecting the mass of the light fermion, f)

$$\Gamma(h \to fX) = (M_h/16\pi)(v^2 + a^2)z^{-2}(1 - 3z^4 + 2z^6)\,, \tag{3.33}$$

with $z \equiv M_X/M_h$ and the couplings normalized as

$$\mathcal{L}_{hfX} = \bar{h}\gamma_\mu(v - a\gamma_5)fX^\mu + \text{h.c.} \tag{3.34}$$

For $M_h \gg M_{W,Z}$ one finds $\Gamma(h \to dZ)/\Gamma(h \to uW) = \frac{1}{2}$, so that the branching fraction for $h \to dZ \to d\ell^+\ell^-$ remains small in this mass regime.

The decay of the exotic leptons is somewhat more complicated due to the lack of knowledge about the ordering of the exotic masses, i.e., is $M_E > M_N$ or vice versa? If $M_E > M_N$ then E decays by the usual charged current process $E \to NW$, with the W being real or virtual, without mixing with the ordinary fermions. For $M_E - M_N < M_W$ the decay rate for $E \to Ne\nu_e$ is [3.2]

$$\Gamma(E \to Ne\bar{\nu}) = \frac{G_F^2 M_E^5 W^2}{24\pi^3} \int_\delta^{1/2(1+\delta^2)} dx\, \frac{(x^2 - \delta^2)^{1/2}[x(1 + \delta^2 - 2x) + 2(1 - x)(x - \delta^2)]}{(1 + \delta^2 - 2x - W)^2 + WG}\,(v^2 + a^2)\,, \tag{3.35}$$

with $W = M_W^2/M_E^2$, $\delta = M_N/M_E$, $G = \Gamma_W^2/M_E^2$, and $x = E_N/M_E$. Note that for V − A couplings, $v = a = 1$. If $M_E - M_N > M_W$ then E undergoes a two-body decay into physical W's with a rate

$$\Gamma(E \to NW) = \frac{g^2 M_E}{128\pi}\left[\left(1 + \frac{M_N^2 - M_W^2}{M_E^2}\right)^2 - \frac{4M_N^2}{M_E^2}\right]^{1/2} \times \left((v^2 + a^2)\left\{\left(1 + \frac{M_N^2 - M_W^2}{M_E^2}\right) + \frac{M_E^2}{M_W^2}\left[\left(1 - \frac{M_N^2}{M_E^2}\right)^2 - \frac{M_W^4}{M_E^4}\right]\right\} - \frac{6M_N}{M_E}(v^2 - a^2)\right)\,, \tag{3.36}$$

with the above normalization for the couplings v and a. Hence for $M_E > M_N$ we see that E decays in a fairly normal manner.

If, however, $M_E < M_N$, then E must decay via ordinary–exotic mixing in analogy to h decay discussed above with corresponding expressions for the various decays. For small mixing, $M_E^2 \ll M_{W,Z}^2$, and taking ν_e^c to be heavy one finds [3.3]

$$
\begin{aligned}
&B(\mathrm{E}\to \nu_e + \text{hadrons}) \simeq 47\% , \qquad B(\mathrm{E}\to \mathrm{e} + \text{hadrons}) \simeq 20\% , \\
&B(\mathrm{E}\to \nu_e \mu \bar{\nu}_\mu) = B(\mathrm{E}\to \nu_e \tau \bar{\nu}_\tau) \simeq 8\% , \\
&B(\mathrm{E}\to \nu_e \mathrm{e} \bar{\nu}_e) \simeq 10\% , \qquad B(\mathrm{E}\to \mathrm{e}\nu_\mu \bar{\nu}_\mu) = B(\mathrm{E}\to \mathrm{e}\nu_\tau \bar{\nu}_\tau) \simeq 2\% , \\
&B(\mathrm{E}\to \mathrm{ee}\bar{\mathrm{e}}) \simeq 1\% , \qquad B(\mathrm{E}\to \mathrm{e}\mu\bar{\mu}) = B(\mathrm{E}\to \mathrm{e}\tau\bar{\tau}) \simeq 1\% .
\end{aligned}
\tag{3.37}
$$

These numbers change somewhat if ν_e^c and ν_e form a Dirac neutrino, e.g., if ν is Dirac (Majorana) and all mixing angles are taken equal, then one finds $\Gamma(\mathrm{E}\to \mathrm{eZ})/\Gamma(\mathrm{E}\to \nu\mathrm{W}) = \frac{1}{4}\,(\frac{1}{2})$ for $M_\mathrm{E} \gg M_{\mathrm{W,Z}}$. When E decays via mixing, the most distinct signature for exotic lepton production is the three charged lepton final state $\mathrm{E}\to \mathrm{e}\ell^+\ell^-$.

Note that for N decays we can merely interchange the rates for E to N in the discussion above.

One of the obvious signals for the FCNC couplings suggested by the E_6 models in which the exotic fermions have conventional B and L assignments is the observation of FC decays of the Z [3.11]. Writing the FC couplings as

$$
(g/4c_\mathrm{w})[\bar{l}_i \gamma_\mu (1-\gamma_5) l_j C_{ij} + \bar{d}_i \gamma_\mu (1+\gamma_5) d_j \tilde{C}_{ij}] Z^\mu , \tag{3.38}
$$

it is clear that C_{ij}, $\tilde{C}_{ij}$ for the first and second generations must be quite small implying Z decay into these modes is highly suppressed. For example, the $\mu\to 3\mathrm{e}$ process can occur via the flavor mixing and u- and t-channel Z exchanges for which we find

$$
\mathrm{d}\Gamma/\mathrm{d}x = (G_\mathrm{F}^2 m_\mu^5/24\pi^3)|C_{\mu\mathrm{e}}|^2 [X(3x^2 - 5x^3) + Yx^3] , \tag{3.39}
$$

with $x = E_{\mathrm{e}^+}/m_\mu$ (for μ^- decay) and

$$
X = \tfrac{1}{2}[1 + (1-4x_\mathrm{w})^2] , \qquad Y = \tfrac{1}{2}(1-4x_\mathrm{w}) , \tag{3.40}
$$

so that $\Gamma(\mu\to 3\mathrm{e})/\Gamma(\mu\to \mathrm{e}\nu\bar{\nu}) = 0.4|C_{\mu\mathrm{e}}|^2 \le 1.1\times 10^{-13}$, which is the present experimental bound [3.12]. The $\mathrm{Z}\to \mathrm{e}\mu$ branching fraction is then given by

$$
\mathrm{BR}(\mathrm{Z}\to \mathrm{e}\mu) = \mathrm{BR}(\mathrm{Z}\to \mathrm{e}^+\mathrm{e}^-) 4|C_{\mu\mathrm{e}}|^2/[1 + (1-4x_\mathrm{w})^2] = 0.12|C_{\mu\mathrm{e}}|^2 \le 3.3\times 10^{-14} , \tag{3.41}
$$

following from the bound on the $\mu\to 3\mathrm{e}$ rate. FC couplings involving the third generation fermions are far less restricted by existing data so that FC Z decays involving them are potentially observable. Data from the ARGUS collaboration on rare τ decays [3.13] can be used to constrain $|C_{\tau\mathrm{e}}|$ and $|C_{\tau\mu}|$. They find $\mathrm{BR}(\tau\to 3\mu) < 2.9\times 10^{-5}$; $\mathrm{BR}(\tau\to \mathrm{e}2\mu)$, $\mathrm{BR}(\tau\to \mu 2\mathrm{e}) < 3.3\times 10^{-5}$; and $\mathrm{BR}(\tau\to 3\mathrm{e}) < 3.8\times 10^{-5}$, from which one obtains $|C_{\tau\mu}|^2 < 3.5\times 10^{-4}$ and $|C_{\tau\mathrm{e}}|^2 < 2.8\times 10^{-4}$, implying

$$
\mathrm{BR}(\mathrm{Z}\to \tau\mathrm{e}) \le 3.2\times 10^{-5} , \qquad \mathrm{BR}(\mathrm{Z}\to \tau\mu) \le 4.2\times 10^{-5} . \tag{3.42}
$$

A possible signature for such decays is $\mathrm{Z}\to \tau\ell \to \pi\nu_\tau\ell$ or $\rho\nu_\tau\ell$. An obvious background comes from $\mathrm{Z}\to \tau^+\tau^- \to \tau\nu_\tau\nu_\ell\ell$ where the ν's are soft and ℓ and τ appear back-to-back. If the lepton energy can be measured to an accuracy of 1 GeV and the angle between the τ and ℓ measured to an accuracy of 10 mrad (1 mrad) then the branching fraction for the background is $3\times 10^{-6}(2\times 10^{-7})$. At a Z factory,

such decays should be observable if 10^7 Z's can be collected and if $|C_{\tau\mu}|$ and $|C_{\tau e}|$ are not too far from their present upper bounds. Similarly, the constraints from $b\to q\ell^+\ell^-$ [3.14] ($BR \le 2.4\times 10^{-3}$) place a bound on $\Sigma |C_{bq}|^2$ and results in $BR(Z\to bq) \le 9.6\times 10^{-5}$. Modes such as this are, of course, much more difficult to see than $\tau\mu$ or τe due to the more severe hadronic background.

3.1.2. h-leptoquarks

In this case h has $B(h) = +\frac{1}{3}$, $L(h) = +1$, $R = -1$, and has interactions which are given by the superpotential terms

$$W_1 = \lambda_6 h u^c e^c + \lambda_7 L h^c Q + \lambda_8 \nu^c h d^c , \tag{3.43}$$

with unknown coupling strength λ_i. Since the couplings λ_i are generation dependent, there is the possibility of flavor universality violations. However, intergenerational Yukawa couplings are highly suppressed from FCNC constraints (as will be discussed in section 3.3) and here we will employ generation conserving couplings only. Mixing with the ordinary down-type quarks is not possible for leptoquarks (as it would violate B and L), so either $\langle \tilde{\nu}^c \rangle = 0$ and $L(\nu^c) = +1$, or we constrain $\lambda_8 = 0$. Note that here, it is the spin-$\frac{1}{2}$ h which has odd R-parity (called a leptoquarkino) and hence decays into supersymmetric particles, while the scalar $\tilde{h}$ (leptoquark) has even R-parity and couples to an ordinary lepton–quark pair. The tree level decays of the h leptoquarkino are then

$$h\to d\tilde{\nu}, \quad h\to \tilde{d}\nu, \quad h\to u\tilde{e}, \quad h\to \tilde{u}e, \tag{3.44}$$

where the super-partner final states may be real or virtual, depending on the relative mass spectrum. If squark and slepton final states are kinematically allowed, then the partial width of $h\to f\tilde{f}'$ for a real $\tilde{f}'$ has the generic form [3.15] (neglecting the mass of f)

$$\Gamma(h\to f\tilde{f}') = (\lambda_i^2/32\pi)K(\chi)M_h(1-\tilde{M}^2/M_h^2)^2 , \tag{3.45}$$

where $\tilde{M}$ is the mass of $\tilde{f}'$ and $K(\chi)$ is a mixing angle factor due to the left–right mixing of the scalar states $\tilde{f}'$. If real $\tilde{f}'$ states are not kinematically accessible then a variety of three-body final states are possible,

$$h\to u\nu\tilde{W}, \quad h\to de\tilde{W}, \quad h\to ue\tilde{Z}, \quad h\to d\nu\tilde{Z}, \quad h\to ue\tilde{\gamma}, \quad h\to d\nu\tilde{\gamma}, \tag{3.46}$$

with relative rates depending on the actual squark or slepton supersymmetric decay chains. The partial width for $h\to q\ell\tilde{\chi}$, including contributions from $h\to \tilde{h}\tilde{\chi}$, where $\tilde{\chi}$ is the lightest neutralino, is found to be (in the limit $M_h \ll M_{\tilde{q}}, M_{\tilde{\ell}}$ and neglecting $M_{\tilde{\chi}}$) [3.16]

$$\Gamma(h\to q\ell\tilde{\chi}) = \frac{3e^2M_h^5}{192\pi^3}\left[\lambda_7^2\left(\frac{1}{M_{\tilde{e}_L}^4} + \frac{(\frac{2}{3})^2}{M_{\tilde{u}_L}^4} + \frac{(-\frac{1}{3})^2}{M_{\tilde{d}_L}^4} - \frac{2(\frac{2}{3})}{M_{\tilde{u}_L}^2 M_{\tilde{e}_L}^2}\right)\right.$$
$$\left. + \lambda_6^2\left(\frac{1}{M_{\tilde{e}_R}^4} + \frac{(-\frac{2}{3})^2}{M_{\tilde{u}_R}^4} + \frac{2(-\frac{2}{3})}{M_{\tilde{e}_R}^2 M_{\tilde{u}_R}^2}\right)\right] . \tag{3.47}$$

The exact amplitude for this mode is given in this reference.

The scalar $\tilde{h}$ leptoquark has the decay modes

$$\tilde{h} \to ue\,, \qquad \tilde{h} \to d\nu\,, \tag{3.48}$$

with partial widths (for massless final states)

$$\Gamma_{\tilde{h}} = (\lambda_6^2 + \lambda_8^2) M_{\tilde{h}}/16\pi\,, \qquad \Gamma_{\tilde{h}^c} = 2\lambda_7^2 M_{\tilde{h}}/16\pi\,, \tag{3.49}$$

neglecting $\tilde{h}$–$\tilde{h}^c$ mixing factors. Since the coupling strengths are unknown, the λ_i are usually scaled to α_{em} for calculational purposes.

It is also possible that the heavier of h and $\tilde{h}$ could decay into the lighter plus a neutralino, i.e., $\tilde{h} \to h\tilde{\chi}$ or $h \to \tilde{h}\tilde{\chi}$. Chargino final states are not allowed since h is an iso-singlet.

3.1.3. h-diquarks

For this assignment we have $B(h) = -2/3$, $L(h) = 0$, and $R = -1$. The relevant superpotential terms are

$$W_2 = \lambda_9 hQQ + \lambda_{10} h^c u^c d^c\,, \tag{3.50}$$

where the coupling strengths are set by the undetermined Yukawa factors λ_i. Intergenerational couplings are restricted from FCNC processes. The spin-$\frac{1}{2}$ h again has odd R-parity and supersymmetric decay modes (and is called a diquarkino), and the scalar $\tilde{h}$ (diquark) has even R-parity and decays into an ordinary quark pair. The h diquarkino has the following tree level decays

$$h \to \bar{u}\bar{\tilde{d}}\,, \qquad h \to \bar{\tilde{u}}\bar{d}\,, \tag{3.51}$$

where the relative mass spectrum again determines whether the u- or d-squarks are real or virtual. In the case where the direct two-body decays are forbidden, the dominant three-body final states are

$$h \to \bar{u}\bar{u}\tilde{W}\,, \qquad h \to \bar{u}\bar{d}\tilde{Z}\,, \qquad h \to \bar{d}\bar{d}\tilde{W}\,, \qquad h \to \bar{u}\bar{d}\tilde{\gamma}\,, \tag{3.52}$$

where $\tilde{q} \to \tilde{g}q$ contributions have been neglected and the rates depend on the relative SUSY decays. The process $h \to \tilde{h}\tilde{\chi} \to \bar{u}\bar{d}\tilde{\chi}$ may also contribute to the above, if kinematically allowed. The exact amplitude for $h \to \bar{q}\bar{q}\tilde{\chi}$ is calculated in ref. [3.16] and simplifies to

$$\Gamma(h \to \bar{q}\bar{q}\tilde{\chi}) = \frac{e^2 M_h^5}{192\pi^3}\left[\lambda_{10}^2\left(\frac{(\frac{1}{3})^2}{M_{\tilde{d}_R}^4} + \frac{(-\frac{2}{3})^2}{M_{\tilde{u}_R}^4} + \frac{2(\frac{1}{3})(-\frac{2}{3})}{M_{\tilde{d}_R}^2 M_{\tilde{u}_R}^2}\right) + \lambda_9^2\left(\frac{(-\frac{1}{3})^2}{M_{\tilde{d}_L}^4} + \frac{(\frac{2}{3})^2}{M_{\tilde{u}_L}^4} + \frac{2(-\frac{1}{3})(\frac{2}{3})}{M_{\tilde{d}_L}^2 M_{\tilde{u}_L}^2}\right)\right], \tag{3.53}$$

in the $M_h \ll M_{\tilde{q}}$ and massless $\tilde{\chi}$ limit.

The scalar $\tilde{h}$ diquark decays via

$$\tilde{h} \to \bar{u}\bar{d}\,, \tag{3.54}$$

with the partial widths

$$\Gamma_{\tilde{h}} = 4\lambda_9^2 M_{\tilde{h}}/16\pi\,, \qquad \Gamma_{\tilde{h}^c} = \lambda_{10}^2 M_{\tilde{h}}/16\pi\,, \tag{3.55}$$

with $\tilde{h}$–$\tilde{h}^c$ mixing factors neglected.

3.2. Constraints on exotic fermion masses

In this section we review the bounds which can be placed on the masses of the exotic fermions from current collider data and various theoretical models. Additional limits on the masses and couplings that can be obtained from rare processes are extensively discussed in section 3.3.

Before we turn our attention to specific experimental searches and theoretical calculations, let us examine the expected exotic mass spectrum due to the ordering of the vev's of the various Higgs fields. In the case where the Higgs fields are contained in the **27**, one can see from the superpotential W, eq. (1.4), that h acquires its mass through the non-zero vev $\langle \tilde{S}^c \rangle$. Since the Z′ mass is also generated by $\langle \tilde{S}^c \rangle$, it is reasonable to expect that h will have a mass of the same order as $M_{Z'}$. However, this same argument applied to the SM would imply that $m_e \sim M_W$; hence h could be lighter than the Z′ if the Yukawa coupling λ_5 is appropriately small. Note that the h masses are completely independent of those for the ordinary quarks and leptons (since they are generated by different Yukawa couplings and vev's), and that the limits from neutral current phenomenology (which set $\langle \tilde{S}^c \rangle > \langle \tilde{N} \rangle, \langle \tilde{N}^c \rangle$) explain the present experimental non-observation of h. The mass spectrum of the scalar partner $\tilde{h}$ is more complicated [3.16], with two possible hierarchies

$$M_{h_a} < M_{\tilde{h}_a^1} < M_{\tilde{h}_a^2}\,, \qquad M_{\tilde{h}_a^1} < M_{h_a} < M_{\tilde{h}_a^2}\,, \tag{3.56}$$

where a is a generation index, and the labels 1, 2 denote the mass eigenstates of the left- and right-handed $\tilde{h}$. Obviously there is large freedom in the h, $\tilde{h}$ mass spectrum, and it is possible that they could be as light as the present e^+e^- collider data allows.

3.2.1. Current collider data

3.2.1.1. Direct production. First we summarize the relevant bounds from direct experimental searches. The present limits on the production of new fermions in e^+e^- annihilation are from TRISTAN [3.17] and are determined from the ratio $R = \sigma(e^+e^- \to \bar{f}f)/\sigma(e^+e^- \to \mu^+\mu^-)$, a jet distribution analysis, or a search for high p_T leptons; the relevant bounds are $M_{-1/3} > 23.8$–26.7 GeV for a new color triplet, $Q = -\frac{1}{3}$ fermion and $M_{-1} > 25.5$–27.6 GeV for a new color singlet, $Q = -1$, unstable fermion with an associated massless neutrino. However, the neutral fields N and N^c can, in principle, be much lighter [3.18]. The production of these fields in e^+e^- annihilation only proceeds through Z exchange and is more difficult to observe for $\sqrt{s} < M_Z$. The ratio of the production cross section $\sigma(e^+e^- \to N\bar{N})$ to $\sigma_{pt}\,(= 4\pi\alpha^2/3s)$ is only $\simeq 8 \times 10^{-3}$ at $\sqrt{s} = 30$ GeV for $M_N \lesssim 10$ GeV, but increases to $\simeq 2.0$ at $\sqrt{s} = 75$ GeV for $M_N \lesssim 35$ GeV. Also, mixing between N and ν_e states can result in single N production for which the single production R ratio, scaled by the appropriate mixing factors, is given by $R^{N\nu}/(s_\nu c_\nu)^2 \equiv \sigma(e^+e^- \to N\bar{\nu} + \bar{N}\nu)/\sigma_{pt}(s_\nu c_\nu)^2 \simeq 8 \times 10^{-3}$ (2.0) at $\sqrt{s} = 30$ (75) GeV for $M_N \lesssim 5$ (25) GeV, where s_ν (c_ν) $= \sin\theta_\nu^R$ ($\cos\theta_\nu^R$) represents the amount of ordinary–exotic mixing. Clearly these production rates become quite small once the mixing is included. Combining all these results together, PEP and PETRA data exclude N's for $10\,\text{MeV} \lesssim M_N \lesssim 3 \sim 14$ GeV [3.18].

Constraints have also been placed on the production of scalar leptoquarks in e^+e^- annihilation. The JADE Collaboration at PETRA has reported [3.19] a search of their data for events of the type $e^+e^- \to \tilde{h}\bar{\tilde{h}} \to \mu^+\mu^-$ + hadrons and have excluded masses in the range 5–20.8 GeV for leptoquarks which decay exclusively into second generation fermions. The UA1 Collaboration at the CERN collider has looked for an excess of events with signatures of (a) $\mu^+\mu^-$ + two jets, (b) $\mu^\pm + \not{p}_T$ + two jets, or (c) $\not{p}_T$ + jet(s) and has placed a limit of $M > 33$ GeV for second generation scalar leptoquarks [3.20].

Barger et al. [3.3] have studied two signatures of $h\bar{h}$ production at the CERN $Sp\bar{p}S$ collider and have set limits on the first generation of h quarks. The first signature arises from the charged current semileptonic decay of either the h or $\bar{h}$, resulting in a single-lepton signal. For a branching fraction $B(h \to ue\bar{\nu}_e) \simeq 8\%$, an integrated luminosity of $0.39\,pb^{-1}$, an efficiency of 50%, and the isolated electron acceptance cuts of the UA1 top-quark search, the resulting number of expected events of the type e + n jets is of order 13–20 with $n \geq 2$ and 6–8 with $n \geq 3$. Comparison of this with the UA1 data of 13 events with $n \geq 2$ and 4 events with $n \geq 3$ yields the limit $M_h \gtrsim 30$ GeV. The second signature of dimuons from charged current decays of both h and $\bar{h}$ and neutral current decays of either h or $\bar{h}$ yields no constraint since the predicted number of events is far below the number of dimuon events in the present UA1 data sample.

The UA1 collaboration limit on the mass of a charged, fourth generation, heavy lepton, L, of $M_L > 41$ GeV [3.21], can be used to extract constraints on both the charged and neutral E_6 exotic leptons, E and N [3.22]. For the mass regions where $M_E + M_N \leq M_W$ and $M_E > M_N$, and in the limit of small ordinary–exotic mixing (i.e., if N is sufficiently long-lived to appear as missing energy in the detector), the process

$$\begin{array}{l} W \to E + N \\ \quad\quad\; \big\lfloor \to N q\bar{q} \end{array} \tag{3.57}$$

will appear quite similar to that of fourth generation lepton production and decay. Since the ordinary–exotic mixing is very well bounded (as discussed in the previous section) the following ratio

$$R = \frac{\Gamma(W \to EN)}{\Gamma(W \to L\nu)} \frac{B(E \to Nq\bar{q})}{B(L \to \nu q\bar{q})} \frac{\Gamma(E \to Nq\bar{q})_w}{\Gamma(E \to Nq\bar{q})_{wo}} \frac{\Gamma(L \to \nu q\bar{q})_{wo}}{\Gamma(L \to \nu q\bar{q})_w} \tag{3.58}$$

can be used to constrain the E and N masses for the above mass regions. R is a measure of the number of events produced from the $W \to EN$ process as compared to $W \to L\nu$. The subscripts w and wo denote widths that are calculated with and without the UA1 energy cuts, respectively. Figure 41 from ref. [3.22] shows the allowed region in the M_E–M_N plane which corresponds to $R \leq 1$ for one or three generations of exotic leptons with N being a Majorana or Dirac neutrino. As can be seen from the figure reasonably strong constraints on M_E and M_N are obtained.

3.2.1.2. Indirect production. Limits on the couplings and mass of scalar leptoquarks have been obtained [3.23] by examining the indirect effects of the virtual exchange of these particles in the process $e^+e^- \to q\bar{q}$. Besides the usual s-channel γ and Z exchange, leptoquarks will also contribute to this process via t-channel exchange. For calculational purposes the leptoquark Yukawa couplings [as given in eq. (1.4)] are generally scaled to the electromagnetic coupling, e, by

$$\lambda^2/4\pi = F\alpha\,, \tag{3.59}$$

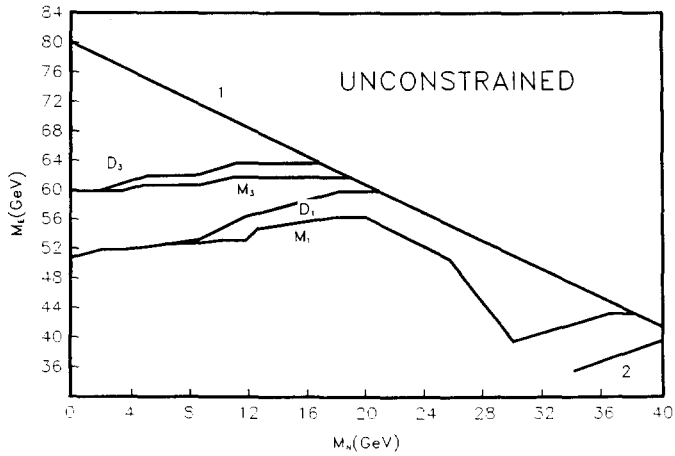

Fig. 41. Regions for which $R \leq 1$ for one or three generations of exotics where N is a Dirac (D) or Majorana (M) neutrino. The allowed regions lie above the curves. Curve 1 corresponds to $M_E + M_N = M_W$ and curve 2 to $M_E = M_N$.

where $\lambda_6 = \lambda_7 = \lambda$ has been taken for simplicity. However, here we shall consider the possibility that $\lambda_6 \neq \lambda_7$ and allow for more general left- and right-handed couplings. Taking the unknown $\tilde{h}\ell q$ coupling to be $A + B\gamma_5$ we then parameterize its strength by

$$k \equiv (|A|^2 + |B|^2)/e^2 , \qquad k' \equiv 2\,\mathrm{Re}(A^* B)/e^2 . \tag{3.60}$$

The differential cross section for $e^+e^- \to q\bar{q}$ is then given by

$$\frac{d\sigma}{d\cos\theta} = \frac{3\pi\alpha^2}{2s}\left(\sum_{i,j} s^2 P_{ij}^{ss}[B_{ij}(1+\cos^2\theta) + 2C_{ij}\cos\theta] \right.$$

$$\left. + \frac{2u^2}{u-M^2}\sum_i \frac{R_i}{s}[k(v_e^i v_q^i + a_e^i a_q^i) + k'(v_e^i a_q^i + a_e^i v_q^i)] + \frac{k^2u^2}{(u-M^2)^2}\right), \tag{3.61}$$

where $u = -\frac{1}{2}s(1+\cos\theta)$, P_{ij}^{ss}, B_{ij}, and C_{ij} are defined in eq. (2.42), R_i is defined in eq. (2.57), the sum over $i\,(j) = (0, 1)$ extends over the neutral gauge bosons γ and Z, respectively, M is the mass of the scalar leptoquark, and the couplings are normalized as

$$\mathcal{L} = e\bar{f}\gamma_\mu(v_i - a_i\gamma_5)fZ_i^\mu . \tag{3.62}$$

A limit on M as a function of k (and k') can be obtained by demanding that neither the total cross section nor the forward–backward asymmetry deviate from the PEP and PETRA data on charm and bottom production (and hence that these quantities do not deviate significantly from their SM predictions). Figure 42 from ref. [3.23] displays these constraints (with $k = k'$) for deviations of not more than 10% (5%) from the data for the curve on the left (right). Small leptoquark masses (<200 GeV) with large couplings ($k \gtrsim 0.5$) are excluded, but the constraints for larger masses are not very strong, as one might expect.

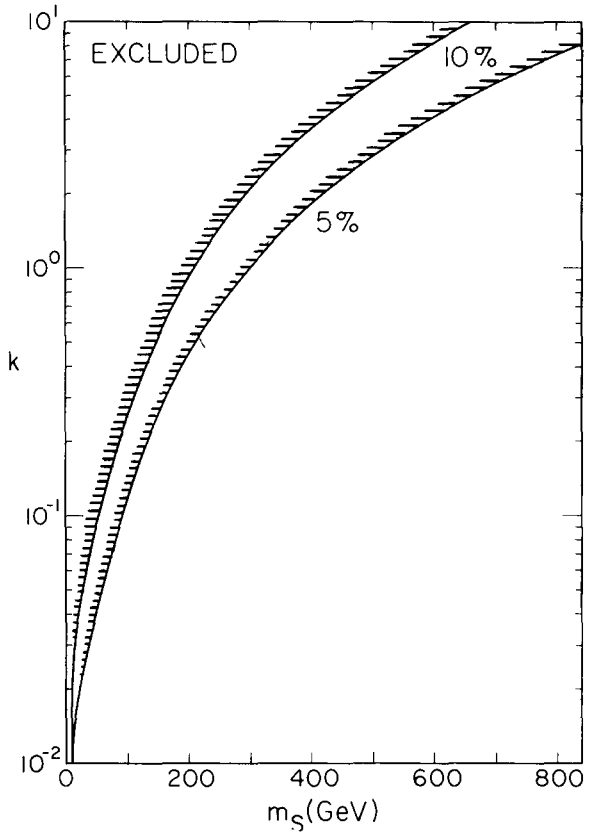

Fig. 42. Constraints on the scalar leptoquark mass as a function of the leptoquark coupling scale parameter, k, as described in the text.

3.2.1.3. Ratio of W to Z events. It is well known that a measurement of the ratio

$$R \equiv \sigma(p\bar{p} \to W^{\pm} \to \ell\nu)/\sigma(p\bar{p} \to Z \to \ell^+\ell^-) \tag{3.63}$$

can be used to extract information on the number of light neutrinos, N_ν [3.24]. However, this ratio can also yield information on new physics, and several authors [3.25] have placed constraints on the exotic fermions using this technique. R is theoretically calculable via

$$R = \frac{\sigma(p\bar{p} \to W^{\pm})}{\sigma(p\bar{p} \to Z)} \frac{\Gamma(W \to \ell\nu)}{\Gamma(Z \to \ell^+\ell^-)} \frac{\Gamma_Z}{\Gamma_W}, \tag{3.64}$$

where $\Gamma(W \to \ell\nu)$ and $\Gamma(Z \to \ell^+\ell^-)$ are completely determined within the SM. The ratio of cross sections in eq. (3.64) is calculable in QCD but is dependent upon the choice of parton distribution functions, e.g., the structure functions of Duke and Owens (DO) [3.26] lead to significantly larger values of this ratio than those of Eichten et al. (EHLQ) [3.27]. Γ_Z and Γ_W depend upon the masses and couplings of *all* new particles which may be light enough to be decay products of the W and/or Z, such as the top quark, additional neutrinos, supersymmetric partners, h, E, or N.

For the case of the h quark, in the absence of ordinary–exotic mixing (hence h only contributes to Γ_Z and not to Γ_W), a comparison of the UA2 data on R [3.28] ($R \leq 10.42$ at 95% CL) with the theoretical

calculation, using the EHLQ set II structure functions and including the QCD radiative corrections to Γ_W and Γ_Z, yields no constraints on M_h for $N_\nu = 4, 5, 6$ if the top quark mass is less than 70–72, 60–62, 52 GeV, respectively, and no limits at all if $N_\nu = 3$ as can be seen in fig. 43 from ref. [3.25]. Note that the EHLQ distribution functions yield the most conservative limits since they give the smallest value for the cross section ratio. The constraints on M_h from this procedure are rather weak (especially when compared to the limits obtained from a similar analysis on the mass of a fourth generation $Q = -\frac{1}{3}$ quark) since the couplings of h to the Z are rather small. However, significant improvements in the experimental data for R would tighten these constraints considerably assuming also an improvement in our knowledge of the structure functions. If the ordinary–exotic mixing (as well as more than one generation of non-degenerate exotics) is included in this analysis, then no useful limits are obtained due to the proliferation of parameters. However, if the mixing is constrained to be small from the absence of FCNC's, then its effect on this calculation is minimal. When the N and E exotics are also included, mass limits from R have been obtained for two different scenarios (with $m_t = 40$ GeV). For three completely degenerate generations of exotics ($M_h = M_E = M_N = M$), $M < M_Z/2$ is excluded if N is a Dirac fermion and $M \leq 31$ GeV is excluded if N is Majorana. In the case of Dirac N's, the inclusion of three degenerate generations of exotics can increase the total Z width by as much as 50%. For the case where all three generations of exotics are degenerate but the masses differ within each generation ($M_h = M_E \neq M_N$) the restrictions are $M_N \geq 30$ GeV if N is Majorana and $M_N \geq 44$ GeV if N is Dirac.

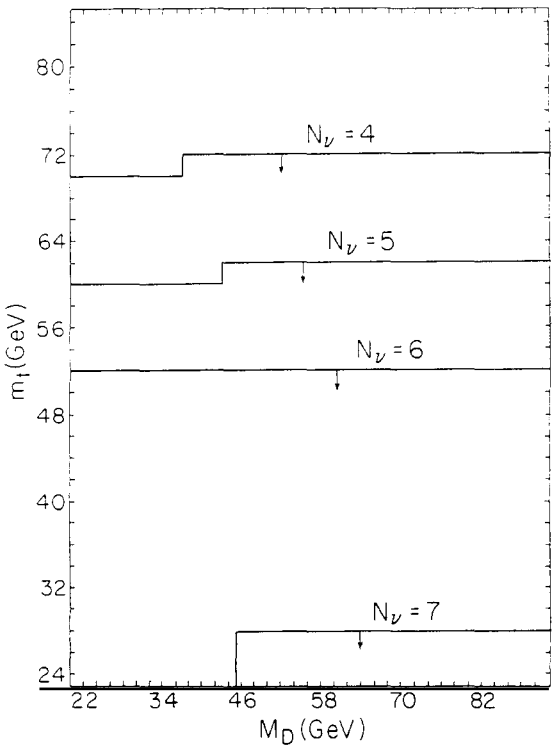

Fig. 43. Allowed regions in the $M_D(m_b)$–m_t plane for different N_ν values using EHLQ II structure functions and $\alpha_s = 0.10$, $x_w = 0.23$, $M_W = 81$ GeV, and $M_Z = 92$ GeV.

3.2.1.4. ρ parameter shift. The existence of new heavy fermions would produce a measurable shift in the value of the ρ parameter ($\rho = M_W^2/M_{Z_1}^2 \cos^2\theta_w$). The heavy fermions contribute to the shift, $\Delta\rho$, via the usual one-loop vacuum-polarization diagrams. Since the exotics are vector-like particles, the usual calculation for $\Delta\rho$ does not apply in this case and a complete analysis for general vector and axial-vector couplings must be performed [3.29]. The results are presented in figs. 44a, b for the contributions from three degenerate generations of N's and E's ($M_E \neq M_N$) which are consistent with the UA1/UA2 Collaboration data of $|\Delta\rho| \leq 0.02\,(0.05)$ [3.28]. Also shown in the figures is the e^+e^- annihilation bound for charged particle production (curve 1) and the limits (curve 2) $M_N \geq 30\,(44)$ GeV if N is Majorana (Dirac) which are obtained from the ratio R as discussed in the previous paragraph. Note that bounds are not placed on h, as h is a vector-like isosinglet and thus does not contribute to $\Delta\rho$.

3.2.2. Theoretical estimates

3.2.2.1. Perturbative unitarity. Perturbative unitarity constraints on the partial-wave decomposition of scattering amplitudes have been used to place limits on the masses of vector leptons [3.30]. Partial-wave unitarity requires that the lth partial wave satisfies $|a^l| \leq 1$, where a^l is proportional to the angular integration of the scattering amplitudes. A calculation of the tree-level amplitudes for $F\bar{F} \rightarrow F\bar{F}$,

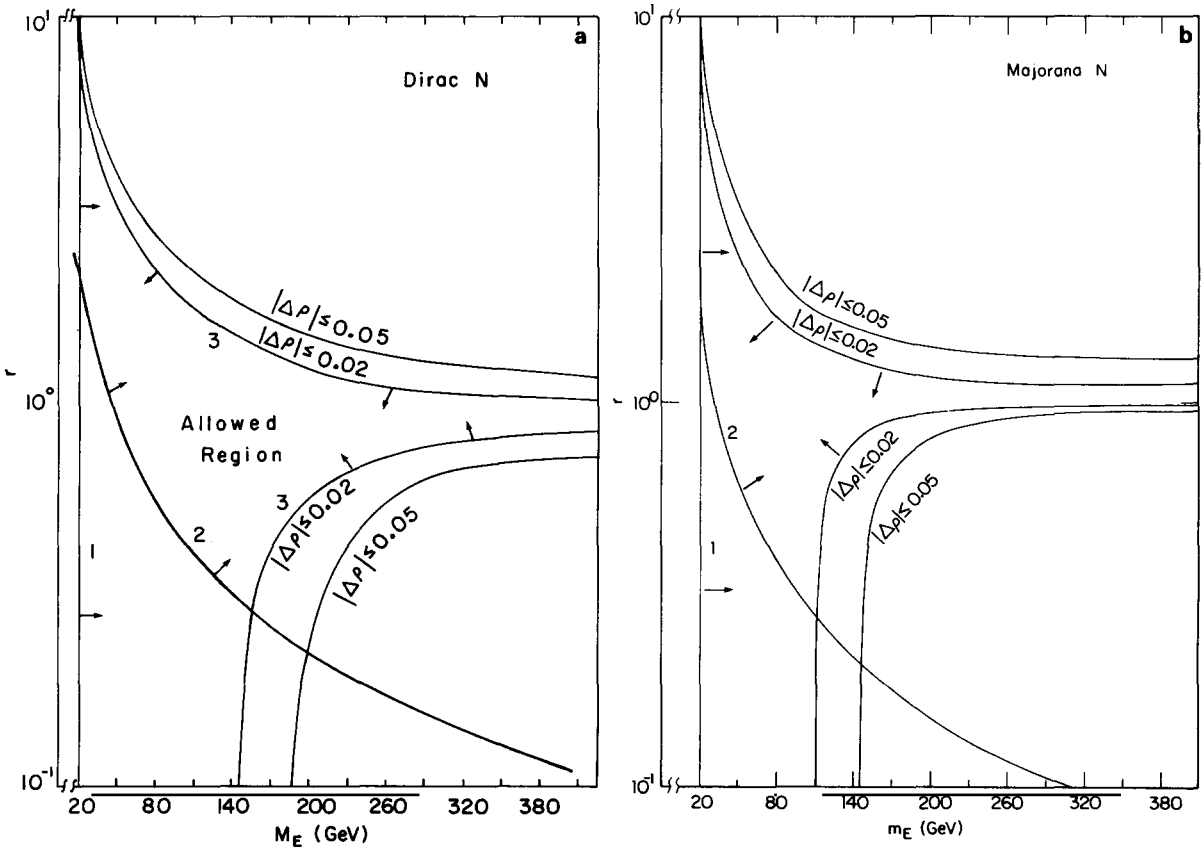

Fig. 44. Contributions to $\Delta\rho$ as allowed by UA1/UA2 data for $r \equiv M_N/M_E$ as a function of M_E for N (a) Dirac or (b) Majorana.

where here F = E or N, and a search for unitarity violation at high energies ($s \to \infty$) yields

$$M_E^2 \sin^4\theta_e \leq 4\pi\sqrt{2}/G_F\,, \tag{3.65}$$

where θ_e is the ordinary–exotic mixing angle. In the absence of mixing there is obviously no bound, and if the mixing scales as $\sin\theta_e \sim M_e/M_E$ there is again no unitarity bound. This constraint is proportional to the mixing because the unitarity violating partial wave depends solely on the axial-vector coupling to the Z and for vector leptons an axial-vector coupling can only be induced via ordinary–exotic mixing. Z′ exchange was not considered in this reference, and if included, would most likely result in a similar restriction as that discussed below. The processes $E\bar{E} \to N\bar{N}$, $e^-E^+ \to W^+W^-$, ZZ, HH, ZH, and $\nu\bar{N} \to W^+W^-$ were also examined, but the non-zero amplitudes are again all proportional to some power of $M_E \sin\theta_e$. No mixing independent bound results from this study.

Similarly, bounds can be obtained on the masses of h quarks [3.31]. Considering the elastic scattering $h_+\bar{h}_+ \to h_+\bar{h}_+$ (where ± denotes the fermion helicity state) with Z′ and Higgs exchange only (in a simplified model with only one Higgs doublet and Higgs singlet), unitarity of the 0th partial wave places the constraint $M_h \lesssim 17.4\, M_{Z'}$ in the rank-5 model. s-channel Z exchange is again dependent on the axial vector $h\bar{h}Z$ coupling which is non-zero only if the h–d mixing is non-vanishing. Constraints on the mixing induced partial wave amplitude for Z exchange then places the restriction $M_h \lesssim (1.2\,\text{TeV})/\sin^2\theta_d$.

3.2.2.2. Perturbative unification. Constraints on the exotics can be set by requiring that their couplings remain perturbative (i.e., not grow too large) at the GUT scale. Drees and Tata [3.32] have studied the renormalization group evolution of the Yukawa couplings for two generations of the neutral exotics, N, N^c, and S^c (the third generation being associated with the Higgs fields) in the class of rank-5 E_6 models where the mass matrix of the neutral exotics decouples from the gaugino–higgsino sector. In the absence of an intermediate scale, the mass scale for the lightest of these neutral exotics is found to be set by M_W rather than by $M_{Z'}$, and an absolute upper bound on this mass obtained from this analysis is $M \lesssim 115$ GeV. The bounds set from this procedure depend on the mass of E and the ratio of vev's, $w \equiv \langle\tilde{N}^c\rangle/\langle\tilde{N}\rangle$, with the weakest constraint of $M \lesssim 115$ GeV given when $M_E \simeq 20$ GeV and $w = 1$. For larger values of M_E and w the bound on M becomes even stronger, e.g., for $M_E = 200$ GeV and $w = 3$, M is constrained by $M \lesssim 35$ GeV. In models with an intermediate scale, these bounds could still hold if $\langle\tilde{S}^c\rangle$ and not $\langle\tilde{\nu}^c\rangle$ were responsible for the breaking of the extra U(1) at the weak scale.

An examination of the infrared fixed points of the renormalization group evolution of the couplings λ_4 and λ_5 [as defined in eq. (1.4)] also results in the limits [3.33]

$$M_h^{\text{heavy}} \lesssim 3.1\, M_{Z_2}\,, \qquad M_E^{\text{heavy}} \lesssim 2.2\, M_{Z_2}\,, \tag{3.66}$$

where "heavy" is defined as the heaviest h and E of the three generations of h's and E's, and

$$M_h^{\text{light}} \lesssim 2.1\, M_{Z_2}\,, \qquad M_E^{\text{light}} \lesssim 1.8\, M_{Z_2}\,, \tag{3.67}$$

where "light" denotes the lightest particle of the three generations. These results hold in E_6 models without an intermediate scale and where the third generation of $\tilde{S}^c$ gives a mass to h and E.

3.3. Rare processes and indirect effects

Processes which are rare or forbidden in the SM have proven themselves useful in placing constraints on or perhaps even eliminating new physics beyond the SM. For instance, the lack of experimental evidence of proton decay prompted the exclusion of SU(5) as a viable GUT [1.3], and the absence of FCNC assisted in the demise of the original extended technicolor theories [3.34]. New and more sensitive rare process experiments have either begun taking data or are on the horizon [3.35] and are on the verge of being able to detect possible SUSY [1.6] and/or fourth generation [3.36] effects. Existing data can already place restrictions on the exotic fermion sector of E_6 theories and the promise of new data may even reveal their presence.

The question of proton decay is worth examining in more detail. As previously discussed, certain terms in the superpotential cannot simultaneously exist in order to ban baryon number violating dimension-four operators which would mediate rapid proton decay. In SU(5) GUTS, nucleon decay is mediated by super-heavy gauge bosons at a scale of $M_X \sim 5 \times 10^{14}$ GeV, while in E_6 theories the mass of the corresponding superheavy gauge bosons is set by the compactification scale, rendering the resulting baryon decay rate unobservable. Dimension-five baryon number violating operators which consist of fields from the **27** alone are found [3.37, 3.38] not to be invariant under the E_6 low-energy gauge group which contains (at least) one extra U(1). Survivors from the additional $\overline{\mathbf{27}}$'s could invoke nucleon decay at the one-loop level if one assigns opposite baryon numbers to each member in the $\overline{\mathbf{27}}$ and the corresponding **27**. In summary, proton decay in E_6 models is rather problematic and is not predicted to occur at observable rates.

A comprehensive analysis of the contributions from the exotic fermions to the FCNC rare processes and precision tests from low-energy K, D, B, and μ physics, *CP* violation, and weak universality is given in Campbell et al. [3.38]. These authors consider the effects of each term in the superpotential (1.4) (i.e., for all possible quantum number assignments of the exotics) on a variety of processes relevant for each type of coupling in the rank-5 model. Comparison of these E_6 contributions to current experimental data for each process places shared constraints on the Yukawa couplings and the mass of the new particles involved. Table 3, from this reference, summarizes their results, where each column represents a term of the superpotential and each rare process examined is listed in the rows. The elements in the table are the bounds which can be placed on the couplings from comparison of the E_6 contributions to experimental data for each process, assuming the specific mass values, $M_{Z'} = 300$ GeV, $M_H = 100$ GeV, and $M_h = 300$ GeV. These limits have been obtained in a generation independent manner. A dashed entry indicates that the particular coupling does not contribute to the interaction, while the question marks listed under $D \to \mu e + X$ denote the coupling restrictions that could be set if experimental bounds for $D \to \mu e + X$ could be obtained which were comparable to those for the decay $D \to \mu\mu$ [$B(D \to \mu\mu) < 1.1 \times 10^{-5}$ [3.39]]). The bottom row of the table displays the best bounds on the real and imaginary parts of each coupling and the process from which it was derived. None of these constraints present any phenomenological difficulties or rule out certain models. Although this analysis is seemingly complete, we point out that coupling restrictions obtained in this manner are generally quite dependent on the masses of the new fermions, gauge bosons, and Higgs bosons which may be present in the interaction, and that the tabulated results only hold for the specific mass values assumed.

In addition to the above analysis, may other authors have also, perhaps more carefully, examined exotic fermion contributions to certain rare processes. We now explore these other studies for each B and L assignment.

Table 3

Constraints on the Yukawa couplings from flavor-changing neutral currents and other rare processes. ε_L and ε_R are the coefficients of the left- and right-handed flavor-changing coupling constants of the Z′, respectively

			Superpotential term									
			1	2	3	4	5	6	7	8	9	10
		Rare process	$\lambda_1 H^c Q u^c$	$\lambda_3 H L e^c$	$\lambda_2 H Q d^c$	$\lambda_9 h Q Q$	$\lambda_{10} h^c u^c d^c$	$\lambda_6 h u^c e^c$	$\lambda_7 L h^c Q$	$\lambda_8 \nu^c h d^c$ $\langle 0\vert\tilde{\nu}^c\vert 0\rangle = 0$	ε_L $\langle 0\vert\tilde{\nu}^c\vert 0\rangle \neq 0$	ε_R $\langle 0\vert\tilde{\nu}^c\vert 0\rangle \neq 0$
K physics	1	$K^0 \leftrightarrow \bar{K}^0$	–	–	3×10^{-5}	0.1	0.1	–	0.1	0.1	1×10^{-2}	3×10^{-2}
	2	$K_L \rightarrow \mu^+ \mu^-$	–	$\sqrt{\lambda_3 \lambda_2} < 8 \times 10^{-4}$		0.4	0.4	–	0.6	0.2	6×10^{-3}	3×10^{-2}
	3	$K \rightarrow \pi \bar{\nu} \nu$	–	–	–	–	–	–	0.2	0.2	2×10^{-2}	0.1
	4	$K \rightarrow \pi e^+ e^-$	–	$\sqrt{\lambda_3 \lambda_2} < 8 \times 10^{-3}$		0.9	0.9	–	–	–	–	–
	5	$K_L \rightarrow \mu^\pm e^\mp$	–	$\sqrt{\lambda_3 \lambda_2} < 6 \times 10^{-4}$		–	–	–	–	–	–	–
	6	$K^+ \rightarrow \pi^+ \mu^\pm e^\mp$	–	$\sqrt{\lambda_3 \lambda_2} < 2 \times 10^{-3}$		–	–	–	–	–	–	–
D physics	7	$D^0 \leftrightarrow \bar{D}^0$	2×10^{-4}	–	–	0.1	0.1	0.1	0.1	–	–	–
	8	$D^0 \rightarrow \mu^+ \mu^-$	$\sqrt{\lambda_1 \lambda_2} < 6 \times 10^{-2}$		–	–	–	–	–	–	–	–
	9	$D^0 \rightarrow \mu^\pm e^\mp$	$\sqrt{\lambda_1 \lambda_2} < 6 \times 10^{-2}$		–	–	–	2	2	–	–	–
	10	$D \rightarrow \mu^\pm e^\mp X$	$\sqrt{\lambda_1 \lambda_2} < 0.2$?		–	–	–	1.0?	1.0?	–	–	–
B physics	11	$B^0 \leftrightarrow \bar{B}^0$	–	–	1×10^{-4}	0.1	0.1	–	0.1	0.1	1×10^{-2}	3×10^{-2}
μ physics	12	$\mu N \rightarrow eN$	–	$\sqrt{\lambda_3 \lambda_2} < 8 \times 10^{-4}$		–	–	4×10^{-3}	4×10^{-3}	–	–	–
	13	$\mu \rightarrow \bar{e}ee$	–	2×10^{-3}	–	–	–	0.02	0.02	–	–	–
	14	$\mu \rightarrow e\gamma$	–	8×10^{-4}	–	–	–	0.1	0.1	–	–	–
	15	$(g-2)_\mu$	–	–	–	–	–	–	–	–	–	–
CP violation (Im λ)	16	$\mathrm{Im}(K^0 \leftrightarrow \bar{K}^0)$	–	–	1×10^{-6}	2×10^{-2}	2×10^{-2}	–	2×10^{-2}	2×10^{-2}	2×10^{-3}	5×10^{-3}
	17	ε'/ε	–	–	–	–	–	–	–	–	–	–
	18	$P(K \rightarrow \pi\mu\nu)$	–	$\sqrt{\lambda_3 \lambda_2} < 6 \times 10^{-3}$		–	–	–	–	–	–	–
	19	d_n	$\sqrt{\mathrm{Im}\ \lambda_1 \lambda_3} < 6 \times 10^{-3}$	–	$\sqrt{\mathrm{Im}\ \lambda_1 \lambda_3} < 6 \times 10^{-3}$	$\sqrt{\mathrm{Im}\ \lambda_6 \lambda_7} < 2 \times 10^{-2}$		$\sqrt{\mathrm{Im}\ \lambda_8 \lambda_9} < 6 \times 10^{-2}$		2×10^{-2}	–	–
weak universality	20	$\pi \rightarrow e\nu$	–	$\sqrt{\lambda_3 \lambda_2} < 1 \times 10^{-3}$		–	–	–	–	–	–	–
	21	$\pi^0 \rightarrow ee$		$\sqrt{\lambda_{1,3} \lambda_2} < 0.2$		–	–	–	–	–	–	–
	22	U_{KM}	–	–	–	–	–	–	–	–	–	–
ν mass	23	m_ν	–	–	–	–	–	–		$\sqrt{\lambda_9 \lambda_{10}} < 1 \times 10^{-3}$		
best limit (process)		Re λ	2×10^{-4} $D^0 \leftrightarrow \bar{D}^0$	8×10^{-4} $\mu \rightarrow e\gamma$	3×10^{-5} $\mathrm{Re}(K^0 \leftrightarrow \bar{K}^0)$	0.1 $\mathrm{Re}(K^0-\bar{K}^0)$ $\mathrm{Re}(D^0-\bar{D}^0)$ $\mathrm{Re}(B^0-\bar{B}^0)$	0.1 $\mathrm{Re}(K^0-\bar{K}^0)$ $\mathrm{Re}(D^0-\bar{D}^0)$ $\mathrm{Re}(B^0-\bar{B}^0)$	4×10^{-3} $\mu N \rightarrow eN$	4×10^{-3} $\mu N \rightarrow eN$	0.1 $K^0 \leftrightarrow \bar{K}^0$ $B^0 \leftrightarrow \bar{B}^0$	2×10^{-3} $\mathrm{Im}(K^0-\bar{K}^0)$	5×10^{-3} $\mathrm{Im}(K^0-\bar{K}^0)$
		Im λ	2×10^{-4} $D^0 \leftrightarrow \bar{D}^0$	8×10^{-4} $\mu \rightarrow e\gamma$	1×10^{-6} $\mathrm{Im}(K^0 \leftrightarrow \bar{K}^0)$	2×10^{-2} $\mathrm{Im}(K^0-\bar{K}^0)$	2×10^{-2} $\mathrm{Im}(K^0-\bar{K}^0)$	4×10^{-3} $\mu N \rightarrow eN$	4×10^{-3} $\mu N \rightarrow eN$	2×10^{-2} $\mathrm{Im}(K^0-\bar{K}^0)$ d_n		

3.3.1. E-leptons and h-quarks

3.3.1.1. Right-handed currents, $g-2$, and $\mu \to e\gamma$. As discussed above, ordinary–exotic mixing in the leptonic sector produces non-chiral couplings (i.e., right-handed currents) and a non-unitary mixing matrix. These ingredients can lead to significant enhancements in leptonic loop-order processes if sizeable mixing angles are realized. Experimental constraints on these rare processes can thus, in turn, be used to constrain various combinations of E_6 model parameters.

As a prelude to a consideration of these loop processes, we note that polarized μ decay itself can be used to constrain parameters. Data on the combination of Michel parameters $R \equiv \xi P_\mu \delta/\rho$ [3.40] and the ρ parameter [3.39] results in the bound $|\sin\theta_R^\nu \sin\theta_R^e| \lesssim 0.03$ if e–μ universality is assumed [3.41]. This bound is independent of the masses of the exotic fermions.

Turning to loop processes, the good agreement between the SM predictions for the anomalous magnetic moments of muons, a_μ, and electrons, a_e, can be used to constrain these parameters further and has been considered by several authors [3.41–3.43]. In general, there are several contributions to these quantities as is represented graphically in fig. 45 from ref. [3.42], in which X is a generic gauge boson and F a generic fermion. As one can see from the general discussion of Leveille [3.44] and emphasized by Maalampi and Roos [3.45], diagrams involving non-chiral couplings and heavy fermions in the loop are substantially enhanced in comparison to other contributions. Since the FCNC couplings to the Z are chiral, the only non-chiral contributions arise from Z′ exchange with F representing the exotic partner of the muon (M) or from W exchange with F portraying the exotic partner of ν_μ (N_μ). All other contributions are found to be at most comparable to those of the SM and will be ignored from here on. Writing the coupling of any fermion to the Z′ as

$$\tfrac{1}{2} g_x \bar{f} \gamma_\mu [(x_L + x_R) - (x_L - x_R)\gamma_5] f Z'^\mu \tag{3.68}$$

and defining $\alpha_x = g_x^2/4\pi$, $s_{L,R}^\mu = \sin\theta_{L,R}^\mu$, and $c_{L,R}^\mu = \cos\theta_{L,R}^\mu$ one finds

$$\Delta a^\mu = (-\alpha_x/\pi)(m_\mu/M_{Z'})(x_L^\mu - x_L^M)(x_R^\mu - x_R^M) s_L^\mu s_R^\mu c_L^\mu c_R^\mu G\,, \tag{3.69}$$

with G being a complicated function of the ratio of the M to Z′ mass and is generally of order unity [3.42]. If we take model χ ($\theta = -90°$) as an example, we get

$$\Delta a_{Z'}^\mu = -18100 \times 10^{-10} (M_Z/M_{Z'})(s_L^\mu c_L^\mu)(s_R^\mu c_R^\mu) G\,, \tag{3.70}$$

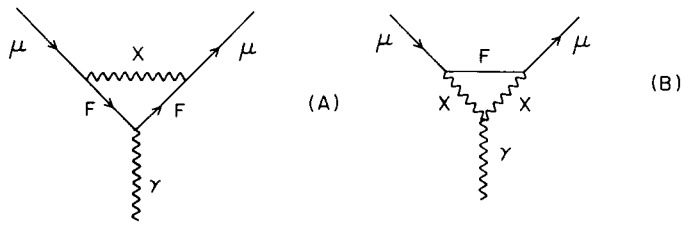

Fig. 45. Diagrams contributing to $(g-2)_\mu$ in a general gauge theory with X a gauge boson and F a fermion.

which with $G \simeq 1$ yields the constraint (assuming $\theta_L^\mu = \theta_R^\mu = \theta^\mu$)

$$(M_Z/M_{Z'})(s^\mu c^\mu)^2 \leq 6.1 \times 10^{-3} \tag{3.71}$$

at 95% CL. Clearly for a heavy Z' the bound on the mixing obtained in this manner becomes quite weak. Other choices for θ yield similar constraints. For the case of W exchange we obtain

$$\Delta a_W^\mu = (-G_F m_\mu M_W/2\sqrt{2}\pi^2) \sin\delta^\mu \sin\theta_R^\mu \cos\theta_R^\nu F\,, \tag{3.72}$$

where F depends on the ratio M_N/M_W in a somewhat sensitive way. For $M_N \simeq 44$ GeV we obtain

$$-0.223 \leq \sin\delta^\mu \sin\theta_R^\mu \cos\theta_R^\nu \leq 0.098\,, \tag{3.73}$$

which strengthens by a factor of $\simeq 10$ for $M_N \simeq 615$ GeV. Hence this bound becomes significantly stronger with increasing M_N.

Further bounds [3.46] are obtainable in the leptonic sector from the process $\mu \to e\gamma$, where strong experimental constraints exist [3.47], i.e., $\Gamma(\mu \to e\gamma)/\Gamma(\mu \to e\nu\bar{\nu}) \leq 4.9 \times 10^{-11}$. The contributions are again potentially largest when non-chiral couplings are present and a heavy, charged fermion is present in the loop as is displayed in fig. 45. For generic couplings, such as

$$\tfrac{1}{2} g_x[\bar{\mu}\gamma_\sigma(v_1 - a_1\gamma_5)M + \bar{e}\gamma_\sigma(v_2 - a_2\gamma_5)E]X^\sigma + \text{h.c.}\,, \tag{3.74}$$

the dominant part of the $\mu \to e\gamma$ amplitude is given by

$$T = +i\bar{e}(p')\Lambda_\lambda \mu(p)\varepsilon_\gamma^\lambda\,, \tag{3.75}$$

with

$$\Lambda_\lambda = \frac{ieg_x^2}{128\pi^2 M_X^2}\,\gamma_\lambda \not{A}(A - B\gamma_5)\sum_j M_j U_{\mu j} U_{ej} + O(m_\mu/M_j)\,, \tag{3.76}$$

where $A = v_1 v_2 - a_1 a_2$, $B = a_1 v_2 - v_1 a_2$, and M_j is the mass of the fermion in the loop. Here, terms of order m_μ/M_j have been neglected and the U's are the mixing matrix elements. Note that for chiral couplings, $A = B = 0$, and an additional suppression of the order m_μ/M_j occurs. Thus

$$R = \frac{\Gamma(\mu \to e\gamma)}{\Gamma(\mu \to e\nu\bar{\nu})} = \frac{\alpha}{4}(A^2 + B^2)\left(\frac{g_x M_W}{g M_X}\right)^2 \left(\sum_j \frac{M_j}{m_\mu} U_{\mu j} U_{ej}\right)^2\,, \tag{3.77}$$

which, e.g., for model χ yields (assuming $\theta_L^\mu = \theta_L^e$ as a two generation example)

$$R = 900\alpha(x_w \alpha_x M_W^2/\alpha M_{Z'}^2)^2 (s_L^e c_L^e)^4 s_\phi^2 c_\phi^2 [(M_M - M_E)/m_\mu]^2\,, \tag{3.78}$$

with ϕ representing the suppression due to intergenerational mixing. Use of the experimental bound results in (taking $M_M - M_E \simeq 100$ GeV)

$$(M_W/M_{Z'})(s_L^e c_L^e)(s_\phi c_\phi)^{1/2} \lesssim 3.9 \times 10^{-4}\,. \tag{3.79}$$

This constraint, although severe for a light Z', becomes quite weak for Z' masses in the TeV range. Similar bounds hold for other E_6 models.

3.3.1.2. Meson mixing and CP violation. A large number of authors have considered the influence of ordinary–exotic mixing on the mixing of mesons and *CP* violation [3.3, 3.48–3.50].

Barger et al. [3.3] use the K_L–K_S mass difference (ΔM_K) and the decay $K_L \to \mu^+\mu^-$ to place a bound on the strength of the $\bar{s}d$ FCNC coupling (which they denote as A_{ds}). They obtain from $K_L \to \mu^+\mu^-$ decay

$$|\mathrm{Re}\, A_{ds}| < 3 \times 10^{-3}\,, \qquad |\mathrm{Im}\, A_{ds}| < 2 \times 10^{-5}\,, \tag{3.80}$$

and $[\mathrm{Re}(A_{ds}^2)]^{1/2} < 3.6 \times 10^{-4}\, B_K^{-1/2}$ from ΔM_K. Here B_K is the usual bag factor. For the B meson system, these authors find that the lack of observation of the $b \to \mu^+\mu^- X$ transition constrains $|A_{qb}| < 0.28|U_{cb}|$, where U_{cb} is the cb KM matrix element. A similar analysis of K_L–K_S mixing and $K_L \to \mu^+\mu^-$ decay by Robinett [3.50] in a simple two-generation model results in the bound

$$[\cos^2(\theta - \phi)\sin^2(\theta - \phi)/\cos^2\theta_c \sin^2\theta_c]\sin^4\alpha\,(M_h^2/m_c^2) \ll 1.0\,, \tag{3.81}$$

where θ (ϕ) is the mixing in the d (h) sector, α is the d–h mixing angle, and M_h is the typical value of the h mass arising from the K_L–K_S mass difference, while the restriction

$$M_h \sin\alpha \lesssim 20\ \mathrm{GeV} \tag{3.82}$$

comes from the process $K_L \to \mu^+\mu^-$. The analysis of Decker [3.48] results in similar bounds.

Raychaudhuri et al. [3.49], in a very interesting set of papers, consider the possibility of the mixing of h with the b quark in a simplified model where only a single generation of exotic fermions is present, but with three generations of ordinary fermions. In this case, one can write the non-unitary 4×4 KM matrix as a 3×4 matrix, since the extra row consists only of null entries; this matrix is, in general, parameterized by six angles and three phases, but simplifies to four angles and one phase if b–d and b–s mixing is set to zero by fiat. These angles and phases can be taken to be the usual KM angles and phase plus one additional angle, α. Tests for the deviation from unitarity of the KM matrix force $\cot\alpha \lesssim 0.11$ at the 90% CL. These authors then proceed to constrain the various angles in the usual manner from the known values of V_{ud} and V_{us}, the b quark lifetime and the upper bound on $\Gamma(b \to u\ell\nu)/\Gamma(b \to c\ell\nu)$ arising from the electron spectrum in semi-leptonic b decay. This additional mixing parameter is found to have little effect on B–$\bar{B}$ mixing, which remains t-quark dominant, but ε'/ε is generally found to be smaller than that predicted by the SM. Since $Q = -1/3$ type quarks appear on the internal lines of the box diagrams for D–$\bar{D}$ mixing, the presence of the h significantly modifies SM expectations and dominates for $M_h > 20$ GeV. The SUSY contributions in this case are also found to be potentially large and can saturate the current experimental bounds. A similar mixing scenario has been considered by Maalampi and Roos [3.51]. An interesting possibility, which can be realized in their scenario, is the rather small value of $|V_{tb}| \simeq 0.15$–0.30 which can lead to a substantial reduction in the t-quark production cross section at hadron colliders since $W \to t\bar{b}$ is now suppressed. Branco and Lavoura [3.52] perform a similar analysis and obtain constraints on FCNC couplings while Pulido [3.53] restricts his analysis to a rank-6 scenario with a relatively high intermediate breaking scale.

3.3.1.3. Comprehensive analysis of mixing limits. A systematic investigation of limits on ordinary–exotic mixing imposed by data from high precision charged and neutral current experiments has been performed by Langacker and London [3.54]. The data set that these authors have considered is that from charged current universality, the W and Z masses, induced right-handed currents, and flavor-diagonal neutral currents. Demanding consistency with the data and allowing for all possible fermionic mixings to occur simultaneously, they have found constraints on all the ordinary–exotic mixing angles discussed in section 3.1, excluding δ. Their results are displayed in fig. 46. Also shown in the figure for comparison are the limits placed from this data on the possible mixing angles of the ordinary fermions with Hermitian mirror fermions and with heavy sequential fourth generation fermions (including both the mixing of one fermion individually as well as all fermions simultaneously). The parameter Λ labels the change in isospin associated with the mixing in the neutrino sector; $\Lambda = 0$ denotes the mixing of ν with a heavy neutrino which is the top member in a left-handed doublet (i.e., N), $\Lambda = 2$ corresponds to mixing with an iso-singlet neutral field (S^c), and $\Lambda = 4$ stands for mixing with a neutrino which is the bottom member of a left-handed doublet (N^c). As can be seen from the figure, the mixing limits in E_6 models are somewhat more stringent than what is found for the other models, with the general restriction $\sin^2\theta_i \lesssim 0.05$.

3.3.2. h-Leptoquarks

3.3.2.1. $g-2$ of μ and e. The anomalous magnetic moment of the muon can receive substantial contributions from both h and $\tilde{h}$ leptoquarks. These new E_6 contributions can be comparable in size to the standard electroweak terms (which are $\sim 2\times 10^{-9}$), even for small values of the Yukawa couplings. These extra terms arise from $h\tilde{c}$ and $\tilde{h}c$ exchange in the loops of the triangle diagrams responsible for this process as shown in fig. 47, and are proportional to the left–right mixing in the c-squark and scalar

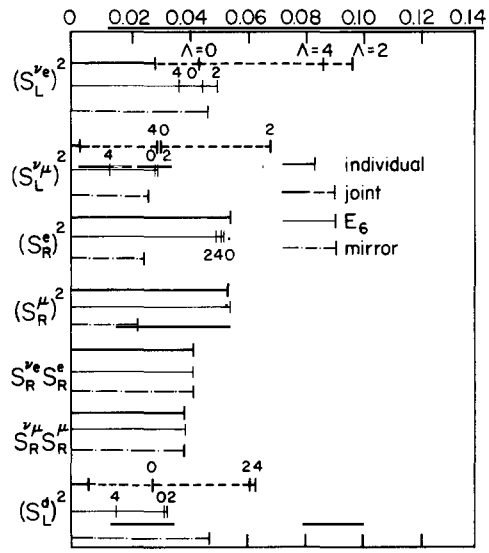

Fig. 46. 90% CL upper limits on mixing for the light left-handed fermions, for individual fits (heavy solid lines), joint fits to all mixings (dashed lines), E_6 models (solid lines), and the Hermitian mirror model (dot-dashed line). The Λ (as described in the text) values are indicated.

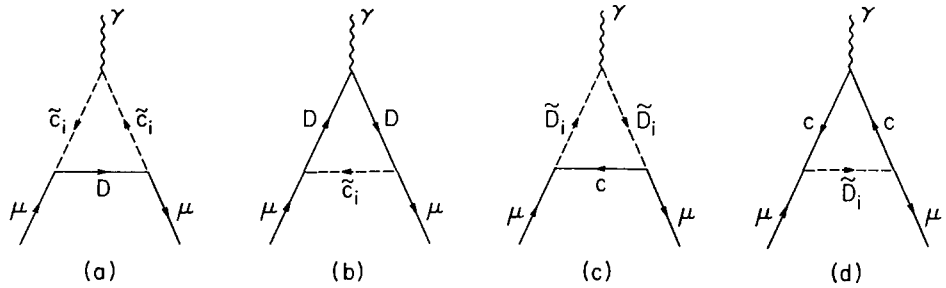

Fig. 47. Lowest order contributions to the muon anomalous magnetic moment involving (a), (b) D (h) exchange and (c), (d) their superpartners.

leptoquark sector, respectively. One then finds [3.55]

$$\Delta a_\mu|_{\tilde{c}h} = \lambda_6\lambda_7(m_\mu/M_h)\sin 2\chi_{\tilde{c}}\,[F(m^2_{\tilde{c}_1}/M^2_h) - F(m^2_{\tilde{c}_2}/M^2_h)]\,,$$
$$\Delta a_\mu|_{c\tilde{h}} = \lambda_6\lambda_7(m_\mu/m_c)\sin 2\chi_{\tilde{h}}\,[G(M^2_{\tilde{h}_1}/m^2_c) - G(M^2_{\tilde{h}_2}/m^2_c)]\,, \tag{3.83}$$

where $\chi_{\tilde{c}(\tilde{h})}$ is the $\tilde{c}$ ($\tilde{h}$) mixing angle and the functions F and G are given in Morris [3.55]. Note that the $\tilde{c}h$ contributions are suppressed by a factor of $1/M_h$ compared to those from $c\tilde{h}$ and hence the $c\tilde{h}$ diagrams are dominant. For squark and leptoquark masses in the range 100–600 GeV and with typical values of the mixing, one finds

$$\Delta a_\mu \sim 2\text{–}1000(\lambda_6\lambda_7)\times 10^{-9}\,, \tag{3.84}$$

which yields the rough bound $|\lambda_6\lambda_7| \lesssim 10^{-2}$ when comparison with experimental data is made. Note that even with these restrictions on the couplings, the leptoquark contributions can be of the same magnitude, or larger, than the electroweak contributions to Δa_μ, as advertised. The electron anomalous magnetic moment is less sensitive to new physics since $(g-2)_e \sim m_e/m_\mu(g-2)_\mu$, and present data only places [3.55] the restriction $|\lambda_6\lambda_7| \lesssim 0.1$–$0.5$.

3.3.2.2. Electric dipole moments. The neutron and electron electric dipole moments, d_n and d_e respectively, which are induced by scalar leptoquark exchange in the usual penguin-type graph presented in fig. 48 can be significantly larger than that predicted by the SM. The SM values lie several

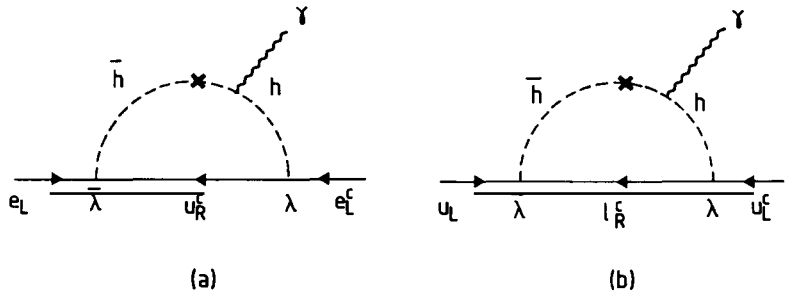

Fig. 48. Diagrams contributing to the electric dipole moment of (a) the electron and (b) the up-quark. There is another set of diagrams where the photon couples to the internal fermion line.

orders of magnitude below the current experimental $1\,\sigma$ limits [3.39] of $d_n < 4.6 \times 10^{-25}\, e$ cm and $d_e < 3.0 \times 10^{-24}\, e$ cm. The electric dipole moment of a fermion f arising from these diagrams is [3.56]

$$d_f = \frac{-e}{16\pi^2}\,\mathrm{Im}(\lambda_6\lambda_7)\,M_F \int_0^1 dx\, \frac{Q_F(1-x)^2 + Q_B x(1-x)}{xM_B^2 + (1-x)M_F^2 + x(1-x)m_f^2}\,, \tag{3.85}$$

where $M_{F(B)}$ and $Q_{F(B)}$ are the mass and charge of the fermion (boson) present in the loop. For generation conserving (λ_i^1) and nonconserving (λ_i^3) couplings (corresponding to first or third generation fermion in the loop) with $M_{\tilde{h}} = 100$ GeV and $m_t = 40$ GeV this yields

$$d_e = 7.8 \times 10^{-22}\,\mathrm{Im}(\lambda_6^1\lambda_7^1)\, e\,\mathrm{cm}\,, \qquad d_e = 2.6 \times 10^{-19}\,\mathrm{Im}(\lambda_6^3\lambda_7^3)\, e\,\mathrm{cm}\,, \tag{3.86}$$

$$d_n = -1.4 \times 10^{-22}\,\mathrm{Im}(\lambda_6^1\lambda_7^1)\, e\,\mathrm{cm}\,, \qquad d_n = -1.4 \times 10^{-17}\,\mathrm{Im}(\lambda_6^3\lambda_7^3)\, e\,\mathrm{cm}\,. \tag{3.87}$$

Comparison with the current data shows that the strongest bounds on the couplings are realized from d_n and are

$$\mathrm{Im}(\lambda_6^1\lambda_7^1) < 3 \times 10^{-3}\,, \qquad \mathrm{Im}(\lambda_6^3\lambda_7^3) < 3 \times 10^{-8}\,. \tag{3.88}$$

The contribution from the electric dipole moment of the d-quark has been neglected in calculating d_n, since it is proportional to the neutrino mass and $Q_F = 0$ in this case.

3.3.2.3. $b \to s\gamma$. Leptoquarks may appear in the loop in two of the contributing electromagnetic penguin-type diagrams which mediate this process via $\tilde{h}\nu$ and $h\tilde{\nu}$ exchange and intergenerational Yukawa couplings. The dominant SM contribution to this process arises from the t-quark diagram and yields a branching ratio of $B(b \to s\gamma) \simeq 10^{-5}$ for $m_t = 60$ GeV [3.57]. This rate may soon be accessible to experiment as the present upper limit [3.58] on the exclusive process $B \to K^*\gamma$ from CLEO is $B(B \to K^*\gamma) < 1.7 \times 10^{-4}$ and the recent calculation [3.59] of the ratio of the exclusive to inclusive rate gives $\Gamma(B \to K^*\gamma)/\Gamma(b \to s\gamma) \simeq 7\%$. Since the SM prediction is close to the experimental limit, one might expect to obtain strong constraints on the contributions from new physics. Dreiner [3.60] has shown that for a variety of values of the parameters (and including the SUSY-SM contributions), experimental data can exclude a wide range in the M_h–$\tilde{m}$ mass plane, where $\tilde{m}$ represents the universal squark mass.

3.3.2.4. K decays, $\mu \to e\gamma$, and μ–e conversion. Both of the Yukawa couplings λ_7 and λ_8 can induce the process $K \to \pi\nu\bar{\nu}$ at tree level via scalar leptoquark exchange as shown in fig. 49, if one allows intergenerational couplings. Taking $\lambda_7 \simeq \lambda_8 = \lambda$ and assuming that the intergenerational couplings are of the same order of magnitude as the generation diagonal ones, Masiero et al. [3.61] infer the following bound using current experimental data:

$$\lambda < (M_{\tilde{h}}/M_W)(8 \times 10^{-3} - 10^{-2})\,, \tag{3.89}$$

assuming that $M_{\tilde{h}}$ is in the range 100–200 GeV. Note that the leptoquark couplings do not allow for tree level $K \to \mu e$ or $K^+ \to \pi^+ \mu e$ decays. The contributions of the fermion leptoquarkino h to the muon

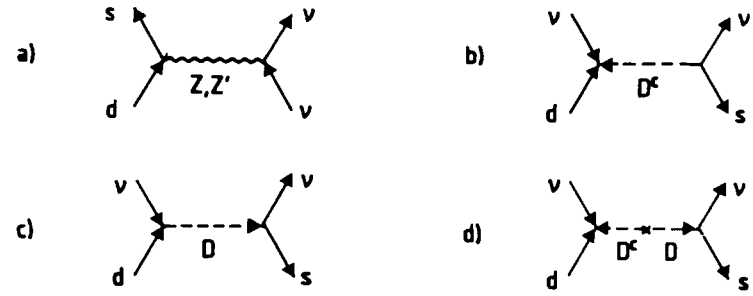

Fig. 49. Possible tree level contributions to $(\bar{s}d)(\bar{\nu}\nu)$ operators relevant for the decay $K \to \pi\nu\bar{\nu}$.

longitudinal polarization in the decay $K_L \to \mu\mu$ have been studied by Liu [3.62], where it was shown that bounds on the couplings λ_6 and λ_7 may be obtained from this process.

The interaction $\mu \to e\gamma$ can also place bounds on the coupling λ_7 when the scalar leptoquark appears in the loop. One approximately finds [3.38, 3.61] the constraint

$$\lambda_7 < (M_{\tilde{h}}/1\ \text{GeV})10^{-5}\,, \tag{3.90}$$

when comparison with the experimental limit is made. Three tree level diagrams with t-channel scalar leptoquark exchange contribute to μ–e conversion via intergenerational couplings, resulting [3.61] in the restriction (assuming $\lambda_1 \simeq \lambda_2 = \lambda$)

$$\lambda < (M_{\tilde{h}}/1\ \text{GeV})(5 \times 10^{-6})\,. \tag{3.91}$$

Thus we see that for $\tilde{h}$ masses of order 100–200 GeV, the above limits (as well as those found in table 3) on the leptoquark Yukawa couplings are not that stringent. The couplings can take on values which are of order of the Yukawa couplings present in the SM and still be in accord with experiment.

3.3.2.5. D^0–$\bar{D}^0$ mixing in the ALRM. In the ALRM discussed in section 2, the exotic h's take on the quantum numbers of leptoquarks and the right-handed W carries lepton number and odd R-parity, thus escaping the stringent mass bounds set on the standard left–right model W_R from K^0–$\bar{K}^0$ mixing. These exotic particles in the ALRM can induce D^0–$\bar{D}^0$ mixing through the W_R couplings of the c- and u-quarks to the exotic h leptoquark via a standard box-type diagram which is presented in fig. 50. The

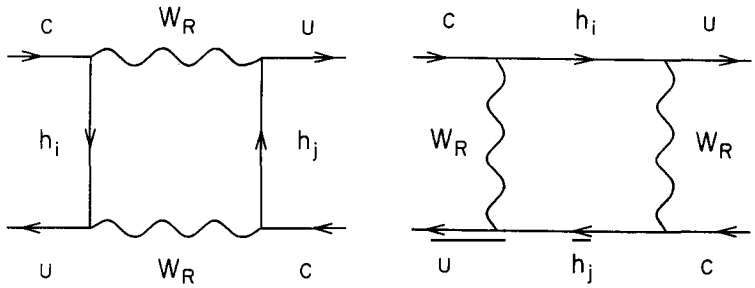

Fig. 50. Box diagrams in the ALRM can lead to an enhancement in D–$\bar{D}$ mixing.

amplitude for this mixing is calculated in ref. [3.63], where it is found that these exotic box diagrams can have significant contributions to D^0–$\bar{D}^0$ mixing for a wide range of h and W_R mass values. Mixing which is close to the present experimental limit is predicted if $SU(2)_R$ is a relevant symmetry below a TeV or so. Note that these new interactions which are present in the ALRM will not affect K^0–$\bar{K}^0$ or B^0–$\bar{B}^0$ mixing.

3.3.3. h-diquarks

With the exception of the general survey in ref. [3.38], the effects of h-diquarks in rare processes have not gained much attention in the literature. Diquark contributions to the general radiative transitions $q \to q'\gamma$ [3.64, 3.65], as well as to the more specific quark-level decay $b \to s\gamma$ [3.60], and to the $\Delta I = 1/2$ rule [3.66] have been analyzed. We will discuss each of these in turn, and refer the reader to table 3 for a more complete summary of the bounds which can be placed on diquark couplings from a larger variety of rare processes.

3.3.3.1. Electric dipole moment of the neutron. Scalar diquark contributions to the electric dipole moment of the neutron, d_n, occur through the Yukawa terms λ_9 and λ_{10} in the superpotential. The dipole moment is mediated by an electromagnetic penguin-type diagram, where $\tilde{h}$ and $\tilde{h}^c$ are present in the loop and the photon is attached in every possible manner, as shown in fig. 51. These diquark contributions are potentially large and are expected to be even larger than the leptoquark contributions to d_n since we now have internal, more massive quarks, instead of internal leptons. The scalar diquark contribution to d_n is given by [3.65]

$$d_n = (e/12\pi^2)\,\mathrm{Im}(\lambda_9\lambda_{10})\,(1/M_{\tilde{h}})(2Q_d x_d \ln x_d^2 - Q_u x_u \ln x_u^2)\,, \tag{3.92}$$

to leading order in x_i, where $x_i = m_i/M_{\tilde{h}}$ and Q_i is the quark charge. Comparing the above expression with the current experimental bound [3.39] on d_n places the restriction (for $M_{\tilde{h}} = 100$ GeV)

$$\mathrm{Im}(\lambda_9^1\lambda_{10}^1) \leq 2 \times 10^{-4}\,. \tag{3.93}$$

For $M_{\tilde{h}} = 300$ GeV, the resulting constraint on the Yukawa couplings is an order of magnitude weaker. If intergenerational mixing is allowed, then present data constrains $\mathrm{Im}(\lambda_9^3\lambda_{10}^3) \lesssim 3 \times 10^{-6}$ with $m_t = 60$ GeV and $M_{\tilde{h}} = 100$ GeV (where the superscripts denote mixing between the first and third generation). These bounds are significantly stronger than the estimates presented in table 3 and are an order of magnitude better than the corresponding limits set in the case of h-leptoquarks, as expected.

Note that h-diquarks only contribute to the electric dipole moment of the neutron and not to that of the electron, which is an important difference between the diquark and leptoquark cases.

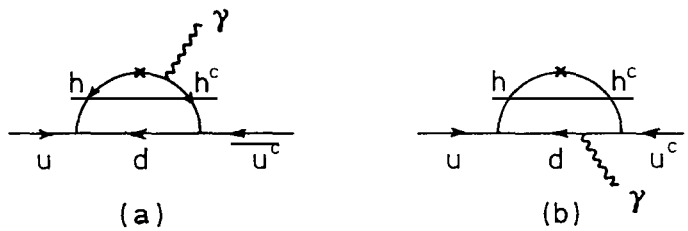

Fig. 51. Diagrams contributing to the neutron electric dipole moment due to the exchange of an h diquark.

3.3.3.2. $b \to s\gamma$. Both the fermion h and scalar $\tilde{h}$ diquarks can have important contributions to this flavor changing radiative transition via their presence in the loop of the penguin-type diagrams which are responsible for this process. Considering the contribution from the scalar diquark only [3.65], the total amplitude is dominated by the graph where the $\tilde{h}$ and t-quark are exchanged in the loop, and the width is given in the leading approximation in $x_t = m_t/M_{\tilde{h}} \ll 1$ by

$$\Gamma(b \to s\gamma) = (8\alpha/9\pi^4 M_{\tilde{h}}^2) E_0^3 (x_t \ln x_t)^2 \lambda^4 . \tag{3.94}$$

Here, $E_0 = (m_b^2 - m_s^2)/2m_b$ is the energy of the photon and

$$\lambda^2 = \lambda_9^{(23)} \lambda_{10}^{(33)} - \lambda_9^{(33)} \lambda_{10}^{(23)} , \tag{3.95}$$

where the superscripts denote the generation indices. Note that intergenerational couplings are involved due to the $\tilde{h}ts$ vertex. The experimental limits on $B(B \to K^* \gamma)$ and the exclusive to inclusive rate ratio discussed above yields the restriction (for $m_t = 60$ GeV and $M_{\tilde{h}} = 100$ GeV)

$$\lambda^2 \lesssim 2 \times 10^{-4} . \tag{3.96}$$

Life becomes more complex if one considers [3.60] the contributions from the odd R-parity h as well as the scalar $\tilde{h}$ diquark exchange due to the introduction of several new parameters. One now has eight contributing penguin-type diagrams, where each diagram is summed over u, c, t or $\tilde{u}$, $\tilde{c}$, $\tilde{t}$ exchange, and one should also keep the SM and SUSY-SM contributions for consistency. For various values of the parameters, there exists a wide range of allowed branching ratios which are either enhanced or suppressed relative to the SM value. The possible depletion in the branching ratio arises from a destructive interference for lower values of the squark mass. Present experimental limits can be used to eliminate regions in the M_h–squark mass plane [3.60].

3.3.3.3. $\Delta I = \frac{1}{2}$ *rule.* The $\Delta I = \frac{1}{2}$ rule in nonleptonic decays of baryons and mesons can also receive contributions from scalar diquark interactions [3.66]. Through intergenerational couplings, diquarks can only mediate $\Delta I = \frac{1}{2}$ decays, and not $\Delta I = \frac{3}{2}$ decays. Hence, in the operator product expansion [3.67], $\tilde{h}$'s only contribute to the $\Delta I = \frac{1}{2}$ operator, and no new operators appear in the effective Hamiltonian. Assuming no mixing between $\tilde{h}$ and $\tilde{h}^c$, diquarks induce only purely left- or right-handed operators, and the resulting enhancement to $\Delta I = \frac{1}{2}$ transitions is only a factor of 25% above the QCD predicted rate for masses of $M_{\tilde{h}} \lesssim 150$ GeV and $\lambda_9 = \lambda_{10} = 0.3$. Once $\tilde{h}$–$\tilde{h}^c$ mixing is included, larger enhancements may occur due to the mixing of left- and right-handed currents. However, even for large values of the couplings and for maximal mixing, there is still only a 20% enhancement for $M_{\tilde{h}} < 200$ GeV. Thus $\Delta I = \frac{1}{2}$ transitions do not receive any sizeable contributions from scalar diquarks.

3.4. Direct production and signals

In this section we review first (in subsections 3.4.1.1–3.4.1.3) the direct production and second (in subsections 3.4.1.4., 3.4.1.5) indirect signals below production thresholds of the exotic fermions (for all possible assignments of baryon and lepton number) at e^+e^-, ep, and $\overset{(-)}{p}p$ colliders. Throughout this section we will generally limit ourselves to one generation of exotics (except where otherwise noted) and will ignore the effects from Z–Z′ mixing, which is constrained to be small.

3.4.1. e^+e^- colliders

The exotics can be produced through a variety of mechanisms in e^+e^- annihilation. For favorable mass values, the exotics could be copiously pair produced in Z_1 decays at the SLC and LEP I. For larger masses exotic pair production in the continuum or perhaps from Z_2 decays can be studied at LEP II or higher energy machines, such as the proposed TeV linear colliders. Exotics may also be singly produced via the off-diagonal flavor mixing as occurs in the more "conventional" E_6 GUTs. A large number of possible indirect effects also exist for the various quantum number assignments and could signal the existence of exotics below their production threshold.

3.4.1.1. Direct production: Z_i decays. If the masses of the exotic fermions (which we generically denote as M_F) are such that $2M_F < M_1$, then pair production from Z_1 decay will be an important production mechanism. The general width for Z_1 decay into a pair of massive fermions is given by (assuming the coupling $g\bar{F}\gamma_\mu(v_1 - a_1\gamma_5)FZ_1^\mu$)

$$\Gamma(Z_1 \to F\bar{F}) = (N_c g^2 M_1/12\pi)(1 - 4M_F^2/M_1^2)^{1/2}[v_1^2(1 + 2M_F^2/M_1^2) + a_1^2(1 - 4M_F^2/M_1^2)], \tag{3.97}$$

where N_c represents the number of colors of F. In the case of Majorana neutrinos the same expression applies with $v_1 = 0$ and $a_1^2 \to 2a_1^2$. It is important to notice that in the limit of zero ordinary–exotic mixing, h, E, and N (if N is a Dirac field) only couple vectorially to Z_1, i.e., $a_1(h) = a_1(E) = a_1(N) = 0$. If on the other hand N and N^c are distinct Majorana fields, then they will only have pure axial-vector couplings. The size of the modification in the overall Z_1 width due to the existence of these exotic decay channels clearly depends on the mass of the exotics, but is consistent with the current CERN Collider data [3.28] on Γ_Z (within experimental error) for $M_F \sim 25$–45 GeV. For this mass range, E, N-leptons and h-quarks will decay via a three-body process yielding a signature of jets + lepton pairs. The leptoquark and diquark quantum number assignments of h will yield final states with missing transverse momentum.

Exotics with quark and lepton quantum numbers in the mass range $M_F < M_1 < 2M_F$ can still be produced in Z_1 (and also W) decays if there is non-zero ordinary–exotic mixing. This mixing results in the final states $Z_1 \to \bar{e}E$ or $e\bar{E}$, $\bar{d}h$ or $d\bar{h}$, and $\bar{\nu}_e N$ or $\nu_e \bar{N}$ with a decay width of

$$\Gamma(Z_1 \to F\bar{f} + \bar{F}f) = (N_c g^2 M_1/6\pi)(v_1^2 + a_1^2)(1 - M_F^2/M_1^2)^2(1 + M_F^2/2M_1^2), \tag{3.98}$$

with v_1 and a_1 as defined in eq. (3.97). Unfortunately, this mechanism is quadratically suppressed by mixing angle factors and may be unobservable except on the Z_1 resonance. Similarly, the W has the potential decay modes $W \to h\bar{u}$, $E\bar{\nu}_e$, and $e\bar{N}$ with partial widths also given by (3.98) with $M_1 \to M_W/2$; these decays are also proportional to the square of the appropriate mixing angles. Since $M_F < M_{1,W}$, the exotics will decay weakly via mixing into three-body final states. This single particle production should not make drastic modifications (<1%) in the Z_1 or W widths due to the mixing angle as well as phase-space suppressions. For completeness we also include the Z_1 width into two distinct massive fermions f_1 and f_2, which can also be induced by mixing,

$$\begin{aligned}\Gamma(Z_1 \to f_1\bar{f}_2 + \bar{f}_1 f_2) = (N_c g^2 M_1/6\pi)(v_1^2 + a_1^2)[(1 + x_1^2 - x_2^2)^2 - 4x_1^2]^{1/2} \\ \times [1 - \tfrac{1}{2}(x_1^2 + x_2^2) - \tfrac{1}{2}(x_1^2 - x_2^2)^2 + 3x_1x_2(v_1^2 - a_1^2)/(v_1^2 + a_1^2)],\end{aligned} \tag{3.99}$$

where $x_{1,2} = M_{f_1,f_2}/M_1$ and QCD radiative corrections have been neglected.

ν_L^c and S^c essentially decouple from the W and SM Z in the absence of mixing between all the neutral fields (such mixing will be discussed in section 3.6) and hence can only be produced in Z′ decays. Z–Z′ mixing, however, can induce a coupling between these fields and the Z_1, but this coupling will be very weak.

The exotic fermions may also be pair or singly produced in Z_2 decays (if $2M_F < M_2$ or $M_F < M_2 < 2M_F$, respectively) with considerable event rates. The partial decay width for $\Gamma(Z_2 \to F\bar{F})$ is given by (3.97) with $M_1 \to M_2$ and where the couplings are furnished in eq. (2.7) and table 2 (these modes are also discussed in section 2.4). The branching fractions for exotic pair production in Z_2 decay as a function of the angle θ (the Z′–Z″ mixing parameter) are displayed in fig. 7c [2.19] (in the figure $n \equiv S^c$, $\nu_E \equiv N$, $N_e \equiv \nu^c$ and $N_E \equiv N^c$). Clearly these branching fractions can be substantial and would provide a copious source of exotic production. The single exotic decay rate $\Gamma(Z_2 \to F\bar{f} + \bar{F}f)$, is as given in (3.98) and (3.99) for massless and massive fermions, respectively, with $M_1 \to M_2$, $v_1 \to v_2$, $a_1 \to a_2$, and are still hampered by mixing angle suppression. Decays into two massive neutral exotic final states such as $Z_2 \to S^c\nu^c$, can also be induced by mixing between the five neutral fields. For illustration we present a list of relative rates (assuming massless exotics) for a few Z_2 decay modes in model η [3.50],

$$d\bar{d}/(d\bar{h} + \bar{d}h)/h\bar{h}/\bar{e}e/(e\bar{E} + \bar{e}E)/E\bar{E} = 15/216(s_L^d c_L^d)^2/51/5/7(s_R^e c_R^e)^2/17\,, \tag{3.100}$$

where s (c) = sin θ (cos θ).

3.4.1.2. Continuum production: E-leptons and h-quarks. The production of E-leptons and h-quarks in e^+e^- collisions has been discussed in refs. [3.3, 3.50, 3.68–3.73]. Exotic pair production in the continuum proceeds through γ, Z_1, and Z_2 s-channel exchange (Z_i exchange only for the neutral exotics) similar to that for SM heavy fermions with a differential cross section [3.68] (for massive Dirac final states)

$$\frac{d\sigma}{dz}(e^+e^- \to F\bar{F}) = \frac{N_c s}{32\pi}\beta \sum_{i,j} P_{ij}^{ss}[B_{ij}(1 + \beta^2 z^2) + 2C_{ij}\beta z + E_{ij}(1 - \beta^2)]\,. \tag{3.101}$$

Here $z = \cos\theta$, where θ is the angle between e^- and F, N_c is the usual color factor, $\beta = (1 - 4M_F^2/s)^{1/2}$, P_{ij}^{ss}, B_{ij}, and C_{ij} are defined in eq. (2.42), the sum extends over the virtual exchange bosons, and

$$E_{ij} = (v_i v_j - a_i a_j)_F (v_i v_j + a_i a_j)_e\,, \tag{3.102}$$

with the couplings normalized as in eq. (2.43). In the case of $E\bar{E}$ ($N\bar{N}$) production there are additional contributions in the t-channel from $Z_{1,2}$ (W) exchange but are suppressed by ordinary–exotic mixing and may be safely disregarded. In E_6 model I, W_I exchange in the t-channel may also mediate $e^+e^- \to E\bar{E}$. The cross section for Majorana pairs is also obtained from the above with $v_F \to 0$, $a_F \to 2a_F$, and an additional factor of $\frac{1}{2}$ due to identical particles in the final state.

Search limits for h-quarks produced at e^+e^- colliders has been recently discussed in ref. [3.69]. The clear signal for their production is the decay $h \to dZ^* \to d\ell^+\ell^-$ which has a small branching fraction of 0.007–0.010% for the mass range $20 \leq M_h \leq 80$ GeV as can be seen in fig. 52a. For this quantum number assignment for h, the current bounds on M_h come from TRISTAN ($\gtrsim$26 GeV) and UA1 ($\gtrsim$32 GeV) as found in ref. [3.69]. If $M_h \lesssim 45$ GeV, $Z \to h\bar{h}$ can be observed via "gold-plated" (two jets + $\ell^+\ell^-\ell^+\ell^-$) or "silver-plated" (two jets + $\ell^+\ell^-\ell^\pm + \not{p}_T$) signatures. For example, if M_h =

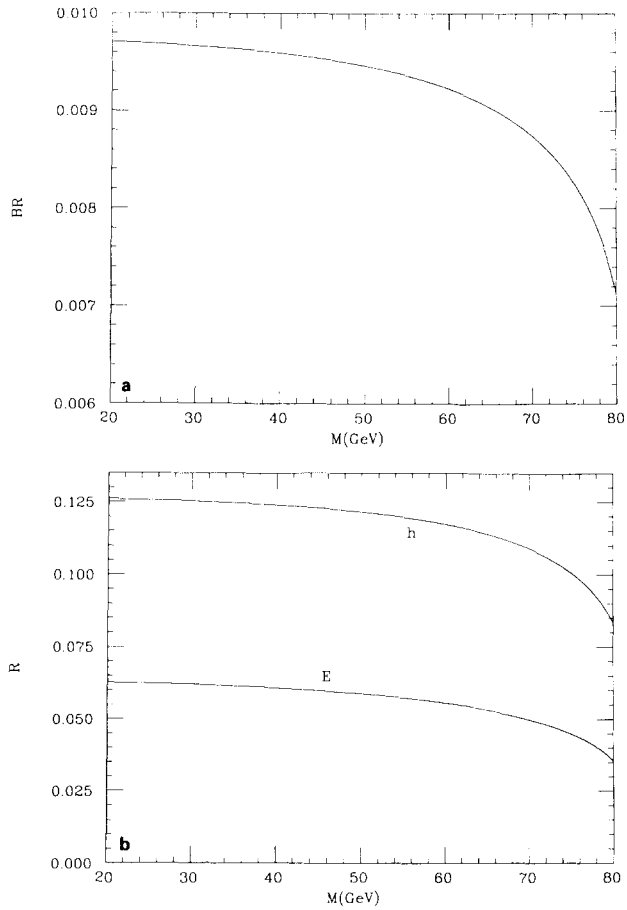

Fig. 52. (a) Branching fraction for $M_h < 80$ GeV, and (b) $\Gamma(h \to d\ell^+\ell^-)/\Gamma(h \to u\ell\bar{\nu})$ and $\Gamma(E \to e\ell^+\ell^-)/\Gamma(E \to \nu_e\ell\bar{\nu})$ as a function of the h or E mass, M.

35 GeV, the number of these events is 2.9 per 10^6 Z's and 46 per 10^6 Z's, respectively, and is approximately a factor of two smaller for $M_h = 43$ GeV. These results follow from the previous figure as well as figs. 52b and 53, which show the ratio $\Gamma(h \to d\ell^+\ell^-)/\Gamma(h \to u\ell\nu)$ and the branching fraction for $Z \to h\bar{h}$. For $M_h > M_Z/2$, the $Z \to h\bar{d}/d\bar{h}$ mode may be observable if θ_L^d is not too small; e.g., if $M_h = 65$ GeV and $\theta_L^d \geq 0.015$ then five events per 10^7 Z's of the type two jets + $\ell^+\ell^-$ will be expected. For this same mass range, LEP II will be required for $h\bar{h}$ pair production. At these energies ($\sqrt{s} = 190$ GeV) and integrated luminosities (200 pb^{-1}) we must also consider "brass-plated" events (in which $h\bar{h} \to$ multi-jets + $\ell^+\ell^-$ with only one jet in the same hemisphere as the charged lepton pair and where two of the jets in the opposite hemisphere come from W decay), since the "gold-plated" events may be unobservable. For "silver-plated" ("brass-plated") signatures, $h\bar{h}$ production for $M_h \lesssim$ 70 (80) GeV should be observable. Figure 54 shows the "brass-plated" event rate per year with the above energy and luminosity.

For $M_h > M_{W,Z}$ even higher energy e^+e^- colliders will be necessary. For $\sqrt{s} = 1$ (2) TeV and an integrated luminosity of 30 fb^{-1}, only the "brass-plated" events occur frequently enough to clearly

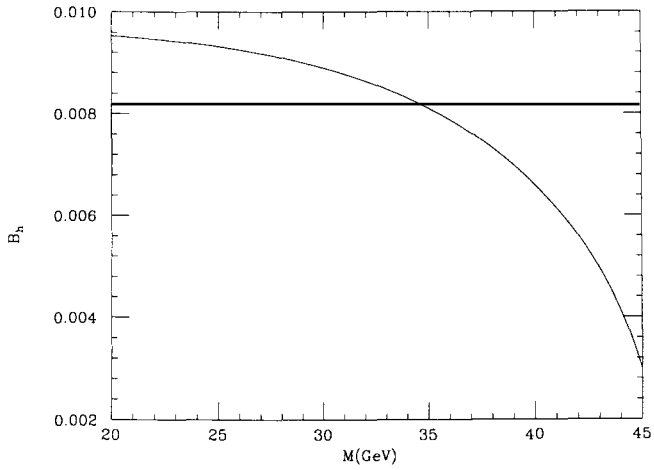

Fig. 53. Branching fraction for $Z \to h\bar{h}$ as a function of the h mass M.

signal $h\bar{h}$ pair production. In this case $h\bar{h}$ produces a two jet + WZ final state with the Z reconstructed from the $\ell^+\ell^-$ and the W from two-jet invariant mass peaks. h's should then be observable up to masses as high as 400–450 (850–900) GeV for $\sqrt{s} = 1$ (2) TeV. For lower integrated luminosities these limits deteriorate rapidly. Figure 55 displays the $h\bar{h}$ production cross section at TeV e^+e^- colliders, while fig. 56 shows the ratio of $\Gamma(h \to dZ)/\Gamma(h \to uW)$ for this mass range. The number of "brass-plated" events at a 1 TeV collider is shown in fig. 57.

Various asymmetry measurements would provide a clear signal for exotic pair production in e^+e^- annihilation. The forward–backward asymmetry (A_{FB}) is defined in eq. (2.45) and is easily calculated via (3.101). Figure 58 from refs. [3.68, 3.70] shows the A_{FB} for (a) h and (b) E pair production with an exotic mass of 30 GeV and taking $M_{Z_2} = 150$ GeV for several E_6 models, as well as the A_{FB} for fourth

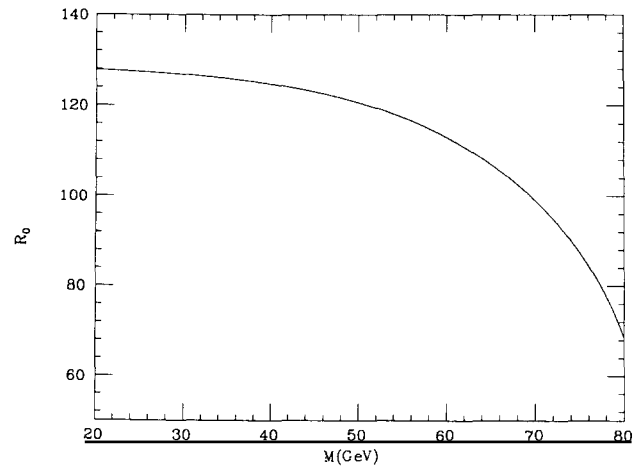

Fig. 54. Number of "brass-plated" events/yr at a $\sqrt{s} = 190$ GeV e^+e^- collider with an integrated luminosity of 200 pb^{-1} as a function of the h mass, M.

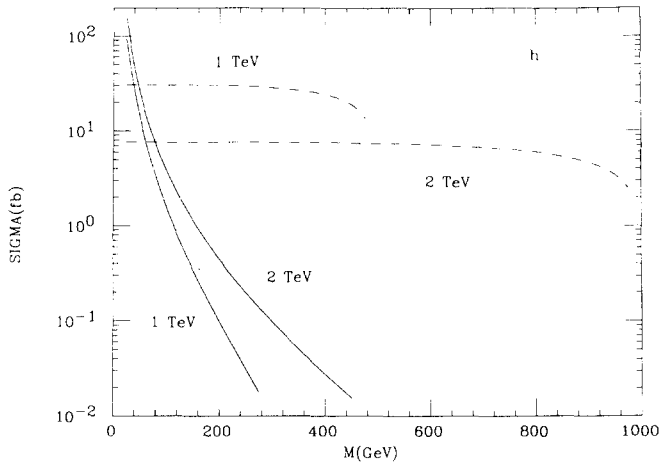

Fig. 55. Production cross sections as a function of the h mass for $h\bar{h}$ at 1 and 2 TeV colliders: solid curves show the $\gamma\gamma \to h\bar{h}$ subprocess while dashed curves correspond to the usual s-channel process.

generation fermions in the SM of the same mass. The exotic A_{FB} is very distinct, with a value near zero below the Z_1 resonance due to the vector-like nature of the exotics, and with a strong dependence on the choice of E_6 model (i.e., θ) once the Z_2 contribution becomes important. The prescription for obtaining the left–right asymmetry (A_{LR}) for longitudinally polarized e^- beams is outlined in section 2.5, eqs. (2.44), (2.45), where one must of course use the production cross section for massive fermions (3.101). A_{LR} is presented in fig. 59 [3.70, 3.71] for 30 GeV (a) h-quarks and (b) E-leptons and compared to that for 30 GeV SM fourth generation fermions of the same charge (with $M_{Z_2} = 150$ GeV). A_{LR} for these particles is quite distinct from that of the SM fermions and the E_6 models are again easily differentiable once the Z_2 contribution is relevant. If transversely polarized e^+e^- beams are available,

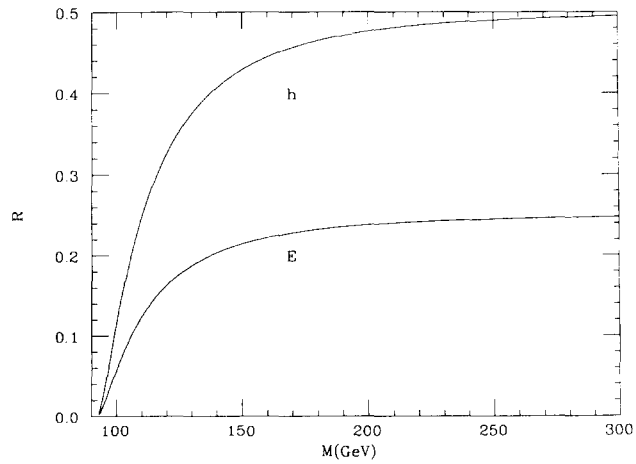

Fig. 56. $\Gamma(h \to dZ)/\Gamma(h \to uW)$ and $\Gamma(E \to eZ)/\Gamma(E \to \nu_e W)$ as a function of the h or E mass, M.

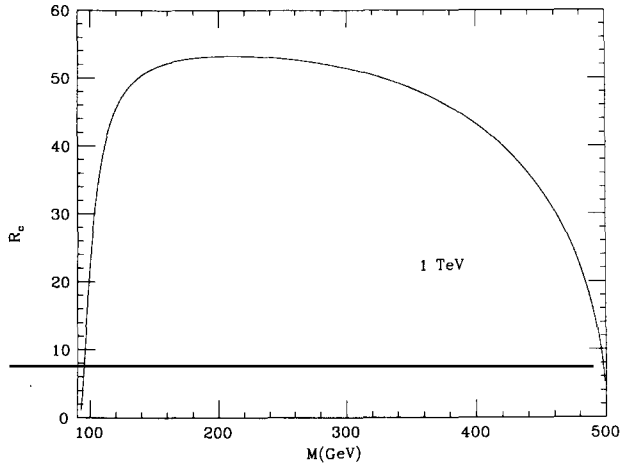

Fig. 57. Number of "brass-plated" events/yr at a $\sqrt{s} = 1$ TeV e^+e^- collider with an integrated luminosity of 30 fb^{-1} as a function of the h mass, M.

one could also form the azimuthal asymmetry (A_ϕ), given in eq. (2.48), with a differential cross section for massive fermions

$$\frac{d\sigma}{d\phi} = \frac{N_c s}{64\pi^2}\,\beta \sum_{i,j} P_{ij}^{ss}[2B_{ij}(1+\tfrac{1}{3}\beta^2) + 2E_{ij}(1-\beta^2) + \tfrac{4}{3}(p^T)^2\beta^2 G_{ij}\cos 2\phi]\,, \tag{3.103}$$

where G_{ij} is defined in (2.46) and p^T is the amount of transverse polarization. Even with maximum polarization ($p^T = 1$), A_ϕ is tiny for h-quarks [3.70] with magnitude generally $\lesssim 0.1$. This asymmetry can be somewhat larger for E-leptons and is shown in fig. 60 from ref. [3.71].

Ordinary–exotic mixing can also induce single exotic production. The process $e^+e^- \to \bar{d}h$ occurs

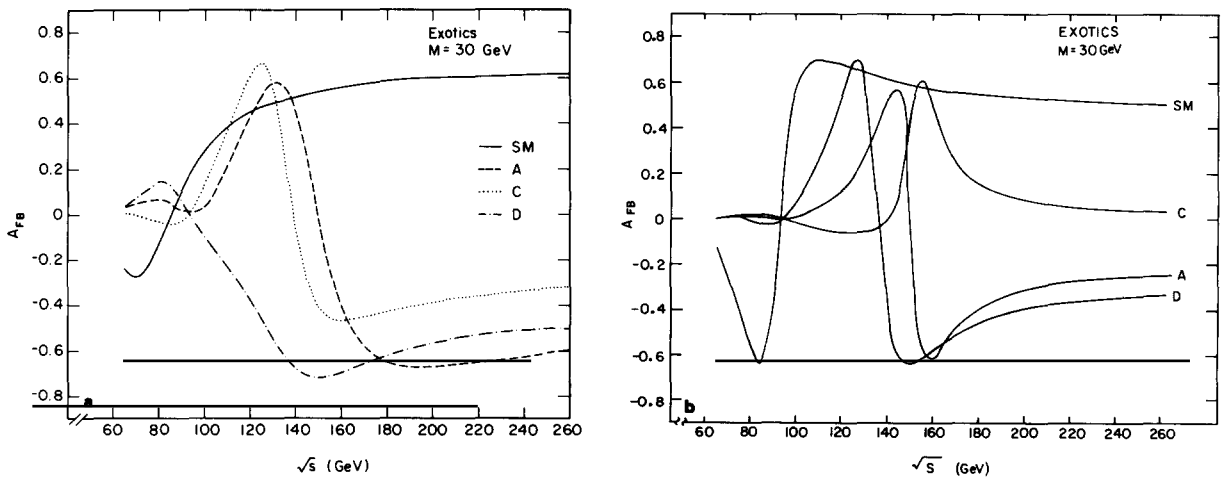

Fig. 58. Forward–backward asymmetry versus $\sqrt{s}$ for 30 GeV (a) and (b) E pair production in e^+e^- collisions for models ψ (A), η (C), and I (D), and for 30 GeV SM fourth generation fermions (SM).

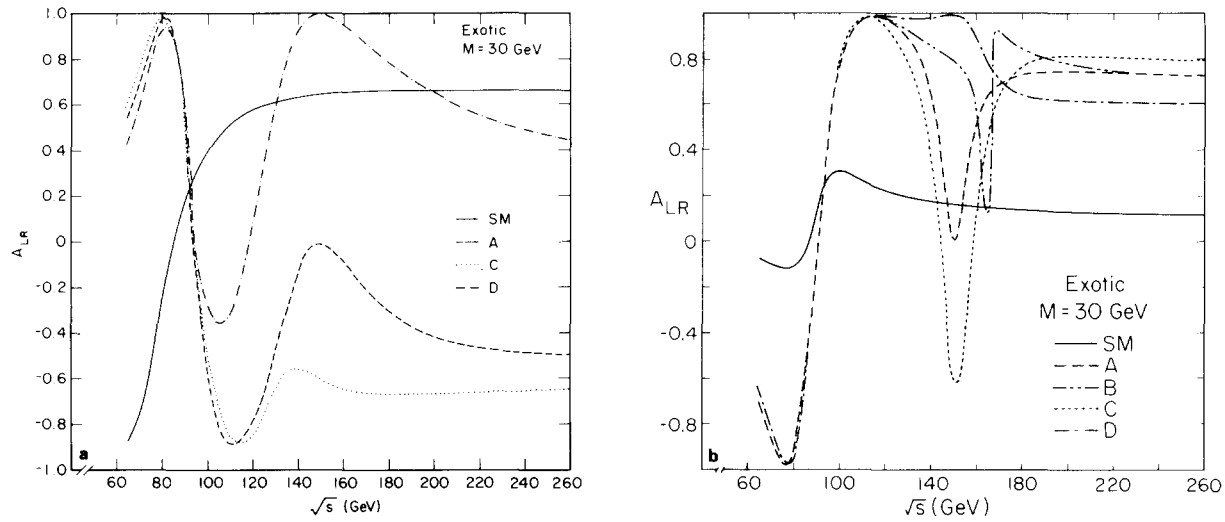

Fig. 59. Left–right asymmetry for (a) h and (b) E pair production for models ψ (A), χ (B), η (C), and I (D) with $M_{Z_2} = 150$ GeV, and for SM fourth generation fermions (SM).

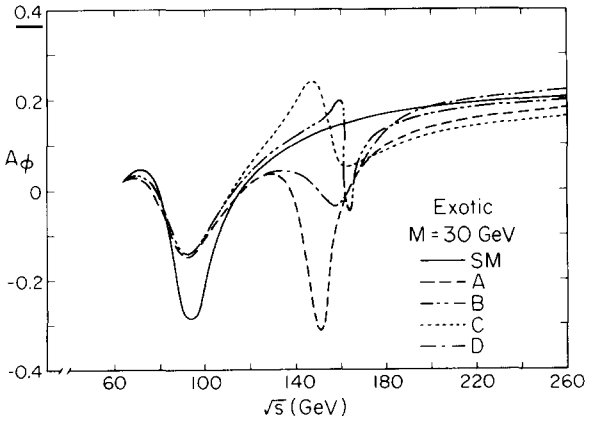

Fig. 60. Azimuthal asymmetry for 30 GeV SM fourth generation and exotic E-leptons for the same E_6 models as in fig. 59.

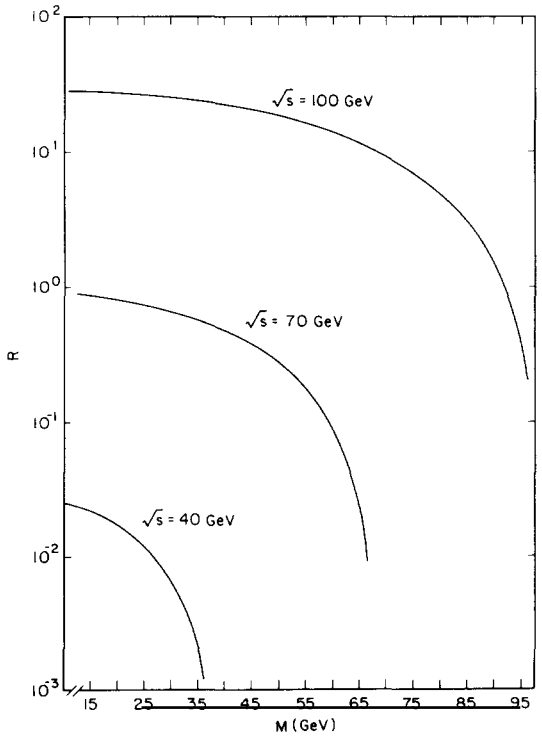

Fig. 61. The ratio R, as defined in the text, for single exotic production via Z_1 exchange only.

through s-channel $Z_{1,2}$ exchange with a cross section [3.72] [for couplings defined in (3.97)]

$$\frac{d\sigma}{dz}(e^+e^- \to \bar{d}h) = \frac{N_c s}{32\pi}\left(1-\frac{M_h^2}{s}\right)\left[1-\left(\frac{M_h^2}{s}\right)^2\right]\sum_{ij} P_{ij}^{ss}[B_{ij}(1+\beta z^2)+C_{ij}(1+\beta)z]\,. \tag{3.104}$$

Here $\beta \equiv (s-M_h^2)/(s+M_h^2)$ and $z=\cos\theta$ where θ is defined as the angle between e^- and h. (3.104) also applies for $e^+e^- \to d\bar{h}$ with $z \to -z$ and keeping the same definition of θ. The ratio $R \equiv \sigma(e^+e^- \to \bar{d}h + d\bar{h})/\sigma(e^+e^- \to \mu^+\mu^-)$ is shown in fig. 61 from ref. [3.72] neglecting the mixing and color factors. The production rates are reduced once σ is scaled by the appropriate mixing factor, $(s_L^d c_L^d)^2$ in this case. Single E production is also mediated by Z_i in the t-channel as well as in the s-channel and the complete cross section for $e^+e^- \to e\bar{E} + \bar{e}E$ is expressed in terms of helicity amplitudes in ref. [3.73]. The reaction $e^+e^- \to \bar{\nu}_e N$ proceeds through W t-channel as well as Z_i s-channel exchange. The cross section for the W t-channel contribution only (assuming $t \ll M_W^2$) can be found in this reference. The signal for single N production depends on the relative masses of N and E, but one interesting possibility is that of monojet events. These single production processes have the advantage of less phase space suppression, but generally have very small rates due to the constraining mixing angle factors.

3.4.1.3. Continuum production: h-leptoquarks and diquarks. Leptoquark production in e^+e^- collisions has been studied by a number of authors [3.23, 3.15, 3.74].

Pair production of the spin-$\frac{1}{2}$ h-leptoquarks occurs through the usual s-channel γ, Z_1, and Z_2 exchange, as well as by u-squark exchange in the t-channel via the Yukawa couplings λ_6 and λ_7. The differential cross section is expressed in terms of the helicity amplitudes (for both the gauge and Yukawa pieces) in ref. [3.74]. Figure 62 from this reference shows the ratio $R \equiv \sigma(e^+e^- \to h\bar{h})/\sigma_{pt}$ for several values of the center-of-mass energy $\sqrt{s}$ and M_{Z_2}, where the solid curves correspond to pure gauge boson exchange and the dashed curves also include the Yukawa interactions (with $\lambda_6 = \lambda_7 = \sqrt{4\pi\alpha}$). The existence of a 500 GeV Z_2 increases the production cross section by roughly a factor of 2 and if resonance production is possible (i.e., $2M_h < M_{Z_2}$) the cross section then becomes quite large. Schaile and Zerwas [3.74] have performed detailed background simulations and found that in the

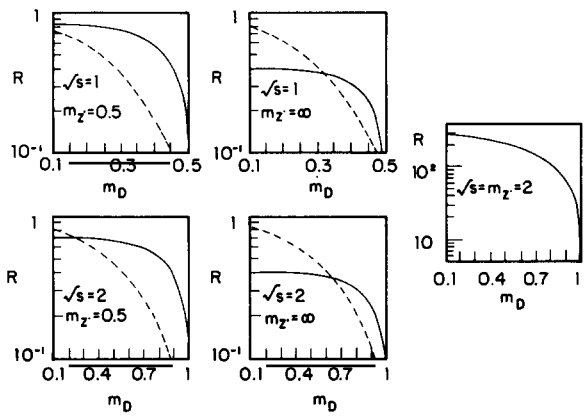

Fig. 62. The R-ratio for $e^+e^- \to h\bar{h}$ as a function of the leptoquark mass for various values of $\sqrt{s}$ and M_{Z_2} as indicated. The solid curves represent the gauge boson exchanges only and the dashed curves demonstrate the effect of additional Yukawa interactions.

scenario where $M_{Z_2} < 2M_h$, and the Yukawa interactions are neglected (assuming a $\sqrt{s} = 2$ TeV e^+e^- collider with an integrated luminosity of 10 fb^{-1}) appropriate background cuts can result in a signal to noise ratio of 10, with 60–90 clean signal events/yr for the decay mode $h \to u\tilde{e}$. In this case, the discovery limit is set at $M_h \simeq 0.9$ TeV. Clearly if resonance production is possible ($2M_h < M_{Z_2}$) or if the Yukawa interactions are stronger, the h-leptoquark signal would be even easier to spot. These authors also simulated diquark production (s-channel only!) and found 45–70 clean signal events/yr for the decay channel $h \to \tilde{u}\tilde{d}$ assuming the same conditions as above.

Scalar leptoquark production, $e^+e^- \to \tilde{h}\tilde{h}$, receives contributions from γ, Z_i s-channel diagrams, as well as u-quark exchange in the t-channel due to Yukawa interactions. Neglecting mixing between the scalar states, the production cross section [3.23] is given by

$$\frac{d\sigma}{dz} = \frac{3\pi\alpha^2}{4}\beta^3 s(1-z^2)\left(\sum_{ij} P_{ij}^{ss} C_i C_j (v_i v_j + a_i a_j) + \frac{1}{st}\sum_i C_i R_i (k v_i - k' a_i) + \frac{1}{4t^2}(k^2 + k'^2)\right), \tag{3.105}$$

with $t = M_{\tilde{h}}^2 - s(1-\beta z)/2$, R_i is defined in eq. (2.57), the couplings are normalized as in (3.62), k and k' are as given in (3.60), C_i is the coefficient of the $Z_i\tilde{h}\tilde{h}$ coupling, and β is defined as usual. The ratio of the total cross section to σ_{pt} is presented in fig. 63 from ref. [3.74] for various values of $\sqrt{s}$ and M_{Z_2} (and setting $k = k' \equiv \frac{1}{2}\lambda^2 = \frac{1}{2}$). Unlike the case of spin-$\frac{1}{2}$ h production, the Yukawa interactions significantly increase the production cross section for scalar leptoquarks. However, the β^3 phase space suppression factor for scalar particles constrains the mass range over which $\tilde{h}$ production can be explored. Assuming only gauge interactions (i.e., $\lambda^2 \ll 4\pi\alpha$) with $M_{Z_2} < 2M_{\tilde{h}}$ the discovery limit is $M_{\tilde{h}} \simeq 0.6$ TeV [3.74] at a $\sqrt{s} = 2$ TeV collider with an integrated luminosity of 10 fb^{-1}, with only 5–40 clean signal events/yr in the decay channel $\tilde{h} \to eu$. But, if Z_2 has a favorable mass or the Yukawa couplings have larger values, the $\tilde{h}$ mass search limit could be close to the beam energy. Likewise, for the case of scalar diquarks with the decay mode, $\tilde{h} \to \bar{u}\bar{d}$, 4–30 clean signal events/yr could be obtained.

Scalar leptoquarks have a non-zero forward–backward asymmetry [3.23] due to the existence of the t-channel Yukawa interactions which modify the angular distribution away from the standard $(1-z^2)$ expected for s-channel scalar pair production. If the Yukawa couplings are large enough, they can lead to significant values of A_{FB} as are shown in fig. 64. In this figure the maximum allowed values of k [as

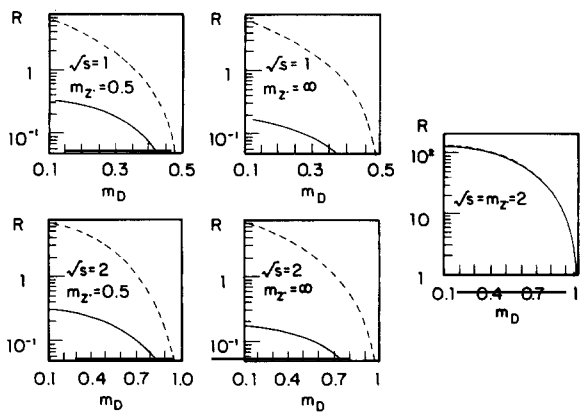

Fig. 63. Same as fig. 62, but for scalar leptoquark production, $\tilde{h}$.

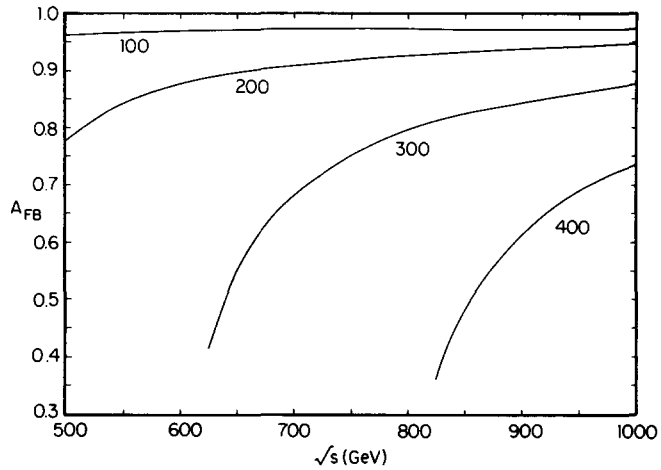

Fig. 64. A_{FB} for $0.5 \leq \sqrt{s} \leq 1$ TeV with $M_{\tilde{h}} = 100$ GeV ($k = 0.25$), $M_{\tilde{h}} = 200$ GeV ($k = 0.9$), $M_{\tilde{h}} = 300$ GeV ($k = 2.0$), and $M_{\tilde{h}} = 400$ GeV ($k = 3.6$).

defined in eq. (3.60) with $k = k'$] for each value of $M_{\tilde{h}}$ as given in fig. 42 have been assumed. Since "ordinary" scalars (such as squarks) do not possess an A_{FB} [due to the $(1 - z^2)$ angular distribution], a non-zero measurement of A_{FB} would be a good signature for scalar leptoquarks and an indication of large Yukawa couplings.

Single production of scalar leptoquarks takes place via the higher order process $e^+e^- \to e\bar{u}\tilde{h}$, which proceeds from a γ bremsstrahlung from the e^+ (or e^-) beam and through the consequent sub-process reaction $\gamma e^- \to \bar{u}\tilde{h}$. The resulting cross section, which was obtained by use of the effective γ approximation, is dependent on the unknown Yukawa coupling strength and is displayed in fig. 65 from ref. [3.75] at $\sqrt{s} = 1$ TeV for $k = 1.0$, and 0.1 (with k as defined as above), and with a p_T cut on the associated jet of $p_{T_{jet}} > 10$ GeV. The pair production cross section is also shown in the figure for

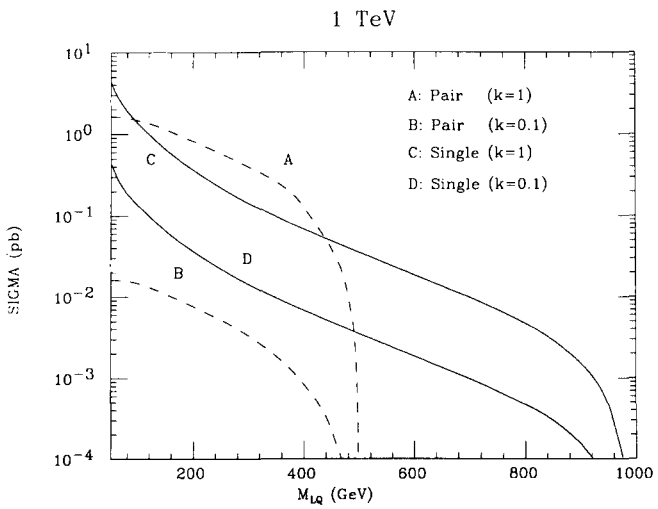

Fig. 65. Single (solid lines) and pair (dashed line) leptoquark production at a $\sqrt{s} = 1$ TeV e^+e^- collider for the values of k as indicated.

comparison, where it is clear that the single production rate is competitive with that for pairs for $k = 1.0$, and will have a larger discovery reach. Since the pair production rate receives substantial contributions from the Yukawa interactions (as discussed above), one would expect the single production mechanism to remain competitive for smaller values of k. The cleanest signal for this process is two jets + $\not{p}_T$ (from the $\tilde{h} \to d\nu$ decay channel) with a small SM background arising from $\gamma\gamma$ events. This mechanism could greatly extend the scalar leptoquark discovery reach at e^+e^- colliders, if the Yukawa couplings are not infinitesimally small.

3.4.1.4. Indirect signals: E-leptons. The E-lepton can contribute to the process $e^+e^- \to Z^0Z^0$ through t- and u-channel exchange via ordinary–exotic mixing, in addition to the usual electron t- and u-channel exchange diagrams for this process. Since only the e_R, E_R mass eigenstates have non-diagonal couplings to the Z, this additional E-lepton exchange channel is only open for incoming right-handed polarized electrons. The effect of this new channel is then maximized by the asymmetry

$$A_{ZZ} = \sigma_R - \sigma_L \,, \tag{3.106}$$

where $\sigma_{R(L)}$ denotes the total cross section for right- (left-)handed incoming electrons. This quantity is very sensitive to the exact value of $\sin^2\theta_w$ and reaches a maximum when the eeZ coupling is purely axial-vector. The work of ref. [3.76] shows that for a value of $x_w = 0.25$, A_{ZZ} has a value of 0.1 (0.06) at $\sqrt{s} = 200$ (400) GeV for $M_E = 100$ GeV and then decreases to zero as M_E is increased to 1 TeV. At $\sqrt{s} = 1$ TeV, $A_{ZZ} \simeq 0.01$ for $M_E = 100$ GeV and then smoothly increases as M_E becomes larger to a value of $A_{ZZ} \simeq 0.2$ for $M_E = 1$ TeV. The values of this asymmetry decrease for smaller values of x_w. We note that the results presented here were obtained by using generally larger values of the ordinary–exotic mixing ($\cos^2\theta_R^e \gtrsim 0.83$).

3.4.1.5. Indirect signals: h-leptoquarks. As discussed in section 3.2, scalar leptoquarks participate in the process $e^+e^- \to q\bar{q}$ through t-channel exchange, where the differential cross section, $d\sigma/d\cos\theta$, is given in eq. (3.61). Figure 66, from the work of Dreiner et al. [3.77], displays contours of $\delta\sigma/\sigma$ in the leptoquark coupling–mass plane at LEP II where $\delta\sigma$ represents the additional terms in the $e^+e^- \to u\bar{u}$ cross section due to leptoquark exchange and σ is the total cross section summed over all quark flavors

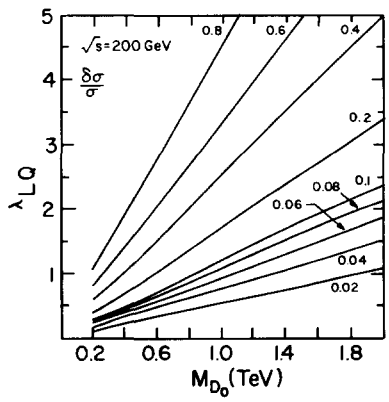

Fig. 66. Contours of $\delta\sigma/\sigma$ in the leptoquark coupling–mass plane for the process $e^+e^- \to q\bar{q}$ at LEP II.

q. Here, $\lambda_{LQ} = \lambda_6 = \lambda_7$ [where λ_{LQ} is related to the factor k in $d\sigma/d\cos\theta$ as in eq. (3.105)] and M_{D_0} is the scalar $\tilde{h}$ mass. For $\lambda_{LQ} = 1.0, 0.5, 0.3$ a sensitivity of $\delta\sigma/\sigma = 2\%$ leads to discovery limits of $M_{\tilde{h}} \simeq 1.8, 0.9, 0.5$ TeV. At LEP I energies, the cross section is dominated by the Z peak and thus is not sensitive to this indirect exchange. The results for a $\sqrt{s} = 2$ TeV e^+e^- linear collider scale roughly by a factor of 10 from the LEP II curves (i.e., $\delta\sigma/\sigma = 2\%$ for $\lambda = 1.0, 0.5, 0.3$ yields discovery limits of $M_{\tilde{h}} = 20, 9, 6$ TeV). The corresponding forward–backward asymmetry for quark pair production will also be modified by the leptoquark t-channel contribution. However, Dreiner et al. show that this asymmetry is not as sensitive to the leptoquark exchange as the cross section, and can only detect $M_{\tilde{h}} \lesssim 0.3$ TeV if $\lambda_{LQ} = 1.0$ for a 2% measurement of δA at LEP II. Obviously, e^+e^- colliders are a good tool for the exploration of indirect leptoquark effects via the process $e^+e^- \to q\bar{q}$, even for very large leptoquark masses.

Virtual t-channel scalar leptoquark exchange can also be responsible for single top-quark production in e^+e^- collisions via the process $e^+e^- \to t\bar{c}$ or $t\bar{u}$ (+ $\bar{t}c$ or $\bar{t}u$). This mechanism could result in the production of t-quarks up to 180 GeV in mass at LEP II, or the production of lighter top quarks at SLC and LEP I, even if pair production is prohibited by kinematics. Remarkably, these non-diagonal Yukawa couplings which are responsible for these intergenerational vertices are not restricted from FCNC data and hence a priori could be large. (However, it seems unnatural to have large $\tilde{h}ec$ or $\tilde{h}et$ couplings, while FCNC's restrict other intergenerational scalar leptoquark couplings to be small, as discussed in section 3.3.) For Yukawa couplings of order of the electric charge, one generation of leptoquarks in the heavy leptoquark limit ($M_{\tilde{h}}^2 \gg s$) results in an approximate change in R of [3.78]

$$\Delta R = \frac{\sigma(e^+e^- \to t\bar{c} \text{ or } \bar{t}c)}{\sigma(e^+e^- \to \text{“}\gamma\text{”} \to \mu^+\mu^-)} \simeq \frac{3}{8}\left(\frac{s}{M_{\tilde{h}}^2}\right)^2\left(1 + \frac{m_t^2}{s}\right)\left(1 - \frac{m_t^2}{s}\right)^2, \tag{3.107}$$

for unpolarized beams. The experimental signatures for these events should be quite distinctive. The change in R for the production of a $t\bar{c}$ quarkonium bound state, T_c^*, is estimated as (for $M_{T_c^*} < M_W$)

$$\Delta R = \frac{2\sigma(e^+e^- \to T_c^*)}{\sigma(e^+e^- \to \text{“}\gamma\text{”} \to \mu^+\mu^-)} \simeq \frac{9}{2}\left(\frac{m_t m_c}{M_{\tilde{h}}^2}\right)^2 \frac{\Gamma(\Upsilon \to e^+e^-)}{(5 \times 10^{-6})\delta W}, \tag{3.108}$$

where δW is the beam spread and $\Gamma(\Upsilon \to e^+e^-)$ is the partial width of the $\Upsilon(b\bar{b})$ state into e^+e^- pairs.

The contribution of third-generation $\tilde{h}_{L,R}$ t-channel exchange to the decays $V_t \to \tau^+\tau^-$, where V_t is the $^3S_1(t\bar{t})$ quarkonium bound state, can influence [3.79] the forward–backward asymmetry of $e^+e^- \to \tau^+\tau^-$. However, a conservative choice of the parameters ($\lambda_6 = \lambda_7 = 0.5$) yields only a slight difference of this asymmetry from its SM prediction. Diquark quantum numbers for the h would influence the A_{FB} for $e^+e^- \to b\bar{b}$ through a similar mechanism ($e^+e^- \to V_t \to b\bar{b}$ with diquark contributions to $V_t \to b\bar{b}$). The resulting change in the b-quark A_{FB} is also small in this case and mimics the effect that would arise from the exchange of charged Higgs bosons in $V_t \to b\bar{b}$.

The t-channel exchange of spin-$\frac{1}{2}$ h-leptoquarks can contribute to the production of squarkonium bound states as well as squark pair production in e^+e^- annihilation, yielding potentially large cross sections. The expected shift in the R-ratio for S-wave squarkonium production near threshold is given by [3.80]

$$\Delta R = \frac{\sigma(e^+e^- \to \tilde{u}_L\bar{\tilde{u}}_R, \tilde{u}_R\bar{\tilde{u}}_L)}{\sigma_{pt}} = \frac{9\lambda^{1/2}(s, m_{\tilde{u}_L}^2, m_{\tilde{u}_R}^2)}{2s}\left(\frac{\lambda_6\lambda_7}{e^2}\right)\left(\frac{mM}{M^2 + m^2}\right)^2, \tag{3.109}$$

where $m^2 = m_{\tilde{u}_L} m_{\tilde{u}_R}$, $\lambda(s, m^2_{\tilde{u}_L}, m^2_{\tilde{u}_R})$ is the usual triangle function (2.36), and M is the leptoquark mass. For favorable values of the parameters, ΔR could be as large as $\Delta R \sim 1$.

3.4.2. ep colliders

ep colliders are especially well suited for leptoquark production and will be the best place to search for these particles. Hence it is not surprising that this subject has received much attention in the literature for leptoquarks specifically within the context of E_6 models, as well as within a more general setting. We will consider this topic first before turning our attention to the production of E-leptons and h-quarks, which generally have smaller production rates at ep machines.

3.4.2.1. h-leptoquarks. First we shall review the production of the supersymmetric partner, $\tilde{h}$, which is a scalar leptoquark and couples directly to a lepton–quark pair. Direct production occurs through an s-channel resonance by $e + u \to \tilde{h}$ with a subsequent decay to eu or νd and has been discussed by many authors [3.16, 3.81–3.86]. The differential cross section for this process ($eu \to \tilde{h} \to eu, \nu d$) is given by

$$\frac{d\sigma}{dx\,dy} = \frac{u(x, Q^2)}{32\pi} \frac{\lambda^4}{(\hat{s} - M^2_{\tilde{h}})^2 + M^2_{\tilde{h}}\Gamma^2}\,\hat{s}\,, \tag{3.110}$$

where $u(x, Q^2)$ is the u-quark distribution function, $\hat{s} = xs$, $Q^2 = sxy$, the width Γ is given in eq. (3.49), and we set the Yukawa couplings $\lambda_6 = \lambda_7 = \lambda$ for simplicity. The total integrated cross section from the work of Angelopoulos et al. [3.16] is presented in fig. 67 for $\sqrt{s} = 314$ GeV at HERA ($D_0 \simeq \tilde{h}$), where F parameterizes the coupling λ by $\lambda^2 = 4\pi F\alpha$. It is clear that this process is particularly sensitive to the value of the Yukawa coupling, but large cross sections are obtainable almost up to the kinematic limit due to the s-channel resonance. Leptoquarks can also contribute to the process $eq \to eq$ via t-channel exchange, but this amplitude is roughly two orders of magnitude smaller than the s-channel resonance and vanishes completely at $y = 1$.

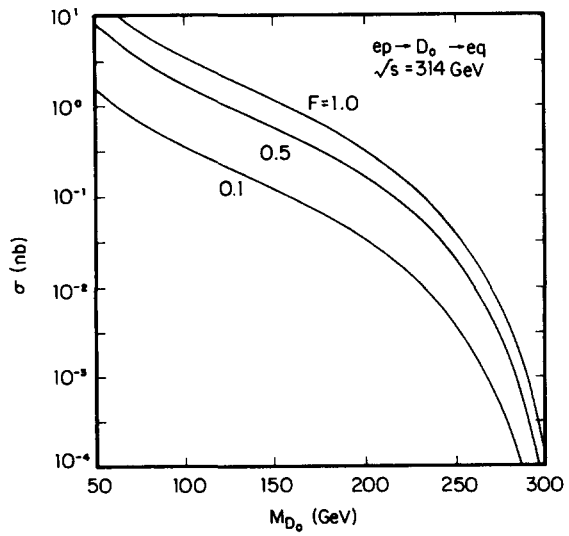

Fig. 67. Total cross section for s-channel scalar leptoquark production at HERA.

Gunion and Ma [3.82] have performed a thorough analysis of leptoquark production signals versus the ordinary electroweak background $eq \to eq$ which arises from γ and Z exchange. The s-channel resonance, $d\sigma/dx \sim \delta(x - M_{\tilde{h}}^2/s)$ yields distinctive peaks in the x-distribution, which are shown in fig. 68 from this reference for the process $eu \to eu$ with leptoquark masses of 100 GeV and 300 GeV. Here, the solid curve represents the leptoquark resonance plus interference plus background, while the dashed curve includes only the background, and the authors have set $\lambda = g$ where g is the weak interaction coupling strength, $\sqrt{s} = 324$ GeV, and have integrated $d\sigma/dx\, d\cos\theta$ over $\cos\theta$ from -0.99 to 0, where θ is the angle between the outgoing and incoming electron in the laboratory. Clearly, the signal peak lies 1–2 orders of magnitude above the ordinary electroweak background, and would stand out even for smaller values of λ. One should be aware that the signal peaks are quite narrow and would be smeared out in an experiment by the finite resolution in x.

Appropriate cuts in the y-distributions can also enhance the signal to background ratio. This is due to the fact that $\tilde{h}$ production is isotropic in y since $\tilde{h}$ is a scalar, whereas the electroweak background is forward peaked. Figure 69, from an analysis by Harnew [3.83], shows the signal to background rate for a 200 GeV leptoquark with cuts of $y > 0.01$ and $y > 0.5$. This analysis was performed for the ZEUS detector, assuming a $15\%/\sqrt{E}$ resolution for the e^- and $35\%/\sqrt{E}$ for jets, and taking $F = 0.01$. A cut of $y > 0.5$ seems to be optimal for enhancing the $\tilde{h}$ production signal over both the deep inelastic scattering neutral current and charged current background.

If the Yukawa coupling λ_8 is non-zero, then the process $e_R^- u \to h \to \nu_R d$ can occur via s-channel exchange. The differential cross section has the same x and y dependence as that in eq. (3.110) and is proportional to $\lambda_6^2 \lambda_8^2$ instead of λ^4. This process could be an important leptoquark signal as there is no standard model background!

A good summary of scalar leptoquark production in ep colliders is presented in fig. 70 from Ellis, Pauss et al. [3.84]. Here, leptoquark discovery limits ($D = \tilde{h}$) are shown in the coupling strength–mass plane ($\lambda^2/4\pi = F\alpha_{em}$) and are compared for HERA, a $\sqrt{s} = 1.4$ TeV, $\mathcal{L} = 10^{32}\,\mathrm{cm}^{-2}\,\mathrm{s}^{-1}$, and a $\sqrt{s} = 1.8$ TeV, $\mathcal{L} = 10^{31}\,\mathrm{cm}^{-2}\,\mathrm{s}^{-1}$ LEP × LHC option, where appropriate cuts in y ($y > 0.5$) have been included. For larger values of the coupling, the 1.8 TeV option has the largest reach as the bigger value of $\sqrt{s}$ eventually wins over luminosity. These machines can detect leptoquarks almost up to the kinematic limit for stronger couplings ($F = 1$), and can explore a wide mass range for smaller values of the coupling as well.

If the $\tilde{h}$-scalar is too massive to be produced directly at HERA, perhaps it could be detected through its indirect effects on the neutral current process $ep \to e + X$. If polarized e^- beams are available then

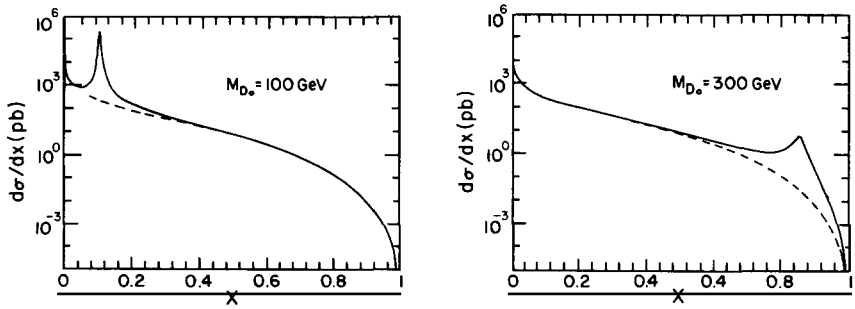

Fig. 68. Signal (solid curve) versus background (dashed curve) for scalar leptoquark production in the process $eu \to eu$ at HERA for 100 GeV and 300 GeV leptoquarks, where a 2% resolution at resonance is assumed.

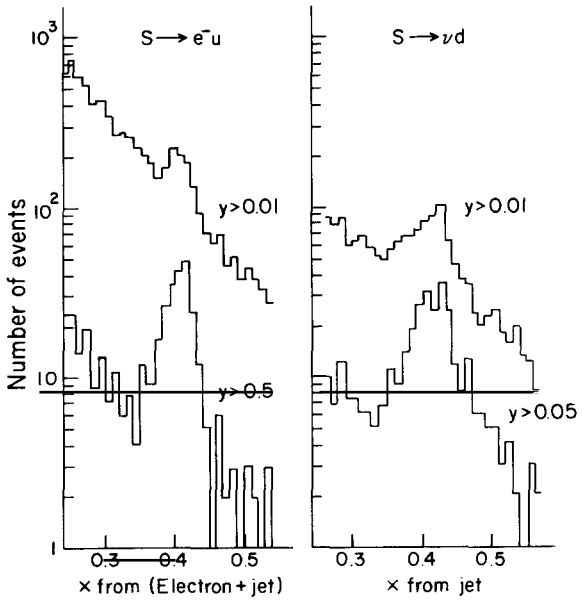

Fig. 69. x-distributions for the different y-cuts as indicated, for resonance leptoquark production at HERA.

various asymmetries, such as ($d\sigma \equiv d\sigma/dx\,dy$)

$$\frac{d\sigma(e_L^- p) - d\sigma(e_R^- p)}{d\sigma(e_L^- p) + d\sigma(e_R^- p)}, \qquad \frac{d\sigma(e_L^- p) - d\sigma(e_R^+ p)}{d\sigma(e_L^- p) + d\sigma(e_R^+ p)}, \qquad \frac{d\sigma(e_R^- p) - d\sigma(e_R^+ p)}{d\sigma(e_R^- p) + d\sigma(e_R^+ p)}, \tag{3.111}$$

could be measured. Buchmüller et al. [3.81] have discussed the first two of these asymmetries and have found that the deviation from the SM prediction due to the presence of scalar leptoquarks is small, even for a $\tilde{h}$ mass of only 400 GeV (setting $\lambda = 0.3$ and $x = 0.3$). Grifols and Peris [3.85] have analyzed the

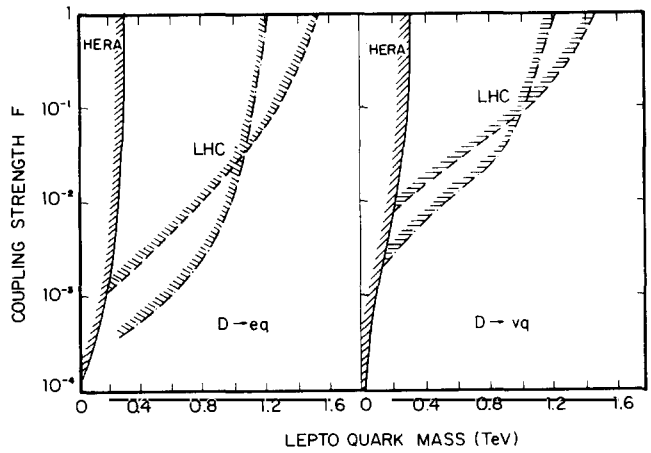

Fig. 70. A comparison of scalar leptoquark discovery limits at HERA and LEP × LHC (with $\sqrt{s}$ = 1.4 or 1.8 GeV) in the leptoquark coupling–mass plane.

last asymmetry in (3.111) and find that $\delta A \equiv A - A_{SM}$ can be substantial (ranging from -0.8 to 1.0) in an x bin of $0.36 \leq x \leq 0.46$ with $y = 0.45$, but these values are for $M_{\tilde{h}} = 200$ GeV and $\lambda = 0.1$, and are in the range where leptoquarks could be directly produced and observed. Hence it is doubtful that leptoquarks with masses above the kinematic limit can be indirectly detected. However, if their mass is such that they have been directly produced, then the polarized beams and the various asymmetries which can be formed could be valuable in probing the nature of the leptoquark couplings (e.g., left- versus right-handedness).

Associated scalar leptoquark production ($\tilde{h} + u$ or $\tilde{h} + g$) can also occur with reasonable rates and has been studied by Dobado et al. [3.86]. The Feynman diagrams responsible for the processes $e^- u \to \tilde{h} g$ and $e^- g \to \tilde{h} u^c$ are shown in fig. 71a, b, respectively (where $\tilde{D} = \tilde{h}$). The resulting cross sections are proportional to λ_6^2 (λ_7^2 for $\tilde{h}^c$ production) and are given explicitly in ref. [3.86]. The total integrated cross sections scaled by λ^2 from this same reference are presented in fig. 72 for (a) the mechanism $e^- p \to \tilde{h} g + X$, and (b) $e^- p \to \tilde{h} u^c + X$ at HERA and the proposed LEP × LHC (with $\sqrt{s} = 2$ TeV). These processes are not as dominant as the single s-channel production mechanism discussed above, but are important in that they produce events with higher p_T. The production signal is two jets + e (or ν). An estimated discovery limit at HERA for $\lambda \sim 0.1$ is $M_{\tilde{h}} \sim 250$ GeV for the first mechanism and ~165 GeV for the second. These authors also consider $\tilde{h}\tilde{\bar{h}}$ pair production, which proceeds via photon–gluon fusion, similarly to squark pair production. This mechanism does not depend on the unknown Yukawa coupling, but is phase-space suppressed, and yields a search limit of approximately $M_{\tilde{h}} \simeq 45$ GeV at HERA.

The spin-$\frac{1}{2}$ leptoquark (with odd R-parity), h, can be produced in ep collisions in association with supersymmetric particles (in order to conserve R-parity) via the subprocesses $eu \to h\tilde{\gamma}$, $eg \to h\tilde{u}$, and $eu \to h\tilde{g}$. Assuming that the $\tilde{\gamma}$ is the lightest supersymmetric particle and given present limits on squark and gluino masses [3.87] ($M_{\tilde{q},\tilde{g}} > 80$ GeV) it is clear that $eu \to h\tilde{\gamma}$ will have the largest production rate of the above processes due to phase space. The Feynman graphs which contribute to $eu \to h\gamma$ are shown in fig. 73. Due to the proliferation of parameters (M_h, $M_{\tilde{h}_{L,R}}$, $M_{\tilde{e}_{L,R}}$, $M_{\tilde{u}}$, $M_{\tilde{\gamma}}$, λ_6, and λ_7) the author of ref. [3.88] considered only the first diagram in the figure, in the limit of a massless $\tilde{\gamma}$. In this approximation the parton level differential cross section is

$$d\sigma/d\cos\theta^* = \alpha\lambda^2\beta t(t - M_h^2)/64s(s - M_{\tilde{e}}^2)^2 , \tag{3.112}$$

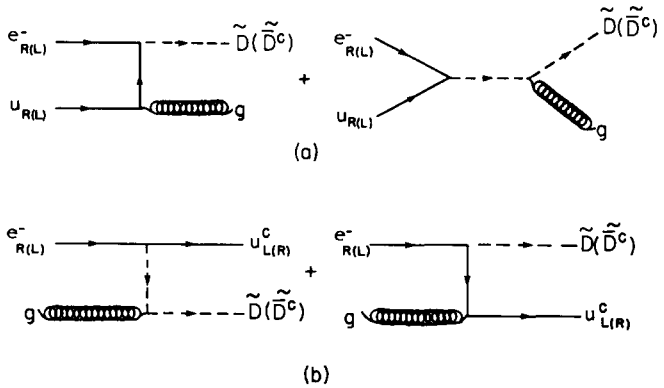

Fig. 71. Feynman graphs contributing to the associated production of scalar leptoquarks in ep collisions.

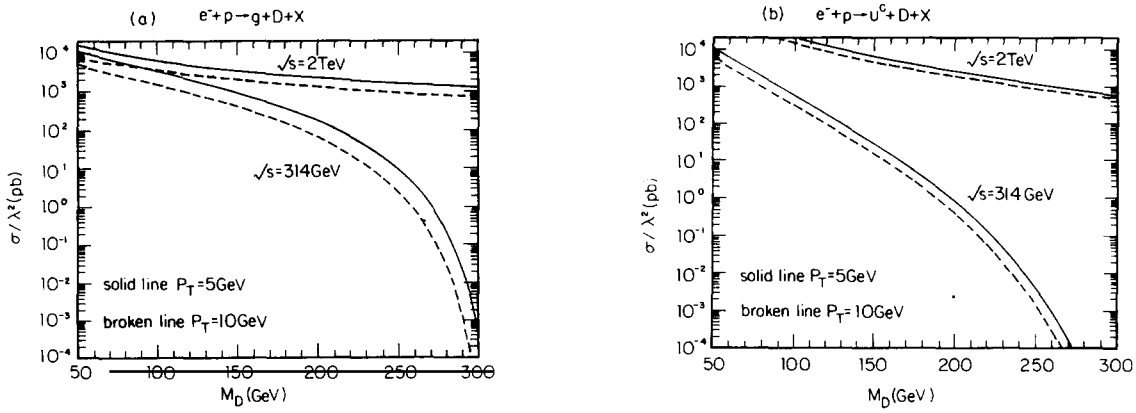

Fig. 72. Total cross section (scaled by λ^2) for leptoquark production via (a) $e^-p \to \tilde{h} + g + X$ and (b) $e^-p \to \tilde{h} + u^c + X$ ($D = \tilde{h}$). The solid (dashed) curves represent a minimum value of 5 (10) GeV for the transverse momentum of the final state particles.

with $\beta \equiv 1 - M_h^2/s$, $\lambda = \lambda_6$, and θ^* is the angle between the photino and electron. For a value of $\lambda = 0.5$, Robinett finds that the total cross section at HERA is about 3 (0.5) pb for masses of $M_h = 60$ (120) GeV and $M_{\tilde{e}} = 80$ GeV. At LEP × LHC with $\sqrt{s} = 2$ TeV the cross section rises to 17 (4) pb for these same masses. The signal for these events would be $h\tilde{\gamma} \to (q\ell\tilde{\gamma})\tilde{\gamma} \to$ jet + charged lepton + missing energy. This mechanism is competitive with that of SM SUSY particle production at ep machines (e.g., $eq \to \tilde{e}\tilde{q}$, etc.), but cannot compete with h production at hadron colliders.

The associated production process $ep \to hS^c$, which proceeds through W_R t-channel exchange in the alternative left–right symmetric model, was discussed in section 2.6 and the resulting cross sections are shown in fig. 38a, b from ref. [2.52]. The cross section can be obtained from the general expressions given in eq. (3.120) with appropriate substitutions.

3.4.2.2. h-diquarks. The production of scalar diquarks, both singly and in pairs, in ep collisions has been recently examined [3.89] using the effective photon approximation. The unknown coupling strength of $qq\tilde{h}$ is parameterized as $k\alpha_{em}$ where k is defined in eq. (3.60).

Pair production of diquarks at ep colliders proceeds through photon–gluon fusion and is hence independent of the unknown coupling strength. The cross section for diquark pairs depends only on the diquark mass and charge, and is shown in fig. 74. For $Q = -\frac{1}{3}$, σ is of order 1 pb at $\sqrt{s} = 314$ GeV for $M_D \simeq 28$ GeV. The $\sqrt{s} = 1.8$ TeV LHC × LEP option yields larger cross sections, with values of 1 pb for $M_D \simeq 75$ GeV. The corresponding signal is four jets with double peaking in the jet–jet invariant mass distribution and is relatively background free.

Single diquark production occurs via photon–quark fusion. The cross section is directly proportional to the unknown quark–quark–diquark couplings (k) and thus is quite sensitive to its value. The single

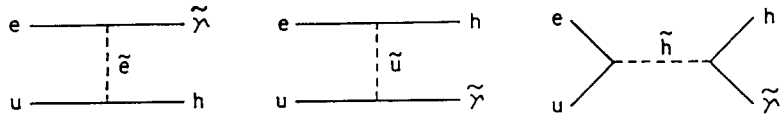

Fig. 73. Diagrams responsible for the subprocess $eu \to h\tilde{\gamma}$.

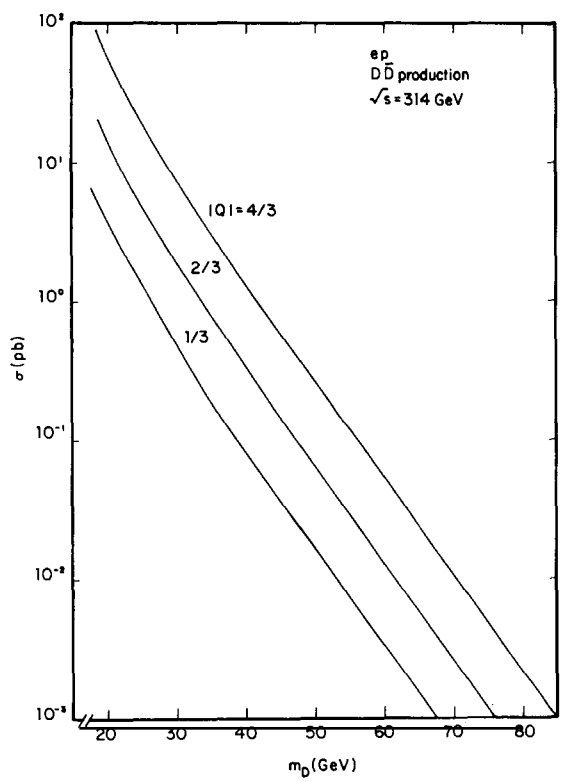

Fig. 74. Production cross section for $D\bar{D}$ (= $h\bar{h}$) pairs as a function of M_D for $Q_D = \frac{4}{3}, \frac{2}{3}$, and $-\frac{1}{3}$ at HERA.

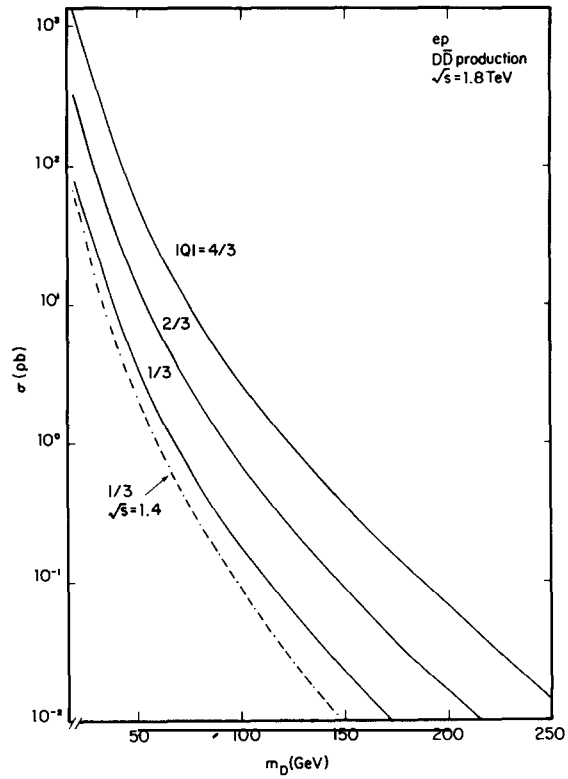

Fig. 75. Same as fig. 74, but for single D (= h) production with $k = 1.0$.

cross section at HERA is presented in fig. 75 from ref. [3.89]. Here, cross sections of order 1 pb are obtained at HERA for $M_D \simeq 65$ GeV and at LHC × LEP ($\sqrt{s} = 1.8$ TeV) for $M_D \simeq 130$ GeV assuming $k = 1$ in all cases. Hence, for $k = 1$ the single production cross sections are larger than those for pair production, but the single production rate decreases substantially for smaller values of k. The signal for single production is three (or two) jets, with the jet from the associated anti-quark preferring to be at small angles. The background results from QCD processes and is potentially larger than that for diquark pairs since the associated antiquark jet produced along with the single diquark comes out at a small angle relative to the beam. Although p_T cuts may decrease the QCD background, they will also substantially reduce the signal. Search limits, assuming 25 events constitute a discovery, are then set at ≃40 GeV and 110 GeV for pair and single production, respectively, with $k = 1.0$.

3.4.2.3. h-quarks and E-leptons. Single production of exotic h-quarks and E-leptons in ep collisions proceeds through ordinary–exotic mixing and has been considered in ref. [3.90]. The subprocess eq → Eq results from neutral current t-channel Z_1 and Z_2 exchange, while ep → h + X has contributions from the charged current reaction eu → ν_eh and neutral current reaction ed → eh. The general double differential cross section for these processes is given by

$$\frac{d^2\sigma}{dz\,dy} = \frac{G_F^2 M_X^4}{4\pi} s \sum_q \sum_{ij} P_{ij}\{\alpha_{ij}^q F_1[q(z) + \bar{q}(z)] + \beta_{ij}^q F_2[q(z) - \bar{q}(z)]\}\,, \tag{3.113}$$

with $P_{ij}(s \to Q^2)$ as defined in eq. (2.42), $Q^2 = sxy$, $q(z)$ is the appropriate parton distribution function, and

$$\alpha_{ij}^{q} = (v_i v_j + a_i a_j)_{q(e)}(v_i v_j + a_i a_j)_{eE(qh)}\,, \qquad \beta_{ij}^{q} = (v_i a_j + a_i v_j)_{q(e)}(v_i a_j + a_i v_j)_{eE(qh)}\,, \tag{3.114}$$

for E (h) production. The couplings are normalized as

$$\begin{aligned}\mathscr{L} &= (g/2c_w)[\bar{e}\gamma_\mu(v_{ie} - a_{ie}\gamma_5)e + \bar{h}\gamma_\mu(v_{iqh} - a_{iqh}\gamma_5)d]Z_i^\mu \\ &\quad + (g/2\sqrt{2})[\bar{h}\gamma_\mu(v_{qh} - a_{qh}\gamma_5)u + \bar{\nu}\gamma_\mu(v_e - a_e\gamma_5)e]W^\mu\,,\end{aligned} \tag{3.115}$$

for h production, with e→q, h→E, and d(q)→e in the NC interaction for E production. In the case of eq→Eq, $M_X = M_{Z_1}$, $z = x$, and ($\lambda \equiv M_E^2/s$)

$$F_1 = x(1-y) - \lambda + (y/2)(xy + \lambda)\,, \qquad F_2 = -xy(1 - y/2) + \lambda y/2\,, \tag{3.116}$$

x and y are constrained to the ranges

$$\lambda \le x \le 1\,, \qquad 0 \le y \le 1 - \lambda/x\,. \tag{3.117}$$

Neglecting the ordinary–exotic mixing, one finds [3.90] that the total cross section is generally small with $\sigma \simeq 0.82$ (0.25) pb at $\sqrt{s} = 314$ GeV for $M_E = 50$ (100) GeV with $M_{Z_2} = 300$ GeV. For a $\sqrt{s} =$ 1.5 TeV ep machine, these production cross sections scale roughly by a factor of 100. It is clear that once these cross sections are also scaled by the appropriate mixing factors, they become quite small.

In the case of h production ($\lambda \equiv M_h^2/s$),

$$F_1 = (\lambda/y)(1-y) + x(1 - y + y^2/2)\,, \qquad F_2 = xy(1 - y/2)\,, \tag{3.118}$$

$z = x + \lambda/y$, and the scaling variables are constrained to lie within the ranges

$$0 \le x \le (1 - \lambda/y) \le 1 - \lambda\,, \qquad \lambda/(1-x) \le y \le 1\,. \tag{3.119}$$

For the NC process, $M_X \equiv M_{Z_1}$ and the sum over q only includes the d-quark [i.e., $q(z) = d(z)$], while in the CC case $M_X \equiv M_W/\sqrt{2}$, and only the u-quark contributes, and the sum over i, j in eq. (3.113) reduces to a single term. The production rates are slightly larger than for ep→E + X, yielding [3.90] $\sigma(ep \to \nu h + X) \simeq 15$ (6) pb for $M_h = 50$ (100) GeV at $\sqrt{s} = 314$ GeV neglecting d–h mixing factors. The NC process results in cross sections which are approximately a factor of 20 smaller. In addition, these cross sections increase by a factor of 3–10 for a $\sqrt{s} = 1.5$ TeV collider. However, these results are again disappointingly small, especially once the ordinary–exotic mixing is included.

Exotic final states can also be obtained via W_I t-channel exchange (see section 2.6), the subprocess ed→Eh, and has been investigated by Godfrey [2.55]. The differential cross section for general couplings [2.52] is

$$\frac{d^2\sigma}{dz\,dy} = \frac{g^4}{64\pi\hat{s}}\left(\frac{\hat{s}^2}{(sxy+M^2)^2+\Gamma^2M^2}\right)$$
$$\times\left\{\frac{(v_1^2+a_1^2)(v_2^2+a_2^2)}{4}\left[1-\left(\frac{M_E^2+M_h^2}{\hat{s}}\right)+(1-y)\left((1-y)+\frac{M_h^2-M_E^2}{\hat{s}}\right)\right]\right.$$
$$+(v_1a_1v_2a_2)\left[1-\left(\frac{M_E^2+M_h^2}{\hat{s}}\right)-(1-y)\left((1-y)+\frac{M_h^2-M_E^2}{\hat{s}}\right)\right]$$
$$\left.+\frac{(v_1^2+a_1^2)(v_2^2+a_2^2)}{2}\frac{M_E^2M_h^2}{M^2}\left[\frac{1}{\hat{s}}+\frac{y}{4M^2}\left(y+\frac{M_E^2-M_h^2}{\hat{s}}\right)\right]\right\}, \tag{3.120}$$

where $M(\Gamma)$ is the mass (width) of W_I, $\hat{s}=sz$, and the interaction Lagrangian is given by

$$\mathcal{L}=(g/2\sqrt{2})[\bar{d}\gamma_\mu(v_1-a_1\gamma_5)h+\bar{E}\gamma_\mu(v_2-a_2\gamma_5)e]W_I^\mu+\text{h.c.} \tag{3.121}$$

The total cross section is obtained via the integration [where $d(z,\hat{s})$ is the d-quark distribution function]

$$\sigma=\int_{z_{min}}^{1}dz\int_{y_{min}}^{y_{max}}dy\,\frac{d^2\sigma}{dz\,dy}\,d(z,\hat{s}), \tag{3.122}$$

with $z\equiv x+M_h^2/sy$, $z_{min}=(M_E^2+M_h^2)/s$, and

$$y_{\substack{min\\max}}=(1/2\hat{s})\{\hat{s}-M_E^2-M_h^2\mp[\hat{s}-(M_E+M_h)^2]^{1/2}[\hat{s}-(M_E-M_h)^2]^{1/2}\}. \tag{3.123}$$

The resulting cross section is not large at $\sqrt{s}=314$ GeV, i.e., $\sigma\lesssim 1\ (0.1)$ pb with $M=200\ (300)$ GeV for all choices of E and h masses. However, the event signature is clean (with the exact signal depending upon the relative masses of the exotics and their resulting decay chains) and Godfrey estimates that the discovery limit is $M_E+M_h\simeq 220\ (170)$ GeV for $M=200\ (300)$ GeV with an integrated luminosity of $600\,\text{pb}^{-1}$ (which corresponds to 3 years of running time). These production rates are slightly smaller than those for the similar subprocess $eu\to\text{"}W_R\text{"}\to nh$ which are shown in fig. 38. Note that W_I exchange could also mediate the related process $\nu_e d\to Nh$, but this reaction would require very high energy neutrino beams which are beyond the scope of present experiments.

h-quarks can also be pair produced via photon–gluon fusion but the resulting cross section is small and falls off rapidly with increasing M_h, with $\sigma\simeq 10^{-3}$ pb for $M_h=80$ GeV [2.55, 3.91].

It is clear from the above discussion that ep colliders are the best place to search for leptoquarks, but do not do as well as e^+e^- or hadron machines for the other types of exotic fermions.

3.4.3. Hadron colliders

Here we will concentrate not only on the different production mechanisms for each set of quantum number assignments for the exotic fermions, but also on the event signatures and possible sources of background.

3.4.3.1. Direct production: E-leptons and h-quarks. E_6 exotic lepton production in hadron colliders parallels that of heavy fourth generation leptons [3.92], where the dominant subprocesses are the Drell–Yan mechanism and the gluon fusion triangle diagram which are shown in fig. 76. The Drell–Yan

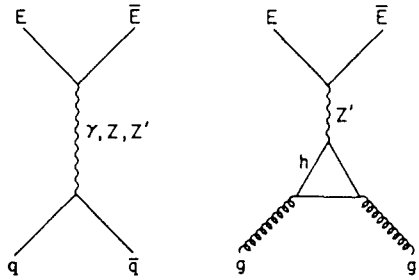

Fig. 76. Diagrams for Drell–Yan and gluon fusion subprocesses for EĒ production.

cross section for heavy leptons is well known [3.27] and we will not repeat it here, however for the case of E_6 lepton production one must also include the contribution from Z_2 exchange. In the gluon fusion subprocess the dominant contribution arises from h-quarks in the triangle (provided that they are the heaviest quarks in the theory) and the spin and color averaged subprocess cross section is (for three generations of approximately mass-degenerate h and E exotics)

$$\hat{\sigma} = \frac{27\alpha^2\alpha_s^2}{8\pi} \frac{\beta(a_{2h}a_{2E})^2}{(1-x_w)^2} \frac{M_E^2}{M_{Z_2}^4} \left| -2 \int_{\substack{\alpha+\gamma\le 1 \\ \alpha,\gamma>0}} d\alpha\, d\gamma \frac{M_h^2}{M_h^2 - \alpha\gamma\hat{s}} \right|^2 , \tag{3.124}$$

where $\beta \equiv (1 - 4M_E^2/\hat{s})^{1/2}$ as usual, and a_{2h}, a_{2E} are the axial-vector coupling constants of h and E to the Z_2. Note that Z_1 intermediate states do not contribute (except through mixing) since the cross section is proportional to the axial-vector coupling constants and h as well as E only couple vectorially to the Z_1. Figure 77 from ref. [3.92] shows the cross sections at the SSC for EĒ production as well as heavy neutral lepton pair production, assuming the neutrals are all Majorana particles, with M_{Z_2} taken to be 200 GeV. The production cross section for heavy Dirac neutral lepton pairs is approximately equal to that for charged leptons. The experimental signature for EĒ production depends on the relative E and N masses, but possible final states include $e^+e^-W^+W^-W^+W^-$, e^+e^-ZZ, or $W^+W^-\not{p}_T$ with high-p_T e^+ and e^- in the first two cases. If the first two signals are dominant, it may be possible to fully

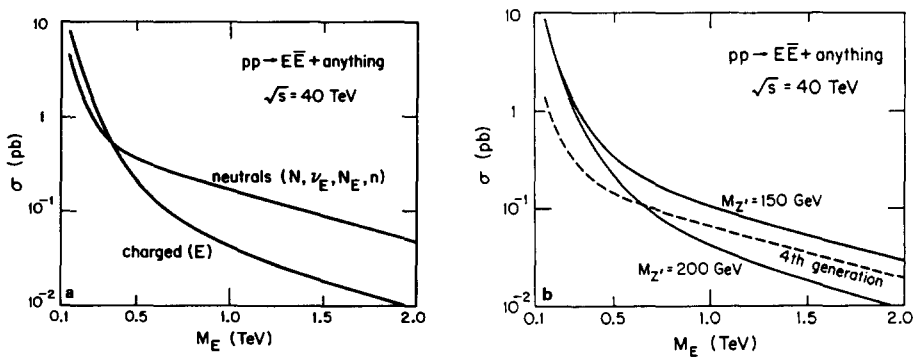

Fig. 77. (a) Drell–Yan and gluon fusion contributions to EĒ production, and (b) total EĒ and neutral Majorana pair production cross sections at the SSC with $M_{Z_2} = 200$ GeV. Three approximately mass-degenerate generations of each lepton type are assumed.

reconstruct the E-lepton masses, which would distinguish them from new SM sequential leptons. These exotic leptons should be observable up to $M_E \sim 1$ TeV at the SSC [3.92].

The forward–backward asymmetry of heavy leptons at hadron colliders could yield information on the lepton–Z_2 couplings as well as be useful in differentiating between SM sequential and E_6 exotic leptons [3.93]. The gluon fusion production mechanism is symmetric in y and hence does not contribute to this asymmetry. Only the Drell–Yan subprocess produces an asymmetry, where the prescription for computing A_{FB}^h for lepton production on the Z_2 resonance has been outlined in section 2.5.3. Here the substitutions

$$\tfrac{4}{3}[(C_L^\ell)^2 + (C_R^\ell)^2] \to \beta\{(1 + \tfrac{1}{3}\beta^2)[(C_L^\ell)^2 + (C_R^\ell)^2] + 2(1-\beta^2)C_L^\ell C_R^\ell\} \tag{3.125}$$

in $d\sigma^+/dy$ and $d\sigma^-/dy \to \beta^2\, d\sigma^-/dy$ in (2.69) must be included for massive leptons ($\beta^2 = 1 - 4M_E^2/\hat{s}$). The Z_2 resonance is used in order to increase the production rates. A_{FB}^h as a function of θ (the Z′–Z″ mixing parameter with $\theta_{E_6} \equiv \theta + \pi/2$) is given in fig. 78 from this same reference for both fourth generation and E_6 E-leptons at the Tevatron and SSC (where a minimum rapidity of $y_{min} = 0.1$ has been used). Note that $A_{FB}^h = 0$ in models η and χ for both types of leptons as well as in model ψ for E-leptons, and has its largest value in model I for both kinds of leptons. Clearly, information can be gathered from this asymmetry only for some E_6 models.

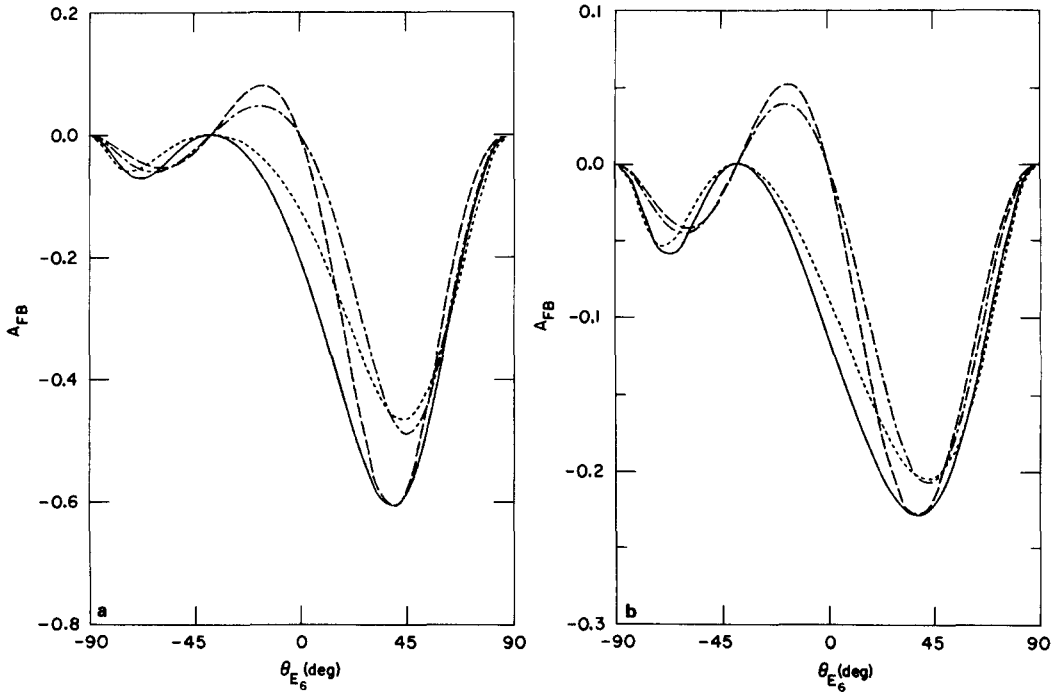

Fig. 78. (a) A_{FB} as a function of θ_{E_6} in $p\bar{p}$ collisions at $\sqrt{s} = 2.0$ TeV with $M_{Z_2} = 200$ GeV. The solid line and the dotted line are for fourth generation heavy leptons with $M_L = 40$ and 80 GeV, respectively. The dashed line and the dot–dashed line are for exotic E_6 heavy leptons with $M_E = 40$ and 80 GeV, respectively. (b) A_{FB} as a function of θ_{E_6} in pp collisions at $\sqrt{s} = 40.0$ TeV with $M_{Z_2} = 1.0$ TeV. The solid line and the dotted line are for fourth generation heavy leptons with $M_L = 100$ and 300 GeV, respectively. The dashed line and the dot–dashed line are for exotic E_6 heavy leptons with $M_E = 100$ and 300 GeV, respectively.

The production of h-quark pairs at hadron colliders is the same as that of any heavy color triplet quark and has been thoroughly studied within the context of the SM [3.27]. At SSC energies gluon fusion, $gg \to h\bar{h}$, dominates over the quark annihilation, $q\bar{q} \to h\bar{h}$. The total cross section is shown for reference in fig. 79a, b [3.3, 3.94]. Note that W_I t-channel exchange can also mediate the subprocess $q\bar{q} \to h\bar{h}$, but with negligible rates compared to the gluon fusion mechanism. The signature resulting from the decay $h \to uW$ is the same as that expected from a heavy SM sequential quark. However, mixing also allows the FCNC decay $h \to dZ_1$ which leads to an outstanding event signature of two jets + $\ell^+\ell^-\ell'^+\ell'^-$ with little SM background and is completely reconstructable. The event rate for this signature is too small (~0.6 events/yr) to be seen at the Tevatron, but the situation is much improved at the SSC as is witnessed by fig. 80 from ref. [3.95]. Folding in $\ell, \ell' = e$, μ, or τ yields a rate of ~67 events/yr for $M_h = 1$ TeV and thus h-quarks could be easily detected in this manner up to this mass.

Single h-quark production may also occur via the subprocesses $Wu \to h$, $gu \to Wh$, $Zd \to h$, and $gd \to Zh$. These mechanisms proceed through the ordinary–exotic mixing, but may have reasonable rates at supercollider energies.

3.4.3.2. Direct production: h-leptoquarks and diquarks. Pair production of h leptoquarks and diquarks is again the same as that for any other heavy color triplet fermion and is shown in fig. 79 for SSC energies. The most promising signatures for $h\bar{h}$ production are (assuming $\tilde{f} \to f + \tilde{\gamma}$ is the dominant supersymmetric decay) $h\bar{h} \to (d\nu\tilde{\gamma})(\bar{d}\bar{\nu}\tilde{\gamma})$ (leptoquark), $h\bar{h} \to (ue\tilde{\gamma})(\bar{u}\bar{e}\tilde{\gamma})$ (leptoquark), and $h\bar{h} \to (ud\tilde{\gamma})(\bar{u}\bar{d}\tilde{\gamma})$ (diquark). The dijet + lepton + missing energy leptoquark mixed final state possesses a more severe background and hence is not a strong signal. Angelopoulos et al. [3.16] have estimated that

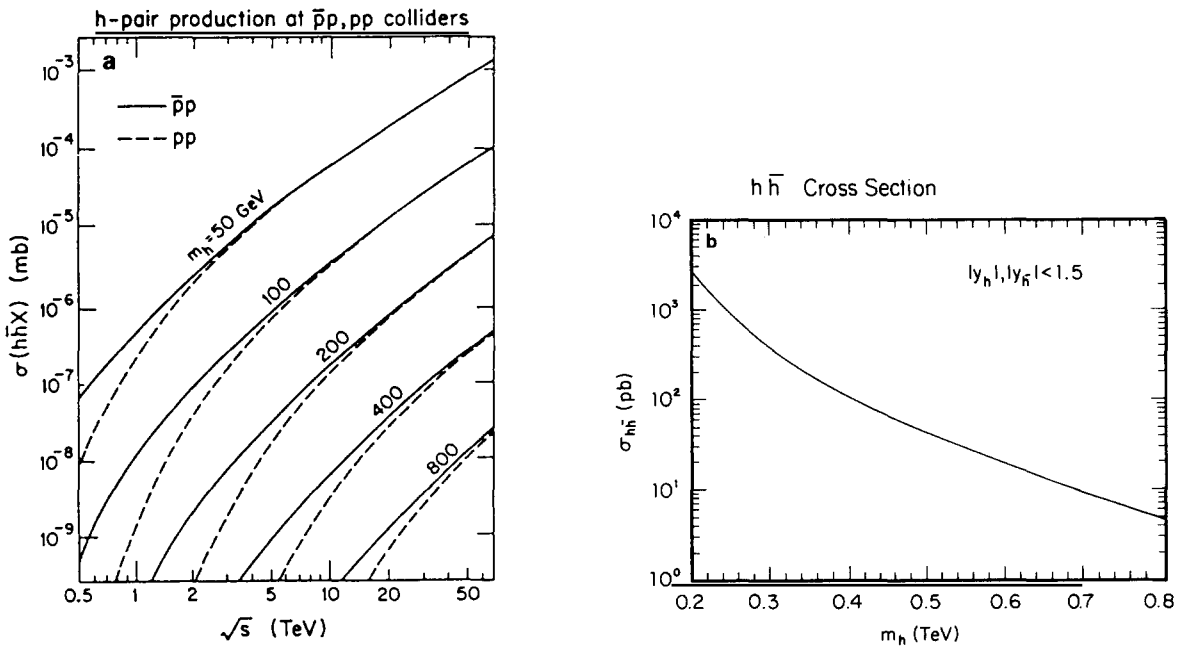

Fig. 79. Total cross section for $p\overset{(-)}{p} \to h\bar{h}$, (a) as a function of $\sqrt{s}$ for various values of M_h, (b) as a function of M_h for $\sqrt{s} = 40$ TeV with rapidity cuts as indicated.

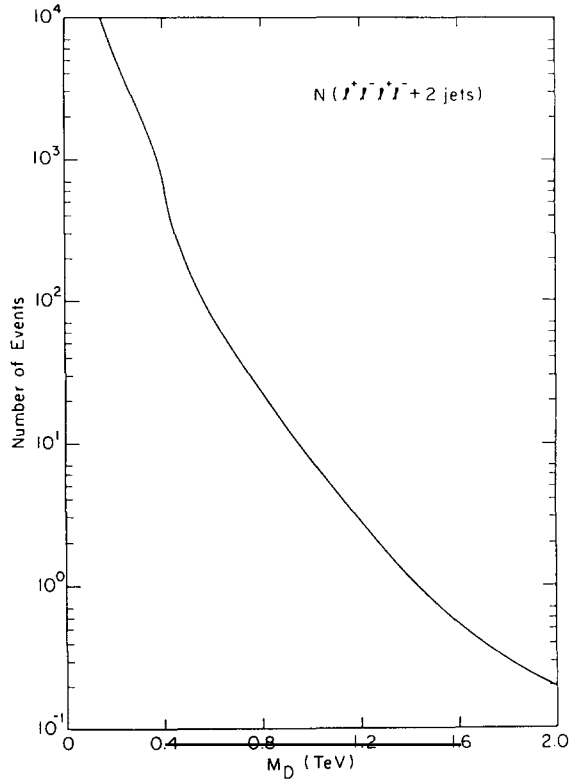

Fig. 80. The number of events of type two jets + $\ell^+\ell^-\ell'^+\ell'^-$ from $h\bar{h}$ production at the SSC as a function of the h mass (D = h).

with $\sqrt{s} = 1.6$ TeV at the Tevatron and with a sensitivity comparable to present CERN collider data, a search limit of $M_h \simeq 120$ GeV for the two jets + $\not{p}_T$ signal, and $M_h \simeq 160$ GeV for two jets + $\ell^+\ell^-$ + $\not{p}_T$ leptoquark signatures, and $M_h \simeq 150$ GeV for the diquark signal can be reached. If one includes other supersymmetric decay chains (such as $\tilde{f} \to f'\tilde{W} \to f'W\tilde{\gamma}$ or $\tilde{f} \to f\tilde{Z} \to f\ell^+\ell^-\tilde{\gamma}$) then other, more exotic, signatures may occur. A thorough analysis of the potential signals and of possible backgrounds at the SSC is presented in Barger et al. [3.94], where the authors conclude that detection of a 500 GeV h fermion should be relatively straightforward.

Single h-leptoquark production in association with W_R in the ALRM is possible via $gu \to W_R h$ as is shown in figs. 36, 37 and is discussed in section 2.6.

Pair production of the scalar partner, $\tilde{h}$, is similar, except for overall combinatorial factors which count the number of relative species, to that of any other color triplet scalar, such as squarks and technipions, which have been thoroughly discussed elsewhere [3.27, 3.96]. We include, for reference, the total production cross section in fig. 81 [3.97] for only one generation of left- or right-handed $\tilde{h}$'s. The cross section should be appropriately scaled to include the number of degenerate generations and/or superposition of left- and right-handed states. Note that in the case of scalar leptoquarks an additional contribution, $q\bar{q} \to$ "ℓ" $\to \tilde{h}\bar{\tilde{h}}$ in the t-channel, exists due to the Yukawa interactions. However, this extra mechanism is negligible due to the expected small size of the Yukawa couplings and the dominance of the gluon fusion process. The signatures for scalar leptoquark production are two jets + $\ell^+\ell^-$, two jets + $\nu\bar{\nu}$, and two jets + $\overset{(-)}{\nu}\ell^{\pm}$ with a relative probability of occurrence (assuming only

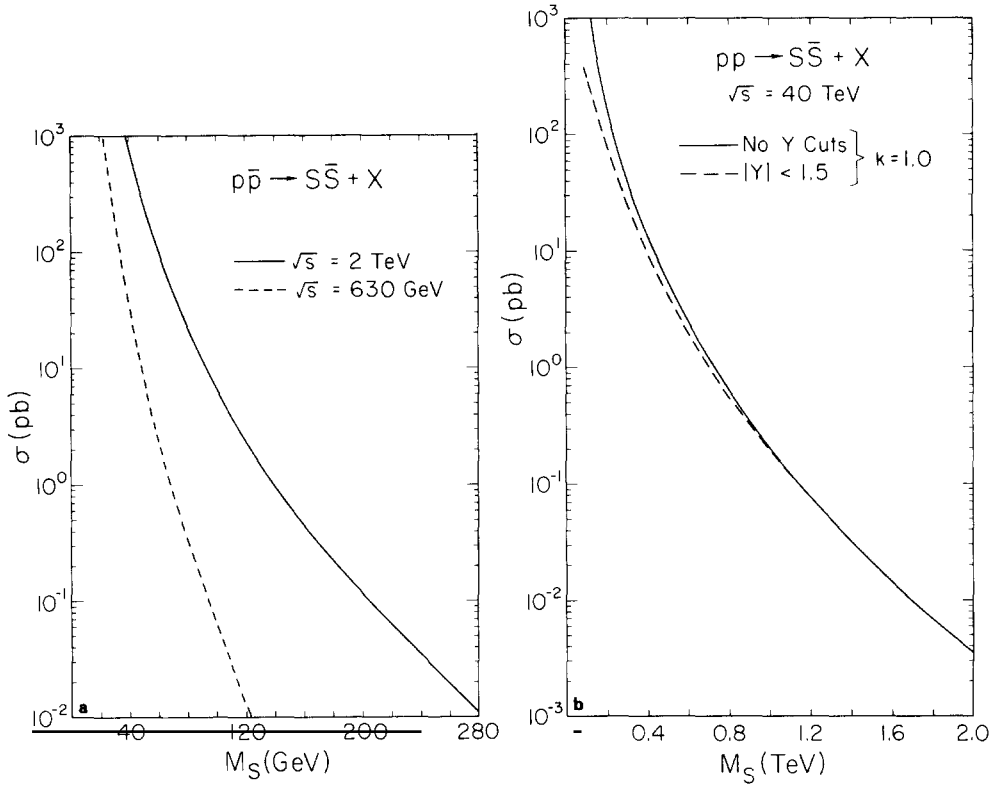

Fig. 81. Pair production of $\tilde{h}$ scalars at (a) the Tevatron and CERN $S\bar{p}pS$ Collider, and (b) the SSC.

left-handed couplings, i.e., $\lambda_6 \neq 0$) of 25%, 25%, and 50%, respectively. The most serious background arises for events of the third type. Estimated discovery limits [3.97] are placed at $M_{\tilde{h}} \simeq 40$–70 GeV, 120 GeV, and 1.7 TeV at the CERN collider, Tevatron, and SSC respectively. A recent calculation [3.98], which includes the CDF detector's capabilities for measuring missing transverse momentum, places an upper search limit of 100 GeV at the Tevatron for only one generation of scalar leptoquarks.

Scalar diquark pair production is best characterized by four jet events with dijet mass bumps, provided that the jets do not coalesce. A comparison of the cross sections for two, three, and four jet final states from diquark $\tilde{h}\tilde{h}$ production with the background QCD n jet cross sections is presented in fig. 82 from Argyres et al. [3.99]. It is evident that only the four jet diquark final states can compete with the QCD background, due to the QCD jet cross section behavior of $\sigma_{n+1} \sim \alpha_s \sigma_n$. These authors compute that with appropriate cuts, four jet measurements could explore mass ranges up to $M_{\tilde{h}} \simeq$ 40 GeV and $\simeq$70 GeV at the CERN Collider and Tevatron, respectively, at a 90% confidence level.

Single scalar leptoquark production at hadron colliders is achieved through the Yukawa interactions via the parton level process $qg \to \tilde{h}\ell$, where ℓ is a charged lepton or a neutrino. The Feynman diagrams which contribute to this process are displayed in fig. 83. The subprocess differential cross section [3.97] is given by

$$\frac{d\hat{\sigma}}{d\hat{t}} = \frac{k\pi\alpha_s\alpha}{6\hat{s}^2}\left(\frac{\hat{s}+\hat{t}-M_{\tilde{h}}^2}{\hat{s}} + \frac{\hat{t}(\hat{t}+M_{\tilde{h}}^2)}{(\hat{t}-M_{\tilde{h}}^2)^2} + \frac{\hat{t}(2M_{\tilde{h}}^2-\hat{s})}{\hat{s}(\hat{t}-M_{\tilde{h}}^2)}\right), \tag{3.126}$$

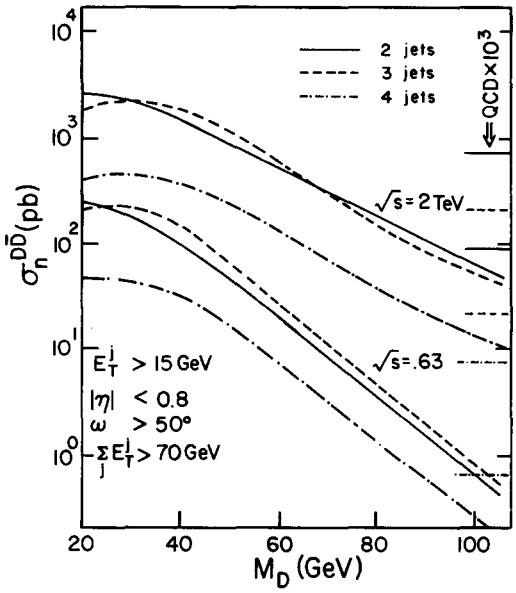

Fig. 82. n jet cross sections for scalar diquark production and the QCD background at the Tevatron and S$\bar{p}$pS Collider. A "jet" is defined as a cluster with angular separation of $\omega < 50°$, total transverse energy of the cluster is $E_T > 15$ GeV, the transverse energy of the jet system is $\Sigma_j E_T > 70$ GeV, and for jets which lie in the pseudorapidity interval $|\eta| < 0.8$.

with k as defined as in eq. (3.60), and $\hat{t} \equiv \frac{1}{2}(M_{\tilde{h}}^2 - \hat{s})(1 - \cos\theta)$ where θ is the quark–lepton scattering angle. It is important to notice that the cross section for this mechanism is directly proportional to the square of the Yukawa coupling, and hence the production rates are very sensitive to the exact value of λ. This is in contrast to the case of pair production which is basically independent of λ. The total production cross section (assuming equal masses and no mixing) is shown in fig. 84 from this reference for various values of k for the CERN Collider, Tevatron, and the SSC. The signatures for this process are quite distinct and are given by jet + $\nu\bar{\nu}$, jet + $\ell^+\ell^-$, or jet + $\nu\ell^\pm$. Events of the first two types have the smallest SM backgrounds which arise from the processes jet + Z($\rightarrow \ell^+\ell^-$) and jet + q($\rightarrow$ jet $\ell\nu$)$\bar{q}$($\rightarrow$ jet $\ell\bar{\nu}$) for the charged lepton pair events and jet + Z($\rightarrow \nu\bar{\nu}$) and W$\rightarrow \tau\nu$ for the monojets. These authors estimate that observable production rates occur up to $M_{\tilde{h}} \simeq 20$–30 GeV and 80 GeV for the CERN Collider and the Tevatron with $k = 0.1$, and $M_{\tilde{h}}$ in excess of 2 TeV at the SSC with $k = 1.0$. Clearly, this mechanism is only important for larger values of the Yukawa coupling.

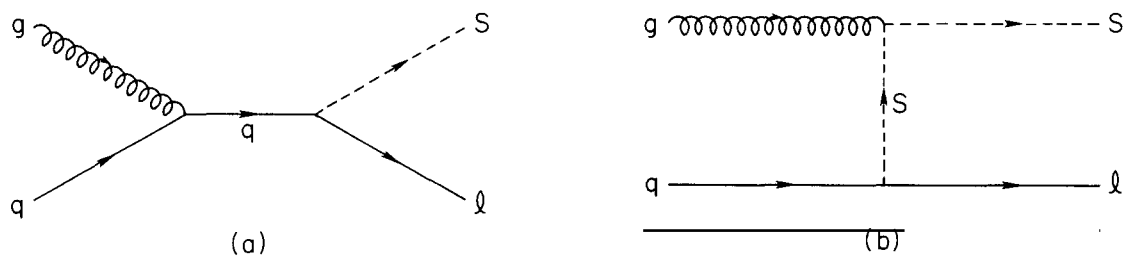

Fig. 83. Diagrams responsible for the single production of scalar leptoquarks in hadron collisions.

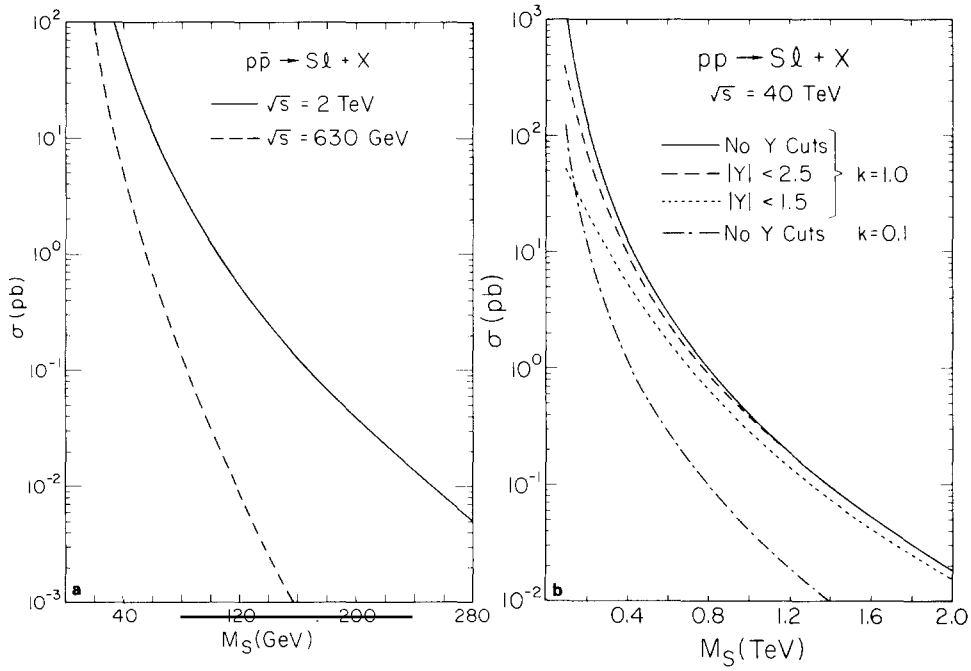

Fig. 84. The total cross section for $p\overset{(-)}{p} \to \tilde{h}\ell + X$ as a function of the leptoquark mass at (a) the Tevatron and S$\bar{p}$pS Collider with $k = 0.1$, and (b) the SSC with values of k and rapidity cuts as indicated.

The Yukawa couplings can also mediate single production of diquark scalars in hadronic collisions via the direct s-channel resonance $\bar{q}\bar{q} \to \tilde{h}$ (or $qq \to \tilde{h}_L^c$). The differential cross section for the process $p\overset{(-)}{p} \to \tilde{h} \to qq + X$ can be written as [3.16] (for $M_{\tilde{h}} = M_{\tilde{h}_L^c}$ and neglecting any mixing between $\tilde{h}$ and $\tilde{h}_L^c$)

$$\frac{d^2\sigma}{dx_1\,dx_2} = \frac{\hat{s}}{108\pi}\,\delta(sx_1x_2 - \hat{s})\left(\frac{16\lambda_9^4 + \lambda_{10}^4}{(\hat{s} - M_{\tilde{h}}^2)^2 + \Gamma_{\tilde{h}}^2 M_{\tilde{h}}^2}\right)\sum_{i,j} q_i(x_1)q_j(x_2)\,, \tag{3.127}$$

where $\lambda_{9,10}$ are the diquark Yukawa couplings in eq. (1.4) and the sum extends over all the contributing initial parton states. Taking $\lambda_9 = \lambda_{10} = \lambda$ and $F\alpha \equiv \lambda^2/4\pi$, fig. 85 from this same reference shows the total cross section for this process at various hadron colliders. Note that again, this single production mechanism is very sensitive to the value of the Yukawa couplings, as opposed to the case of pair production. The experimental signature is a peak in the number of two jet events and is unfortunately overwhelmed by the QCD two jet background by one to two orders of magnitude; even for large Yukawa couplings, it will be difficult to detect scalar diquarks from this mechanism.

3.4.3.3. Indirect signals: h-leptoquarks. Just as scalar leptoquarks can participate in $q\bar{q}$ production in e^+e^- annihilation, they also contribute to the inverse subprocess $q\bar{q} \to e^+e^-$ via virtual u-channel exchange. The subprocess differential cross section is as given in eq. (3.61) [with $s(u) \to \hat{s}(\hat{u})$] and the hadronic cross section is obtained by integrating over the appropriate quark distribution functions where only the u-quark contributes to the t-channel terms. Figure 86 from Dreiner et al. [3.77] shows contours of $\delta\sigma/\sigma$ in the leptoquark coupling–mass plane at the Tevatron and CERN Collider, where $\delta\sigma$

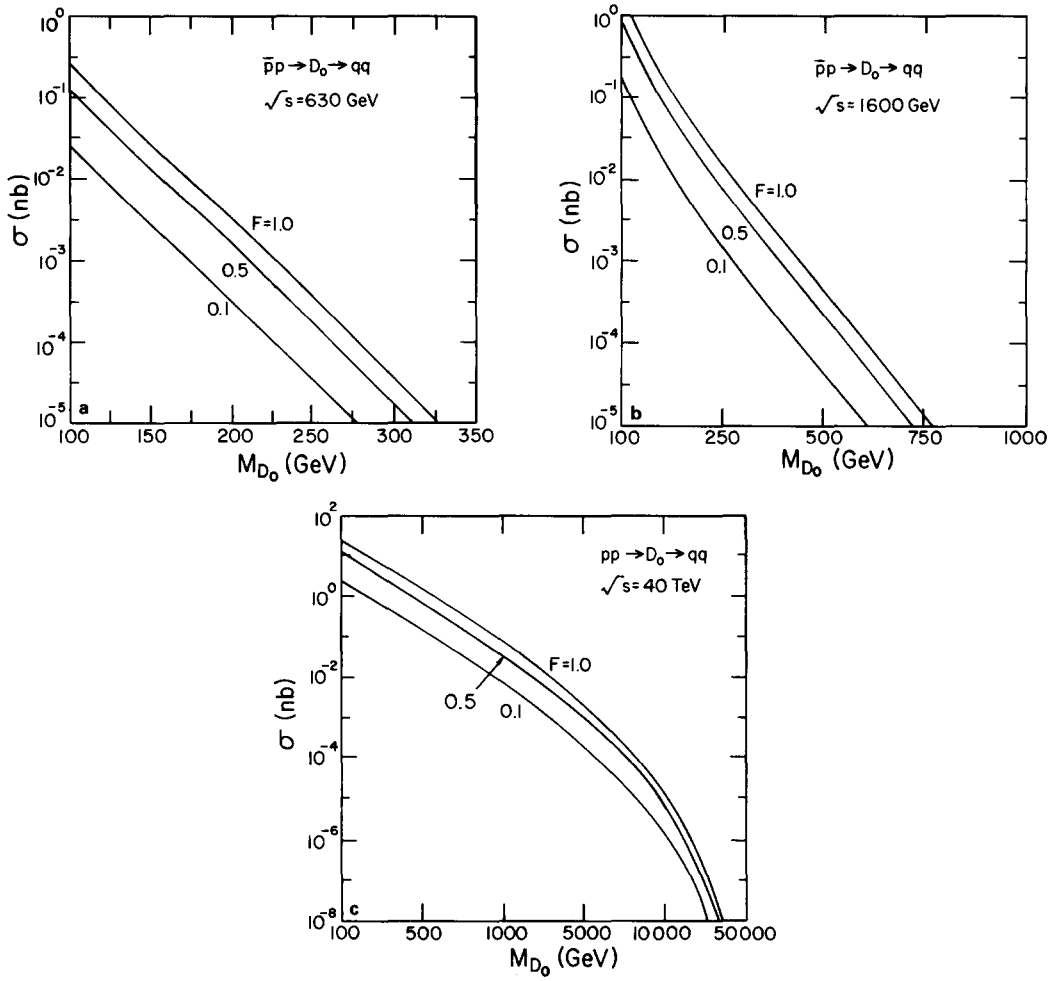

Fig. 85. Total cross section for the production of single scalar diquarks and subsequent decay into quark pairs at the (a) CERN Collider, (b) Tevatron, and (c) SSC for $F = 1.0$, 0.5, and 0.1.

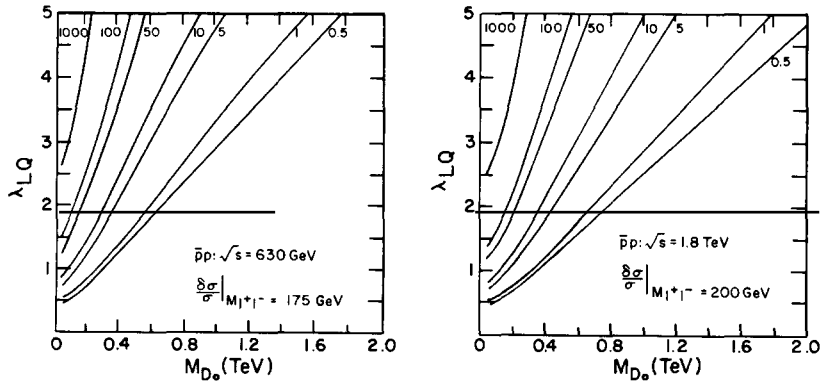

Fig. 86. Contours of $\delta\sigma/\sigma$ in the leptoquark coupling–mass plane for the Drell–Yan process at the (a) CERN Collider and (b) Tevatron for minimum invariant mass values of the $\ell^+\ell^-$ pair as indicated.

represents the additional terms due to the leptoquark exchange, and σ is the total cross section. These curves were obtained by first choosing the invariant mass value, $M_{\ell^+\ell^-}$, of the $\ell^+\ell^-$ pair which corresponds to a minimum observable $d\sigma/dM^2_{\ell^+\ell^-}$ of one event/yr for the usual Drell–Yan process (for an integrated luminosity of $10^{37}\,cm^{-2}$ at both colliders). A sensitivity of $\delta\sigma/\sigma \geq 1\%$ could probe leptoquark masses up to 250 (300) GeV at the CERN Collider (Tevatron) for couplings of electromagnetic strength. At higher energy colliders, such as the LHC or SSC, this mechanism is unlikely to be sensitive to leptoquark masses greater than that which can be produced directly, with the following limit [F is as defined in eq. (3.59)]

$$M_{\tilde{h}} \lesssim 1.2\,\text{TeV}\sqrt{F}\,, \tag{3.128}$$

at the LHC [3.100]. Comparing figs. 66 and 86 it is clear that e^+e^- machines are much more sensitive than hadron colliders to these virtual leptoquark exchanges.

3.4.4. Other production mechanisms

The possibility that leptoquarks may be resonantly produced by the interaction of ultra high energy neutrinos (from the atmosphere or astrophysical sources) with nucleons has been considered [3.101]. Such interactions can explore different coupling terms in the superpotential W than those relevant for leptoquark production in ep collisions. Explicitly, the pertinent W terms are

$$\lambda_6(\bar{e}u^c_L)\tilde{h}_L + \lambda_7(\bar{\nu}^c d_L - \bar{e}^c u_L)\tilde{h}^*_R\,. \tag{3.129}$$

(Note that $\tilde{h}_L$ and $\tilde{h}^*_R$ can, in principle, mix.) While ep interactions probe both λ_6 and λ_7, νN interactions probe only λ_7. Through the subprocess $\nu_e d \to \tilde{h}^*_{1R}$ and $\nu_\mu s \to \tilde{h}^*_{2R}$, leptoquarks of both the first and second generation can be produced. In the $\tilde{h}_2$ case, the smallness of the s-quark sea is offset by the much larger ν_μ flux. For the first and second generations, the λ_7 coupling is constrained to satisfy [3.102]

$$\lambda_7 \lesssim M(\tilde{h}_1)/2\,\text{TeV}\,, \qquad \lambda_7 \lesssim M(\tilde{h}_2)/0.4\,\text{TeV}\,, \tag{3.130}$$

and the cross section for the $\nu N \to \nu X$, e^-X process is given by ($x = M^2/s$, with M the leptoquark mass)

$$\sigma = \pi\lambda_7^2 x q(x, Q^2 = M^2)/4M^2\,, \tag{3.131}$$

and $q = d$ or s. Figure 87 from ref. [3.101] shows the relative size of the leptoquark and charge current cross sections for $\nu N \to e^-X$ as a function of the ν energy for the first generation using the bound from (3.130) and different choices of λ_7 and M. As can be seen from the figure, the leptoquark and charged current cross sections are comparable over a large range of neutrino energies.

The exchange of leptoquarks (either $\tilde{h}_L$ or $\tilde{h}_R$) in the t-channel can also significantly modify the expectations for the decay of the $^3S_1$ $t\bar{t}$-onium decay into $\tau^+\tau^-$ (which usually takes place only via s-channel γ and Z exchange) [3.79]. The effective vector and axial-vector couplings of $t\bar{t}$-onium to $\tau^+\tau^-$ can be written as

$$\begin{aligned}
\lambda_\tau &= e_\tau e_t + v_\tau v_t X_Z/y^2 - (\lambda_7^2/3e^2)X_R - (\lambda_6^2/3e^2)X_L\,,\\
\lambda'_\tau &= a_\tau a_t X_Z/y^2 - (\lambda_7^2/3e^2)X_R - (\lambda_6^2/3e^2)X_L\,,
\end{aligned} \tag{3.132}$$

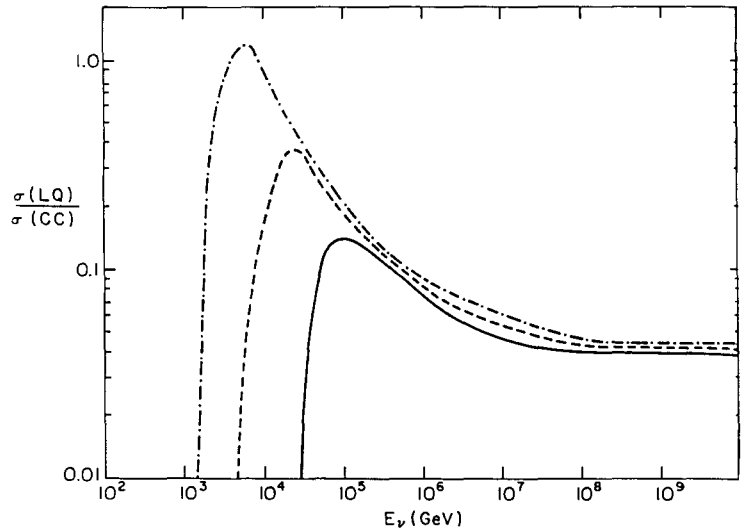

Fig. 87. Ratio of the cross sections for the leptoquark mediated $\nu_e N \to e^- X$ process to that for ordinary charged currents as a function of the neutrino energy for $M = 50$ GeV, $\lambda = 0.025$ (dot-dashed); $M = 100$ GeV, $\lambda = 0.05$ (dashed); and $M = 200$ GeV, $\lambda = 0.1$ (solid).

where $e_\tau = -1$, $e_t = \frac{2}{3}$, $v_\tau = -1 + 4x_w$, $a_\tau = -1$, $v_t = 1 - 8x_w/3$, $y^2 = 16x_w(1 - x_w)$, $X_Z = M^2/(M^2 - M_Z^2 + i\Gamma_Z M_Z)$, and $X_{L,R} = M^2/[M^2 + 4M^2(\tilde{h}_{L,R})]$. Here, M is the mass of the toponium system which is $\simeq 2m_t$. Figure 88a shows the fractional change in the decay rate for toponium decay into $\tau^+\tau^-$ due to leptoquark exchange while fig. 88b displays the corresponding changes in the forward–backward asymmetry in $e^+e^- \to \tau^+\tau^-$. We see that large changes are possible in the toponium decay rate, while rather small deviations are expected in the asymmetries.

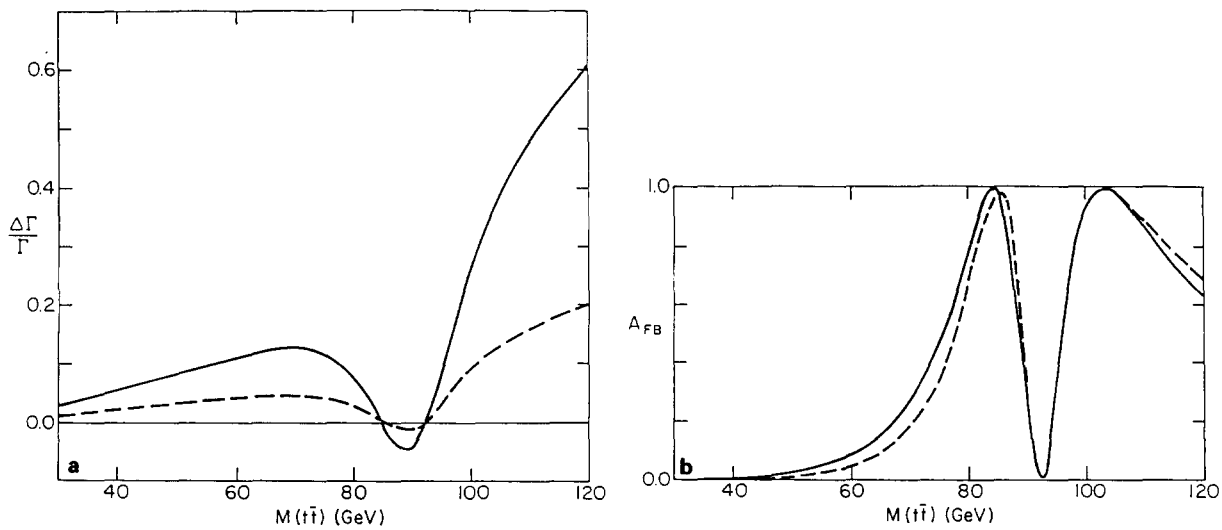

Fig. 88. (a) Fractional change in rate $\Delta\Gamma/\Gamma$, for the process $V_t \to \tau^+\tau^-$ due to leptoquarks with $M = M(\tilde{h}_{L,R}) = 200$ GeV and $\lambda_6 = \lambda_7 = 0.5$ (0.3) for the solid (dashed) curves, and (b) A_{FB} in $e^+e^- \to \tau^+\tau^-$ for the SM (solid) and with leptoquarks with $M = 200$ GeV and $\lambda_6 = \lambda_7 = 0.5$ (dashed).

If, on the other hand, h's have diquark quantum numbers, then t-channel scalar $\tilde{h}$ exchange can analogously modify toponium$\rightarrow b\bar{b}$ decay [3.79]. In this case the effective vector and axial-vector couplings are given by (including W exchange for which the KM element V_{tb} has been set to unity)

$$\lambda_b = e_b e_t + v_b v_t X_Z/y^2 - X/24x_w - (4\lambda_9^2/3e^2)X_L - (\lambda_{10}^2/3e^2)X_R\,,$$
$$\lambda_b' = a_b a_t X_Z/y^2 - X/24x_w - (4\lambda_9^2/3e^2)X_L - (\lambda_{10}^2/3e^2)X_R\,, \tag{3.133}$$

where $e_b = -\frac{1}{3}$ and $X = (M^2/M_W^2)(M_W^2 + M^2/8)(M_W^2 + M^2/4)^{-1}$ with λ_9, λ_{10} given in the superpotential W. Figure 89a, b from this reference shows the modification in toponium decay and bb A_{FB} from t-channel scalar diquark exchange. Again, we see that contributions can influence the decay rate substantially, but that the asymmetries remain relatively unchanged.

If leptoquarks are lighter than the top-quark, then decays such as $t\rightarrow \tilde{h}\bar{\ell}$ may dominate or compete with the usual three-body decay mode $t\rightarrow b\bar{\ell}\nu$, as has been considered in refs. [3.15, 3.79]. If the corresponding Yukawa coupling $\lambda \gtrsim G_F m_t^2/\pi \simeq 25\times 10^{-3}\ (m_t/40\,\text{GeV})^2$, then $\tilde{h}$ decays will clearly be dominant. With the subsequent decay of $\tilde{h}\rightarrow \ell u$, the t decay final state of a lepton pair plus a jet should be quite spectacular. If, however, the decay $\tilde{h}\rightarrow \nu d$ takes place, the t decay final state would be somewhat similar to the usual $t\rightarrow b\bar{\ell}\nu$ mode, but with slightly different kinematics. It should be noted that even if leptoquarks are heavier than the top-quark, their virtual exchange can also lead to the above final states with a reasonable rate.

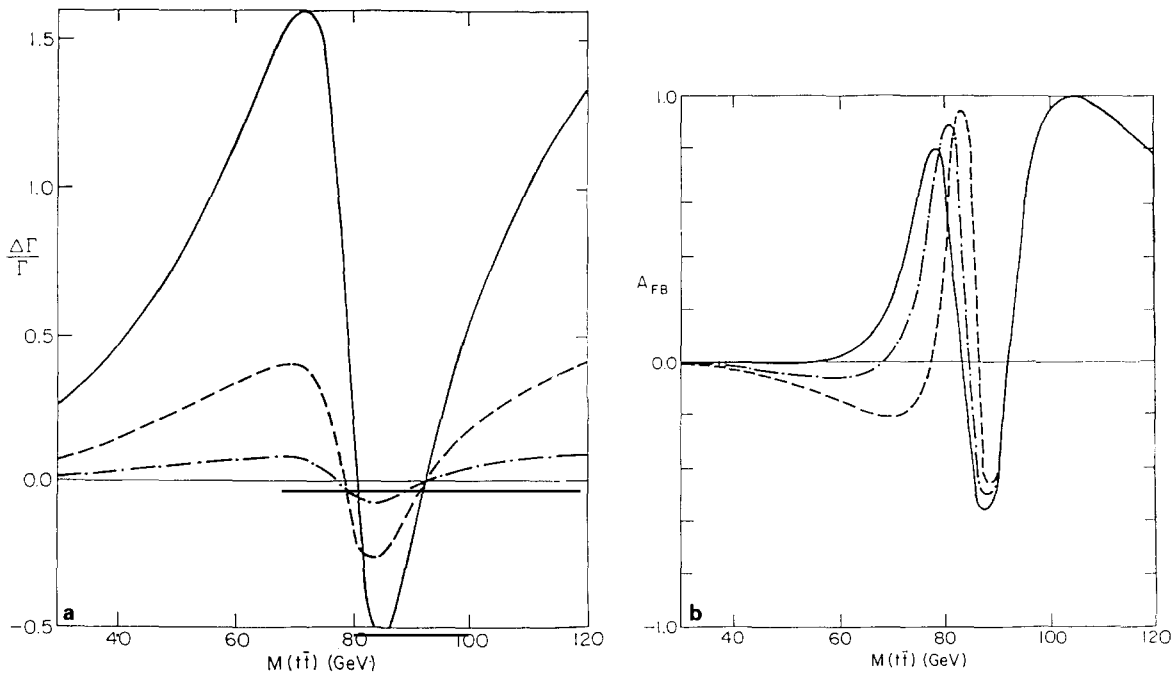

Fig. 89. (a) Fractional change in the decay rate for $V_t\rightarrow b\bar{b}$ for $M = 250$ GeV diquarks with λ_9, $\lambda_{10} = 0.5$ (0.3, 0.1) for the solid (dashed, dot-dashed) curves and (b) A_{FB} in $e^+e^-\rightarrow b\bar{b}$ for the SM and for diquarks with $M = 200$ GeV and λ_9, $\lambda_{10} = 0.5$ (0.3) for the dashed (dot-dashed) curves.

Diquarks may also influence top-quark decay via processes such as $t \to \tilde{h}\bar{d}$ with subsequent $\tilde{h}$ decay into ud. These decays would, however, be essentially impossible to search for at a hadron collider.

To conclude this section, we present in table 4 a summary of expected discovery limits from the various production mechanisms discussed above for the three distinct quantum number assignments of the exotic h. At e^+e^- colliders, the numbers inside the parentheses for the cases of scalar leptoquarks and spin-$\frac{1}{2}$ h-quarks are the mass search limits for single production via the Yukawa interactions and ordinary–exotic mixing, respectively. These single production limits, which are highly dependent on the strength of the Yukawa coupling or mixing, are the maximum limits obtainable and, in reality, could be much lower if the respective interaction strength is weaker. The numbers listed outside the parentheses are the limits from pair production and are model independent. The limits that we have quoted for the h-quark at ep and hadron colliders include only its semi-leptonic branching ratio, and not the other possible flavor changing decay modes which would distinguish it from a fourth generation, $Q = -\frac{1}{3}$ b′-quark. The inclusion of these FC decay modes would lower the h-quark search limits due to their smaller branching fractions. Scalar diquark production at the SSC has not been examined, but its detection will be hazardous due to the overwhelming QCD background. If these exotic fermions are present at or slightly above the electroweak scale, they should be detectable at these present or future colliders.

3.5. Bound states

The quarkonium ($h\bar{h}$) and open flavor hadron ($h\bar{q}$) bound states of the exotic h-quark have gained some attention in the literature [3.103–3.108]. These bound states are able to form since the spectator decays of the heavy h quark constituent (i.e., $h \to q + W/Z, q + H$) are expected to be suppressed due to the small ordinary–exotic mixing. It is important to note that the strong and purely electromagnetic interactions of both the $h\bar{h}$ and $h\bar{q}$ bound systems will be identical to those of bound states that are composed of SM down-type quarks (e.g., $b'\bar{b}'$ and $b'\bar{q}$) of the same mass, since the h and SM down-type quarks have the same color and electric charges. Hence, only the weak interactions of the h bound states will differ from their SM counterparts.

3.5.1. Quarkonium

Bigi et al. [3.103] have estimated, by requiring that the $h\bar{h}$ system lifetime be longer than its characteristic binding time, that heavy quarkonium bound states will not form for quark masses in

Table 4
Summary of discovery limits for the three possible quantum number assignments of the exotic fermion h and its SUSY partner at various colliders

	LEP I/SLC (GeV)	2 TeV CLIC (TeV)	HERA (GeV)	Tevatron (GeV)	SSC (TeV)
Leptoquark h	44	0.9	40	120	0.5–1.0
$\tilde{h}$	40(80)	0.6–1.2	300	100	1.7–2.0
Diquark h	44	0.9	40	120	0.5–1.0
$\tilde{h}$	40	0.6	110	70	–
Quark h	44(80)	0.85	40–50	120	0.5–1.0
$\tilde{h}$	40	0.8–0.9	40–80	120	0.5–1.0

excess of $125 \times |U_{hq}|^{-2/3}$ GeV, where U_{hq} represents the mixing between h and a light quark q into which h may decay. Since the ordinary–exotic mixing is constrained to be small by the absence of FCNC's, very heavy h quarkonia could form and satisfy the above bound. (Even for unacceptably large values of the mixing, such as, $|U_{hq}| \sim \sin\theta_c$, where θ_c is the Cabibbo angle, h-quarkonium masses up to 650 GeV are allowed.) In this section, only the lowest-lying $^3S_1$ quarkonium state (V_h) will be considered, except where noted otherwise. The corresponding $^3S_1$ system composed of heavy SM charged $-\frac{1}{3}$ quarks (i.e., a fourth generation b′) will be denoted by V_{SM}.

The production mechanisms for V_h are basically the same as for a heavy SM quarkonium system and hence will only be briefly surveyed here. In e^+e^- annihilation the production cross section is given by [3.109]

$$\int d\sqrt{s}\, \sigma(e^+e^- \to V_h \to X) = \frac{6\pi^2}{M_{V_h}^2} \frac{\Gamma_{ee}\Gamma_X}{\Gamma}, \tag{3.134}$$

where $\Gamma_{ee(X)}$ is the width of $V_h \to e^+e^-(X)$, Γ is the total width, and the energy integration is performed since the V_h resonance is expected to be narrower than the energy resolution of the beams. Since Γ_{ee} is expected to be tiny (as will be discussed below) reasonable cross sections are only obtainable near a Z or Z′ resonance or if a suitably small beam spread can be maintained. At hadron colliders the dominant quarkonium production mechanism is by gluon fusion. The $^1S_0$ quarkonium state (η_h) yields the largest production cross section, which is given [3.104] at the parton level by

$$\sigma(gg \to \eta_h) = (2\pi^3\alpha_s^2/3sM_{\eta_h}^3)|\psi(0)|^2, \tag{3.135}$$

where $|\psi(0)|$ is the total wave function taken at the origin. For the SSC at $\sqrt{s} = 40$ TeV, $\sigma(pp \to gg \to \eta_h)$ is 1 (100) pb for $M_{\eta_h} \simeq 700$ (100) GeV for the Wisconsin and Richardson potential models, and is larger by a factor of 20 for the Cornell potential. The lowest order process for V_h production is $gg \to V_h g$ since $V_h \to gg$ is forbidden due to Yang's theorem and color conservation, where

$$\hat{\sigma} = (20\pi^2\alpha_s^3/9M_{V_h}^5)|\psi_V(0)|^2 I(\hat{s}/M_{V_h}^2), \tag{3.136}$$

and $I(x)$ is given in Barger et al. [3.104]. The total production cross section at the SSC is roughly two orders of magnitude less than that for $\sigma(pp \to gg \to \eta_h)$, resulting in $\sigma(pp \to gg \to V_h g) \simeq 1\ (10^{-2})$ pb for $M_{V_h} \simeq 100\ (700)$ GeV for the Wisconsin and Richardson potentials. Quark annihilation, radiative decay of excited states, and WW fusion can also contribute to quarkonium production, but these mechanisms are smaller than that from gluon fusion by factors of 10^{-2}, 10^{-1}, and 10^{-3} respectively, for SM quarkonium systems (unless $M_{Q\bar{Q}} \simeq M_Z$). As shall be discussed below, $\Gamma(V_h \to q\bar{q}, W^+W^-)$ is much smaller than for SM quarkonia due to the iso-scalar nature of h, hence, these other V_h production mechanisms are negligible compared to gluon fusion.

Now we turn our attention to the decay modes of the V_h. Since, as previously discussed, h and SM $Q = -\frac{1}{3}$ quarks have the same strong and purely electromagnetic interactions, the partial widths $\Gamma(V_h \to ggg)$, $\Gamma(V_h \to gg\gamma)$ and $\Gamma(V_h \to \gamma \to \ell^+\ell^-)$ will be identical to the corresponding partial widths for a V_{SM} of the same mass.

The general annihilation decays, $V_h \to f\bar{f}$, proceed via s-channel γ, Z_1, and Z_2 exchange as well as t-channel W, Z_1, Z_2 exchange. The t-channel processes are due to the existence of FCNC's and are all

proportional to the small ordinary–exotic mixing, and hence are negligible compared to the s-channel graphs. The general annihilation decay rate [3.105] for massless final states is

$$\frac{\Gamma(V_h \to f\bar{f})}{\Gamma(V_h \to \gamma \to \ell^+\ell^-)} = \frac{9N_c M_{V_h}^4}{16\pi^2\alpha^2}\Bigg[\sum_{i,j=X_s} P_{ij}^{ss} v_1^i v_1^j (v_2^i v_2^j + a_2^i a_2^j) - \frac{1}{N_c}\sum_{i=X_s}\sum_{k=X_t} P_{ik}^{st}\left(1+\frac{M_{V_h}^2}{8M_{t_k}^2}\right) \times [(v_1^i v_3^k v_2^i v_4^k + a_1^i a_3^k a_2^i a_4^k) + (v_1^i a_3^k v_2^i a_4^k + v_3^k a_1^i v_4^k a_2^i)] + \frac{1}{N_e^2}\sum_{k,l=X_t}\frac{P_k^{tt}}{2}\left(1+\frac{M_{V_h}^2}{8M_{t_k}^2}\right)\left(1+\frac{M_{V_h}^2}{8M_{t_l}^2}\right)(v_4^k v_4^l + a_4^k a_4^l)(v_3^k v_3^l + a_3^k a_3^l)\Bigg], \tag{3.137}$$

where the rate has been scaled to $\Gamma(V_h \to \gamma \to \ell^+\ell^-)$ to avoid the question of the value of $\psi_V(0)$. Here, P_{ij}^{ss} is given in eq. (2.42), P_{ik}^{st} and P_{kl}^{tt} are obtained from P_{ij}^{ss} with the appropriate substitutions, N_c is the number of colors of f, the sums over $i, j\,(k, l)$ extend over the $s\,(t)$-channel bosons $X_{s(t)}$, and the couplings are normalized via

$$\mathcal{L} = \sum_i [\bar{h}\gamma_\mu(v_1^i - a_1^i\gamma_5)hX_s^{i\mu} + \bar{f}\gamma_\mu(v_2^i - a_2^i\gamma_5)fX_s^{i\mu} + \bar{h}\gamma_\mu(v_3^i - a_3^i\gamma_5)fX_t^{i\mu} + \bar{f}\gamma_\mu(v_4^i - a_4^i\gamma_5)hX_t^{i\mu}]\,. \tag{3.138}$$

The ratio

$$R_f = \Gamma(V_h \to f\bar{f})/\Gamma(V_{SM} \to f\bar{f}) \tag{3.139}$$

as a function of M_{V_h} is displayed in fig. 90 from ref. [3.105], (a) for $V_h \to \ell^+\ell^-$, and (b) $V_h \to \Sigma\, q\bar{q}$ for V_h and V_{SM} of equal mass and $M_{Z_2} = 250$ GeV. Note that this ratio is also independent of $\psi_V(0)$ as well as QCD and QED radiative corrections. As can be seen from the figures, once the photon contribution is no longer dominant ($M_{V_h} \sim 60$ GeV), $R_{\ell,q} < 1$. The corresponding ratio R_ν for $V_h \to \nu\bar{\nu}$ is always less than unity since there is no photon contribution in this case. These ratios are also roughly E_6 model independent until M_{V_h} nears the Z_2 pole. In this region, with M_{V_h} near M_{Z_2}, the effects of Z_2–V_h mixing should be included in order to see the proper behavior.

For heavier h quarks, the decays $V_h \to W^+W^-$, Z_1Z_1, and γZ_1 are also kinematically allowed. Obviously, these decay modes are extremely sensitive to the constituent quark's weak isospin properties. The process $V_h \to W^+W^-$ proceeds through s-channel exchange via virtual γ, Z_1, and Z_2 bosons, where the Z_2 contributes only through the Z–Z′ mixing. A t-channel contribution with virtual $Q = +\frac{2}{3}$, SM quark exchange is also present, but is proportional to the square of the ordinary–exotic mixing (as well as a KM mixing angle factor) and thus is small compared to the s-channel contributions. The decay rate [3.106] (neglecting the t-channel) is given by

$$\frac{\Gamma(V_h \to W^+W^-)}{|\psi_V(0)|^2} = \frac{\alpha^2}{16x_w^2}\frac{M_{V_h}^6}{M_W^4}(1-4r_W)^{3/2}\sum_{i,j} F_iF_jP_{jj}^{ss}(1+20r_W+12r_W^2)\,, \tag{3.140}$$

with $r_W = M_W^2/M_{V_h}^2$, P_{ij}^{ss} defined in eq. (2.42), $F_i = C_iv_i$, where C_i and v_i are normalized as

$$\mathcal{L} = \sum_i [\tfrac{1}{2}g\bar{h}\gamma_\mu(v_i - a_i\gamma_5)hX_s^{i\mu} + gC_i\Gamma_{\mu\nu\lambda}X_s^{i\mu}W^\nu W^\lambda]\,, \tag{3.141}$$

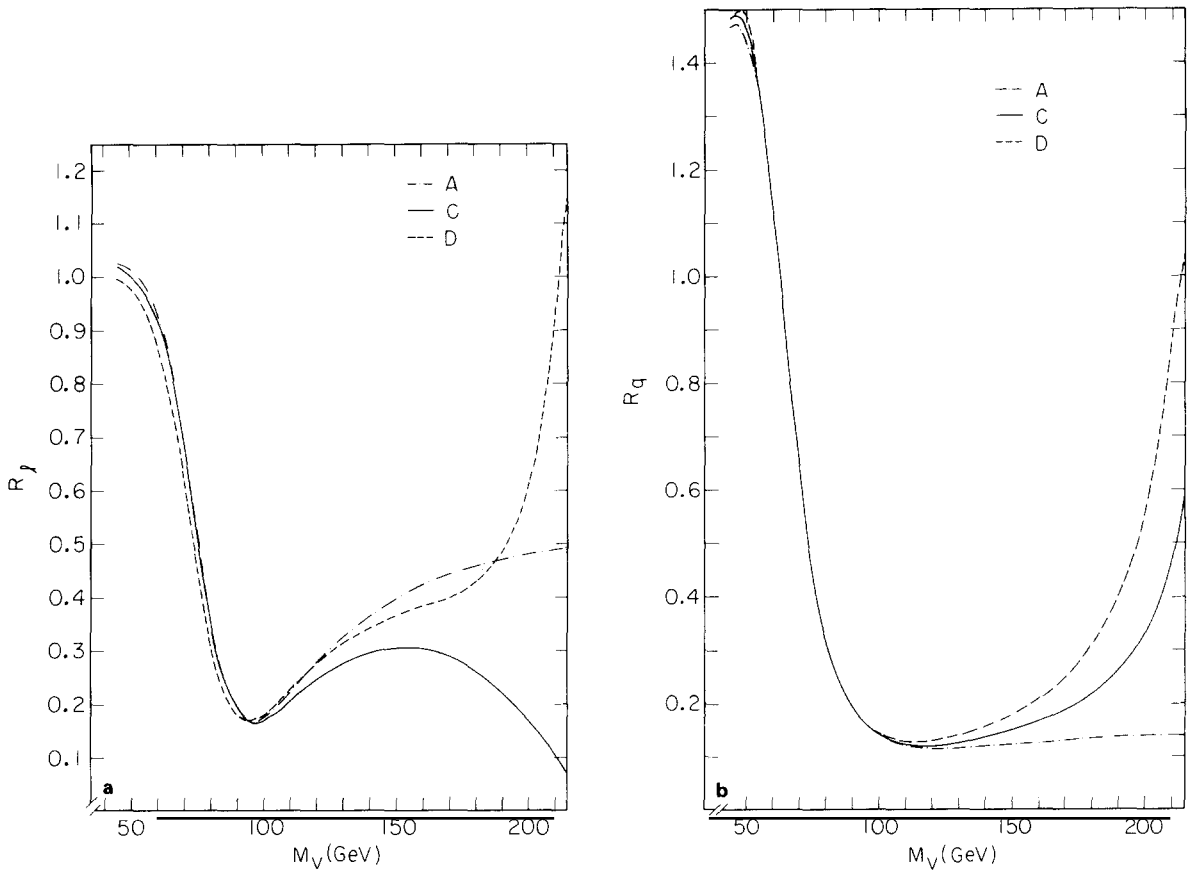

Fig. 90. The ratio (a) R_ℓ, (b) R_q as a function of M_{V_h} in E_6 models ψ (corresponding to label A), η (C), and I (D).

and $\Gamma_{\mu\nu\lambda}$ is the standard triple gauge boson vertex. It is important to notice that the decay width is proportional to the vector coupling constants only. The ratio, R_W, defined as

$$R_W = \Gamma(V_h \to W^+W^-)/\Gamma(V_{SM} \to W^+W^-)\,, \tag{3.142}$$

is examined in fig. 91a as a function of the Z–Z′ mixing parameter, ϕ, and in fig. 91b as a function of the quarkonium mass, from the work of ref. [3.106]. It is clear that the value of R_W is quite dependent on the amount of Z–Z′ mixing as well as the particular E_6 model, but R_W is very small nevertheless (ranging from 10^{-5} to 10^{-1}) for all values of the parameters. This is in stark contrast to $\Gamma(V_{SM} \to W^+W^-)$ which has a very large t-channel contribution and is the dominant decay mode of the V_{SM} if it is kinematically allowed. The partial widths $\Gamma(V_h \to Z_1Z_1)$ and $\Gamma(V_h \to \gamma Z_1)$ are given in Barger et al. [3.104] and are proportional to a^2 and a, respectively, where a is the axial-vector coupling constant of h to the Z_1. Since a only obtains a small, but non-zero, value through Z–Z′ mixing (i.e., $a = 0$ if $\phi = 0$), these decay rates will be quite small, and are bounded [3.106] from mixing constraints by

$$R_{\gamma Z_1} \lesssim 0.03\,, \qquad R_{2Z_1} \lesssim 0.006\,, \tag{3.143}$$

where R is again the ratio $\Gamma(V_h \to \gamma Z_1, 2Z_1)/\Gamma(V_{SM} \to \gamma Z_1, 2Z_1)$.

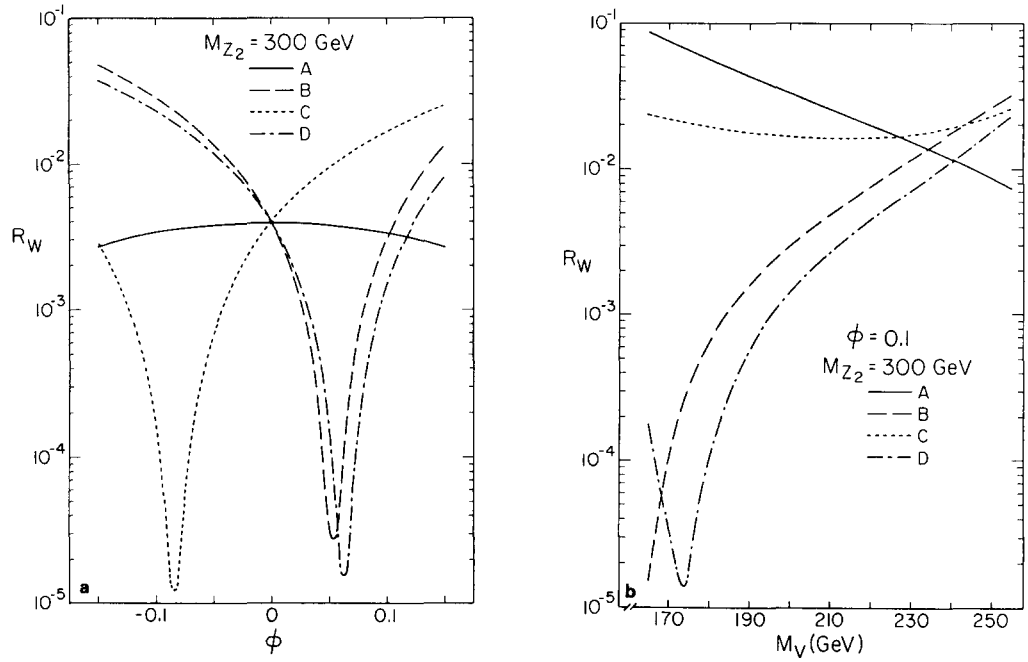

Fig. 91. The ratio R_W as a function of (a) ϕ (with $M_{V_h} = 200$ GeV), and (b) M_{V_h} (with $\phi = 0.1$) in E_6 models ψ (label A), χ (B), η (C), and I (D).

Thus the dominant decay modes of V_h are to ggg and gγ. The $f\bar{f}$, WW, Z_1Z_1, and γZ_1 modes are all suppressed due to the isoscalar and vector-like properties of the h. The single constituent decays are also suppressed by the small ordinary–exotic mixing. However we note that V_h couples mainly to the isosinglet Higgs field and could have enhanced decay rates into Higgs final states.

As discussed extensively in section 2, deviations from SM predictions in the forward–backward and left–right asymmetries in $e^+e^- \to \mu^+\mu^-$ could signal the presence of a Z_2 boson. However, the values of these asymmetries would also be different if they were measured on top of a heavy quarkonium resonance, i.e., $e^+e^- \to V \to \mu^+\mu^-$. With A_{FB} and A_{LR} as defined in eqs. (2.41)–(2.45), and summing over the contributions $e^+e^- \to \gamma, Z, V \to \mu^+\mu^-$, fig. 92 from the work of Robinett [3.107] shows the values of these asymmetries as a function of the V mass for h, t, and b′ quarkonium systems. A_{FB} and

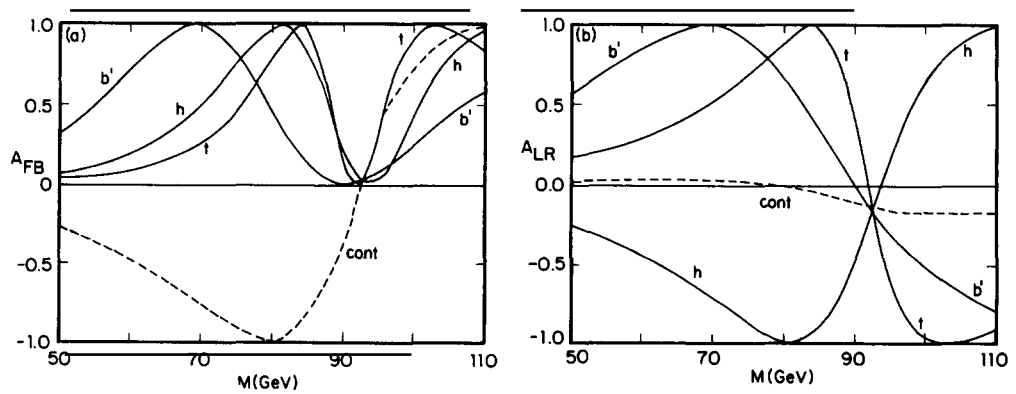

Fig. 92. (a) A_{FB}, and (b) A_{LR} in $e^+e^- \to \mu^+\mu^-$ on a quarkonium resonance for V_h, $V_{b'}$, and V_t. The dashed line corresponds to the continuum.

A_{LR} in the continuum ($M = \sqrt{s}$) in the absence of a V resonance are also displayed for comparison. It is clear that the presence of a new quarkonia could greatly affect these asymmetry measurements at SLC and LEP. Robinett has also included the contribution from a new Z_2 and the effect of Z–Z′ mixing and found that the deviations, δA_{FB} [$= A_{FB} - A_{FB}(SM)$] and δA_{LR}, are very E_6 model dependent but can have values up to 0.05 on a V_h resonance.

3.5.2. Open flavor hadrons

Bigi et al. [3.103] have also placed a limit of

$$M_h \lesssim 100 \times |U_{hq}|^{-2/3} \text{ GeV}, \tag{3.144}$$

for open flavor hadrons above which the heavy h quark would decay before it had time to bind into a meson. This restriction is slightly stronger than the corresponding limit placed on the formation of quarkonia systems, but very heavy open flavor hadrons could still occur since the mixing factor is constrained to be small.

The possibility of $H^0 (= h\bar{d})$–$\bar{H}^0$ mixing has been studied [3.108]. This mixing could proceed in lowest order via FCNC's and hence could be maximal, even for small ordinary–exotic mixing. Assuming that H_d^0–$\bar{H}_d^0$ transitions occur via tree-level Z_1 and Z_2 exchange and proceeding with the usual mixing analysis one finds

$$\Delta M/\Gamma = 1.43(f_H/f_\pi)^2 B(1+\xi^2)(M_H/23 \text{ GeV})^{-4}, \tag{3.145}$$

where f_H is the H decay constant, B is the usual bag factor, and $\xi = 2\sqrt{x_w}\, M_{Z_1}/M_{Z_2}$ (in the absence of Z–Z′ mixing) measures the relative strength of the Z_1 and Z_2 contributions to the transition. $|\Delta\Gamma/\Delta M|$ is estimated to be small for $M_H < M_Z/2$ and thus its contributions to the mixing is neglected. Using $f_H = f_\pi$, and $B = 1$ yields a value for ε, the fractional mean probability of $H_d^0 \to \bar{H}_d^0$, of $\varepsilon \simeq 0.40$ (0.27) for $\xi = 0.96$ (0.0) with $M_H = 25$ GeV, and $\varepsilon \simeq 0.05$ (0.02) with $M_H = 40$ GeV. It is important to note that ε is independent of the h–d mixing as it cancels out in the ratio $\Delta M/\Gamma$.

3.6. Neutrino masses

As is well known, one of the best explanations for the (possibly) small value of the mass of the ordinary left-handed neutrino (ν_L) is the so-called seesaw mechanism (SSM) [3.110] which is most commonly discussed within the context of the LRSM [2.5] and/or SO(10) [1.7]. In such models, Higgs isotriplets [belonging to the **126** representation of SO(10)] obtain large vev's (V) and induce a large Majorana mass term for the right-handed neutrino (ν_R), while a Dirac neutrino mass term is also generated in the usual way by mixed doublets (belonging to, e.g., the **10** of SO(10)]. Diagonalization of this mass matrix results in a heavy Majorana ν_R, and a light Majorana ν_L whose mass is suppressed in comparison to the ordinary charged fermions by $\sim m_f/V$. One of the basic problems with E_6 superstring-inspired models is how such a suppression can come about when large Higgs representations, such as the isotriplets (now in the **351** of E_6), are absent since the **27** contains only Higgs doublets and singlets.

Given the renormalizable superpotential W (eq. 1.4) and R-parity conservation the most general mass matrix for a single generation of the neutral fields in the **27** of E_6 (including only these fields!) must take the following form:

$$\begin{array}{c} \\ N \\ N^c \\ S^c \\ \nu \\ \nu^c \end{array} \begin{array}{c} \begin{array}{ccccc} N & N^c & S^c & \nu & \nu^c \end{array} \\ \begin{bmatrix} 0 & \lambda_4\langle\tilde{S}^c\rangle & \lambda_4\langle\tilde{N}^c\rangle & 0 & 0 \\ \lambda_4\langle\tilde{S}^c\rangle & 0 & \lambda_4\langle\tilde{N}\rangle & \lambda_{11}\langle\tilde{\nu}^c\rangle & 0 \\ \lambda_4\langle\tilde{N}^c\rangle & \lambda_4\langle\tilde{N}\rangle & 0 & 0 & 0 \\ 0 & \lambda_{11}\langle\tilde{\nu}^c\rangle & 0 & 0 & \lambda_{11}\langle\tilde{N}^c\rangle \\ 0 & 0 & 0 & \lambda_{11}\langle\tilde{N}^c\rangle & 0 \end{bmatrix} \end{array}. \tag{3.146}$$

Note that the R-parity of ν^c is a priori unspecified whereas it is completely fixed for ν, N, N^c, and S^c. Immediately several possibilities present themselves, if as stated above, we assume R-parity is conserved when the vev's are generated. If (i) ν^c has $R=+1$, then necessarily $\langle\tilde{\nu}^c\rangle = 0$ and the mass matrix for the $R=-1$ fields N, N^c, and S^c decouples from that for ν and ν^c. However, if (ii) ν^c has $R=-1$, then W forces $\lambda_{11} \doteq 0$ and $\langle\tilde{\nu}^c\rangle$ can be non-zero. Scenario (i) is the one which is played out in the rank-5 case since $\langle\tilde{\nu}^c\rangle$ must be zero for phenomenological reasons in such models as discussed previously in section 1. Since $\langle\tilde{N}^c\rangle$ also produces u-quark masses it is difficult to explain why λ_{11} is tuned to such a small value under these circumstances unless it is absent by virtue of a discrete symmetry. In this case as well, the N, N^c, and S^c fields will, in general, mix with other negative R-parity neutralinos in a complex way and we will no longer be concerned with them here since such states will usually be heavy. In rank-6 models, on the other hand, $\langle\tilde{\nu}^c\rangle \neq 0$ is required and so it is scenario (ii) which must be realized in this case. The generation of a non-zero $\langle\tilde{\nu}^c\rangle$ may, however, be problematic in such models as previously discussed. In these models, ν's are massless at the tree level since they decouple (as usual) from N, N^c and S^c and there are no entries in the ν–ν^c submatrix. A situation such as this can even occur in some effective rank-5 models, as has been demonstrated in the case of the alternative left–right symmetric model. In these models, ν_L could remain massless to all orders in perturbation theory depending on which terms in eq. (1.4) survive as long as new fields are not introduced, non-renormalizable terms are not added to the superpotential, or R-parity remains unbroken. If the mass of ν_L is found experimentally to be non-zero but small, how can such small values be generated?

We now turn to an overview of a number of possible solutions to the ν mass problem discussed in the literature where, essentially, one or more of the above assumptions are relaxed. These approaches can be classified as follows. First (in subsection 3.6.1) *discrete symmetries* are applied to the superpotential, W, so that ν_L remains massless at tree level. However, higher order radiative corrections arising from W (or the gauge sector) induce small ν_L masses. These discrete symmetries can sometimes occur as part of an enlarged gauge symmetry as in the ALRM. Second (in subsection 3.6.2) *additional neutral fermions* (and their SUSY partners) coming from possible E_6 singlets and/or surviving parts of $\overline{\mathbf{27}}$'s could mix with the ordinary members of the **27**. In addition, new terms in W are generated which lead to modifications in the neutral fermion mass matrix. Third (in subsection 3.6.3) *higher-dimensional operators* representing non-renormalizable interactions which are suppressed by inverse powers of some large scale are added to W and produce new terms in the neutral fermion mass matrix. This also can change the neutral fermion mass matrix structure and introduces mixing with the other neutralinos. In general not all of these approaches are mutually exclusive and the modifications they make in the mass matrix can be quite different. A last worry with such models is how to prevent too many of the additional neutral fermions from becoming light and upsetting the limit on the number of such fields from cosmological considerations. This certainly is more problematic in models which introduce additional neutral fields. We will also discuss neutrino magnetic moments and radiative decays in subsection 3.6.4.

3.6.1. Discrete symmetries and radiative breaking

This approach is particularly popular in the literature (see refs. [3.61, 3.111–3.118] since it requires the introduction of no new interactions or particles beyond those which already exist in the superpotential (W) and the electroweak gauge sector of the model under consideration. However, such an approach might be viewed as somewhat ad hoc and certain models of this kind were initially controversial [3.61, 3.111, 3.112], where it has now been emphasized that such discrete symmetries, if they exist, must be able to differentiate between generations in a realistic model with three (or more) generations [3.111, 3.112]. As a generic example of this kind of model we follow the work of ref. [3.111].

In order to forbid rapid proton decay, have zero tree-level neutrino mass, *and* to be able to generate such masses only at the one loop level, there must be some discrete symmetry G such that $\lambda_{11} = 0$ and $\lambda_{9,10} = 0$. One *cannot* make the choice that $\lambda_{6,7,8}$ vanish since only $\lambda_{7,8}$ can be used to generate a small Dirac ν mass via a diagram such as fig. 93. A short analysis shows that such a symmetry which demands that $\lambda_{2,4,5,7,8}$ be non-zero while simultaneously demanding $\lambda_{11} = 0$ is inconsistent unless generation freedom is taken into account. The simplest symmetry of this kind was found to be [3.111] $Z_2 \times Z_3$ under which

$$
\begin{aligned}
&Z_2\colon\ [Q, u^c, d^c, h, h^c]_i \to -[Q, u^c, d^c, h, h^c]_i\,,\\
&Z_3\colon\ [Q, d^c, L, \nu^c, h, h^c]_i \to e^{i(2\pi/3)}[Q, d^c, L, \nu^c, h, h^c]_i\,,\\
&H_1 \to e^{-i(2\pi/3)}H_1\,, \quad H_{2,3} \to H_{2,3}\,, \quad \bar{H}_1 \to e^{-i(2\pi/3)}\bar{H}_1\,, \quad \bar{H}_2 \to e^{i(2\pi/3)}\bar{H}_2\,, \quad \bar{H}_3 \to \bar{H}_3\,,\\
&S_1^c \to e^{-i(2\pi/3)}S_1^c\,, \quad S_2^c \to e^{i(2\pi/3)}S_2^c\,, \quad S_3^c \to S_3^c\,,
\end{aligned}
\tag{3.147}
$$

where the index labels generation number. Such a symmetry not only allows for one-loop Dirac neutrino masses and avoids rapid proton decay but leads to realistic mass matrices for u, d, and e, as well as avoiding FCNC couplings in the scalar sector at the tree level. A rough estimate of the size of the generated masses is given in refs. [3.111, 3.112] by taking suggestive masses for $\tilde{h}$, $\tilde{h}^c$ of order 100–200 GeV and Yukawa couplings consistent with limits from flavor changing processes such as $K \to \pi\nu\bar{\nu}$, $\mu N \to eN$, and $\mu \to e\gamma$ with the results: $m_{\nu_e} \lesssim 0.1$ eV, $m_{\nu_\mu} \lesssim 1$ eV, and $m_{\nu_\tau} \lesssim 50$ eV without any fine tuning. The symmetry $Z_2 \times Z_3$ is not unique and other symmetries of a similar nature have been discussed in the literature such as $Z_2 \times Z_5$ [3.113, 3.117]. In general, the ν mass matrix is proportional to that for the down-type quarks and can even be in the Fritzsch form [3.119]. The same class of diagrams which produce ν masses in these models can also produce radiative decays, $\nu' \to \nu\gamma$, merely by attaching a photon line in all possible ways. These rates are found to be quite rapid since they tend not to be helicity suppressed and can be used together with astrophysical limits to constrain model parameters [3.114]. Similarly, the diagonal versions of the above $\nu'\nu\gamma$ loop-induced couplings can

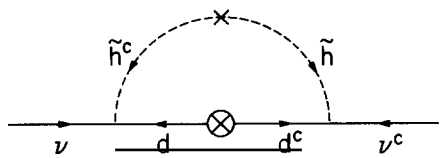

Fig. 93. Loop order contribution to the neutrino mass from leptoquark exchange.

produce a large magnetic moment for the ν which may help in solving the solar ν-problem [3.115]. This will be discussed further below. These models seem to be quite attractive.

3.6.2. Additional neutral fermions

The possibility of using E_6 singlets (**1**'s) or neutral fields remaining from the $\overline{\mathbf{27}}$'s to deal with the neutrino mass problem was first considered by Witten [3.120] and subsequently by a number of authors [3.117, 3.121–3.124]. In addition to the usual $(\mathbf{27})^3$ terms in the superpotential, W, there are now extra terms containing these new fields which are still renormalizable: $(\overline{\mathbf{27}})^3$ and $\mathbf{27}\cdot\overline{\mathbf{27}}\cdot\mathbf{1}$. We will give an overview of a specific pair of models of this kind [3.122] since they typify the general features of this approach.

H and J will denote the two Higgs fields in the additional two pairs of $\mathbf{27}+\overline{\mathbf{27}}$ representations (with Betti–Hodge number $b_{1,1}=2$) that will be added to the usual set of fields as well as the E_6 singlets ϕ_a. In H and J, it will be assumed that the ν^c-like and S^c-like components $(\nu^c_{H,J}, S^c_{H,J})$ remain light and can obtain vev's which are associated with an intermediate scale. The relevant part of the superpotential is given by (where a labels the various fields and is summed over)

$$W_0 = \lambda_7^a d^c h \nu_a^c + \lambda_8^a h^c h S_a^c + \lambda_9^a L H \nu_c^a + \lambda_{10}^a H H^c S_a^c + \lambda_{11} L H e^c + \beta_1 \nu_H^c \bar{\nu}_J^c \phi + \beta_2 S_H^c \bar{S}_J^c \phi \,. \tag{3.148}$$

In the first model presented in ref. [3.122] W_0 is supplemented by (assuming only one singlet, ϕ)

$$W_1 = \lambda_{12} S^c \bar{S}_J^c \phi + \lambda_{13} \nu^c \bar{\nu}_J^c \phi \,, \tag{3.149}$$

while in the second model, which contains two additional singlets $(\phi_{1,2})$, the additional term is

$$W_2 = \lambda_{14} S^c \bar{S}_J^c \phi_2 + \lambda_{15} \nu^c \bar{\nu}_J^c \phi_2 + \lambda_{16} S^c \bar{S}_H^c \phi_1 + \lambda_{17} \nu^c \bar{\nu}_H^c \phi_2 \,. \tag{3.150}$$

In W_1, the neutral fields originating in H are eliminated by a discrete symmetry under which ϕ, J, and $\bar{J}$ are odd while all others are even. We assume that $\langle \tilde{S}^c \rangle_H = V_6$, and $\langle \tilde{S}^c \rangle_J = \mu$, $\langle \tilde{\nu}^c \rangle_{\bar{J}} = V_{BL}$ with a $\mu \ll V_{BL} \ll V_6$ hierarchy assumed. V_{BL} is the scale at which $B-L$ is spontaneously broken. N, N^c as well as h, h^c pick up a large mass $\sim V_6$ and decouple. If we also assume $\beta_1 \ll \lambda_{13}$, then defining $(\nu^c)' = \nu^c + (\beta_1/\lambda_{13})\nu_H^c$ and $(S^c)' = (\beta_2 S_H^c + \lambda_{12} S^c)/(\beta_2^2 + \lambda_{12}^2)^{1/2}$ one finds that the combinations orthogonal to $(\nu^c)'$ and $(S^c)'$ remain massless (and invisible), while the remaining neutral fields form the 4×4 mass matrix

$$\begin{array}{c} \\ \nu \\ (S^c)' \\ (\nu^c)' \\ \phi \end{array} \begin{array}{c} \begin{array}{cccc} \nu & (S^c)' & (\nu^c)' & \phi \end{array} \\ \begin{bmatrix} 0 & 0 & m_D & 0 \\ 0 & 0 & 0 & \mu \\ m_D & 0 & 0 & V_{BL} \\ 0 & \mu & V_{BL} & 0 \end{bmatrix} \end{array} . \tag{3.151}$$

Diagonalizing this matrix produces two Dirac fields with masses $m_1 = \mu m_D / V_{BL}$ and $m_2 = V_{BL}$ with m_D being the typical Dirac ν mass term: $m_D = O(m_e) \simeq 1$ MeV. If $V_{BL} \simeq 10^{12}$ GeV and $\mu < 10^6$ GeV then $m_1 < 1$ eV. Note that the light ν in this model is Dirac so that neutrinoless double-beta decay is forbidden.

In the second model from ref. [3.122] a discrete symmetry is imposed under which the J, $\bar{J}$, and ϕ_2 fields are odd while all others are even. It is now assumed that $\langle \tilde{S}^c \rangle_H = \langle \tilde{S}^c \rangle_H = V_6$ and $\langle \tilde{\nu}^c \rangle_J = \langle \tilde{\nu}^c \rangle_{\bar{J}} = V_{BL}$ which leads to N, N^c, and S^c becoming heavy and hence leaving a 3×3 mass matrix (assuming $\beta_1 \ll \lambda_{15}$)

$$\begin{array}{c} \\ \nu \\ \nu^c \\ \phi_2 \end{array} \begin{array}{c} \begin{array}{ccc} \nu & \nu^c & \phi_2 \end{array} \\ \begin{bmatrix} 0 & m_D & 0 \\ m_D & 0 & V_{BL} \\ 0 & V_{BL} & 0 \end{bmatrix} \end{array}, \tag{3.152}$$

which produces the eigenstates of a massless Majorana neutrino: $\nu_{phy} \simeq \nu - (m_D/V_{BL})\phi_2$ and a heavy Dirac neutrino with a mass of order $\simeq V_{BL}$. SUSY breaking could induce a small Majorana mass (m_ϕ) for ϕ_2 leading to a small Majorana mass for ν: $m_\nu \simeq m_\phi (m_D/V_{BL})^2$ which, if $m_D \simeq 1$ MeV, $V_{BL} \gtrsim 1$ TeV, and $m_\phi \simeq 10^2$–10^3 GeV, would predict $m_\nu \simeq 0.1$–1 eV. Models of this kind can lead to n–$\bar{\text{n}}$ mixing times of order $\simeq 6 \times 10^9$ s, which may be accessible in future experiments.

For both of the models considered above one can easily extend the results to more realistic situations where $n_g = 3$ or 4 by adding additional singlet fields, ϕ. Note that models can be easily constructed in which the light ν is either a Dirac or Majorana field. It is also possible to construct models of this kind where a neutral gaugino plays the role of ϕ [3.122]. It is clear that while this approach leads to interesting results, it appears to be even more ad-hoc than the radiative breaking scenario since not only are discrete symmetries necessary but the vev's of the new neutral fields must be chosen properly in a hierarchial fashion.

3.6.3. Higher-dimensional operators

The usual Yukawa interactions in the renormalizable superpotential are of the form

$$\mathcal{L}_4 = f\psi\psi H\,, \tag{3.153}$$

with ψ being the **27** of E_6 containing the matter fields and H being the **27** containing the Higgs fields. In addition to these terms, non-renormalizable terms could also be generated by world-sheet instantons on Calabi–Yau backgrounds which are suppressed by powers of the compactification (or Planck) scale. Such new terms could be sufficiently large and hence contribute significantly to the neutral fermion mass matrix [3.125–3.129]. To be specific, we will follow the work in ref. [3.125] as a typical example of this kind of approach where new terms in W up to dimension 7 were considered: $\mathcal{L} = \mathcal{L}_4 + \mathcal{L}'$,

$$\mathcal{L}' = (1/M_c) f_2 \psi\psi\bar{H}\bar{H} + (1/M_c^2) h\psi\psi H(H\bar{H}) + (1/M_c^3)[y_1 \psi\psi\bar{H}\bar{H}(H\bar{H}) + y_2 \psi\psi H(HHH)]\,. \tag{3.154}$$

The leading correction will, of course, come from the dimension-5 terms. If m_i (M_i) represent SU(2)-doublet (singlet) vev's, we expect $M_i \gg m_i$ with M_i of order the intermediate scale. In the notation of ref. [3.125], $\langle \tilde{\nu}^c \rangle_H = M_1$, $\langle \tilde{S}^c \rangle_H = M_2$, $\langle \tilde{\nu} \rangle_H = m_3$, $\langle \tilde{N} \rangle_H = m_2$, and $\langle \tilde{N}^c \rangle_H = m_1$ with $m_i \sim 100$ GeV. A short analysis indicates that the usual quark and charged lepton masses are not affected much by these higher-dimensional terms. However, the neutral mass matrix now takes the form

$$\begin{array}{c} \\ \nu \\ N \\ N^c \\ \nu^c \\ S^c \end{array} \begin{array}{c} \begin{array}{ccccc} \nu & N & N^c & \nu^c & S^c \end{array} \\ \begin{bmatrix} 0 & 0 & M_1 & m_1 & 0 \\ 0 & 0 & M_2 & 0 & m_1 \\ M_1 & M_2 & 0 & m_3 & m_2 \\ m_1 & 0 & m_3 & M_1' & M_{12}' \\ 0 & m_2 & m_2 & M_{12}' & M_2' \end{bmatrix} \end{array}, \tag{3.155}$$

where $M_i' = M_i^2/M_c$ and $M_{12} = 2M_1M_2/M_c$. Diagonalization of this matrix leads to the eigenvalues $\lambda_1 \sim m_1^2/M'$, $\lambda_{2,3} \sim M'$, and $\lambda_{4,5} \sim M$, with which, if we take $M_1 \sim 10^{11}$ GeV, $M_c \sim 10^{18}$ GeV (then $M' \sim 10^4$ GeV), and $m_1 \sim 10$ MeV, we obtain $\lambda_1 \sim 10$ eV. The light Majorana ν is then a combination of weak SU(2) doublet members, and for $M_2 > 10\,M_1$ weak universality is satisfied. All other neutral leptons obtain very large masses. It is interesting to note that if the intermediate scale, M_1 is larger ($\sim 10^{14}$ GeV or so) then the light Majorana isodoublet neutrino mass will be extremely small.

While models of this kind generally produce light, Majorana neutrinos they appear to be as ad-hoc as the models of the type treated in section 3.6.2 in that additional fields with well-ordered vev's, as well as the existence of discrete symmetries are necessary in obtaining the desired result. It would appear that models of the type of section 3.6.1 are the most economical at this time.

3.6.3. Neutrino magnetic moments and radiative decay

A number of scenarios have been proposed to give a large rate for neutrino radiative decay within the E_6 context. These models can be classified by what quantum number assignments are assumed for the exotic fermions.

If the exotic fermions have conventional quantum number assignments, FCNC and RHC are both present and mixing matrices are generally non-unitary. From the discussion above, it is clear that in this case the dominant contribution comes from the diagrams shown in fig. 93 from ref. [3.111]. One finds that in Bohr magneton units the anomalous magnetic moments for ν_e and ν_μ ($\kappa_{e,\mu}$ respectively) are given by

$$\kappa_{e,\mu} = (G_F m_e M_W/2\sqrt{2}\pi^2) \sin\theta_R^\nu \sin(\theta_L^e - \theta_L^\nu)\, G(x)\,, \tag{3.156}$$

with

$$G(x) = x[1 + 3(1-x^2)^{-1} + 6x^2(1-x^2)^{-1} \ln x]\,, \tag{3.157}$$

and $x = M_E/M_W$. Since $M_E \gtrsim 27$ GeV based on data from TRISTAN we obtain

$$\kappa_{e,\mu} \gtrsim 1.9 \times 10^{-8} \sin\theta_R^\nu \sin(\theta_L^e - \theta_L^\nu)\,. \tag{3.158}$$

As M_E increases this result gets larger, e.g., if $M_E \simeq 760$ GeV this prediction increases by a factor of 10. Existing bounds on $\kappa_{e,\mu}$ come from several sources: accelerator and reactor data (AR) impose the constraints [3.130] $|\kappa_e| \lesssim 1.52 \times 10^{-10}$ and $|\kappa_\mu| \lesssim 1.19 \times 10^{-9}$ while big bang nucleosynthesis (BB) results in $|\kappa_e| \lesssim 2.2 \times 10^{-11}$ [3.131]. Using these constraints one finds

$$\begin{aligned} |\sin\theta_R^\nu \sin(\theta_L^e - \theta_L^\nu)| &\leq 8.00 \times 10^{-3}\ (\mathrm{AR})\,, \\ &\leq 1.16 \times 10^{-3}\ (\mathrm{BB})\,. \end{aligned} \tag{3.159}$$

Stronger limits on κ_{ν_e} may arise when data from the supernova SN1987A is considered (this has been discussed by a number of different authors [3.132–3.137]) and are generally in the range of $|\kappa_e| \lesssim (0.5\text{–}3) \times 10^{-12}$ which could substantially strengthen the constraint on the mixing angles. These supernova constraints are, however, model dependent and it may be possible to evade these stronger limits [3.134]. If the Voloshin et al. [3.138] solution to the solar ν problem is to be realized then significantly larger values of $|\kappa_e| \simeq (0.1\text{–}1) \times 10^{-10}$ would be required. Their scenario proposes that the ordinary left-handed neutrinos are rotated into non-interacting (or very weakly interacting) right-handed neutrinos by their helicity-flipping magnetic dipole interaction with the solar magnetic field.

It should be pointed out that models of this kind which can give such a large value for κ_ν have a naturalness problem if they also want to keep the neutrino from getting a large radiative mass [3.139]. It is not completely clear how the rather complex nature of the ν mass generation in E_6 models may resolve this problem.

With these same B and L assignments, radiative decay of a heavy neutrino, $\nu_H \to \nu_L \gamma$, can proceed by the same types of diagrams as shown in fig. 93 except that the initial and final fermions are now distinct. Using the $V_{L,R}$ matrix notation developed in section 3.1, the $\nu_H \to \nu_L \gamma$ matrix element can be written as [3.140]

$$M = C\bar{\nu}_L \sigma_{\mu\nu} \varepsilon_\gamma^\mu q^\nu (v - a\gamma_5) \nu_H \,, \tag{3.160}$$

which leads to

$$\Gamma(\nu_H \to \nu_L \gamma) = (C^2/8\pi) M_H^3 (1 - M_L^2/M_H^2)^3 (|v|^2 + |a|^2) \,. \tag{3.161}$$

For the case of Dirac neutrinos one obtains

$$\begin{aligned} &C = eG_F M_W / 8\sqrt{2}\pi^2 \,, \\ &v, a = \sum_i G(\delta_i)[(V_L^*)_{iH}(V_R)_{iL} \pm (V_L)_{iL}(V_R^*)_{iH}] \,, \end{aligned} \tag{3.162}$$

with $\delta_i = M_i/M_W$ (M_i being the exotic fermion mass in the loop) and

$$G(\delta) = \delta(1 - \delta^2)^{-2}(4 - 5\delta^2 + \delta^4 + 6\delta^2 \ln \delta) \,. \tag{3.163}$$

Note that $G \simeq 2.5$ for $\delta \simeq 1$. For $M_H \gg M_L$, this results in a lifetime

$$\tau_{\text{Dirac}} = 2.46 \times 10^6 \text{ s} \times (1 \text{ keV}/M_H)^3 \left(\sum |G(\delta_i)|^2 [|(V_L^*)_{iH}(V_R)_{iL}|^2 + |(V_L)_{iL}(V_R^*)_{iH}|^2] \right)^{-1} \,. \tag{3.164}$$

For Majorana neutrinos, v and a become (with β being the $\nu_{H,L}$ relative phase)

$$v, a = \sum_i G(\delta_i)\{(V_L^*)_{iH}(V_R)_{iL} \pm (V_L)_{iL}(V_R^*)_{iH} - e^{i\beta}[(V_L^*)_{iL}(V_R)_{iH} \pm (V_L)_{iH}(V_R^*)_{iL}]\} \,, \tag{3.165}$$

and produces a similar prediction for τ for most values of β. If we demand that ν's in the 10^2–10^6 GeV mass range have $\tau \lesssim 10^4$ s (see, for example, ref. [3.141]) from cosmological considerations and taking

all V's comparable with $\delta_i \simeq 1$ we obtain the constraint

$$2.5 \leq (M_H/1\,\text{keV})^{3/4} V\,, \tag{3.166}$$

so that $V \lesssim 0.1$ (0.01) implies $M_H \gtrsim 73$ keV (1.6 MeV). Thus light neutrinos would not be able to decay quickly enough in this scenario to avoid the cosmological bounds for reasonable values of the parameters. The interplay of the cosmological constraints, naturalness, and the assumption of the Voloshin et al. solution to the solar neutrino problem [3.138] has been considered at some length in a somewhat model independent way by Pulido and Ralston [3.142].

Similar calculations can be done for the other assignments of B and L for the exotic fermions particularly in the case where h is a leptoquark. Enqvist and Maalampi [3.114] considered the leptoquark coupling terms in the superpotential which generate a Dirac mass (as discussed above) and produce an off-diagonal magnetic moment via loop diagrams allowing for the $\nu_H \to \nu_L \gamma$ decay. Existing astrophysical and cosmological data as well as present constraints on the neutrino masses result in the bounds (if the typical h mass is $\simeq$100 GeV) $\lambda_{e,\mu,\tau}, \bar{\lambda}_{e,\mu,\tau} < 10^{-3}$–$10^{-4}$ with λ, $\bar{\lambda}$ defined by the structure of the superpotential ($\bar{\lambda} QLh^c + \lambda d^c \nu^c h$). The enhancement in the $\nu_H \to \nu_L \gamma$ rate found by these authors is due to the fact that the amplitude is proportional to the down-quark masses instead of the neutrino masses as in the SM. Grifols and Sola [3.115] consider the parallel situation for the neutrino magnetic moment with these B and L assignments for the exotics. In a model where a reasonable value for the ν Dirac mass is generated, a magnetic moment of order $\simeq 2 \times 10^{-11}$ Bohr magnetons is obtained but is somewhat sensitive to the values assumed for the d-squark masses. Liu [3.143] addresses the problem of naturalness in these models which produce such large magnetic and transition moments and suggests that the only natural value for these quantities is of order of those obtained in the SM.

4. The Higgs sector

4.1. Theoretic overview and mass spectrum

The scenario which is the most extensively studied in the literature is that where all matter superfields, including the Higgs fields which provide electroweak symmetry breaking, lie in three generations of **27** representations of E_6. In this scenario there are no light survivors from the $(\mathbf{27} + \overline{\mathbf{27}})$ representations; this corresponds to case A discussed in section 1. Here the Higgs fields are chosen from amongst the scalar components of the five colorless supermultiplets, $\tilde{H}$, $\tilde{H}^c$, $\tilde{S}^c$, $\tilde{\nu}^c$, and $\tilde{\nu}$. However, a non-zero vev for $\tilde{\nu}$ would violate lepton number (as well as R-parity) and thus the constraint $\langle \tilde{\nu} \rangle = 0$ is imposed. In order to break the electroweak symmetry and provide masses for all the gauge bosons, we must have $\langle \tilde{N} \rangle$ and $\langle \tilde{N}^c \rangle \neq 0$, and in rank-5 models at least one of $\langle \tilde{\nu}^c \rangle$ or $\langle \tilde{S}^c \rangle$ must be non-zero as well, while for rank-6 models both of these vev's must be non-vanishing. As can be seen from the superpotential (eq. 1.4), $\tilde{H}$ and $\tilde{H}^c$ also provide masses for the $T_{3L} = -\frac{1}{2}$ and $+\frac{1}{2}$ fermions, respectively, while $\tilde{S}^c$ gives a mass to the exotic fermion h and the Higgs super-partner, E. $\tilde{S}^c$ is also responsible for mixing within the Higgs sector via the superpotential term $\lambda_4 S^c H H^c$ and hence $\langle \tilde{S}^c \rangle$ should not be much larger than of O(1 TeV).

It has been demonstrated that $\langle \tilde{\nu}^c \rangle \neq 0$ can lead to phenomenological difficulties [4.1]. For rank-5 low-energy gauge groups, an essentially massless pseudo-Goldstone boson, a_ν, is present if $\langle \tilde{\nu}^c \rangle$ is non-vanishing. h–d mixing will also occur due to the superpotential term $\lambda_8 \nu^c h d^c$ and induces the flavor

changing decay $K \to \pi + a_\nu$ at an unacceptably large rate. In order to make this decay rate compatible with experiment, the vev must satisfy the bound $\langle \tilde{\nu}^c \rangle \lesssim 40$ keV. In rank-6 models it is difficult to obtain large enough Yukawa couplings to drive the $\tilde{\nu}^c$ mass squared negative and produce $\langle \tilde{\nu}^c \rangle \neq 0$ and simultaneously keep the superpotential couplings λ_8 and λ_{11} small in order to be consistent with FCNC constraints and limits on neutrino masses, respectively. These arguments may be evaded by the use of discrete symmetries, which would conveniently set the troublesome Yukawa couplings to zero.

Following the literature, we will focus on the Higgs sector within the context of the simplest E_6 superstring-inspired model, the rank-5 model η, and will set $\langle \tilde{\nu}^c \rangle = 0$ for the remainder of this section, except where otherwise noted. We are then left with three generations of two iso-doublets and one iso-singlet Higgs fields whose neutral components acquire a non-vanishing vev. We follow the notation of ref. [4.2], which was outlined in section 2, and label the multiplets by

$$\tilde{H} \equiv \Phi_1 = \begin{pmatrix} \phi_1^0 \\ \phi_1^- \end{pmatrix}, \qquad \tilde{H}^c \equiv \Phi_2 = \begin{pmatrix} \phi_2^+ \\ \phi_2^0 \end{pmatrix}, \qquad \tilde{S}^c \equiv \Phi_3 = \phi_3^0, \tag{4.1}$$

with $\langle \phi_i^0 \rangle = v_i/\sqrt{2}$. Without loss of generality, the phases of the Higgs fields can be rotated such that the vev's are all real and positive.

It is possible to work in a basis where only one set of these fields (usually defined as the third generation) obtains vacuum expectation values. This avoids dangerous tree-level flavor changing neutral currents [4.3] as well as serving as a simplification. However, mixing between all three generations can occur through the superpotential term $\lambda_4^{ijk} H_i^c H_j S_k^c$, where $i, j, k = 1, 2, 3$ are generation indices, and can induce vev's for the first and second generations (since if any two of the scalar components of the three fields in such a tri-linear term acquire vev's then the third scalar component must also have a non-vanishing vev). Hence, to preserve this basis where only the third generation fields receive vev's, it is necessary to require that

$$\lambda_4^{i33} = \lambda_4^{3j3} = \lambda_4^{33k} = 0 \quad \text{for } i, j, k = 1, 2,$$

while

$$\lambda_4^{333}, \lambda_4^{ij3}, \lambda_4^{i3k}, \lambda_4^{3jk} \neq 0, \tag{4.2}$$

are possible. This can be achieved by use of discrete symmetries. An example of one such symmetry [4.4] is given by $(H_3, H_3^c, H_i, H_i^c) \to (H_3, H_3^c, -H_i, -H_i^c)$ where $i = 1, 2$, and $S^c \to S^c$. The first two generations of scalars then do not acquire vev's and are called unHiggs [4.5].

As previously stated, all three vev's $v_{1,2,3}$ must be non-zero, not only to provide masses for all the fermions, but also to break the rank-5 group $SU(3)_C \times SU(2)_L \times U(1)_Y \times U(1)_\eta$ down to $SU(3)_C \times U(1)_{em}$. The gauge symmetry breaking is furnished by the renormalization group evolution of the scalar masses, where one or more of the mass squared terms is driven from a positive value at the GUTS scale (M_c for model η) to a negative value at the electroweak scale. This is achieved by the presence of large Yukawa couplings between the Higgs fields and the fermions within the same multiplet (here, the third generation fermions). In order to obtain $M_{Z_2} > M_{Z_1}$, and thus be consistent with neutral current phenomenology, the parameter $M_{\phi_3}^2$ becomes negative first, not much above the electroweak scale, and induces $v_3 > v_2, v_1$. Due to the presence of the large top quark Yukawa coupling, the mass-squared term for ϕ_2 is driven downwards faster than that for ϕ_1 (which couples to the lighter b-quark), but need

not go negative. This results in the inequality $M^2_{\phi_2}(M_W) < M^2_{\phi_1}(M_W)$ and consequently $v_2 > v_1$. From various phenomenological considerations the authors of ref. [4.6] find that typical values of v_1/v_2 and v_3/v_2 in no-scale models lie in the ranges $0.4 \le v_1/v_2 \le 0.6$ and $2.8 \le v_3/v_2 \le 10$, while Cohen et al. [4.7] extend the range of v_1/v_2 to 0.2–0.6. More details of the renormalization group analysis are given in refs. [4.3, 4.4, 4.6–4.8].

The most general scalar Higgs potential is given by [4.2–4.10]

$$\begin{aligned} V = {} & \mu_1^2 \Phi_1^+ \Phi_1 + \mu_2^2 \Phi_2^+ \Phi_2 + \mu_3^2 \Phi_3^+ \Phi_3 - i(\lambda A/\sqrt{2})(\Phi_1^+ \tau_2 \Phi_2 \Phi_3 + \text{h.c.}) \\ & + \lambda^2 (\Phi_1^+ \Phi_1 \Phi_2^+ \Phi_2 + \Phi_1^+ \Phi_1 \Phi_3^+ \Phi_3 + \Phi_2^+ \Phi_2 \Phi_3^+ \Phi_3) + \tfrac{1}{8}(g_L^2 + g_Y^2)(\Phi_1^+ \Phi_1 - \Phi_2^+ \Phi_2)^2 \\ & + \tfrac{1}{72} g_\eta^2 (\Phi_1^+ \Phi_1 + 4\Phi_2^+ \Phi_2 - 5\Phi_3^+ \Phi_3)^2 + (\tfrac{1}{2} g_L^2 - \lambda^2) |\Phi_1^+ \Phi_2|^2 . \end{aligned} \tag{4.3}$$

We specifically define the coupling constants via the covariant derivative

$$D_\mu = \partial_\mu - i g_L \boldsymbol{T} \cdot \boldsymbol{B}_\mu - i g_Y \tfrac{1}{2} Y C_\mu - i g_\eta \tfrac{1}{2} Y_\eta C^\eta_\mu , \tag{4.4}$$

where the charges are normalized such that $g_Y = g_\eta$. (In more realistic models, g_Y and g_η vary at most by a few percent [4.4, 4.6].) In eq. (4.3) $\lambda \equiv \lambda_4^{333}$, A is the associated soft supersymmetry breaking parameter, and in order to keep the minimum of the potential stable, λA is real and positive. Since the vev's are also defined to be real and positive, the scalar potential is then CP invariant. In addition to the gauge coupling constants, the potential contains five parameters, λ, A, and the three μ_i^2 which can be expressed in terms of the three v_i at the minimum. The v_i in turn can be completely determined by parameters in the gauge boson sector. The W mass is obtained by $M_W = (g_L/2)(v_1^2 + v_2^2)^{1/2}$ where $v^2 = v_1^2 + v_2^2$ is the SM vev, M_{Z_2} (as well as the Z–Z′ mixing angle ϕ) is related to the vev's $v_{1,2,3}$ in the Z–Z′ mass matrix as presented in eqs. (2.11)–(2.14), and the third parameter is given by the ratio of the doublet vev's, $\tan\beta = v_2/v_1$. Thus once M_{Z_2} and $\tan\beta$ are specified, only two free parameters remain, λ and A. Here we would like to note that, along with other assumptions, the authors of ref. [4.4] have set $A = 0$ and consequently found that radiative symmetry breaking in model η is problematic; we will discuss this point further in section 5.

After spontaneous symmetry breaking five physical Higgs fields remain: one charged scalar, $H^\pm$, one pseudoscalar, P^0, and three neutral scalars, H_1^0, H_2^0, H_3^0 with masses which we will take as $M_1 < M_2 < M_3$. The charged Higgs mass matrix as determined from the potential is given by [4.5]

$$\mathcal{M}^2_{H^\pm} = \frac{1}{2} \begin{pmatrix} (\frac{1}{2} g_L^2 - \lambda^2) v_1^2 + \lambda A v_3 v_1/v_2 & (\frac{1}{2} g_L^2 - \lambda^2) v_1 v_2 + \lambda A v_3 \\ (\frac{1}{2} g_L^2 - \lambda^2) v_1 v_2 + \lambda A v_3 & (\frac{1}{2} g_L^2 - \lambda^2) v_2^2 + \lambda A v_3 v_2/v_1 \end{pmatrix}, \tag{4.5}$$

where one eigenvalue is a massless Goldstone boson which is eaten by the W, and the mass of the physical charged Higgs is

$$M^2_{H^\pm} = (\lambda A v_3/\sin\beta\cos\beta) + M_W^2(1 - 2\lambda^2/g_L^2) . \tag{4.6}$$

Note that due to the $-\lambda^2$ contribution, it is possible for $M_{H^\pm}$ to be less than M_W (although the product Av_3 must not be too large); this is in contradiction to the minimal SUSY SM with two Higgs doublets where one always finds $M_{H^\pm} > M_W$ [4.12].

Since CP is conserved in the Higgs potential, the neutral scalar and pseudoscalar mass matrices decouple. Diagonalization of the pseudoscalar mixing matrix [4.5]

$$\mathcal{M}^2_{PS} = \frac{\lambda A v_3}{2}\begin{pmatrix} v_1/v_2 & 1 & v_1/v_3 \\ 1 & v_2/v_1 & v_2/v_3 \\ v_1/v_3 & v_2/v_3 & v_1 v_2/v_3^2 \end{pmatrix} \tag{4.7}$$

yields two zero mass Goldstone bosons which are eaten by the Z and Z', and the physical pseudoscalar of mass

$$M^2_{P^0} = \frac{\lambda A v_3}{\sin\beta\cos\beta}\left(1 + \frac{v_1^2 + v_2^2}{v_3^2}\sin^2\beta\cos^2\beta\right), \tag{4.8}$$

which is proportional to λA. It is clear that M_{P^0} can be quite large in the $v_3 \gg v_2, v_1$ limit.

The mass matrix for the neutral scalars as derived from eq. (4.3) is found to be [4.10]

$$\mathcal{M}^2_{H^0} = \frac{1}{2}\begin{pmatrix} B_1 v_1^2 + \lambda A v_2 v_3/v_1 & B_2 v_1 v_2 - \lambda A v_3 & B_3 v_1 v_3 - \lambda A v_2 \\ B_2 v_1 v_2 - \lambda A v_3 & B_4 v_2^2 + \lambda A v_1 v_3/v_2 & B_5 v_2 v_3 - \lambda A v_1 \\ B_3 v_1 v_3 - \lambda A v_2 & B_5 v_2 v_3 - \lambda A v_1 & B_6 v_3^2 + \lambda A v_1 v_2/v_3 \end{pmatrix}, \tag{4.9}$$

where we have defined

$$\begin{aligned} &B_1 = \tfrac{1}{2}(g_L^2 + g_Y^2) + \tfrac{1}{18}g_\eta^2, \quad B_2 = 2\lambda^2 + \tfrac{2}{9}g_\eta^2 - \tfrac{1}{2}(g_L^2 + g_Y^2), \quad B_3 = 2\lambda^2 - \tfrac{5}{18}g_\eta^2, \\ &B_4 = \tfrac{1}{2}(g_L^2 + g_Y^2) + \tfrac{8}{9}g_\eta^2, \quad B_5 = 2\lambda^2 - \tfrac{10}{9}g_\eta^2, \quad B_6 = \tfrac{25}{18}g_\eta^2. \end{aligned} \tag{4.10}$$

The eigenvectors, H_j^0, are then related to the ϕ_i by

$$\phi_i = \sum_{j=1}^{3} U_{ij} H_j^0, \tag{4.11}$$

where the matrix U_{ij} is real (due to CP conservation) and in the large v_3 limit is approximately [4.2]

$$\begin{aligned} &U_{11} = \cos\alpha, \quad U_{12} = -\sin\alpha, \quad U_{13} = \tilde{B}_3 v\cos\beta/\tilde{B}_6 v_3, \\ &U_{21} = \sin\alpha, \quad U_{22} = \cos\alpha, \quad U_{23} = \tilde{B}_5 v\sin\beta/\tilde{B}_6 v_3, \\ &U_{31} = -(v/\tilde{B}_6 v_3)(\tilde{B}_3\cos\beta\cos\alpha + \tilde{B}_5\sin\beta\sin\alpha), \\ &U_{32} = -(v/\tilde{B}_6 v_3)(-\tilde{B}_3\cos\beta\sin\alpha + \tilde{B}_5\sin\beta\cos\alpha), \quad U_{33} = 1. \end{aligned} \tag{4.12}$$

Here, $\tilde{B}_j = 2B_j/(g_L^2 + g_Y^2)$ and the angle α is given by

$$\tan 2\alpha = N/D, \tag{4.13}$$

where

$$N = 4yz^2\tilde{B}_6 + 4y^2 \sin 2\beta - 4y(\tilde{B}_3 \cos^2\beta + \tilde{B}_5 \sin^2\beta) - (\tilde{B}_2\tilde{B}_6 - \tilde{B}_3\tilde{B}_5) \sin 2\beta ,$$
$$D = 4yz^2\tilde{B}_6 \cot 2\beta - 4y^2 \cos 2\beta - 2y \sin 2\beta(\tilde{B}_3 - \tilde{B}_5)$$
$$- (\tilde{B}_1\tilde{B}_6 - \tilde{B}_3^2) \cos^2\beta + (\tilde{B}_4\tilde{B}_6 - \tilde{B}_5^2) \sin^2\beta , \tag{4.14}$$

$$z \equiv v_3/v , \qquad y \equiv \lambda A/[2zM_{Z_2}(g_L^2 + g_Y^2)^{1/2}] . \tag{4.15}$$

Notice that in this limit where v_3 is large, the doublets ϕ_1 and ϕ_2 essentially decouple from ϕ_3, i.e., substantial mixing only occurs between ϕ_1 and ϕ_2, and ϕ_3 essentially becomes H_3^0 and is quite massive. It is important to also note that the ϕ_1–ϕ_2 mixing angle, α, is different from that which mixes the two Higgs doublets in the minimal supersymmetric model.

The neutral scalar Higgs mass spectrum is found by diagonalization of (4.9) and is reasonably complex. For large v_3, approximate expressions for the eigenvalues are obtained via perturbation in powers of λA. For values of $\lambda A \gtrsim v$ [corresponding, for example, to theories where the gauginos are responsible for spontaneous symmetry breaking and hence A is of order of the gaugino mass ~O(1 TeV)] the smallest eigenvalue is given by [4.5, 4.9–4.11]

$$M_1^2 = M_Z^2 \cos^2 2\beta + \tfrac{1}{2}v^2[\lambda^2 \sin^2 2\beta + \tfrac{1}{18}g_\eta^2(4 \sin^2\beta + \cos^2\beta)^2] - \gamma^2 v_3^2/2 ,$$
$$\gamma = (-18v/25g_\eta^2 v_3)[(2\lambda^2 - \tfrac{5}{18}g_\eta^2) \cos^2\beta + (2\lambda^2 - \tfrac{10}{9}g_\eta^2) \sin^2\beta - (2\lambda A/v_3) \sin 2\beta] . \tag{4.16}$$

M_1 rises with increasing λ and an absolute upper bound on M_1 cannot be determined unless constraints on λ (or equivalently M_{P^0}) are imposed; we will return to this point later. Alternatively, the authors of ref. [4.10] assumed that $v_3 \gg |A|$ and obtained the limit $M_1 \leq 108$ GeV, independent of the value of λ. In the case of $\lambda A \ll v$, the values of both M_1 and M_2 (as well as M_{P^0}) are of order M_Z or less [4.2, 4.9].

Upper and lower bounds on the charged and neutral scalar Higgs bosons are presented in fig. 94 from ref. [4.9] as a function of M_{P^0} (denoted as $M_{H_3^0}$ in the figure) for fixed values of M_{Z_2} and the Z–Z′

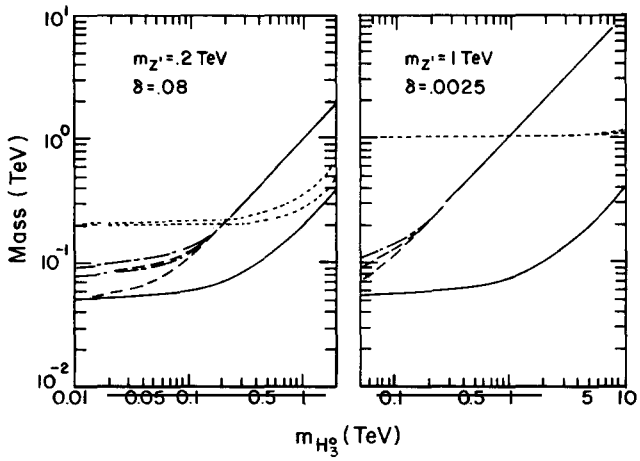

Fig. 94. Plots of upper and lower bounds for the masses of H_1^0 (solid curves), H_2^0 (dash–dotted), H_3^0 (dots), and $H^\pm$ (dashes) as a function of the P^0 mass (labeled as H_3^0 in the figure) for $M_{Z'} = 0.2$ and 1 TeV. The dashed curve is buried under the dash–dotted curve for $M_{P^0} \geq M_{Z'}$. The solid curve is the upper bound for M_1; the lower bound for M_1 is zero. The allowed regions are mapped out as λ is varied at any fixed M_{P^0} as described in the text.

mixing angle ϕ (labeled δ in the figure). These bounds were obtained by numerical diagonalization of the scalar mass matrix and subsequent variation of all parameters subject to the constraint that all physical Higgs have positive squared masses. As can be seen from the figure, of the two heavier neutral scalars, H_2^0 and H_3^0, one is approximately degenerate with Z_2, while the other has mass of order M_{P^0}. Whether H_2^0 or H_3^0 is actually the heaviest neutral scalar depends on the relative ordering of M_{Z_2} and M_{P^0}, where "level crossing" takes place at $M_{Z_2} \simeq M_{P^0}$. The charged Higgs is also nearly degenerate with P^0 and has a lower mass bound [4.2] of $M_{H^+} \gtrsim 50$ GeV when M_1 and M_{P^0} approach zero.

Constraints on the parameters λ and A also provide useful restrictions on the Higgs mass spectrum. By requiring that $M_1^2 > 0$, it is possible to obtain maximum and minimum allowed values of λ. This allowed region is illustrated in fig. 95, also from Gunion et al. [4.9], as a function of M_{P^0}. Also shown in the figure are ranges of A which have been obtained by numerical variation of all parameters such that all physical squared masses are positive. The requirement that the electroweak vacuum be a true minimum of the low energy theory implies that A is no larger than the gravitino mass [4.8] and thus suggests that $|A| \lesssim 1$ TeV. This gives an upper bound on the P^0 mass of approximately 1 TeV, which in turn places constraints on the rest of the spectrum which can be deduced from fig. 94. Additional restrictions on λ can be obtained from the requirement of perturbative unification. Drees [4.11] has found from the renormalization group evolution (assuming a light top quark, $m_t \sim 40$ GeV) that $\lambda(M_W) \lesssim 0.95$ in no-scale models, which sets the limit

$$M_1 \lesssim 170 \text{ GeV} \tag{4.17}$$

(while models with an intermediate mass scale imply $\lambda(M_W) \lesssim 1.2$, which yields $M_1 \lesssim 210$ GeV). The bound (4.17) can be improved if one requires that SUSY breaking effectively occurs due to gaugino masses and gives $\lambda(M_W) \lesssim 0.65$ and $M_1 \lesssim 120$ GeV, but this result is more model dependent.

Mass bounds for the iso-singlet Higgs boson (in the limit where ϕ_1 and ϕ_2 mix only with each other and ϕ_3 remains unmixed) have been calculated [4.13, 4.14] from perturbative unitarity constraints on the S matrix, analogous to the procedure for the SM Higgs boson [4.15]. The strongest unitarity constraint is obtained from the scattering process $Z_2Z_2 \to Z_2Z_2$, where demanding that the lth partial

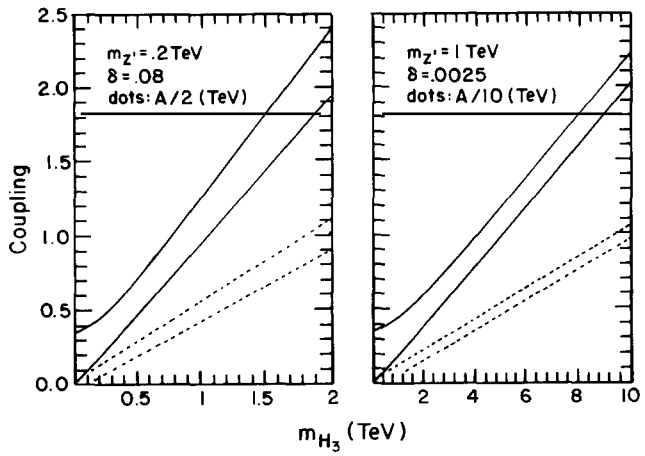

Fig. 95. Allowed regions of λ and A. The solid curves give the maximum and minimum values of λ for a given M_{P^0} (labeled in the figure as M_{H_3}), and correspond to $M_1 = 0$. The dotted curves represent maximum and minimum values of A (corresponding to λ_{min} and λ_{max}, respectively).

wave satisfies $a^l \lesssim 1$ leads to the limits

$$M_{\phi_3} \leq 13.8\, M_{Z_2}\,, \quad \text{in model } \eta\,, \qquad M_{\phi_3} \leq 11.0\, M_{Z_2}\,, \quad \text{in model } \psi\,. \tag{4.18}$$

Hence the mass of the iso-singlet ϕ_3 cannot be much larger than that of the Z_2, which is consistent with the mass bounds discussed above.

The mixing matrices for the unHiggs are given explicitly in ref. [4.5]. Here the authors find that eleven of the neutral eigenstates are expected to have masses of order v_3, whereas, for certain ranges of the parameters, it is possible that the charged unHiggs are relatively light with $25 \leq M_{h_i^\pm} \leq 100$ GeV, where the lower bound is the present e^+e^- collider limit. Since the unHiggs do not acquire vev's, their Yukawa couplings to fermions of all generations cannot be very large.

The supersymmetric mass spectrum is closely associated with the Higgs sector since the gauginos and higgsinos mix to form the physical neutralino and chargino states. The mass matrices (which are analyzed in refs. [4.5, 4.8, 4.9]) are simplified due to our choice of basis for the Higgs fields, where in both the neutralino and chargino cases the first and second generation higgsino sector decouples from the gaugino and third generation higgsino sector. For certain values of the parameters the charginos can be relatively light and it is possible that as many as three charginos can have masses less than $M_Z/2$. The neutralino spectrum is more complicated and model dependent, but two of the neutralinos are expected to have masses determined by M_{Z_2} while the lightest one is a candidate for the LSP (lightest supersymmetric particle). The first and second generation higgsino sector is less well determined as it depends on the superpotential couplings λ_{ij3}, λ_{i3k}, λ_{3jk} where $i, j, k = 1, 2$.

Haber and Sher [4.10] have briefly considered the Higgs sector in the case of effective rank-5 and rank-6 models. In effective rank-5 theories, a rank-6 subgroup of E_6 breaks at some intermediate scale by either $\langle \tilde{\nu}^c \rangle$, $\langle \tilde{S}^c \rangle$, or some linear combination of the two acquiring a vev. If $\langle \tilde{\nu}^c \rangle$ or a combination of $\langle \tilde{\nu}^c \rangle$ and $\langle \tilde{S}^c \rangle$ gets an intermediate scale size vev, the $\lambda_4 H^c H S^c$ term cannot exist in the superpotential since comparable vev's would be generated for H and H^c. The absence of such a term, however, leads to the vanishing of the tree-level pseudoscalar as well as one of the scalar Higgs masses. These masses can then only be non-zero due to small corrections from gaugino loops. If $\langle \tilde{\nu}^c \rangle$ gets an intermediate scale size vev, then model ψ is obtained at low energies. In this case, the bound on the lightest scalar mass is somewhat stronger (due to the change in the couplings of the Higgs fields) in comparison to that found for model η.

In the rank-6 case with two additional U(1) factors, in order to break the electroweak symmetry $\tilde{\nu}^c$ ($\equiv \Phi_4^0$) must acquire a vev which we denote as

$$v_4/\sqrt{2} = \langle \phi_4^0 \rangle = \langle \tilde{\nu}^c \rangle\,. \tag{4.19}$$

If we take these two extra U(1)'s as $U(1)_\psi \times U(1)_\chi$ with an arbitrary angle θ defining the appropriate mixing, the most general scalar potential is given by [4.10]

$$\begin{aligned} V = {} & \mu_1^2 \Phi_1^+ \Phi_1 + \mu_2^2 \Phi_2^+ \Phi_2 + \mu_3^2 \Phi_3^+ \Phi_3 + \mu_4^2 \Phi_4^+ \Phi_4 - i(\lambda A/\sqrt{2})(\Phi_1^+ \tau_2 \Phi_2 \Phi_3 + \text{h.c.}) \\ & + \lambda^2 (\Phi_1^+ \Phi_1 \Phi_2^+ \Phi_2 + \Phi_1^+ \Phi_1 \Phi_3^+ \Phi_3 + \Phi_2^+ \Phi_2 \Phi_3^+ \Phi_3) \\ & + (\tfrac{1}{2} g_L^2 - \lambda^2) |\Phi_1^+ \Phi_2|^2 + \tfrac{1}{8} (g_L^2 + g_Y^2)(\Phi_1^+ \Phi_1 - \Phi_2^+ \Phi_2)^2 \\ & + \tfrac{1}{72} g_1^2 [c_\theta (\Phi_1^+ \Phi_1 + 4\Phi_2^+ \Phi_2 - 5\Phi_3^+ \Phi_3 - 5\Phi_4^+ \Phi_4) - \sqrt{15}\, s_\theta (\Phi_1^+ \Phi_1 - \Phi_3^+ \Phi_3 + \Phi_4^+ \Phi_4)]^2 \\ & + \tfrac{1}{72} g_2^2 [\theta \to \theta + 90°]^2\,, \end{aligned} \tag{4.20}$$

where $s_\theta = \sin\theta$, $c_\theta = \cos\theta$, and $g_{1,2}$ are the gauge couplings of the two U(1) factors. In this case the lightest scalar is found [4.10] to have a mass ≤ 107 GeV assuming $g_1 \simeq g_2 \simeq g_Y$ [for which the angle θ drops out of (4.20)].

Another possible rank-6 group discussed by these authors is the rank-6 left–right symmetric model, $SU(3)_C \times SU(2)_L \times SU(2)_R \times U(1)_L \times U(1)_R$, under which H, H^c form a (2, 2) representation, ν^c is in a (1, 2) representation denoted by

$$\eta = \begin{pmatrix} \tilde{e}_R \\ \tilde{\nu}^c \end{pmatrix} = \begin{pmatrix} \tilde{e}_R \\ \Phi_4 \end{pmatrix}, \tag{4.21}$$

and S^c is a singlet. The most general scalar potential in this case is found to be [4.10]

$$\begin{aligned} V = {} & \mu^2(\Phi_1^+\Phi_1 + \Phi_2^+\Phi_2) + \mu_3^2\Phi_3^+\Phi_3 + \mu_\eta^2\eta^+\eta - i(\lambda A/\sqrt{2})(\Phi_1^+\tau_2\Phi_2\Phi_3 + \text{h.c.}) \\ & + \lambda^2(\Phi_1^+\Phi_1\Phi_2^+\Phi_2 + \Phi_1^+\Phi_1\Phi_3^+\Phi_3 + \Phi_2^+\Phi_2\Phi_3^+\Phi_3) + \tfrac{1}{8}g_{2L}^2(\Phi_1^+\Phi_1 - \Phi_2^+\Phi_2)^2 \\ & + \tfrac{1}{2}(g_{2L}^2 + g_{2R}^2 - \lambda^2)|\Phi_1^+\Phi_2|^2 + \tfrac{1}{8}g_{2R}^2[(\Phi_1^+\Phi_1 - \Phi_2^+\Phi_2 + \eta^+\eta)^2 \\ & + 4\tilde{e}_R^*\tilde{e}_R(\Phi_2^+\Phi_2 - \Phi_1^+\Phi_1) + 4(\tilde{e}_R^*\Phi_4\Phi_1^+\Phi_2 + \text{h.c.})] \\ & + \tfrac{5}{72}g_{1L}^2(\Phi_1^+\Phi_1 + \Phi_2^+\Phi_2 - 2\Phi_3^+\Phi_3 - 2\eta^+\eta)^2 + \tfrac{5}{72}g_{1R}^2(\Phi_1^+\Phi_1 + \Phi_2^+\Phi_2 - 2\Phi_3^+\Phi_3 + \eta^+\eta)^2, \end{aligned} \tag{4.22}$$

where g_{2L}, g_{2R}, g_{1L}, and g_{1R} are the appropriate gauge couplings. If $\tan\beta > 1$ is assumed (in order that the top quark be heavier than the bottom quark), the bound in this case on the lightest scalar is 100 GeV, but increases to 117 GeV if this assumption is relaxed.

4.2. Couplings and decay modes

Here we present the general Higgs boson interaction Lagrangians, as given in ref. [4.2], for the rank-5 model η in the weak eigenstate basis with the Goldstone bosons removed. To transform these couplings to the physical basis, one must produce the mass eigenstates Z_1 and Z_2 via eq. (2.13) and $H^0_{1,2,3}$ via eq. (4.11). In the large v_3 limit, these transformations become quite simple as $Z_1 \to Z$, Z_2 becomes heavy, and the Higgs mixing matrix, U_{ij}, is as given in eq. (4.12), where the neutral doublet members ϕ_1 and ϕ_2 essentially decouple from the singlet ϕ_3. However, terms proportional to $v_3\phi_3$ will give non-negligible interactions with H_1^0 and H_2^0 due to the magnitude of v_3.

The general quark–Higgs Yukawa couplings are given by

$$\begin{aligned} \mathcal{L} = {} & \frac{g_L}{2M_W}\frac{m_u}{\sin\beta}(\bar{u}u\phi_2 - i\bar{u}\gamma_5 u P^0\cos\beta) + \frac{g_L}{2M_W}\frac{m_d}{\cos\beta}(\bar{d}d\phi_1 - i\bar{d}\gamma_5 d P^0\sin\beta) \\ & - \frac{g_L V_{ud}}{2\sqrt{2}M_W}\{H^+\bar{u}[(m_d\tan\beta + m_u\cot\beta) + (m_d\tan\beta - m_u\cot\beta)\gamma_5]d + \text{h.c.}\}, \end{aligned} \tag{4.23}$$

with obvious extensions to the second and third generations and are the same as in the two Higgs doublet SUSY-SM. Here V_{ud} is the appropriate KM matrix element. The corresponding lepton–Higgs Yukawa couplings are given by the above with $d \to e$ and $u \to \nu$. The ϕ_3 coupling to the exotic fermion h is simply

$$\mathscr{L}_{\bar{h}h\phi_3} = (M_h/\sqrt{2}v_3)\bar{h}h\phi_3 \,, \tag{4.24}$$

and the super-partner coupling, $\bar{E}E\phi_3$, is obtained from the above with $h \to E$. Notice that the exotic–Higgs coupling is inversely proportional to v_3, and hence will be weak in strength unless the Z′ is relatively light.

The three-boson interaction Lagrangian is

$$\begin{aligned}
\mathscr{L} = {} & \tfrac{1}{2}\cos\beta\; g_Z M_Z (ZZ + \tfrac{2}{3}\sqrt{x_w}ZZ' + \tfrac{1}{9}x_w Z'Z')\phi_1 \\
& + \tfrac{1}{2}\sin\beta\; g_Z M_Z (ZZ - \tfrac{8}{3}\sqrt{x_w}\,ZZ' + \tfrac{16}{9}x_w Z'Z')\phi_2 \\
& + (25x_w v_3/18v) g_Z M_Z Z'Z'\phi_3 + g_L M_W W^+W^-(\phi_1\cos\beta + \phi_2\sin\beta) \\
& + \tfrac{5}{3}x_w \sin\beta\cos\beta\; g_Z M_Z Z'(W^+H^- + W^-H^+) \\
& + \mathrm{i}[eA + \tfrac{1}{2}(1-2x_w)g_Z Z + \tfrac{1}{6}\sqrt{x_w}(4\cos^2\beta - \sin^2\beta)g_Z Z'](H^- \overleftrightarrow{\partial} H^+) \\
& + \tfrac{1}{2}\mathrm{i}\sin\beta\; g_L[W^+(\phi_1 \overleftrightarrow{\partial} H^-) - W^-(\phi_1 \overleftrightarrow{\partial} H^+)] - \tfrac{1}{2}\mathrm{i}\cos\beta\; g_L[W^+(\phi_2 \overleftrightarrow{\partial} H^-) - W^-(\phi_2 \overleftrightarrow{\partial} H^+)] \\
& + \tfrac{1}{2}(v_3 v/N) g_L[W^+(P^0 \overleftrightarrow{\partial} H^-) + W^-(P^0 \overleftrightarrow{\partial} H^+)] + (v_3 v/N)\sin\beta\; g_Z(\tfrac{1}{2}Z + \tfrac{1}{6}\sqrt{x_w}\,Z')(\phi_1 \overleftrightarrow{\partial} P^0) \\
& - (v_3 v/N)\cos\beta\; g_Z(\tfrac{1}{2}Z - \tfrac{2}{3}\sqrt{x_w}Z')(\phi_2 \overleftrightarrow{\partial} P^0) - \tfrac{5}{6}\sqrt{x_w}(v^2/N)\sin\beta\cos\beta\; g_Z Z'(\phi_3 \overleftrightarrow{\partial} P^0) \,,
\end{aligned} \tag{4.25}$$

where we define

$$N^2 = v_3^2 v^2 + v_1^2 v_2^2 \,, \qquad g_Z^2 = g_L^2 + g_Y^2 = e^2/x_w(1-x_w) \,. \tag{4.26}$$

The four-boson quartic couplings are given by

$$\begin{aligned}
\mathscr{L} = {} & \sin^2\beta\,[\tfrac{1}{2}g_Z(1-2x_w)Z - \tfrac{1}{6}\sqrt{x_w}\; g_Z Z' + eA]^2 H^+H^- \\
& + \cos^2\beta\,[\tfrac{1}{2}g_Z(1-2x_w)Z + \tfrac{2}{3}\sqrt{x_w}\; g_Z Z' + eA]^2 H^+H^- \\
& + \tfrac{1}{2}g_L^2 W^+W^-H^+H^- + \tfrac{1}{4}g_L^2 W^+W^-[\phi_1\phi_1 + \phi_2\phi_2 + (v^2v_3^2/N^2)P^0P^0] \\
& + \tfrac{1}{8}g_Z^2(ZZ + \tfrac{2}{3}\sqrt{x_w}\,ZZ' + \tfrac{1}{9}x_w Z'Z')[\phi_1\phi_1 + \sin^2\beta\,(v^2v_3^2/N^2)P^0P^0] \\
& + \tfrac{1}{8}g_Z^2(ZZ - \tfrac{8}{3}\sqrt{x_w}\,ZZ' + \tfrac{16}{9}x_w Z'Z')[\phi_2\phi_2 + \cos^2\beta\,(v^2v_3^2/N^2)P^0P^0] \\
& + \tfrac{25}{72}x_w g_Z^2 Z'Z'[\phi_3\phi_3 + \sin^2\beta\cos^2\beta\,(v^4/N^2)P^0P^0] \\
& - \tfrac{1}{2}\sin\beta\; g_L(eA - x_w g_Z Z - \tfrac{1}{3}\sqrt{x_w}\; g_Z Z')(W^+H^- + W^-H^+)\phi_1 \\
& + \tfrac{1}{2}\cos\beta\; g_L(eA - x_w g_Z Z + \tfrac{4}{3}\sqrt{x_w}\; g_Z Z')(W^+H^- + W^-H^+)\phi_2 \\
& - \tfrac{1}{2}\mathrm{i}(v_3 v/N) g_L(eA - x_w g_Z Z)P^0(W^+H^- + W^-H^+) \\
& + \tfrac{1}{6}\mathrm{i}\sqrt{x_w}(v_3 v/N)(4\cos^2\beta - \sin^2\beta) g_L g_Z Z' P^0(W^+H^- + W^-H^+) \,.
\end{aligned} \tag{4.27}$$

While the couplings of Higgs bosons to a fermion ($Hf\bar{f}'$) and gauge boson (HVV') pair are expected to dominate in their production, other coupling may be as important in studying their decay signatures. Among these which produce two-body final states are (i) $HH'V$, (ii) $HH'H''$, and (iii) $H\chi\chi'$, where χ is a neutralino or a chargino. These have been discussed by a number of authors [4.2, 4.9, 4.16]. Couplings of type (i) can be read off from eq. (4.25), while types (ii) and (iii) are listed in the above references. Here we will make a few comments about each of these couplings in turn.

$HH'V$. Due to the existence of longitudinal V polarization states, the VH final states, ZP^0 and W^-H^+, are found to be important in the decay of H_3^0 if it is heavy, but these modes are not kinematically allowed for the case of either H_1^0 or H_2^0. Due to longitudinal Z' modes and the large coupling, the $P^0 \to Z'H_1$ decay is found to be important for large M_{P^0}. The H^+ modes $W^+H_1^0$ and $W^+H_3^0$ are coupling suppressed and since the W^+Z' channel has a large coupling strength, these modes will be difficult to observe. $H^+ \to W^+H_2^0$, W^+P^0 are absent due to the near degeneracy of H^+, H_2^0, and P^0 in the large v_3 limit. Note that $Z' \to HH'$ may in general be large.

$HH'H''$. $H_3^0 \to HH$ modes are potentially large leading to the possibility that HH final states dominate H_3^0 decay, with the $2H_1^0$ channel being strongest for large M_3. For smaller M_3 values, almost all modes are comparable with H^+H^- being slightly dominant. If level crossing has occurred and M_2 is large ($\sim M_{P^0}$) the allowed $2H_1^0$ and $2H_3^0$ are suppressed by small couplings but $2H_1^0$ becomes significant if P^0 is light. If P^0 is light, the $H_1^0 \to 2P^0$ decay channel is expected to dominate conventional fermion decays except close to threshold as shown in fig. 96 from ref. [4.2].

$H\chi\chi'$. An analysis of the parameter space indicates that relatively few of these couplings are important for Higgs decay. However, for any particular Higgs there will always be one (or more) neutralino or chargino decay mode(s) which has a substantial coupling and can potentially dominate for the case where the Higgs is heavy. This is particularly stressed by the authors of ref. [4.16].

As can be seen from the above discussion, the rather large number of parameters in the Higgs sector of E_6 superstring-inspired rank-5 models makes it quite difficult to fully analyze all the possible Higgs decay signatures. Gunion et al. [4.9] have examined all of these possible decay modes for a single, yet hopefully representative, choice of model parameters: $M_{Z_2} = 0.6$ TeV, $m_t = 70$ GeV, $M_h = 250$ GeV

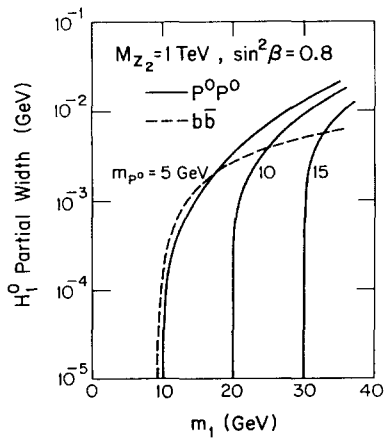

Fig. 96. Partial width for H_1^0 as a function of M_1 for several values of the P^0 mass with $\tan\beta = 2$ and a Z_2 mass of 1 TeV. The curves for the $2P^0$ final state cut off below $M_1 = 40$ GeV since larger M_1 values are not allowed for the chosen value of M_{P^0}. Note that the $q\bar{q}$ pair decay curves are relatively insensitive to M_{P^0}.

(where h is the third generation exotic with the others assumed to be light), and a gluino mass $m_{\tilde{g}} = 0.5$ TeV, which determines the mass of the neutralinos and charginos. Note that in this scenario, the squark and slepton masses are larger than the gluino mass and will probably not be important SUSY decay modes. $\lambda > 0$ and $\tan\beta = 1.1$ will also be assumed.

Some general comments are in order. Whenever a Higgs has an available VV′ (V, V′ = Z or W) channel the relevant coupling is small with the V = Z′ modes being further suppressed (only $H^{\pm}$, P^0, and H_2^0 possess such modes). Since H decays to longitudinal gauge bosons are responsible for their large widths, the Higgs in this model are generally quite narrow in comparison to the SM. In fact, for the above parameter choices, H_1^0 is always quite narrow, whereas, for $M_{P^0} = 3$ TeV, P^0, $H^{\pm}$, and H_2^0 have $\Gamma \lesssim 100$ GeV and H_3^0 has $\Gamma \lesssim 15$ GeV. Thus over most of the M_{P^0} parameter space non-SM decay channels are generally found to dominate the various H final states. H_1^0 still has many modes which are similar to those of the SM Higgs.

For the above set of parameters, the prospect for Higgs decay and detection are now summarized.

H_1^0 decay. H_1^0 will decay predominantly to light SM fermions until M_{P^0} values $\gtrsim 3$ TeV are reached, when it becomes massive enough to have $t\bar{t}$, W^+W^-, and 2Z modes as well. If neutralinos/charginos (χ) are light, then $\chi\chi$ final states will also be important if M_1 is sufficiently large.

H_3^0 decay. The situation for H_3^0 decays is quite complicated. For large values of M_{P^0}, the $\chi\chi$ modes are small, but VV (W^+W^- and 2Z channels occur with the ratio 2 : 1) and HH (completely $2H_1^0$ once M_{P^0} is amply large) may or may not dominate but for large M_1 values the $h\bar{h}$ modes (with their distinctive decay signature) dominate instead. If M_{P^0} is smaller, although VV, HH, and $h\bar{h}$ modes are still important, other channels can be significant, including $\chi\chi$, ZP^0, with $W^{\pm}H^{\mp}$ (the latter two in the ratio 1 : 2). If M_3 is too small, many of these modes may not be allowed kinematically, e.g., the $h\bar{h}$ and $\chi\chi$ final states. In general, however, H_3^0 may be difficult to find due to its small production cross sections, which will be discussed below.

P^0 decay. Except when M_{P^0} is small, $\chi\chi$ modes tend to be important. For larger M_{P^0}, in addition to $\chi\chi$ decays, $t\bar{t}$ and other SM channels can also be significant, but fade in importance when very large P^0 mass values are reached, where $\chi\chi$ again dominates. For low M_{P^0} values, the ZH_1^0 channel can also be important but only for a narrow mass region. $Z'H_1^0$ rates become significant for larger P^0 mass values. If $\chi\chi$ modes dominate, then P^0 should be observable at the SSC for $M_{P^0} \lesssim 0.5$ TeV. The $\gamma\gamma$ channel is relevant at small P^0 masses when SM final states dominate. Due to its tiny couplings, the P^0 will probably not be observable at e^+e^- colliders.

H_2^0 decay. H_2^0 is somewhat similar to P^0 in that $\chi\chi$ modes tend to dominate for most M_{P^0} values, even for small M_{P^0} for which $\chi^0\chi^0$ final states can be very important. For larger M_2 values, in addition to $\chi\chi$, the ZZ′ is also significant and can be of order ~30% of the total width for $M_3 \sim 3$ TeV. For small M_{P^0}, $t\bar{t}$ and $2H_1^0$ states can be important with the latter dominating for $M_2 < 2m_t$. VH modes are either coupling or phase space suppressed. gg fusion allows for H_2^0 detection at the SSC out to $M_2 \simeq 0.5$ TeV using the $\chi\chi$ decay signature. The $\gamma\gamma$ channel is important for small M_2 where SM fermion final states are dominant.

$H^{\pm}$ decay. For low values of M_{H^+} the $t\bar{b}$ final state is clearly dominant, making $H^{\pm}$ detection difficult except at e^+e^- colliders. For $M_{H^+} \gtrsim 0.3$ TeV, the $\chi^+\chi^0$ modes can be ~50% of the total width and may allow for its detection at the SSC as well as a TeV e^+e^- collider. For larger masses, the $Z'W^+$ channel becomes increasingly important and provides a clean signature at a hadron collider if W or Z′ decays leptonically (but with a low event rate). Overall detection of H^+H^- production in e^+e^- machines is only phase space limited, whereas the $g\bar{b} \to H^+\bar{t}$ process provides a significant event rate for only a modest range of charged Higgs masses.

From the above discussion it is clearly obvious that the resulting final states in Higgs decay are very complex and backgrounds will need to be carefully explored. This task will be difficult and will require detailed Monte Carlo simulations.

4.3. Signals for new Higgs bosons

Here we concentrate on the production mechanisms and signals for the Higgs sector which are unique to E_6 theories and which are not contained in the SM or SUSY-SM. SM and SUSY-SM Higgs production modes and signatures are reviewed elsewhere [4.17].

4.3.1. Production mechanisms

4.3.1.1. e^+e^- colliders. The dominant production mechanism in e^+e^- annihilation for the SM Higgs (allowing for the possibility of more than one neutral gauge boson) is $e^+e^- \to Z_i \to Z_1 H^0$, where the final state Z_1 is either virtual (setting a Higgs search limit of 40 GeV at LEP I [4.18]) or real (with a discovery limit up to 90 GeV at LEP II [4.18]) depending on the kinematics. In E_6 theories for the case of $\lambda A \geq v$, the interactions of H_1^0 are approximately the same as for the SM Higgs (since $\alpha \simeq \beta$) and this reaction will proceed at the SM rate with large cross sections at LEP I and II. The rest of the Higgs spectrum is likely to be too heavy to be produced by real Z_1 decay or with a real Z_1 at LEP. E_6 Higgs production at higher energy e^+e^- colliders has not been examined.

The case where $\lambda A \ll v$ is more interesting and yields many deviations from SM Higgs production. The rates for $e^+e^- \to f\bar{f}H_1^0$, $Z_1H_1^0$ are less than their SM predictions since the $Z_1Z_1H_1^0$ coupling is proportional to $\cos(\alpha - \beta)$. This can be seen in fig. 97 from ref. [4.2], which compares the branching fractions for $Z_1 \to H_1^0 e^+e^-$ (as well as for $W \to H_1^0 e\nu$) in this model, assuming a 1 TeV Z_2 and $\sin^2\beta = 0.8$, to their SM values. These weaker couplings could reduce the discovery limit for H_1^0 to 30 GeV or less at LEP I. The modes $Z_1 \to W^{\pm}H^{\mp}$ and $W^{\pm} \to Z_1H^{\pm}$ with one of the final state particles being off-shell proceed via Z–Z′ mixing and hence have suppressed rates. If the value of α is such that the $Z_1Z_1H_1^0$ coupling strength is very weak, the channel $Z_1 \to P^0H_1^0$ will open up, where the branching fraction is found [4.2] to have possible values of order a few percent. If the charged Higgs is light

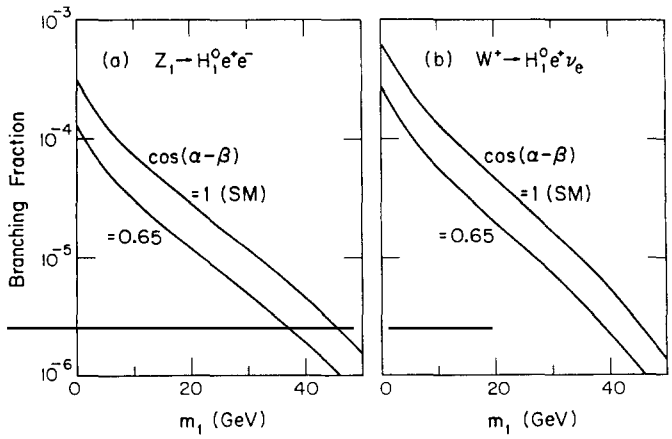

Fig. 97. Branching fraction for (a) $Z \to H_1^0 e^+e^-$ and (b) $W^+ \to H_1^0 e^+ \nu_e$ versus the H_1^0 mass (M_1) for $M_{Z'} = 1$ TeV and $\sin^2\beta = 0.8$ in two cases, for a large P^0 mass with $\cos(\alpha - \beta) = 1$, and for $20 < M_{P^0} < 35$ GeV with $\cos(\alpha - \beta) = 0.65$.

enough, the decays $W^{\pm} \to H^{\pm} H_1^0$, $H^{\pm} P^0$ will proceed at roughly the same rate as $Z_1 \to P^0 H_1^0$. Above the Z_1 resonance at LEP II, a real Z_1 may be produced with H_1^0 with event rates that are lower than those expected in the SM. The cross section is found [4.2] to be of order $\sigma \sim 0.5$–1.2 pb at $\sqrt{s} = 200$ GeV for $\sin^2\beta = 0.8$. The new modes $e^+e^- \to P^0 H_1^0$, $P^0 H_2^0$ are also possible, if kinematically allowed, with production cross sections of order 0.1–0.3 pb at LEP II. H^+H^- production is independent of the angles α and β, and in the limit of a large Z_2 mass the cross section is $\sigma \simeq 1$ pb for $M_{H^+} \leq 80$ GeV at $\sqrt{s} = 200$ GeV.

The reaction $e^+e^- \to Z_2 \to Z_1 H_1^0$ will proceed with large rates on resonance. Nandi [4.19] finds that the ratio of resonance production to the point cross section is

$$\sigma_{\text{res}}/\sigma_{\text{pt}} \simeq 10\text{–}230\,, \tag{4.28}$$

for $\sqrt{s} = 200$ GeV. Hence, if the Z_2 exists within the reach of LEP II, this process could be the dominant source of H_1^0 production, depending on the value of β. The Z_2 may also be virtually produced in association with H_1^0 via $e^+e^- \to Z_2 \to Z_2^* H_1^0 \to \ell^+\ell^- H_1^0$ as discussed in ref. [4.14].

4.3.1.2. Hadron colliders: gluon fusion. The gluon fusion mechanism via a heavy quark triangle diagram is the dominant SM Higgs production mode at hadron colliders for a low mass Higgs ($M \lesssim 400$–500 GeV) [3.27]. Since the quark–anti-quark couplings to H_1^0, H_2^0, and P^0 are essentially of SM strength, as seen in eq. (4.22) (apart from the parameters $\tan\beta$ and the mixing angle α), the gluon fusion mechanism for these Higgs bosons will proceed at roughly the same rate as for the SM Higgs. Since H_1^0 is constrained to have a mass $\lesssim 170$ GeV this mechanism will be its dominant production mode. For the case of the mostly iso-singlet Higgs, H_3^0, the largest cross section occurs when the exotic fermion h is present in the loop. Since there are (at least) three generations of h's with a large mass, one would expect a substantial cross section. However, the $h\bar{h}\phi_3$ coupling is inversely proportional to v_3, and its strength will be much weaker than the SM Higgs–top-quark coupling unless the Z′ is reasonably light. Hence the H_3^0 gluon fusion cross section will not be significant unless Z′ and h have favorable masses. As in the case of the SM, the decay $H_3^0 \to Z'Z' \to \ell^+\ell^-\ell'^+\ell'^-$ will give the best signal above numerous backgrounds.

The charged Higgs is produced via the parton level process $g\bar{b} \to \bar{t}H^+$ with a sizeable cross section (~ 1 pb at the SSC for $M_{H^+} \sim 1$ TeV) and has been studied [4.20] within the context of the SUSY-SM. Reasonable cross sections ($\sigma \sim 0.1$–1 pb) are also obtainable [4.21] for various values of the parameters from the subprocesses $t\bar{t}(b\bar{b}) \to W^{\pm}H^{\mp}$ and $gg \to W^{\pm}H^{\mp}$ which proceeds via a box and triangle diagrams with top and bottom quarks in the loops.

4.3.1.3. Hadron colliders: gauge boson fusion. Gauge boson fusion [3.27, 4.22], which dominates over the gluon fusion mechanism for SM Higgs production for the mass range $M_H \gtrsim 300$–500 GeV, could be of diminished importance in E_6 theories. As seen in eq. (4.25), the H_1^0 couplings to ZZ and WW are of essentially SM strength (in the limit of $\lambda A \geq v$, such that the ϕ_1 and ϕ_2 mixing angle α is of magnitude $\alpha \simeq \beta$), thus yielding ZZ and WW fusion production rates which are comparable to those found in the SM. However, since the H_1^0 is constrained to have a mass $\lesssim 170$ GeV, gauge boson fusion will most likely give insignificant contributions to its production (depending of the value of the top quark mass). In this same limit where $\alpha \simeq \beta$, the H_2^0ZZ and H_2^0WW couplings tend to zero, such that H_2^0 production via gauge boson fusion is expected to be negligible unless this limit does not apply and both

Z′ and P^0 are light. The WW and ZZ fusion cross sections for H_3^0 are also unimportant in the large v_3 limit due to the small mixing between ϕ_3 and ϕ_1, ϕ_2. Despite the fact that the $H_3^0Z'Z'$ coupling is enhanced by a factor of $\sim M_{Z'}$, the contributions to H_3^0 production from virtual Z′Z′ fusion will be suppressed by a factor of $(1/M_{Z'})^2$ due to the small Z′ content of quark. ZZ′ fusion processes suffer a similar fate resulting from weaker couplings and reduced quark structure functions. The pseudoscalar Higgs, P^0, does not couple to gauge boson pairs at the tree level, so these production mechanisms will not be relevant for the P^0. The $W^{\pm}H^{\mp}Z_i$ vertex will be discussed later. So we see that gauge boson fusion yields only relatively unimportant production rates for E_6 bosons, as advertised.

4.3.1.4. Hadron colliders: Z_2 decays. Z_2 decays can yield a copious source of E_6 Higgs bosons at hadron colliders. As discussed in section 2.4 the decays $Z_2 \to Z_1H_1^0$, $Z_1H_2^0$, $P^0H_1^0$, $P^0H_2^0$, H^+H^-, $W^{\pm}H^{\mp}$ can occur with reasonable rates (their total contribution is of order of a few percent of the total ordinary fermionic width). These partial widths are calculated via eq. (2.37) and their branching fractions are shown in fig. 10 as a function of β in the rank-5 model for large M_2 with $n_g = 0$ (where n_g is the number of generations of exotic fermions which are kinematically accessible in Z_2 decays). As can be seen from the figure, these branching fractions can vary substantially (especially if one allows for the possibility of Z_2 decay into SUSY particles or the exotic fermions) and can thus introduce large uncertainties in the cross section for Higgs production. Given the possible mass spectrum, one would expect that the $Z_1H_1^0$ channel would be the most favored by phase space, and Baer et al. [4.16] have thoroughly studied this mode for the SSC. The total production cross section for $pp \to Z_2 \to Z_1H_1^0$ at $\sqrt{s} = 40$ TeV as a function of M_2 (neglecting Z–Z′ mixing as well as SUSY and exotic decays) is presented in fig. 98 from this reference for several values of tan β and M_{H^0}. The cross section is fairly insensitive to the value of M_{H^0}, but is quite sensitive to the assumed value of tan β. The event rate is seen to be quite large with as many as 10^{4-5} $Z_1H_1^0$ pairs being produced per SSC year. Also shown in the figure for comparison, is the cross section when the Z_2 is also allowed to decay into the full spectrum of

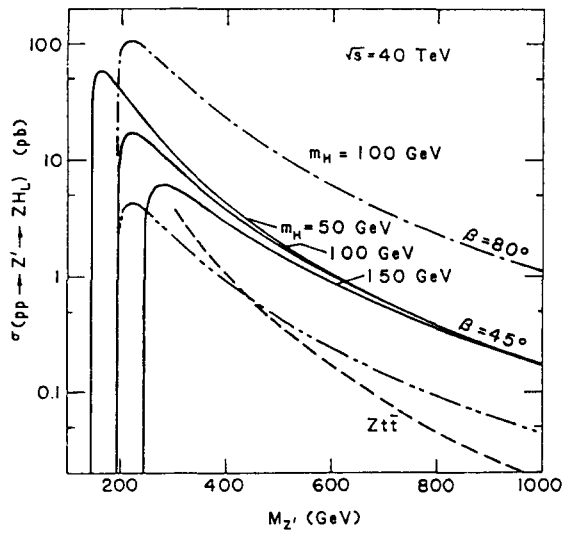

Fig. 98. Total cross section for $pp \to Z' \to ZH_1^0$ (H_1^0 is denoted as H_L in the figure) at the SSC as a function of $M_{Z'}$ for model η. In all but the lowest dashed–double dotted curve the exotic Z′ decays are forbidden. The SM background $Zt\bar{t}$ production is shown by the dashed curve.

exotic fermions (which results in a decrease of the production rate by a factor of ~4), and the cross section for the SM $Z_1 t\bar{t}$ background, where an invariant mass cut of $M_{t\bar{t}} = 100 \pm 15$ GeV has been imposed. Note that the background is smaller than the signal for all of the cases shown. The large event rate for this process allows the use of the decay $Z_1 \to \ell^+\ell^-$ as a trigger and these authors find that $t\bar{t}$ and SUSY H_1^0 decay channels provide a clean signal to background ratio for a wide range of parameters. For Z_2 masses in excess of ~1 TeV this production mechanism becomes of decreasing importance.

In summary, E_6 Higgs boson production rates at hadron colliders are quite dependent on the mass spectrum. Lower mass Higgs have the highest event rates via the gluon fusion mechanism or Z_2 decays. Higher mass Higgs will be produced via gauge boson fusion with event rates which are smaller than those expected from this process in the SM. Unfortunately, the H_3^0 will be difficult to produce, no matter what its mass may be.

4.3.1.5. Toponium decays. Toponium has several possible Higgs decay channels and may provide an abundant source of Higgs bosons. These decay modes, most of which do not exist in the SM, are all present in the two Higgs doublet SUSY-SM and have been discussed elsewhere [4.17, 4.23], and will only be briefly examined here. Since the Higgs couplings are slightly different in E_6 models than in the SUSY-SM, the resulting branching fractions for these decay channels will be somewhat altered from their SUSY predictions. The possible vector (V_t) and pseudoscalar (η_t) toponium Higgs decay modes and their corresponding allowed intermediate state particles are listed in table 5 from ref. [4.2], where Z_2 is assumed to be relatively heavy. Processes with a photon, Z_1, or P^0 intermediate states are *s*-channel, while quark intermediate states are *t*- and/or *u*-channel. We remind the reader that the $^3S_1$ vector states (V_t) are produced copiously at e^+e^- colliders, whereas the $^3S_0$ pseudoscalar states (η_t) have the largest production rates at hadron colliders.

The Wilczek mechanism [4.23], $V_t \to H_i^0\gamma$, proceeds with a rate of (in the large Z_2 mass limit)

$$\Gamma(V_t \to H_1^0\gamma)/\Gamma(V_t \to H^0\gamma)_{SM} = \sin^2\alpha/\sin^2\beta\,, \qquad \Gamma(V_t \to H_2^0\gamma)/\Gamma(V_t \to H^0\gamma)_{SM} = \cos^2\alpha/\sin^2\beta\,, \tag{4.29}$$

if $V_t \to H_2^0\gamma$ is not phase space suppressed. Similarly, the $P^0\gamma$ rate is given by (neglecting QCD corrections)

$$\Gamma(V_t \to P^0\gamma)/\Gamma(V_t \to H^0\gamma)_{SM} = \cot^2\beta\,. \tag{4.30}$$

Table 5
Summary of the various vector and pseudoscalar toponium Higgs decay modes and the allowed intermediate particles

Final state	V_t	η_t
$H^0\gamma$	t	–
$P^0\gamma$	t	–
H^0Z_1	t, Z_1	Z_1, P^0
P^0Z_1	t	–
H^0P^0	Z_1	t, Z_1, P^0
H^+H^-	b, γ, Z_1	–
W^+H^-	b, Z_1	b, Z_1, P^0

It is found that these rates can be slightly more or slightly less than the SM value depending on the choice of parameters, with the ratios being of order unity when the H_i^0 and P^0 masses are close to their lower bounds [4.2, 4.5]. If the decay channels $H_1^0 Z_1$ and $P^0 Z_1$ are allowed by phase space, their rates may be up to an order of magnitude larger than the corresponding SM prediction for certain choices of the parameters. $\Gamma(V_t \to H_1^0 P^0)$ is proportional to $\sin^2(\alpha - \beta)$ and hence will be suppressed if $\alpha \sim \beta$, but the branching fraction for this process can reach a few percent for some values of α and β. The H^+H^- decay mode has a small branching fraction which is of order 10^{-4}–10^{-3}, and the $W^{\pm}H^{\mp}$ channel is suppressed by a factor of m_b/m_t for the quark intermediate states or by the small Z–Z′ mixing for the s-channel Z_1 exchange. If kinematically allowed, the single quark decay $t \to H^+ b$ will be the dominant toponium decay mode. The general expressions, including QCD corrections, for these toponium decay modes may be found in ref. [4.2].

4.3.1.6. Flavor changing couplings. If the exotic fermions have the same B and L assignments as do the ordinary fermions, then ordinary–exotic mixing can result in flavor-changing couplings to the neutral scalars. We can generically parameterize these couplings as

$$\mathscr{L} = (\sqrt{2} G_F)^{1/2} [M_h \bar{h}(a_h^i + b_h^i \gamma_5) d + M_E \bar{E}(a_E^i + b_E^i \gamma_5) e] H_1^0 , \tag{4.31}$$

with a and b being coupling matrices and $M_{h,E}$ being typical exotic fermion masses. In order to insure hermiticity, a must be hermitian while b must be anti-hermitian. The couplings in $\mathscr{L}$ allow for the pair production of neutral Higgs scalars at both e^+e^- and hadron colliders via $e^+e^- \to 2H_i^0$ or $d\bar{d} \to 2H_i^0$, with a t- and u-channel exotic fermion exchange. The cross section [4.24, 4.25] for either process (at the parton level in the hadronic case) is ($z = \cos\theta$)

$$\begin{aligned} d\sigma/dz = {} & (G_F^2 M^4/256\pi N_c)\beta s (D_1^{-1} + D_2^{-1})^2 \\ & \times \{\beta^2 [(|a|^2 + |b|^2)^2 + (2 \operatorname{Re} a^* b)^2](1 - z^2) + (4M^2/s)(|a|^2 - |b|^2)^2\} , \end{aligned} \tag{4.32}$$

where N_c is a color factor (= 1 for e^+e^- or 3 for $d\bar{d}$), M is the exotic fermion mass, $\beta = (1 - 4M_{H^0}^2/s)^{1/2}$ where M_{H^0} is the Higgs mass, θ is the center-of-mass scattering angle, a and b are the appropriate elements of the coupling matrices, and

$$D_{1,2} = (M_{H^0}^2 - M^2) - \tfrac{1}{2} s(1 \mp \beta z) . \tag{4.33}$$

For the parton case $s \to \hat{s}$. The total cross section for e^+e^- annihilation is obtained by a simple angular integration of (4.32), while at hadron colliders integration over z, rapidity, and the $2H_i^0$ invariant mass is required. Note that for fixed M_{H^0}, the second term in (4.32) dominates if $|a| \neq |b|$; for simplicity we will assume that a and b are relatively real.

The results of these calculations for e^+e^- at LEP energies are summarized by fig. 99, where an overall factor of $|a|^4$ has been removed from $d\sigma/dz$, and from which one can draw several conclusions: (i) When $|a| = |b|$, corresponding to chiral couplings, the cross section is relatively small, grows very slowly with increasing M_E for fixed M_{H^0}, and vanishes as $z \to 1$. Clearly, in the limit of small ordinary–exotic mixing (e.g., $|a|^4 \sim 10^{-3}$), which we would naively expect to hold, tiny cross sections are obtained. (ii) For $|a| \neq |b|$, the dominance of the second term in (4.32) is clearly visible and results in a flat angular distribution and produces a strong sensitivity to the value of M_E. For example, with

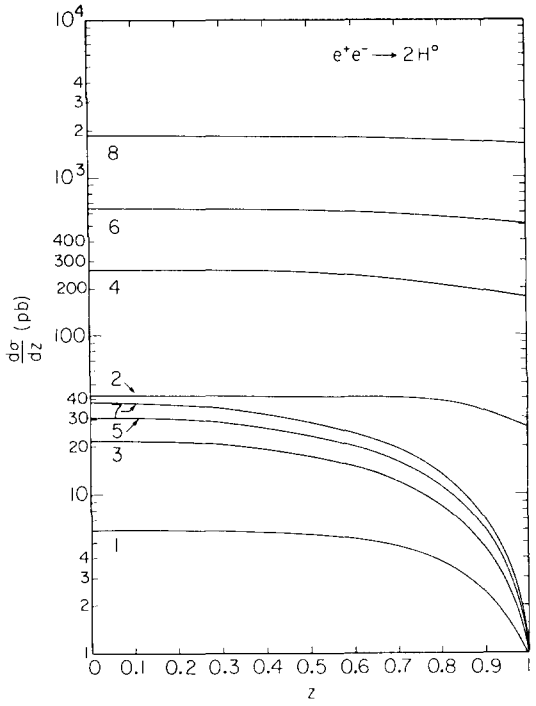

Fig. 99. Differential cross section for $e^+e^- \to 2H^0$ with various values of M_E and $|b/a|$: (1) $M_E = 100$ GeV, $|b/a| = 1$; (2) $M_E = 100$ GeV, $|b/a| = 2$; (3) and (4) are the same as (1) and (2), but with $M_E = 200$ GeV; (5) and (6) are the same as (1) and (2) but with $M_E = 300$ GeV; (7) and (8) are the same as (1) and (2) but with $M_E = 500$ GeV.

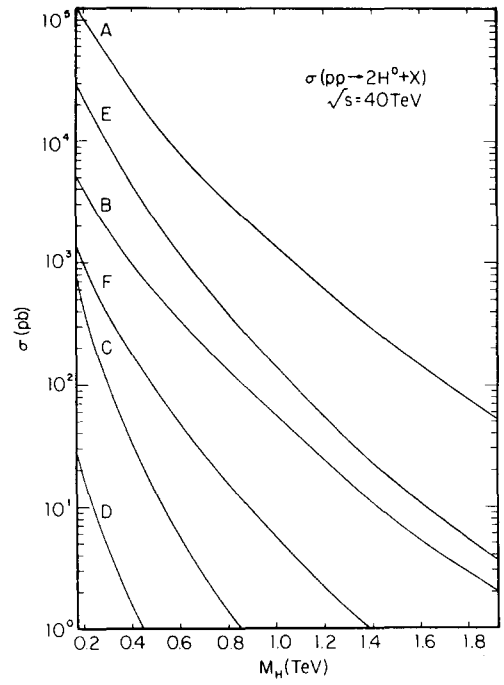

Fig. 100. Total cross section for $pp \to 2H^0 + X$ at SSC energies as a function of the Higgs mass M_H: (A) $M_h = 1$ TeV, $r \equiv |b/a| = 2$; (B) $M_h = 1$ TeV, $r = 0$; (C) $M_h = 0.2$ TeV, $r = 2$; (D) $M_h = 0.2$ TeV, $r = 0$; (E) $M_h = 0.6$ TeV, $r = 2$; and (F) $M_h = 0.6$ TeV, $r = 0$.

$M_{H^0} = 60$ GeV, $M_E = 500$ GeV, and assuming an integrated luminosity of 200 pb^{-1}, $7.2 \times 10^5 |a|^4$ events are expected for $r \equiv |b/a| = 2$. Since the process $e^+e^- \to 2H_i^0$, when enhanced, is fairly isotropic and H^0 prefers to decay into heavy particles, it should be relatively easy to separate $2H_i^0$ production from W^+W^- and $2Z^0$ production.

For heavy $2H_i^0$ production at the SSC, fig. 100 clearly summarizes the situation, where again, an overall factor of $|a|^4$ has been removed from σ. For purposes of comparison, the SM prediction for Higgs pair production from W^+W^- and ZZ fusion with $\sqrt{s} = 40$ TeV and $M_{H^0} = 1$ TeV is in the range of $\sim 5 \times 10^{-4}$ pb [4.26]. Thus for reasonable values of the parameters, $|a| \sim |b| \sim 0.1$, there is a significant enhancement over the SM expectation.

4.3.2. *Indirect signatures*

If the exotic h fermions have the B and L assignments of conventional quarks, then there will in general be an off-diagonal coupling to a neutral scalar field (ϕ) of the form [4.27]

$$\mathcal{L}_{\text{int}} = (g_1 \bar{d} h_1 + g_2 \bar{s} h_2)\phi + \text{h.c.}\,, \tag{4.34}$$

where $h_{1,2}$ are not mass eigenstates, and the subscripts 1 and 2 are a generation index. Such an

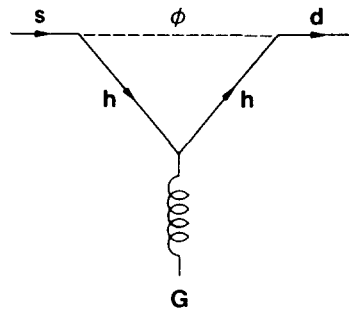

Fig. 101. The s→dg vertex arising from the exchange of a flavor changing neutral scalar φ.

interaction may lead to an enhancement of the $\Delta I = \frac{1}{2}$ amplitude via the penguin-type diagram shown in fig. 101 from ref. [4.27]. $\Delta I = \frac{1}{2}$ amplitudes larger than those from the SM are easily obtainable for a wide range of parameter values, while the ε'/ε ratio is not significantly increased. The above interaction can also contribute to the K_L–K_S mass difference via the box diagrams in fig. 102 and values of the parameters can be found such that this contribution remains small even when the $\Delta I = \frac{1}{2}$ amplitude is enhanced.

These off-diagonal couplings of the fermions to the neutral scalars cannot, of course, be totally arbitrary and mixing must be somewhat suppressed. One constraint, for example, comes from the scalar contributions to the anomalous magnetic moments [3.2] of e and μ given by [3.44]

$$a_{e,\mu} = \frac{m^2}{8\pi^2}\sqrt{2}G_F M^2 \int_0^1 dx \, \frac{(M/m)(|a|^2 - |b|^2)x + x^2(1-x)(|a|^2 + |b|^2)}{M^2 x + M_H^2(1-x)}, \tag{4.35}$$

with m being the e or μ mass and M the corresponding exotic fermion mass. One again sees the very strong M dependence, especially in the non-chiral case $|a| \neq |b|$. Bounds on $|a|$ and $|b|$ from (4.35) have been discussed in the literature [3.2].

4.3.3. *The WHZ vertex*

There are many extensions of the SM in which the Higgs sector is enlarged to include two (or more) scalar doublets for a variety of reasons. Although all such models lead to the existence of physical charged Higgs bosons it has been shown that the tree level $W^{\pm}H^{\mp}Z$ coupling vanishes even if there are an arbitrary number of Higgs doublets and singlets [4.28]. This result is due to the fact that the neutral members of these doublets (which can obtain vev's and contribute to gauge boson masses) have the

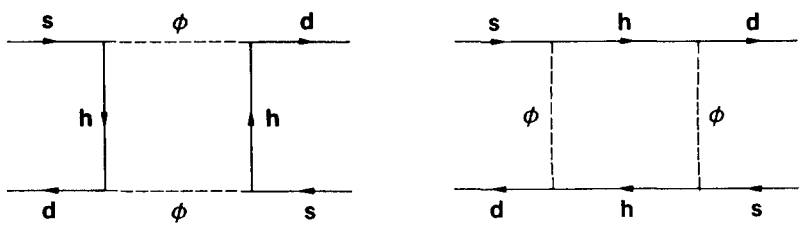

Fig. 102. Box diagram contribution due to φ exchange for the K_L–K_S mass difference.

same isospin, and therefore couple to the W and Z in an identical manner. E_6 models offer a way around this apparently general result by the introduction of a new Z′ gauge boson which couples differently to the various scalar doublets and results in a $W^{\pm}H^{\mp}Z'$ coupling. Once the Z and the Z′ mix to form physical eigenstates, the $W^{\pm}H^{\mp}Z'$ coupling becomes $W^{\pm}H^{\mp}(Z_2\cos\phi + Z_1\sin\phi)$, so that $W^{\pm}H^{\mp}$ now couples to the lighter neutral gauge boson which is a mass eigenstate. Thus, in a model with only doublet and singlet scalars, a coupling of $W^{\pm}H^{\mp}$ to the Z_1 implies the existence of a new and heavier neutral gauge boson, Z_2. In particular, one finds

$$\mathscr{L}_{WHZ} = 2eM_Z \sin\beta\cos\beta\,(Y_1' + Y_2')\begin{pmatrix}\sin\phi\\ \cos\phi\end{pmatrix}(W^+H^-Z_{1,2} + \text{h.c.})\,, \tag{4.36}$$

with $\tan\beta = v_2/v_1$ (the ratio of the doublet vev's), $Y'_{1,2}$ are the U(1)′ couplings of these two doublets whose normalization is defined by the Z' term in the covariant derivative $(-ig/c_w\sqrt{x_w}\,Y'Z')$, and M_Z is the SM mass of the Z. The angles β and ϕ are related via

$$\tan\phi = 2\sqrt{x_w}\,(-Y_1'\cos^2\beta + Y_2'\sin^2\beta)M_Z^2/(M_2^2 - M_Z^2)\,. \tag{4.37}$$

In addition to the $Z_2\to W^{\pm}H^{\mp}$ decay process discussed above, how can such couplings be probed if they exist? Various possibilities within the rank-5 scenario have been discussed in ref. [4.29], which we will now survey. One likelihood is $W^{\pm}H^{\mp}$ off-resonance production in e^+e^- annihilation with a cross section ($t = \tan\beta$) given by

$$\frac{d\sigma}{dz} = \frac{25\pi\alpha^2M_Z^2}{72x_w(1-x_w)}\,\frac{t^2}{1+t^2}\left[\left(1+\frac{M_W^2-M_H^2}{s}\right)^2 - \frac{4M_W^2}{s}\right]^{1/2}$$
$$\times\left[(1+z^2) + \frac{E_W^2}{M_W^2}(1-z^2)\right]\sum_{i,j} c_ic_j(v_i^e v_j^e + a_i^e a_j^e)P_{ij}\,, \tag{4.38}$$

where P_{ij} is the propagator matrix of section 2, $E_W/M_W = (s + M_W^2 - M_H^2)/2\sqrt{s}M_W$, $c_1\,(c_2) = \sin\phi\,(\cos\phi)$, $z = \cos\theta$, and the couplings v_i^e, a_i^e are normalized as in eq. (2.55). Figure 103 shows the integrated cross section for the $e^+e^-\to W^{\pm}H^{\mp}$ process at LEP II ($\sqrt{s} = 200$ GeV) as a function of M_H for different values of $\tan\beta$ and assuming $M_2 = 250$ GeV. With reasonable luminosities and values of $\tan\beta \simeq 0.5$, this corresponds to at least several hundred events/yr. (Note that in the rank-5 model, a light $M_2 \simeq 250$ GeV implies the constraint $\tan\beta \lesssim 0.6$ [4.29].) The backgrounds from W^+W^-, 2Z, and H^+H^- are easily eliminated by demanding a production signal of one W (reconstructed from its leptonic decays and the fixed value of $\sqrt{s}$) plus heavy quark jets ($t\bar{b}$) in the opposite hemisphere. Although, e.g., the W^+W^- cross section is much larger than that for $W^{\pm}H^{\mp}$, an additional angular cut ($z \lesssim 0$) reduces this background by an extra factor of $\simeq 10$ so that when combined with the heavy quark trigger from $t\bar{b}$ jets on the opposite side, the signal is larger than the background. This is due to the fact that $W\to t\bar{b}$ will be very suppressed kinematically and $H\to t\bar{b}$ will be the dominant mode. At higher energy e^+e^- colliders, this cross section falls off like $\sim s^{-2}$, so that it is quite small unless the Z_2 resonance is nearby.

At higher energy e^+e^- colliders, one might imagine that $H^{\pm}$ production via $W^{\pm}Z_{1,2}$ fusion may occur with a significant cross section; explicit calculation shows this not to be the case. With $\sqrt{s} = 1$ TeV, $M_H = 0.5$ TeV, $\tan\beta = 0.6$, and $M_2 = 150$ GeV, one finds $\sigma \simeq 0.016$ fb, which is far too small to be observable.

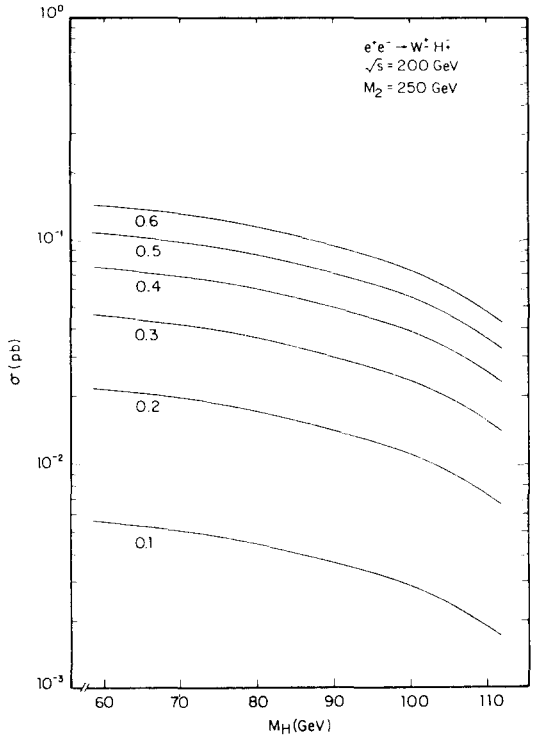

Fig. 103. Cross section for $e^+e^- \to W^\pm H^\mp$ at $\sqrt{s} = 200$ GeV as a function of M_H with $M_2 = 250$ GeV for different values of $\tan\beta$.

Two processes may contribute to $W^\pm H^\mp$ production and probe the $W^\pm H^\mp Z_i$ vertices at hadron colliders: (i) $q\bar{q} \to Z_i \to W^\pm H^\mp$ and (ii) $W^\pm Z_i \to H^\pm \to W^\pm Z_j$. For a reasonable, yet optimistic, choice of parameters, however, process (ii) is far too small to be observable since it is swamped by the $q\bar{q} \to W^\pm Z_j$ continuum as shown in fig. 104 from ref. [4.29]. The only hope then is process (i) for which the cross section is

$$\frac{d\sigma}{dM} = \sum_q \frac{2M}{s} \int_{-Y}^{Y} dy\, [q(x_1, M^2)\bar{q}(x_2, M^2) + \bar{q}(x_1, M^2)q(x_2, M^2)] \int_{-z_0}^{z_0} dz\, \frac{d\hat{\sigma}_q}{dz}\,, \tag{4.39}$$

where $d\hat{\sigma}_q/dz$ is obtainable from eq. (4.38) by letting $s \to M^2$ and dividing by a color factor of 3. As usual, we have

$$\begin{aligned} &x_{1,2} = (M/\sqrt{s})\, e^{\pm y}\,, \qquad z_0 = \min(\beta^{-1} \tanh(Y - |y|), 1)\,, \\ &\beta = \{[1 - (M_W^2 + M_H^2)/M^2]^2 - 4M_W^2 M_H^2/M^4\}^{1/2}[1 + (M_W^2 - M_H^2)/M^2]^{-1}\,, \end{aligned} \tag{4.40}$$

and Y is a rapidity cut on the $W^\pm H^\mp$ final state (which is taken to be $Y = 2.5$).

The major backgrounds to the $q\bar{q} \to Z_i \to W^\pm H^\mp$ process come from gluon-initiated triangle and box diagrams involving heavy b- or t-quarks (e.g., $gg \to t\bar{t} \to H_i^0 \to W^\pm H^\mp$ and $gg \to t\bar{t} \to W^\pm H^\mp$) and

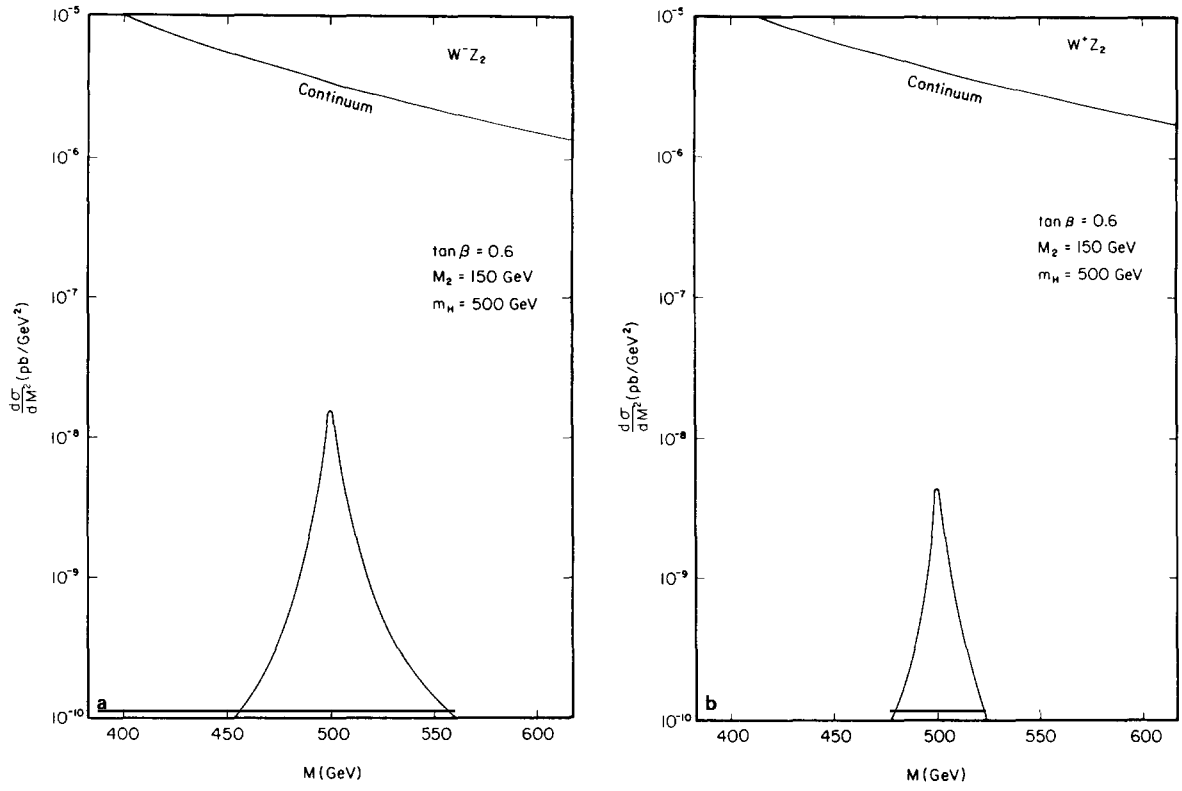

Fig. 104. Differential cross sections $d\sigma/dM^2$ for (a) $pp \to W^- Z_2 + X$ and (b) $pp \to W^+ Z_2 + X$ from the continuum $q\bar{q} \to W^{\pm} Z_2$ process and from resonant charged Higgs production, $W^{\pm} Z_i \to H^{\pm} \to W^{\pm} Z_2$ at $\sqrt{s} = 40$ TeV.

tree-level diagrams with heavy quarks in the initial state, $b\bar{b}$, $t\bar{t} \to W^{\pm} H^{\mp}$. The relative sizes of the signal and background are, of course, quite sensitive to the choice of model parameters, m_t and $\tan\beta$, which together with the charged scalar mass determine all couplings and masses in the minimal SUSY-SM which was used to calculate various background processes [4.21]. Basically, for fixed M_H, one finds that the background increases relative to the signal with increasing (decreasing) m_t ($\tan\beta$). If, at the SSC, we take for example $M_2 = 800$ GeV, $\tan\beta = 0.8$, and $M_H = 600$ GeV, the signal to background ratio is $\simeq 5/1$ (30/1) for $m_t = 100$ (40) GeV with a signal cross section of $\simeq 0.1$ pb. If the $W^{\mp}$ is reconstructed in one of its leptonic modes and $W^{\pm}Z$ final states can also be reconstructed from the $H^{\pm}$ decay, then $\simeq 330$ events should be observable with the SSC design luminosity. This situation improves, of course, with increasing $\tan\beta$. It thus seems likely that the $q\bar{q} \to Z_i \to W^{\pm} H^{\mp}$ process should be observable above background and with a sufficient rate for a reasonable range of model parameters so that the $W^{\pm} H^{\mp} Z_i$ coupling can be explored.

5. Implications elsewhere

In addition to the possible extensions of the gauge, fermion, and scalar parts of the effective low-energy sector in superstring-inspired E_6 models, there are a number of other theoretical and

phenomenological implications of such models which we will briefly survey in this section. Many of these results are not directly linked to E_6 but are general features of these kinds of superstring-inspired models. Note that there is a fair amount of overlap among the subjects surveyed in the various subsections. In areas which are not phenomenological in nature, a brief review is given and the reader is referred to the original references.

5.1. Gaugino masses and SUSY breaking

For superstring-inspired E_6 models to be phenomenologically viable they must provide a mechanism for SUSY breaking and generation of the electroweak scale [1.11, 1.13]. Of the several possible approaches to SUSY breaking, non-perturbative breaking by gaugino condensation in the hidden (E_8') sector seems to be the most promising. SUSY breaking is then transmitted to the observable sector via gravitational couplings inducing soft-SUSY breaking scalar/gaugino mass terms in the potential which then produce electroweak breaking. In this subsection we briefly survey the work done in this area by a number of different groups. It should be noted that some of this work is also discussed in the other parts of this section since it impacts strongly on a number of separate topics.

An extensive amount of work on this subject has been done by the Berkeley group (Binétruy, Dawson, Gaillard, and Hinchliffe) in a series of papers [5.1–5.4]. In the scenario presented in the first paper of the series [5.1], SUSY breaking does not initially generate a mass for the gaugino (in the observable sector) or induce any A-terms but generates soft masses for all scalars which take on a common value at the compactification scale. Gaugino masses are then induced at the one-loop level from the scalar masses while radiatively induced A-terms are neglected since they arise only at the two-loop level. A renormalization group equation (RGE) analysis of the scalar field masses within the context of the minimal rank-5 model is then used to place a bound of $\langle \tilde{S}^c \rangle \lesssim 125$ GeV, or $\lesssim 440$ GeV, depending on the ratio of the doublet vev's, which leads in either case to a phenomenologically unsuccessful result: Z_2 is either too light ($\lesssim 65$ GeV) or the shift in the Z mass is too large ($\gtrsim 4$ GeV). The authors consider several rank-6 models which have no intermediate scales (i.e., light $Z_{2,3}$ gauge bosons) and show that such models are also inconsistent with present data using the same analysis as in the rank-5 case. One possibility not considered by these authors is the alternative left–right model [2.48, 2.49] discussed in sections 2 and 3 which avoids the strong constraints on the W_R mass and could remain viable. These authors conclude that only models with intermediate scales may be compatible with existing phenomenology, assuming the above method of SUSY breaking.

In the second paper in the series [5.2] the authors consider the details of SUSY breaking by gaugino condensation in the hidden sector. The ten-dimensional $E_8' \times E_8$ gauge group after compactification leads to the four-dimensional group $K \times G$, with G being the group relevant for the observable sector. Fields in the adjoint of K (which form the hidden sector) are singlets under G while fields transforming non-trivially under G are K singlets. The two sectors communicate only by gravitational interactions. The existence of a scalar field S coupling to both K and G gauge sectors (and originating from the dilation field) is essential for gaugino condensation to break SUSY. The condensation of the gauginos in K occurs when their respective couplings become strong at some scale Λ. A gravitino mass ($m_{3/2}$) is generated but the net vacuum energy of the system (i.e., the cosmological constant) remains zero at the tree level due to a cancellation with the vev of the antisymmetric field strength tensor H. The observable sector is unaware of the SUSY breaking at this order and scalar masses remain zero even at one-loop.

The authors then investigate the gaugino masses at the one-loop level which arise from diagrams containing the gravitino and a generic scalar field S (as well as its SUSY partner). The gaugino masses

are found to depend only on $\langle S \rangle$, the scale Λ, the gravitino mass ($m_{3/2}$), and the K sector one-loop beta function. The scalars in the observable sector then obtain masses via the RGE's. The gauginos are found to have universal masses $m_{1/2} \simeq M_W$ with $m_{3/2} \simeq 10^{13}$ GeV when the requirement of the stability of the Higgs vev's is imposed. The latter value is also favored by some supersymmetric inflationary models (for a brief discussion of this topic see section 5.4). If the various contributions to $m_{1/2}$ were to cancel in a particular model then SUSY breaking could only be transferred to the observable sector in a non-perturbative manner. These non-perturbative SUSY breaking effects are examined in later papers [5.3, 5.4] where several different models are studied. Since the field theory resulting from string compactification is non-renormalizable, the natural physical cut-off is the condensation scale Λ. Note that the gravitino contributions to $m_{1/2}$ are found to cancel in a theory with a cut-off. The authors find $m_{1/2} \sim (m_{3/2})^3/M_p^2$ for the resulting gaugino masses and $m_{\text{scalars}} \simeq \sqrt{\alpha/\pi}\, m_{1/2}$. This result implies that squarks and sleptons are expected to be lighter than gauginos in superstring-inspired models. R symmetry breaking and the production of one-loop gaugino masses could lead to A-terms, which are potentially dangerous in that both color and electric charge conservation could be broken. For the models examined, however, it is found that such terms are absent in the ground state.

This analysis was extended in later publications [5.3, 5.4] and it is reasonable to conclude that their results should be applicable to a broad class of models where one finds $m_{1/2} \sim \mathrm{O}(1\text{–}100)(m_{3/2})^3(16\pi^2 M_p^2)^{-1}$. In their analysis the authors stress the importance of integrating over the region between Λ and the compactification scale to stabilize the one-loop effective potential.

SUSY breaking has also been considered by the Oxford group [5.5–5.7] in a scheme where the one-loop effective potential is bounded from below [5.8, 5.9] and with a single fine tuning yields a gauge hierarchy and an acceptable cosmological constant. In addition to the possibility of breaking SUSY in the hidden sector by gaugino condensation [5.10–5.12] and/or through the vev for the field strength tensor $\langle H_{lmn} \rangle = c\varepsilon_{lmn}$ [5.10–5.12], these authors propose that gauge singlet fields, N [5.13], develop non-zero vev's so that the superpotential satisfies $\langle W(N) \rangle = c$. If c originates from $\langle H_{lmn} \rangle$, then in units of M_p one expects $c \sim \mathrm{O}(1)$, but if $\langle W(N) \rangle = c$ then c may be much smaller.

The authors discuss some of the difficulties in obtaining a one-loop effective potential which is bounded from below and how such a potential can be obtained in two classes of models. For the two classes of models (I and II) these authors find

$$\text{I:} \quad m_{1/2} \sim (\alpha/\pi)^{4/3}(m_{3/2})^{5/3} M_p^{-2/3}, \qquad m_0 \sim (\alpha/\pi)^{1/2} m_{1/2}, \tag{5.1a}$$

$$\text{II:} \quad m_{1/2} \sim (m_{3/2})^3 M_p^{-2}, \qquad m_0 \sim (\alpha/\pi)^{1/2} m_{1/2}, \tag{5.1b}$$

so that scalar masses are always induced by radiative corrections. The second class of models is similar to that considered by Binétruy et al. [5.1–5.4], while in the first class the mechanism is that of Ellis et al. (to be discussed below) in which radiative corrections modify the Kähler potential. An important point of their analysis is that between Λ_c and M_p there is a drastic change in the particle mass spectrum which cannot be neglected when calculating SUSY breaking effects.

The problem of SUSY breaking has been examined by two groups at CERN, Ibañez et al. [5.12, 5.14] and Ellis et al. [5.11, 5.15]. The first set of authors emphasize the need for non-trivial gauge kinetic terms (i.e., the analytic f_{ab} function) as a crucial ingredient for the breaking of SUSY by gaugino condensation in the hidden sector, which occur in $d = 4$ models. Once condensates form, the gravitino gets an induced mass, $m_{3/2} \sim \Lambda^3/M_p^2$, so that $\Lambda \sim 10^{13\text{–}14}$ GeV would lead to $m_{3/2} \sim \mathrm{O}(1\ \text{TeV})$. However, the quadratic Casimirs of E_8' are so large, these authors claim, that Λ will be too close to M_p unless E_8' itself breaks to some smaller group. Breaking E_8' to large gauge groups, such as $SU(5) \times SU(5)$,

SO(16), SU(9), $E_7 \times SU(2)$ or $E_6 \times SU(3)$, will not help since their Casimirs are also quite large. To get $\Lambda \lesssim 10^{14}$ GeV one needs to break $E_8' \to [SU(2)]^n \times [U(1)]^m$ in order to generate a light gravitino mass according to these authors [5.12, 5.14]. One way out of this problem is that soft terms in the observable sector may be much smaller than $\sim m_{3/2}$. The breaking of E_8' to a small group by the Hosotani mechanism, as in the case of E_6, is found to be quite difficult. They emphasize that gaugino condensation and $\langle H_{lmn} \rangle$ both break SUSY and that the advantage of using both is that the two contributions to the cosmological constant cancel.

Even though SUSY is broken in the hidden sector at the tree level, there is still no SUSY breaking in the observable sector, i.e., $m_0 = m_{1/2} = 0$ and the A-terms (soft trilinear couplings) in the superpotential are still absent. Scalar masses are generated at two-loop order as opposed to one-loop [5.8, 5.16] and are not universal, making the suppression of flavor changing neutral currents extremely difficult. These problems may be avoided if one includes one-loop contributions coming from the exchange of heavy string modes and leads to a gaugino mass $m_{1/2} \sim m_{3/2}(2\pi)^{-5}$ [5.12, 5.17] implying $m_{3/2} \lesssim 10^7$ GeV.

Ellis et al. [5.11, 5.15] claim that the kinetic energy function f_{ab} is modified in a very particular manner, which disagrees with what is found by Ibañez and the Oxford group [5.5, 5.6]. These authors also emphasize that E_8' must be broken if the gaugino condensation scale (and hence, the gravitino mass) is to be somewhat lower than the Planck scale. They also note [5.11, 5.15] that if E_8' is broken by the Hosotani mechanism to an $SU(N)$ subgroup (with $N \leq 4$) then the scale of gaugino condensation, Λ_c, will necessarily be somewhat below M_p and the gravitino mass is given by $m_{3/2} \sim \Lambda_c^3/M_p^2$. Without inflation (or if condensation occurs after inflation) the universe will be filled with $SU(N)$ flux tubes which form cosmic strings producing density perturbations $\delta\rho/\rho \sim 10^2(\Lambda_c^2/M_p^2)$ which could initiate galaxy formation (see the discussion in section 5.4). The bounds on $\delta\rho/\rho$ are satisfied if $\Lambda_c \lesssim 10^{16}$ GeV and $m_{3/2} \lesssim 10^{12}$ GeV so that one expects $m_{3/2} \ll M_p$.

Ellis et al. consider several possible contributions to SUSY breaking in the observable sector. One contribution to $m_{1/2}$ at one-loop is of order $\langle N \rangle m_{3/2}/M_p$ where $\langle N \rangle$ is the vev of some generic gauge non-singlet field. But if $\langle N \rangle$ is not too much larger than M_W and $m_{3/2} \ll M_p$ this contribution is small. Another contribution comes from the two-loop induced scalar mass $m_0 \sim (m_{3/2})^2/M_p$ which these authors claim is also too small. A further contribution to $m_{1/2} \sim (m_{3/2})^3/M_p^2$, as calculated by Binétruy et al. [5.1–5.4], is also claimed by Ellis et al. [5.11, 5.15] to be too small to be the dominant contribution to SUSY breaking. Ellis et al. find a new contribution to $m_{1/2} \sim (\alpha/\pi)^{4/3}(m_{3/2})^{5/3}M_p^{-2/3}$ which they claim is dominant; here α is a typical gauge coupling. This new contribution arises due to one-loop corrections to the effective scalar potential, shifting the value of the S field's vev, thus allowing it to contribute to $m_{1/2}$ (which it did not do at tree level). The authors claim that the sum of the gravitino, gauge boson, and S contributions to $m_{1/2}$ cancel in the momentum space regularization scheme, leaving their new term dominant. Numerically, they find that $m_{3/2} \simeq (0.3\text{–}1.3) \times 10^{11}$ GeV and $\Lambda_c \simeq (2.7\text{–}4.2) \times 10^{15}$ GeV. These authors go on to show that two-loop order scalar mass terms can also be generated by the same mechanism, giving $m_0 \sim m_{3/2}^2(\alpha\lambda/16\pi^2)^{1/2}/M_p$, where $\alpha(\lambda)$ is a gauge (Yukawa) coupling constant. Universal A-terms are similarly generated with a coefficient $A = -(g/12\sqrt{3})m_{1/2}$ where $\alpha = g^2/4\pi$. Given $m_{3/2} \ll M_p$, one then sees that $m_{1/2} \gg A \gg m_0$ which should be used as the initial conditions in an RGE analysis of effective low energy theories.

In an interesting paper, Drees [5.18] performed a detailed analysis of the parameter space of the rank-5 model under the assumption that no intermediate scale exists with SUSY breaking in the observable sector parametrized by $m_{1/2}$, m_0, and A. He shows that large Yukawa couplings are possible, thus allowing for a low SUSY breaking scale and for SUSY particle masses within the range of existing accelerators even if the Z′ is very heavy. Bounds on the masses of the exotic fermions relative

to that of the Z′ are obtained via an RGE analysis: the heaviest exotic quark (lepton) has to have a mass less than 3.1 (2.2) $M_{Z'}$, while the lightest of these particles must have masses which are less than 2.1 (1.8) $M_{Z'}$. For large Yukawa couplings the exotic fermions may be more massive than their SUSY partners, so that decays into partners plus neutralinos become possible. It is possible to make right-handed d-squarks or all sleptons quite light; one chargino and two neutralinos can also be made light in this model.

5.2. *The Oxford three-generation superstring model*

Ross and collaborators [5.19] have constructed an extremely interesting model in which compactification takes place on a specific manifold: the only known Calabi–Yau manifold (M_3) which leads to just three generations [5.20]. In this model the $E_8 \times E_8'$ superstring/supergravity model in ten dimensions compactifies at 10^{18-19} GeV on M_3 while $E_8 \to SU(3)_C \times SU(3)_L \times SU(3)_R$ (with $N=1$ SUSY) via Wilson loops. It is then believed to be energetically favorable in this model for two large vev's to develop producing a pair of very high intermediate scales: $\langle \tilde{\nu}^c \rangle \simeq 10^{17}$ GeV, $\langle \tilde{S}^c \rangle \simeq 10^{15}$ GeV which result in the $SU(3)_C \times SU(2)_L \times U(1)_Y$ SM below $\simeq 10^{15}$ GeV. The unbroken E_8' group interactions become strong (due to the large beta function) at a scale of $\sim 10^{18}$ GeV causing confinement and gaugino condensation in this hidden [5.10–5.12] sector. This can be used as a source of SUSY breaking which is transmitted to the SM observable sector via gravitational radiative corrections producing a non-zero gaugino mass [5.10–5.12, 5.14, 5.21]. Further SUSY breaking from these gaugino masses is then reliably calculable [5.22] and involves the RGE analysis of gauge as well as large Yukawa couplings.

Because the model involves a specific Calabi–Yau manifold there are many known details in this case which would be otherwise unconstrained. The multiplet structure, number of generations, and new discrete symmetries of the low-energy Lagrangian are completely determined. Thus, although there is still some uncertainty in the model due to the complexity of the possible breaking patterns it is likely that the particle content below the SUSY breaking scale ($\lesssim M_W$, say) is completely determined and consists of three usual SM generations, a pair of Higgs doublets and some additional (three neutral and one charged) leptons. Figure 105 from Ross [5.19] shows a schematic representation of this model. In units of a common gaugino mass ($m_{1/2}$) the SUSY particle masses are expected to scale as

$$\tilde{q}/\tilde{g}/\tilde{\ell}_L/\tilde{\ell}_R/\tilde{W}, \tilde{Z}/\tilde{\gamma} = 1.9/1/0.7/0.4/0.3/0.16\,, \tag{5.2}$$

as would be roughly the case in any model in which gauginos generate the dominant SUSY breaking scale in the observable sector. With a reasonable value for $m_{1/2} \simeq 300$ GeV or so, most of the SUSY particle masses are predicted to be much larger than the present experimental lower limits as is shown in fig. 106 from Ross [5.19]. Thus we should not be disappointed in the lack of existing evidence for SUSY at this point if this model is correct. We now turn to a short discussion of some of the details of this model.

The specific manifold, R, under consideration [5.19, 5.20] leads to Betti–Hodge parameters $h_{2,1}=9$ and $h_{1,1}=6$, hence Euler number $\chi=-6$. The chiral structure is thus $9(\mathbf{27})+6(\overline{\mathbf{27}})$ or simply $n_g(\mathbf{27})+\delta(\mathbf{27}+\overline{\mathbf{27}})$ with $n_g=3$ and $\delta=6$. Note that in obtaining R, a discrete symmetry group $G=Z_3$ has been used to form a quotient manifold, hence reducing $h_{2,1}$ and $h_{1,1}$. Wilson line breaking leaves three possible unbroken groups, assuming unbroken E_8' (note R is not simply connected): $[SU(3)]^3$, $SU(6)\times U(1)$, or E_6. It is assumed that $[SU(3)]^3$ is the most promising starting point for a realistic

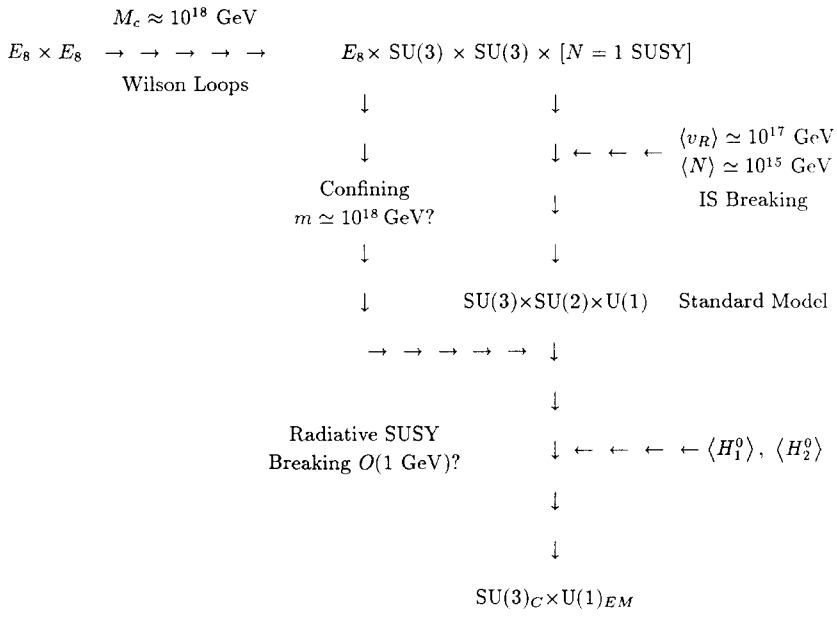

Light States ($m_i \lesssim O(M_W)$) : $3 \times \left[\begin{pmatrix} u \\ d \end{pmatrix}_L u_R d_R \begin{pmatrix} \nu \\ \ell \end{pmatrix}_L \ell_R \right] + \begin{pmatrix} H_1^+ \\ H_1^0 \end{pmatrix}_L + \begin{pmatrix} H_2^0 \\ H_2^- \end{pmatrix}_L$ + Three Neutral, One Charged Leptons

Yukawa Coupings Known

Fig. 105. The three generation Calabi–Yau superstring model examined by Ross et al. [5.19].

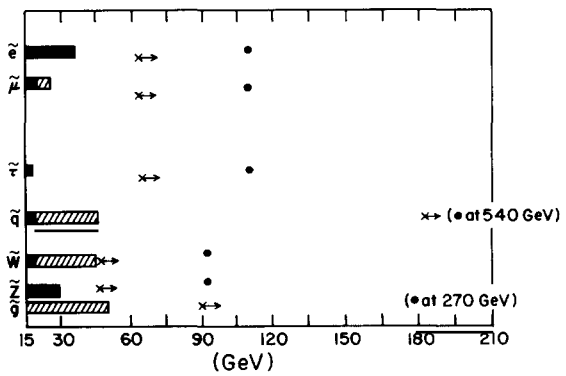

Fig. 106. Bounds and expectations for SUSY particle masses. The crosses denote the lower bounds obtained by choosing $m_{1/2}$ to give a Wino mass at the current CERN Collider experimental limit. The dots correspond to choosing $m_{1/2} = 270$ GeV. The shaded bars represent data.

model. Use of the discrete Z_3 symmetry can determine which states are light after Wilson breaking: for each **27** one is left with nine light "lepton" and seven "quark" (and "antiquark") components whereas in the $\overline{27}$ one obtains six light "lepton" and four "quark" (and "antiquark") components. At this point "lepton" ("quark") means color singlet (triplet) under $SU(3)_C$. Thus, after compactification and Wilson line breaking the number of massless states is drastically reduced. The superpotential, W, of the remaining fields is then determined by using the unbroken gauge symmetry and any additional unbroken discrete symmetries of which there are several.

To study SUSY breaking a model of the low-energy Lagrangian is required but since the Calabi–Yau metric is unknown one assumes a general form consistent with all of the symmetries. This leads to an effective "no-scale" theory [2.8, 5.13] which may provide a good approximation to the true theory. SUSY breaking can occur via a non-zero vev for the field strength antisymmetric tensor, $\langle H_{ijk} \rangle \equiv c\varepsilon_{ijk}$, or by the scalar fields which produce a non-zero vev for W, i.e., $\langle W \rangle = c$. In the former case one would expect $c \sim M_p$ whereas it could be much smaller in the latter case. SUSY breaking is then intimately connected to intermediate scale breaking since the form of the effective potential after compactification determines whether $\langle \tilde{S}^c \rangle$ and $\langle \tilde{\nu}^c \rangle$ are non-zero and the magnitude of their scales. Without SUSY breaking all massless fields will have zero vev's. Self-consistency shows that such intermediate scales can be $\gtrsim 10^{16}$ GeV.

One of the discrete symmetries remaining after compactification is a Z_2 subgroup of E_6 under which the fields transform as

$$\begin{pmatrix} u \\ d \\ h \end{pmatrix}_L \to \begin{pmatrix} -u \\ -d \\ h \end{pmatrix}_L , \quad \begin{pmatrix} u^c \\ d^c \\ h^c \end{pmatrix}_L \to \begin{pmatrix} -u^c \\ -d^c \\ h^c \end{pmatrix}_L , \quad \begin{pmatrix} N & E^c & \nu \\ E & N^c & e \\ e^c & \nu^c & S^c \end{pmatrix}_L \to \begin{pmatrix} N & E^c & -\nu \\ E & N^c & -e \\ -e^c & -\nu^c & S^c \end{pmatrix}_L . \tag{5.3}$$

Note that the ordinary quarks and leptons are odd under this Z_2 while the pair of Higgs doublets (as well as the SUSY partners to N, E, N^c, E^c) is even. This is just what is needed in order to forbid possible baryon number violating dimension-four operators. However, once $\langle \tilde{\nu}^c \rangle \neq 0$, Z_2 is broken explicitly unless an additional discrete symmetry which when combined with the Z_2 symmetry remains unbroken. Such a symmetry has been found to exist leaving the above matter parity assignments unaltered after intermediate scale breaking and the usual fields remain light: three ordinary generations and a pair of Higgs doublets together with their SUSY partners. There is also an additional set of light ($\sim$1 TeV) leptons (three neutral and one charged). All components of the $\overline{27}$ which are still massless after compactification obtain masses of order M_I at this stage. The Higgs supermultiplets remain light (and do not pair up and become heavy) due to the existence of discrete symmetries. Electroweak breaking is triggered if the soft-SUSY breaking Higgs masses are driven negative due to radiative corrections.

Nucleon decay is suppressed in this model since dimension-four baryon number violating ($\Delta B \neq 0$) terms in the superpotential are forbidden by the discrete symmetries. Dimension-five $\Delta B \neq 0$ operators do exist but their contributions are suppressed (by $M_I \gtrsim 10^{16}$ GeV) to be below current limits. Neutrino masses can be made small since there is an active see-saw mechanism due to ν^c and S^c acquiring masses at the scale M_I. One generally expects $m_\nu \sim m_q^2/M_I$ so that with $M_I \sim 10^{16}$ GeV, neutrino masses are in the range 10^{-11} to 10^{-5} eV. $\sin^2\theta_w$ is determined at low energy using the usual RGE analysis; if $M_I = 10^{16}$ GeV one obtains $\sin^2\theta_w \simeq 0.225$, whereas for $M_I \simeq 10^{14}$ GeV, $\sin^2\theta_w \simeq 0.25$ is found. We thus see that the larger value of M_I is favored by the current experimental value of $\sin^2\theta_w = 0.230 \pm 0.005$. The strong CP problem can potentially be dealt with in this model since the discrete symmetries can

give rise to an approximate Peccei–Quinn symmetry which may be adequate to suppress *CP* violation. Implementation of this scenario is made somewhat difficult due to the large value of M_I in this model. *CP* violation arises in the quark mass matrix due to the complex Yukawa couplings. Due to the six unknown field normalizations, one cannot as yet determine the masses of the quarks or leptons, although it is hoped they will be calculable in the future leading to predictions of fermion masses and mixing angles.

It is clear that this highly interesting model shows some of the potential power of a true superstring model even though the detailed physics behind this model is still not fully understood.

5.3. Intermediate scales and particle masses

Subsequent to E_6 breaking by Wilson loops (yielding a rank-5 or rank-6 model) further breaking to the SM requires additional vev's, $\langle \tilde{S}^c \rangle$ and/or $\langle \tilde{\nu}^c \rangle$, at some intermediate mass scale(s) M_I. The problems associated with intermediate scales have been addressed by a large number of groups. In this section we briefly survey the work that has been done in trying to understand the generation of intermediate scales and phenomenological constraints on the allowed range for M_I. Such intermediate scale physics is also discussed in the other parts of this section since it is intimately connected to SUSY breaking, the existence of the fourth generation in E_6 superstring-inspired models, and axions in such theories.

Ellis, Enqvist, Nanopoulos, Olive and collaborators have performed a systematic study of physics associated with the intermediate mass scale in a series of papers. In early work [5.23], these authors examined bounds on M_I from baryon nucleosynthesis. The existence of the scale M_I induces a phase transition as the universe cools below the critical temperature when the scalar field gets a non-zero vev. Entropy is released from the decay of the scalar field as it moves away from the origin toward the true minimum of the potential and oscillates around this minimum. When the decay temperature of the scalar field into light matter coincides with the critical temperature, the amount of entropy released is given by $\Delta \sim (M_I/m)^{3/2}$ where m characterizes the electroweak/SUSY breaking scale: $m \sim 0.1$–1 TeV. Since entropy generation dilutes the baryon to entropy ratio, Δ is bounded from above [5.24], implying $M_I \lesssim 10^{5-7}$ GeV. (This is far too low if dimension-five or six operators linked to the scale M_I can induce proton decay.) If, however, the lifetime of the scalar field is longer than the age of the universe during nucleosynthesis then $\Delta \lesssim O(10)$, otherwise scalar decays will alter the abundances of light nuclei. Therefore, in order that the scalar can decay sufficiently rapidly, one finds that $M_I \lesssim 10^{8-10}$ GeV. This may rule out models with four generations since they require M_I to be quite large as will be discussed below. It should be rembered that unless they are somehow forbidden, effective dimension-5 operators will induce too rapid a proton decay unless $M_I \gtrsim 10^{16}$ GeV. Similarly, if above M_I there are many states (including mirrors) contributing to the RGE, the requirement of perturbative unification demands that M_I not be more than two orders of magnitude below the compactification/Planck scale.

Assuming that M_I is indeed high ($\gtrsim 10^{16}$ GeV), Enqvist et al. [5.25] have analyzed the particle spectrum in a class of models with three generations, a stable proton, and massless neutrinos. These models are effectively rank-5 below M_I until the weak scale is reached. These authors find that the Higgs fields tend to have masses in the 10^6 GeV range due to higher order non-renormalizable interactions and cannot then be used to break the electroweak symmetries. In particular these authors assume $\langle \tilde{\nu}^c \rangle \gtrsim 10^{16}$ GeV, while $\langle \tilde{S}^c \rangle \ll \langle \tilde{\nu}^c \rangle$ is used to break the rank-5 model down to the SM. At a similar higher order in perturbation theory the physical mass eigenstates become general mixtures of the original massless modes, opening up the possibility of dangerous flavor changing interactions. Due

to the large number of light fields below M_I (including mirror states) $\sin^2\theta_w$ is probably in disagreement with experiment. The inclusion of extra E_6 singlets or the existence of certain discrete symmetries may help avoid many of the above mentioned problems with these models.

In a later work, Ellis et al. [5.26] continued their analysis of models with intermediate scales and examined the question of whether one can obtain a consistent model of this type. They discuss the difficulties associated with generating an intermediate scale associated with radiative symmetry breaking unless $M_I \lesssim 10^{10}$ GeV, a result similar to the earlier cosmological constraints ($M_I \lesssim 10^{12}$ GeV) using the Affleck–Dine mechanism [5.27]. However, non-perturbative behavior of the couplings and limits on proton decay force $M_I \gtrsim 10^{16}$ GeV. It would thus appear that there are multiple and contradictory demands on the size of the scale M_I. Some of these problems are solvable by judicious use of discrete symmetries, but most still remain.

Drees [5.28] considers intermediate scale breaking and the spectrum of the SUSY partners in the context of superstring-inspired models. He stresses the possible importance of non-negligible D-terms contributing to the scalar partner masses which is a subject not much discussed in the literature. The origin of these terms is easy to see. In a general potential of the form

$$V = m_\phi^2|\phi|^2 + m_{\bar\phi}^2|\bar\phi|^2 + a(|\phi|^2 - |\bar\phi|^2)^2 + (\lambda^2/M_c^2)(|\phi|^2|\bar\phi|^4 + |\bar\phi|^2|\phi|^4)\,, \tag{5.4}$$

where ϕ is in the **27** and $\bar\phi$ in the $\overline{\mathbf{27}}$ of E_6, the parameter a depends on the gauge group breaking at M_I. Usually the soft-breaking masses $m_{\phi,\bar\phi}$ are expected to be O(1 TeV) and to be equal at M_c. At lower energies, m_ϕ^2 is easily driven negative by large Yukawa couplings to the exotics, whereas this does not happen for $m_{\bar\phi}^2$ since the $\overline{\mathbf{27}}$ consists mostly of very heavy fields. This implies that $m_\phi^2(M_I) < m_{\bar\phi}^2(M_I)$ and $\langle\phi\rangle > \langle\bar\phi\rangle$ so that the D-term proportional to a in (5.4) is non-negligible. Drees proceeds to examine two scenarios of E_6 breaking to a rank-5 model with an additional U(1) factor. In one scenario, scalar masses are the main source of SUSY breaking, whereas in the second scenario gauginos play this role. Using the rough bound on $M_{Z'}$ ($\gtrsim$175 GeV or so) the common scalar mass (m_0) is found to be $\gtrsim$145 GeV whereas the common gaugino mass (M) is $\gtrsim$195 GeV. Detailed mass calculations for all the SUSY partners in units of m_0 or M is possible. Some $\tilde q$'s are quite light (even lighter than some $\tilde\ell$'s) and could be observable at the Tevatron. In the first model the scalar masses are in the range 0.45–1.41 m_0 whereas in the second model one finds the range 0.56–1.88 M. Clearly symmetry breaking at the scale M_I induces significant contributions to the scalar mass spectrum.

Yamamoto [5.29] investigated problems associated with domain walls and Nambu Goldstone bosons in a class of models with an intermediate scale and a global symmetry imposed to maintain the hierarchy $M_W/M_I \ll 1$. The author found that under certain circumstances these problems could be avoided: (1) there are no SM singlet fields with vev's of order M_W thus avoiding the necessity of the above global symmetry; (2) there exist certain classes of scalar fields with vev's of order M_I which transform in different ways under the global symmetry causing it to break at M_I.

Costa et al. [5.30] consider the radiative generation of intermediate mass scales in superstring-inspired models. They perform a detailed RGE analysis of the $SU(3)_C \times SU(2)_L \times [U(1)]^3$ model using constraints from $\sin^2\theta_w(M_W)$ and $\alpha_s(M_W)$. The authors stress that acceptable intermediate scale breaking must correspond to an approximate flat direction of the potential in order not to spoil SUSY. Thus scalar gauge non-singlet fields acquiring large vev's must be in self-conjugate multiplets, i.e., $\mathbf{27} + \overline{\mathbf{27}}$ pairs. These vev's must be nearly equal to prevent a large D-term, and superpotential terms that could induce a big F-term must also be absent. Thus the generation of M_I is impossible in these models without light "survivors" from the $\mathbf{27} + \overline{\mathbf{27}}$'s being present, i.e., Betti–Hodge parameters

$(b_{1,1}) \geq 1$. These authors assume only a minimal set of survivors in their analysis. For reasonable values of the model parameters, these authors find that radiatively induced intermediate scales in the range 10^7–10^{14} GeV are compatible with the low-energy parameters $\sin^2\theta_w$, α_s etc. and can lead to perturbative unification (PU) for $n_g = 3$. The assumption of $n_g = 4$ leads to well-known problems associated with PU. The value of M_I is most constrained by the dimension of the non-perturbative (NP) terms in the scalar potential: $M_I \lesssim 10^9$ GeV is consistent with NP terms of any dimension, whereas for larger M_I, the NP terms need to be dimension six (or even higher for $M_I \gtrsim 10^{13}$ GeV). An analysis along similar lines has been performed by Gabbiani [5.31].

It is clear from the above survey that the problems associated with generating the scale M_I and the constraints on its magnitude are still somewhat controversial.

5.4. *Axions and cosmology*

Any physical theory which involves new physics at high mass scales (>TeV) can have important astrophysical and cosmological consequences; superstring-inspired models are no exception to this. In addition, if string theories are indeed "theories of everything" there will be strong links between low-energy phenomena, cosmology, and physics at mass scales which are inaccessible directly by accelerator experiments. Cosmology thus may provide us with important constraints on superstring-inspired E_6 models as it has already done for other models previously considered [5.32]. In this section we wish to briefly survey some of the consequences of these models in relation to the strong *CP* problem (i.e., axions) [5.33] and cosmology in general.

5.4.1. *Axions*

As is well known, one of the ways to deal with the so-called strong-*CP* problem is through the imposition of the Peccei–Quinn symmetry [5.34] which, when spontaneously broken, produces a light pseudoscalar, the axion, which couples to fermions. The size of the axion decay constant, f_a, sets the scale of the mass and effective coupling strength of the axion. The only phenomenologically acceptable axions are those for which $f_a \gg 250$ GeV, thus ruling out the "standard" axion [5.34] and rendering it "invisible" [5.35]. In fact, f_a needs to be quite large ($\gtrsim 10^8$ GeV) otherwise axions will transport away too much energy from stellar cores [5.36]. Even stronger lower bounds on f_a may be possible using data from the supernova SN1987a. On the other hand, cosmological considerations of the energy density carried by primordial axions and the critical density of the universe constrain $f_a \lesssim 10^{12}$ GeV, *if* axions are produced during a radiation dominated era (as in the standard big-bang scenario) [5.37]. Models which predict f_a outside the above range may not be phenomenologically viable.

Witten [5.38] has shown that superstring theories have one or more Peccei–Quinn symmetries and therefore one or more axions. In the heterotic $E_8 \times E_8'$ scenario of interest to us here, there exist at least two axion-like degrees of freedom (a_1 and a_2) when compactified on a Calabi–Yau manifold with SU(3) holonomy. a_1 is referred to as the "model-independent" axion since it is insensitive to the particulars of the string theory considered and is present in all models. Let $M, N, \ldots$ represent ten-dimensional indices; $\mu, \nu, \ldots$ represent the usual four-dimensional indices; and $m, n, \ldots$ represent coordinate indices on the manifold K. In order to have anomaly cancellation there must exist an antisymmetric tensor gauge field B_{MN}; a zero mode of this field $B_{\mu\nu}$ corresponds to the model-independent axion, a_1. In terms of the field strength tensor, H_{MNP}, this means that (F_1 being the a_1 decay constant)

$$H_{\mu\nu\rho} = 16\pi^2 \varepsilon_{\mu\nu\rho\sigma}(F_1 \partial^\mu a_1)\,. \tag{5.5}$$

To see that a_1 is indeed an axion, taking the curl of (5.5) leads to (omitting gravitational terms)

$$\partial^2 a_1 \sim (1/F_1)\,\mathrm{Tr}(F\tilde{F}) + \cdots , \tag{5.6}$$

so that (5.6) can originate from an effective Lagrangian

$$\mathscr{L}_{\mathrm{eff}} = \tfrac{1}{2}(\partial_\mu a_1)^2 - \frac{a_1}{32\pi^2 F_1}\left(\frac{1}{30}\sum_a \mathrm{Tr}\, F_a \tilde{F}_a\right), \tag{5.7}$$

with the sum being over distinct unbroken non-abelian gauge groups. The second, model-dependent axion, a_2, with decay constant F_2, originates from the Green–Schwarz counter term [1.10] which is necessary for anomaly cancellation, i.e., from the zero modes of B_{mn},

$$H_{\mu mn} = 16\pi^2 \varepsilon_{mn}(F_2 \partial_\mu a_2)\,. \tag{5.8}$$

In both cases, one finds that $F_{1,2} \simeq 10^{15\text{–}16}$ GeV, well outside the upper limit of $\simeq 10^{12}$ GeV given above [5.36], which is a serious problem. If E_8' breaks down to some unbroken non-abelian gauge group (as is required to obtain hidden-sector gaugino condensation) at some scale M_c [5.12, 5.15, 5.39] there are then at least two unbroken non-abelian groups: $SU(3)_C$ and the non-abelian remnant of E_8'. In this case a_i are both true axions, a disconnected vacuum manifold exists, and a problem with domain walls develops [5.40] since different regions fall into distinct vacuum states. If, however, E_8' breaks to some abelian group, domain wall problems may still arise [5.41] so that in either case inflation may be needed to "inflate away" the domain walls. Inflation may also help with the large values of F_i since in superstring models with a super-heavy intermediate scale, M_I, the universe enters an inflationary phase at temperatures not far above the electroweak scale. In such scenarios values of F_i as large as $10^{15\text{–}16}$ GeV may be possible without causing any conflict with observation since the decay of the false "inflation" vacuum releases entropy thus diluting the relative axion number density substantially.

Another possible solution to the axion problem in the superstring-inspired model framework is to impose the condition that other independent, Peccei–Quinn symmetries exist, such that their total number is greater than the number of unbroken non-abelian groups [5.40]. If the axion scale (f_A) associated with these new symmetries *is* in the range $\simeq 10^8$–10^{12} GeV, then the linear combination of the new intermediate scale axions A and a_1 coupling to the gluon sector ends up with an effective scale [5.41]

$$f_a' = (f_A/M_1 + M_1/f_A)^{-1}(M_1^2 + f_A^2)^{1/2} \simeq f_A\,. \tag{5.9}$$

The orthogonal combination is a real Goldstone boson which we can eliminate via the Higgs mechanism. This possibility has been examined with the context of both rank-5 $SU(3)_C \times SU(2)_L \times U(1)_Y \times U(1)_\eta$ and rank-6 $SU(3)_C \times SU(2)_L \times U(1)_Y \times U(1)_\chi \times U(1)_\psi$ models [5.41], where M_I is associated with the breaking scale of $U(1)_\eta$ or some combination of $U(1)_\chi$ and $U(1)_\psi$. The axions in these models are "hadronic" in that they do not have tree level couplings to leptons [5.41] and the Peccei–Quinn symmetry is chosen to act non-trivially on the exotic fermion fields in analogy to the heavy-quark axion model [5.42]. Self-consistent analyses of much models lead to values of $f_A \simeq$ few $\times 10^8$ GeV, just inside the allowed range.

It is clear that such more work needs to be done in order to understand the detailed nature of axions in superstring-inspired models.

5.4.2. Dark Matter

The invariance of the superpotential (W) under R-parity transformations implies that there must exist among the SUSY partners of the matter of gauge fields a lightest supersymmetric particle (LSP) which is stable. The LSP may play the role of the invisible "dark" matter of which most of the universe consists. The arguments for the existence of such dark matter are many and will not be reviewed here. In ordinary SUSY models, it was found to be quite natural for the LSP dark matter density, ρ_D, to be comparable to the closure density as is required by observation and inflationary scenarios [5.43]. As in the SUSY extension of the SM, the generic tendency is for one of the spin-$\frac{1}{2}$ particles described by W to be less massive than any of the spin-0 particles, so that the most likely candidate for dark matter is some combination of the neutral weakly interacting gauginos and matter fermions. In the minimal model of rank-5, the LSP is thus some combination of $\tilde{N}$, $\tilde{N}^c$, $\tilde{S}^c$, $\tilde{\gamma}$, $\tilde{Z}$, and $\tilde{Z}_\eta$ [5.44], all of which have $R=-1$. (Additional possibilities for the LSP exist in rank-6 models.) To determine the LSP (χ) one needs to diagonalize the (symmetric) mass matrix involving the above fields. For a reasonable range of parameters, one finds that χ is dominantly a linear combination of the $\tilde{\gamma}$ and $\tilde{Z}$ [5.44]. One can then proceed to calculate the relic cosmological mass density of χ's (ρ_χ) which is primarily determined by the $\chi\chi$ annihilation cross section. Comparing with the critical density $\rho_c = 1.88\times 10^{-29} h_0^2\ \mathrm{g\,cm^{-3}}$ [where $h_0 = (H/100\ \mathrm{km\,s^{-1}})\ \mathrm{Mpc}^{-1}$ and H is the Hubble parameter] one finds [5.44]

$$\Omega_\chi \equiv \frac{\rho_\chi}{\rho_c} = 2.6\times 10^{-11} h_0^{-2}\left(\frac{T_\chi}{T_\gamma}\right)^3\left(\frac{T_\gamma}{2.8\ \mathrm{K}}\right)^3 N_F^{1/2}\left(\frac{\mathrm{GeV}^{-2}}{ax_f + \frac{1}{2}bx_f^2}\right), \tag{5.10}$$

where N_F is the effective number of relativistic degrees of freedom when the annihilation rate, Γ, satisfies $\Gamma < H$ (i.e., at "freeze-out"). $T_\gamma = 2.8\ \mathrm{K}$ is the present temperature of the microwave background radiation, T_χ is the corresponding relic χ temperature. Here $\langle \sigma v_{rel}\rangle = a + bx$ ($x \equiv T/m_\chi$) is the annihilation rate with $\langle v_{rel}^2\rangle = 6x$; in (5.10), $x_f = T_f/m_\chi$ with T_f being the χ "freeze-out" temperature. To proceed further a and b are then calculated with the result that they depend on two other parameters: $m_{1/2}$, the gaugino mass responsible for SUSY breaking, and λ, the NN^cS^c coupling in the superpotential. For a wide but reasonable range of these parameters (e.g., $100\ \mathrm{GeV} \le m_{1/2} \le 1000\ \mathrm{GeV}$) one finds

$$\Omega_\chi (h_0/0.5)^2 \simeq 2^{0\pm 2}, \tag{5.11}$$

which indicates that χ makes a very substantial contribution to the overall mass density of the universe. m_χ turns out to lie in the range 20–200 GeV from this analysis.

It should be noted that if the dark matter in the galactic halo consists of χ's, elastic scattering with the sun will trap these particles if $m_\chi \gtrsim 6\ \mathrm{GeV}$ [5.45] with an equilibrium maintained by $\chi\chi$ annihilation in the solar interior. Such annihilations could be observable since they lead to high energy prompt neutrinos [5.46] via $\chi\chi \to \mathrm{ff}$, $\mathrm{f} \to \mathrm{f}' + \ell + \nu_\ell$ whose flux is calculable. In the case where χ is mainly a combination of $\tilde{\gamma}$ and $\tilde{Z}$ with $m_\chi \gtrsim 20\ \mathrm{GeV}$, this flux is relatively small in comparison to, say, the $\tilde{\gamma}$ flux in the SUSY extension of the SM.

5.4.3. Cosmological bound on Z_η

In the rank-5 scenario it is possible to derive [5.47] a bound on the mass of Z_η from big bang nucleosynthesis if a number of conditions hold: (1) N, N^c, and S^c get large masses and decouple from the ν, ν^c system, (2) loop corrections do not induce a large mass for ν^c or allow it to decay rapidly. The

most likely possibility here is that ν and ν^c form a (necessarily!) light stable Dirac neutrino. For three generations of stable Dirac neutrinos the effective number of neutrinos (N_ν) is 6, which is in conflict with the well-known limit on N_ν ($\lesssim 4.6$) from big bang calculations of light element abundances [5.48]. Since ν^c is an $SU(2)_L \times U(1)_Y$ singlet, only the couplings to Z_η can be used to speed up its decoupling at the time of nucleosynthesis, hence reducing its relative abundance. In particular the ratio of ν^c to ν decoupling temperatures (T^c and T respectively) is given by

$$(T^c/T)^3 \simeq (M_{Z_\eta}/M_{Z_{SM}})^4 , \tag{5.12}$$

and leads to a bound of $M_{Z_\eta} \gtrsim 400$ GeV [5.47], which is significantly stronger than the others discussed above. The same bound constrains the vev's in this model and potentially the SUSY breaking scale $M_{1/2} > 450$ GeV [5.22, 5.44]. Using the analysis of the previous subsection, one finds $m_\chi \gtrsim 70$ GeV and $\Omega_\chi (h_0/0.5)^2 \gtrsim 1.4$ which agrees remarkably well with inflation and observation. One must remember the two caveats above, neither of which may apply in a realistic model that incorporates an explanation of light neutrinos masses, allows for unstable neutrinos, or additional Z bosons.

5.4.4. Magnetic monopoles

't-Hooft–Polyakov monopoles can occur in superstring-inspired models when the four-dimensional gauge group G which remains after symmetry breaking by Wilson lines is further broken by vev's. Such monopoles do not carry any $SU(3)_C$ color magnetic fields if G explicitly contains an $SU(3)_C$ factor, e.g., $G = SU(3)_C \times SU(3)_L \times SU(3)_R$. The mass of the monopole (m) then depends on the intermediate scale (M_G) at which G is broken, $m \sim M_G/\alpha_G$, with α_G being the coupling constant of G. If G contains a group larger than $SU(3)_C$ in which $SU(3)_C$ is embedded [e.g. $SU(4)_C$], the breaking of G then produces monopoles which also carry color quantum numbers.

Monopole production in these models is somewhat different from that in normal GUT scenarios [5.32, 5.38]. The effective potential of the field(s) ϕ responsible for SSB of G, including finite temperature corrections, is typically of the form ($T \gg |\phi|$)

$$V \sim -M_s^2|\phi|^2 + \lambda|\phi|^{10}/M_c^6 + \sigma T^2|\phi|^2 , \tag{5.13}$$

with $M_s \sim 1$ TeV being the SUSY-breaking and $M_c \sim 10^{18}$ GeV the compactification scale. For $T \gg M_s$, ϕ sits at the local minimum ($\phi = 0$), G remains unbroken, and no monopoles exist. But, as T approaches its critical value $\sim M_s$, the overall $|\phi|^2$ term goes negative causing symmetry breaking so that the origin is no longer a minimum of the potential. Then ϕ rolls down toward the new minimum at $\langle\phi\rangle \sim M_G$, creating large quantities of entropy by performing damped oscillations around this minimum thus diluting the initially large number of monopoles produced. Monopoles only begin to form when ϕ moves away from the origin at $T \sim M_s$. The resulting relative monopole density, after taking into account annihilations (from which there is little, if any, effect [5.38, 5.49], see also ref. [5.32]) and the growth of the scale factor, is found to be roughly

$$r \sim 10^{-30}(M_G/10^{15}\ \text{GeV})^{-3} , \tag{5.14}$$

whereas initially $r \sim 10^{-2}$. The predicted monopole flux for $M_G \sim 10^{15}$ GeV is not far from the Parker bound: $\sim 10^{-(15\text{–}16)}\ \text{cm}^{-1}\,\text{s}^{-1}\,\text{sr}^{-1}$.

5.4.5. Inflation and cosmic strings

String theories may provide a novel way of producing inflation which is not present in the usual SUSY–GUT approach, i.e., the transition from ten to six plus four dimensions could involve an inflationary phase. Shafi and Wetterich [5.50] have investigated such a class of models in $4+D$ dimensions with a generic gravitational action containing several a priori undetermined parameters. In early times the scale of the D-dimensional internal space L and the usual scale factor R are comparable, but in later times solutions with small L and Friedman-type cosmologies involving R were found. The asymmetric evolution can be due to inflation; a value of L different from its ground state value, L_0, induces a positive cosmological constant and an exponential growth in R. Such a scenario would then not only provide inflation in order to deal with known cosmological problems but would also explain the disparity between L and R. More realistic models of this kind would need to be constructed.

The breaking of additional U(1) factors in superstring-inspired models produces topologically stable cosmic strings which, if the breaking scale is sufficiently large, may be relevant for galaxy formation [5.51]. Thus, unlike the situation in normal GUTS, the appearance of cosmic strings is not tied to the simultaneous existence of magnetic monopoles. As in the case for monopoles, however, the phase transition giving rise to cosmic strings takes place at temperatures close to the weak scale so that cosmic strings could be created after the end of an inflationary period. One also finds that cosmic strings in superstring-inspired models turn out to be superconducting [5.51] which, as pointed out by Witten [5.52], may lead to a number of astrophysical implications.

5.4.6. Baryogenesis

Scenarios for baryogenesis in superstring-inspired models necessarily involve an intermediate scale, M_I, if one forbids baryon number violating terms in the superpotential. One of these scenarios for generating a net baryon number is the Affleck–Dine mechanism [5.27]. This involves the decays of initially large classical slepton field configurations sitting away from the origin along the flat directions of the potential after the inflationary epoch.

In an alternate scenario, models with intermediate scales can lead to low energy ($<M_p$) baryogenesis which is closer in spirit to the conventional out-of-equilibrium decay of heavy particles in GUTs. The details of models such as these are somewhat sensitive to M_I and the nature of the group G after Wilson line breaking of E_6 [1.15]. In these scenarios it is the decays of the heavy exotic fermions (h, E, N, N^c and S^c) which are baryon number, C, and CP violating that produce the baryon asymmetry. Such terms can appear in the superpotential (W) and are in agreement with experimental limits on proton stability provided, e.g., h is reasonably massive ($\sim 10^8$ GeV or so). It is also possible to generate such interactions from higher-dimensional non-renormalizable terms in W. In almost all models of this kind [5.53] the baryon asymmetry is generated at temperatures of at most a few TeV (and perhaps somewhat smaller). Depending on the magnitude of the intermediate scale, M_I, the baryon asymmetry is generated either before or after the associated phase transition and determines how easy it is to construct a reasonable model. Generally, for low M_I, a model producing the right amount for the baryon asymmetry is easy to construct [5.53]. The model needs a mechanism to minimize the dilution of this asymmetry from the entropy produced by the decaying of the scalar field which induces the intermediate scale. As M_I is increased this becomes more difficult to arrange although successful models have been constructed [5.53]. It is also possible, in some models, to link the scale M_I to the new large scale needed to solve the neutrino mass problem [5.54]. Physics at the M_I scale could also induce other new phenomena such as neutron–antineutron oscillations [5.54] with time scales, accessible to future experiments.

5.5. The top-quark mass and the fourth generation

Superstring-inspired models based on E_6 can lead to predictions on the mass of the t-quark and constraints on the existence of a fourth generation of fermions. We briefly overview these possibilities in this section. As will be seen from the discussion below, these results are extremely model dependent.

5.5.1. The top-quark mass

The top (t) quark together with the usual neutral Higgs boson are the two essential pieces necessary to complete the SM. As we will review here, several groups of authors have tried to determine the mass of the t-quark (m_t) from E_6 superstring-inspired models. In some scenarios, m_t turns out to be quite small (as low as $\simeq$30 GeV), whereas in others m_t is found to be large ($\simeq$220 GeV). In the latter case this slightly over-saturates the bound on m_t from the ρ parameter [2.13, 2.14] so that additional new physics (Z–Z′ mixing, exotic fermion loops, etc.) needs to be included to maintain consistency with low energy neutral current data and the values of the W and Z masses (see the discussion in section 2 above). One might wonder if such small values of m_t ($\simeq$30 GeV) are still allowed given the recent bounds on m_t from B_d–$\bar{B}_d$ mixing (for a critical analysis see ref. [5.55]) and the direct search limits from UA1 ($m_t >$ 44–56 GeV) [2.33, 5.56].

In the case of B_d–$\bar{B}_d$ mixing, it is usually claimed that within the three-generation SM large mixing can only occur for large m_t ($\gtrsim$80–100 GeV). When matrix element uncertainties are taken into account and all parameters are pushed to the very end points of their allowed ranges then m_t can be as low as 40–60 GeV. Although somewhat smaller values of m_t may be possible they are highly unlikely given the data from the ARGUS Collaboration [5.57]. The UA1 bound also seems difficult to avoid in the three-generation SM. However, in extensions of the SM these bounds can be evaded quite easily. The UA1 search assumes a significant branching fraction for semileptonic t decay: $t \to bW^* \to b\ell\nu_\ell$ as is reasonable in the SM. If, however, there exist charged Higgs scalars (as in the SUSY-SM or E_6 models) such that $m_t > m_H + m_b$ then the decay $t \to H^+ b$ is by far dominant so that the semileptonic branching fraction is suppressed. The t-quark in this scenario could be much lighter and still have evaded the UA1 search. In addition, such a light charged scalar ($m_H \sim 25$–30 GeV) could make a substantial contribution to B_d–$\bar{B}_d$ mixing, thus compensating for the light t-quark [5.58]. Four generation extensions of the SM can also yield large B_d–$\bar{B}_d$ mixing with a light t-quark [5.59] but cannot evade the UA1 bound. Thus, if light charged scalars are present, as may be the case in some superstring-inspired models, the only limit on m_t comes from direct searches in e^+e^- annihilation at TRISTAN [5.60] which yield $m_t > 28$ GeV.

Predictions/bounds on m_t in superstring-inspired models arise from the consideration of the evolution of the t-quark Yukawa coupling and its role in electroweak symmetry breaking, i.e., the soft SUSY breaking mass terms of the relevant Higgs fields can be rendered negative by the large radiative corrections due to Yukawa couplings. Nakamura et al. [5.61] have considered the possibility that m_t can be large ($\sim$200 GeV) in a consistent superstring-inspired minimal rank-5 model. The relevant part of the superpotential (involving only the third generation) is given by

$$W = \lambda_t t^c q N + \lambda_h h h^c S^c + \lambda_N N N^c S^c \,, \tag{5.15}$$

and is supplemented by additional soft SUSY breaking terms, mass terms for the quarks, sleptons, and gauginos, as well as the additional W terms

$$W'_{\text{soft}} = \lambda_t A_t \tilde{t}^c \tilde{q} N + \lambda_h A_h S^c \tilde{h} \tilde{h}^c + \lambda_N A_N \tilde{N} \tilde{N}^c S^c + \text{h.c.} \tag{5.16}$$

These authors constrain the $SU(3)_C \times SU(2)_L \times U(1)_Y \times U(1)_\eta$ coupling so that at the compactification scale $\alpha_3 = \alpha_2 = \alpha_1 = \alpha_\eta$ and $\lambda_i^2/4\pi \lesssim 1$; a common value of the $A_i (= A)$ is assumed, as well as a common mass scale for the gauginos $\sim$1 TeV. They then find that stable vacua exist, which are consistent with the above constraints and the experimental value of $\sin^2\theta_w$, that lead to large values of $m_t \sim 200$ GeV. This is quite different from what happens in minimal SUSY versions of the SM, which generally demand a light t-quark ($\lesssim$70 GeV) in order to stabilize the scalar potential [5.62]. The extra fields as well as new D terms naturally present in the rank-5 model produce additional quartic couplings stabilizing the potential and allowing for a heavy top quark. The vev's in this model are highly ordered, $\langle \tilde{S}^c \rangle^2 \gg \langle \tilde{N} \rangle^2 \gg \langle \tilde{N}^c \rangle^2$. A similar analysis by Cohen et al. [5.63], but with different constraints, suggests that a more natural value for m_t is substantially smaller, $\sim$55 GeV. In both of these analyses, no intermediate scale is assumed to exist in order to simplify the calculation.

Ibañez and Mas [5.14] consider the constraints on m_t from consistent radiative gauge symmetry breaking within the context of different effective rank-5 and rank-6 models. These authors stress the importance of the $A_N \neq 0$ terms in W' and noted that other authors [5.63] who have neglected such terms have found radiative symmetry breaking problematic. In the rank-5 model, these authors only find consistent solutions for radiative breaking when $\langle \tilde{N}^c \rangle < \langle \tilde{N} \rangle$ and $50 \lesssim m_t \lesssim 70$ GeV where the lower bound on m_t comes from the existing bound on the Z_η mass. In the effective rank-4 models which leave only the SM at low energies, these same authors show that the opposite situation, $\langle \tilde{N}^c \rangle > \langle \tilde{N} \rangle$ and $m_t \gtrsim 70$ GeV, holds.

Another analysis of this kind by Volkes et al. [5.64] studied the parameter space of A, λ_t, λ_N, and λ_h using the RGE for the gauge couplings, gaugino masses, trilinear A terms, and Yukawa couplings. These authors assume $M_x = 2 \times 10^{16}$ GeV with $Z_\eta > 130$ GeV within the rank-5 model and find that light top quarks ($m_t \simeq 30$–40 GeV) are consistent with their assumptions and constraints.

Pulido [5.65] has analyzed the rank-6 left–right symmetric model, $SU(3)_C \times SU(2)_L \times SU(2)_R \times U(1)_L \times U(1)_R$, for bounds on m_t and finds that $m_t \lesssim 46$ GeV. In this analysis the vanishing of tree level neutrino masses and proton decay (i.e., B-violating terms) reduces the superpotential to only four terms by means of a discrete symmetry [5.66]. The fields h^c and d^c as well as H and L are allowed to mix by an a priori undetermined amount. In order to break the symmetry down to $U(1)_{em}$, $\langle \tilde{\nu}^c \rangle$, $\langle \tilde{S}^c \rangle$, $\langle \tilde{N} \rangle$, and $\langle \tilde{N}^c \rangle$ all need to be non-zero. The bound on m_t originates from a comparison of the relative magnitudes of the lepton number violating to lepton number conserving terms in the superpotential resulting from the above mixing. If ϕ measures the amount of H–L mixing then Pulido finds

$$m_t = m_b/\eta \sin\phi \,, \tag{5.17}$$

where $\eta \equiv \langle \tilde{N}^c \rangle / \langle \tilde{N} \rangle$ and can be bounded in this model by consideration of the masses of the fermions in the second generation. In addition, $\sin\phi$ is found to be confined to the range $1/\sqrt{2} < \sin\phi < 1$. Putting the various results together and using the RGE for the running t-quark mass the author finds the above quoted result and the bound $0.094 \leq \eta \leq 0.15$. He also shows that m_t in this range is consistent with the radiative symmetry breaking within the context of this model.

It is quite clear from the above survey that considerations in the above analysis are still quite far from making definitive predictions about the t-quark mass.

5.5.2. Fourth generation fermions

The existence of a possible fourth generation of fermions is more problematic in E_6 superstring-inspired models than it is in the SM or its SUSY extension. The reason for this is easily seen by

considering the one-loop beta function (β_1) for QCD in such models. In the SM, $\beta_1 \sim 11 - \frac{2}{3}n_g$, so that the number of generations (n_g) can be quite large before asymptotic freedom (AF) and (possibly) perturbative unification (PU) are lost. Above the SUSY scale, where all colored particles fully contribute to β_1, one finds $\beta_1 \sim 9 - 2n_g$ so that $n_g = 4$ is still consistent with AF and PU. In E_6 superstring-inspired models, the existence of an h exotic (and its SUSY partner $\tilde{h}$) in each generation modifies β_1 above the intermediate scale (M_I) responsible for the $\tilde{h}$ (h) mass; here $\beta_1 \sim 9 - 3n_g$ so that for $n_g > 3$ one loses AF and possibly jeopardizes PU as well. Of course, to be truly reliable, for such small values of β_1, a two-loop analysis is probably required but one begins to see that the $n_g = 4$ situation is perhaps not as trivial as it is in the SM.

In the analysis of Drees, Enqvist, and Nanopoulos [5.67], these authors considered the constraints imposed on M_I in a four-generation model assuming: (1) the unification scale M_x is not far from the Planck scale, i.e., $M_x \geq 10^{17}$ GeV; (2) $\Lambda_{\overline{MS}} = 200 \pm 50$ MeV; (3) $\sin^2\theta_w(M_W) = 0.227 \pm 0.010$; (4) two-loop corrections due to heavy quark Yukawa couplings are small; (5) the relevant gauge groups above the scale M_I are of one of the forms

$$\text{(a)}\ \ SU(3)_C \times SU(2)_L \times G', \qquad \text{(b)}\ \ SU(3)_C \times SU(3)_L \times G', \qquad \text{(c)}\ \ SU(4)_C \times SU(2)_L \times G', \tag{5.18}$$

with G' being different combinations of U(1) and SU(2) factors; (6) the analysis was performed at the two-loop level but contributions from U(1) factors were neglected since their contributions are small; (7) the scale (M_s) for which SUSY partners begin to make full contributions to the RGE is taken to lie in the range $M_W \leq M_s \leq 1$ TeV. For models of type (a) these authors find that M_I must be in the range $\gtrsim 10^{13-14}$ GeV, whereas in cases (b) and (c) $M_I \gtrsim 10^{11}$ GeV in order to obtain PU. In none of the cases is the simple scaling law $M_I \simeq (M_W M_x)^{1/2}$ allowed by the constraints, and typical values of the parameters lead (if $M_x \simeq M_p$ is assumed) to large (10^{13-14} GeV) values of M_I in all cases.

This analysis has, more recently, been extended by the same authors [5.68] to a variety of other models. In SUSY E_6 models (so long as $M_I \gtrsim 10^6$ GeV) the usual constraint, which arises from the demand that the Yukawa couplings remain perturbative up to M_x [1.13, 5.67], on the mass of the fourth generation $Q = 2/3$ $(-1/3)$ quark t′ (b′) is found to continue to hold if

$$m_{t'} \lesssim 190\text{–}210\ \text{GeV}, \tag{5.19}$$

with the range depending on whether $m_{b'} \ll m_{t'}$, or $m_{b'} \simeq m_{t'}$. The authors conclude that it is perhaps quite difficult in E_6 models to satisfy all of the above constraints as well as cosmological limits on M_I ($\lesssim 10^{10}$ GeV) if a fourth generation exists. However, bounds on M_I from cosmology, in particular baryogenesis, are still somewhat controversial [5.32], so that probably the most one could conclude from these analyses is that M_I should be quite high ($\gtrsim 10^{13}$ GeV) if a fourth generation exists, at least for the models so far examined.

5.6. More on left–right symmetric and other extended electroweak models

In this sub-section, we briefly survey some of the more technical implications of left–right symmetric (LRS) and other extended electroweak models that arise from superstring-inspired E_6.

5.6.1. LRS models

These models have a natural origin in E_6 which is easily seen by considering the following breaking patterns:

$$\begin{aligned}
&\text{(a)}\quad E_6 \to SO(10) \to SU(4)_C \times SU(2)_L \times SU(2)_R \to SU(3)_C \times SU(2)_L \times SU(2)_R \times U(1)\,, \\
&\text{(b)}\quad E_6 \to SU(3)_C \times SU(3)_L \times SU(3)_R \to SU(3)_C \times SU(2)_L \times SU(2)_R \times U(1)_L \times U(1)_R \\
&\qquad \to SU(3)_C \times SU(2)_L \times SU(2)_R \times U(1)\,.
\end{aligned} \tag{5.20}$$

Note that the so-called rank-6 or extended LRS model with a $U(1)_L \times U(1)_R$ factor only arises in pattern (b). (Note that in what follows, we will not discuss the alternative LRS model since it has already been discussed at some length in section 2.) Occasionally the $SU(3)_C \times SU(2)_L \times SU(2)_I \times U(1)_L \times U(1)_R$ subgroup of E_6 is also considered to be among the LRS gauge groups. As discussed above in section 2, the $SU(2)_I$ generators are orthogonal to the electric charge Q and the superpotential of this model is similar to that of the LRS model. Much of the analysis of LRS models has been done by two groups, Pulido [5.65, 5.66, 5.69] and del Aguila, Gonzalez, and Quiros [5.70]. We will follow the work of these authors in the following summary (see also ref. [5.71]).

Pulido analyzes the mixing of the h and d quarks in the $SU(2)_I$ model and finds that such a scenario is internally inconsistent owing to the sizes of the required vev's and dismisses the model from further consideration. It should be noted, however, that a rank-5 version of this model may arise in which $\langle \tilde{\nu}^c \rangle = 0$ allowing for internal consistency due to different quantum number assignments for the exotics.

A similar analysis for the usual rank-6 LRS model does, however, lead to a consistent solution for the h–d mixing matrix, with a mixing (θ) between these two states of order $\theta \sim 10^{-2} M_W / M_I$, with M_I being the breaking scale of the rank-6 LRS model. In addition, this model, when combined with appropriately chosen discrete symmetries, can lead to a light neutrino mass and a consistent pattern of radiative breaking. An RGE analysis of the model leads to reasonable values of $\sin^2\theta_w$ and values of M_x close to the Planck scale. In a separate work, the same author extends his analysis to include the groups $SU(3)_C \times SU(2)_L \times SU(2)_R \times U(1)_S$ and $SU(4)_C \times SU(2)_L \times SU(2)_R \times U(1)$, and the scale M_I is argued to be rather low ($\lesssim$ few $\times 10^4$ GeV) in all cases. For both $SU(3)_C \times SU(2)_L \times SU(2)_R \times U(1)_S$ and $SU(3)_C \times SU(2)_L \times SU(2)_R \times U(1)_L \times U(1)_R$, including mixing between the ordinary and exotic fermions (h being a quark and N, E being leptons), the couplings of the fermions to the SM Z (i.e., Z_1) are found not to be in agreement with data in the heavy M_2 limit, although $\sin^2\theta_w$ comes out correctly. The origin of this problem, as one might guess, is the ordinary–exotic mixing. The group $SU(4)_C \times SU(2)_L \times SU(2)_R \times U(1)$ is found to lead to too large a value of $\sin^2\theta_w$ ($\simeq 0.291$) for such small values of the scale M_I in the case of three generations of fermions. Better agreement is obtained for the case of four generations. It would appear that many of these conclusions may be altered in a model without ordinary–exotic mixing.

Del Aguila et al. [5.70] address the problem of lowering the value of $\sin^2\theta_w$ obtained in LRS superstring-inspired models so that agreement with data is obtained. They emphasize that in almost any minimal model of this kind it is difficult to get good values for $\sin^2\theta_w$ with the unification scale at or below the Planck scale, M_p, unless additional fields are added or additional discrete symmetries are imposed. Their philosophy is that the absence of true unification due to the $\sin^2\theta_w$ constraint implies a spreading of the gauge couplings near M_p, perhaps due to detailed string dynamics (of which we are presently ignorant). Taking the values of $\alpha_s(M_W)$ and $\sin^2\theta_w(M_W)$ as input together with the assumption

of the turning on of SUSY contributions to the RGE at 1 TeV [and the assumption that the effective electroweak group above this scale is $SU(3)_C \times SU(2)_L \times SU(2)_R \times U(1)$] they perform a complete RGE analysis of a large number of E_6 subgroups which break to $3_C 2_L 2_R 1_{B-L}$ at a scale M_I and can arise from Wilson line breaking. M_I is thus free to lie anywhere between 1 TeV and M_p. These authors find that the splitting of the couplings at M_p, $s = \max|\alpha_L - \alpha_j|$ is comparable to the values of the couplings themselves and conclude that string renormalization effects at this scale should thus be of order unity.

5.6.2. General extended models

Del Aguila et al. [5.70] have, in a very impressive work, completely analyzed by a one-loop RGE program all superstring-inspired E_6 models with one additional neutral gauge boson at low energy, i.e., those with an additional U(1) factor. This U(1) group is assumed to break to the SM at about 1 TeV. Below the compactification scale ($\sim M_p$) the relevant E_6 subgroup is obtained by Wilson-loop breaking. If the Wilson-loop phase is abelian, the resuting rank-6 subgroup must be further broken down to a rank-5 subgroup at some intermediate scale, $1\,\text{TeV} \ll M_I < M_p$. For non-abelian loop phases the resulting rank-5 group is assumed to be broken at $\simeq 1$ TeV as mentioned above. Perturbative unification ($\alpha_i < 1$), $\sin^2\theta_w(M_Z) = 0.230 \pm 0.005$, $\alpha_s(M_Z) = 0.12$, and $10^{10}\,\text{GeV} \leq M_I \leq M_x$ (with M_x being the unification scale: $10^{17}\,\text{GeV} \leq M_x \leq 10^{19}\,\text{GeV}$) are assumed by these authors in their analysis. SUSY contributions to RGE are also assumed to turn on at a scale $M_s = 1$ TeV. In the breaking of rank-6 groups down to rank-5, either $\langle \tilde{S}^c \rangle \neq 0$ *or* $\langle \tilde{\nu}^c \rangle \neq 0$ is assumed but *not* both since the second vev is assumed to be necessary at the ~1 TeV level to recover the SM. Models which lead to rapid proton decay through dimension-four or dimension-five operators (unless M_I is large) and/or give large Dirac neutrino masses are eliminated. The matter content at M_x is assumed to be n_g complete **27**'s and n_i ($\boldsymbol{R}_i + \bar{\boldsymbol{R}}_i$) mirror representations which appear in the decomposition of $\mathbf{27} + \overline{\mathbf{27}}$ under the various E_6 subgroups. The only surviving groups at the TeV scale are found to be $SU(3)_C \times SU(2)_L \times U(1)_Y \times U(1)$, $SU(3)_C \times SU(3)_L \times U(1)$ and $SU(3)_C \times SU(2)_L \times SU(2)_R \times U(1)$, and the particle content in each case depending on its parent group was determined. Additional properties of the Z-boson mixing matrix were also calculated in each case which follow from the renormalization of new coupling constants and new gauge boson mixing angles. Out of the huge class of possible models a reasonable fraction remains viable after all the various constraints are imposed. In some cases the results may be somewhat questionable since rather large couplings due to the rather weak $\alpha_i < 1$ constraint occur. A two-loop analysis and a more careful study including, e.g. threshold effects may be required. The results are, however, quite lengthy and exhaustive and the reader is referred to the original reference [5.70] for details about any specific model.

It is clear from the above discussion that analyses of extended electroweak models in E_6 superstring-inspired models will continue for some time.

6. Summary and conclusions

In this section we summarize some of the basic implications of superstring-inspired E_6 models for low-energy phenomenology and the possible signals for these kinds of extensions to the SM.

Most, if not all, of the various models discussed in the previous sections have a number of basic features in common: (1) the existence of at least one (and possibly two) new neutral gauge boson(s), i.e., the breaking of E_6 at the compactification scale leads to electroweak gauge groups larger than that of the SM. If the extension of the SM electroweak group contains an SU(2) factor, new charged gauged

bosons may also be present. As we have seen, new gauge bosons in the few hundred GeV mass range may be probed at LEP/SLC and the Tevatron either by their direct production or their indirect effects on SM processes, such as forward–backward asymmetries in e^+e^- annihilation. New limits on (or discoveries of) these types of particles can be expected in the near future from both kinds of machines. For heavier gauge bosons, up to several TeV in mass, direct discovery awaits new hadron colliders (such as the SSC or LHC) or new e^+e^- linear colliders with $\sqrt{s} = 1$ TeV or higher. As we have seen e^+e^- machines are especially good at probing for new neutral gauge bosons with masses several times larger than their center-of-mass energies, although the "reach" of such machines is model (as well as machine) dependent.

Another common feature (2) of E_6 models is the existence of at least three generations of exotic, vector-like fermions which have definite color, weak isospin, and electric charge quantum numbers, and whose masses are set by the same vev(s) which determine the mass(es) of the new gauge boson(s). Mirror generations of these exotics from $\overline{\mathbf{27}}$'s may also be present. The signals for these exotic fermions are not unique since the superpotential allows several possible assignments of B, L, and R-parity quantum numbers to these states consistent with tree-level proton stability. Although most of the production mechanisms for these states depend only on their transformation properties under the low-energy gauge group, specific assignments of B, L, and R-parity allow for exciting new possibilities via Yukawa terms in the superpotential (W). The decay signatures are, in particular, most sensitive to these assignments as are the contribution of these new particles to rare process (via loops) involving ordinary quarks and leptons. Particular B, L and R-parity assignments are usually the result of a discrete symmetry imposed on W but can also result from particular extensions of the gauge symmetries. In the latter case (for all models so far examined) the color triplet exotics are leptoquarks with negative R-parity while the color singlet fermions do not carry B or L quantum numbers and also have negative R-parity. For exotics with masses in the 30–200 GeV range, LEP and the Tevatron should be able to see them directly for all possible quantum number assignments. For higher masses, the SSC or LHC can probe the exotic color-triplet masses out to several TeV, while high energy e^+e^- colliders are better suited for the study of color-singlet states unless a Z' exists in the right mass range to boost color-singlet production cross sections at hadron colliders. The production of such exotics is the true hallmark of E_6 theories since other extensions of the SM can lead to new gauge bosons, e.g. SO(10), but do not contain all of the exotic fermions.

(3) Since all E_6 superstring-inspired models have $N = 1$ SUSY broken at low energies, we should expect to observe all of the partner states contained within the SUSY version of the SM in addition to the SUSY partners of the exotic fermions, new gauge bosons, and new Higgs bosons. In some models, depending on quantum number assignments, the SUSY partners of the iso-doublet, color singlet exotics can act as the usual pair of Higgs doublets responsible for W and Z masses. As is the case for their ordinary partners, these SUSY states have many production mechanisms which are independent of the B, L and R-parity quantum number assignments, but their decay signatures depend critically upon them. In addition to collider searches, these states can also contribute to a number of rare processes which may signal their existence before they are actually produced. If these states are not too heavy ($\lesssim$ a few TeV) they should be observable at the SSC, LHC, and new high energy e^+e^- linear colliders. In the case where the color-triplet exotics have leptoquark quantum numbers, ep machines are especially suited to the production of their SUSY partners (which have positive R-parity) for masses almost as large as the kinematic limit.

(4) The Higgs sector of the SM (or SUSY-SM) is extended to include at least two $SU(2)_L$ doublets and one or more $SU(2)_L$ singlets. As discussed above, these fields can be the SUSY partners of one of

the generations of the colorless $B = L = 0$ exotic fermions, but this depends on the particular assignment of their quantum numbers. Though this sector of the theory is greatly extended in the comparison to the SM, the imposition of SUSY and further discrete and/or gauge symmetries on the superpotential severely restricts the number of independent parameters. Even so, analyses of the scalar mass spectrum and couplings are still quite complex since there remain at least five independent parameters. The physical spectrum of Higgs fields in the minimal model consists of a singly charged state, one neutral pseudoscalar, and three neutral scalars and their decay signatures depend critically on the ordering of their masses with respect to each other as well as the gauge bosons. In general, the widths of the Higgs fields in these models are somewhat narrower than one might expect based on the SM, and, in many cases, non-SM decay channels tend to dominate. Perhaps one of the best signals for the extension of the Higgs sector is the existence of charged scalars which may provide clear signatures at colliders. The production rates for E_6 Higgs bosons at hadron colliders is quite dependent on their mass spectrum; lower mass Higgs have event rates comparable to the SM via the gluon fusion production mechanism or Z_2 decays, while the gauge boson fusion processes, which give large production rates for higher mass Higgs in the SM, are of diminished importance in E_6 models. In addition to the more general properties listed above, we have seen that several specific models discussed in the previous sections can lead to very distinct signals which reveal their origin uniquely within the SUSY-E_6 context, e.g., Ma's alternative left–right model.

It seems clear that the signals for superstring-inspired E_6 models at low energy, while model dependent, are many and will hopefully be observed directly at colliders or indirectly via the observation of rare processes at rates greater than those predicted by the SM. We encourage the continued exploration, both theoretically and experimentally, of the phenomenological implications of superstring-inspired E_6 models.

Acknowledgements

We would like to thank our colleagues V. Barger, G. Belanger, F. Cornet, G. Couture, N.G. Deshpande, D. Dicus, M. Drees, G. Eilam, S. Godfrey, J. Gunion, P. Langacker, E. Ma, S. Nandi, J. Ng, S. Pakvasa, and K. Whisnant for suggestions, helpful interactions, fruitful collaborations, and for providing us with figures that appear in this review. We also thank S.S.C. Willenbrock for continuously urging us to finish this report. J.H. would like to thank her husband and T.R. would like to thank his wife for their patience while this report was written. The authors would also like to thank the Center for Particle Theory, University of Texas, Austin, and TGR thanks the Phenomenology Institute at the University of Wisconsin, Madison, for their hospitality during the course of this report.

This work was supported in part by the University of Wisconsin Research Committee with funds granted by the Wisconsin Alumni Research Foundation, and in part by the U.S. Department of Energy under contract DE-AC02-76ER00881 and W-7405-Eng-82, Office of Basic Science (KA-01-01), Division of High Energy and Nuclear Physics. The work of JLH was also supported in part by the American Association of University Women and ZONTA International.

Appendix. New gauge bosons at high energy colliders: recent results

The purpose of this appendix is to summarize some new results on the production of new gauge bosons from E_6 superstring-inspired models at colliders.

A.1. Search limits at e^+e^- and hadron colliders

In this section we will discuss the search limits for new neutral gauge bosons, Z', at e^+e^- [A.1] and hadron colliders [A.2] within the context of the effective rank-5 model (ER5M), the ALRM, and the LRSM for purposes of comparison. We will also discuss the search limits at hadron colliders for the W_R in the ALRM [A.2]. Z–Z' mixing will be neglected in the discussion below since for such heavy Z' bosons of interest to us here this mixing is constrained to be extremely small.

In setting Z' discovery limits at hadron colliders we will initially assume $N = 5$ events in either lepton channel (e^+e^- and $\mu^+\mu^-$) as setting the limit and return later to examine what happens for larger values of N. Clearly, such search limits are quite sensitive to the u and d quark Z' couplings as well as its leptonic branching fraction (B_ℓ) which, as we have already seen in section 2, is very sensitive to n_g. For $n_g = 0$, the search limits can be found for the various models in table A.1 and figs. A.1a,b for a number of different hadron colliders (the machine parameters for three possible Tevatron upgrades and two possible SSC luminosities are also listed in table A.1). We only plot the range $-90° \leq \theta \leq 90°$ since $\theta \to \theta + 180°$ leaves these search limits unaltered. Note that the "reach" of all these machines is greater for the LRSM and the ALRM than in the ER5M case since the former have stronger couplings. What happens when $N \neq 5$ and/or $n_g \neq 0$? Table A.2 shows the results of these variations. Note that the effect of increasing N to 10 for $n_g = 0$ is similar to increasing n_g to 3 for $N = 5$.

In e^+e^- annihilation the situation is somewhat different. Here we can search for Z' bosons with masses $> \sqrt{s}$ by looking for indirect effects such as modifications of production cross sections and the various asymmetries discussed in section 2. In the analysis below we will assume that $\phi = 0$ (since Z' is so heavy), neglect QCD radiative corrections, and assume that 100% longitudinal e^- beam polarization is available. For fixed $\sqrt{s}$, we can ask for which values of M_2 the shift in the asymmetries ($\delta A_{FB}, \delta A_{LR}$) or cross section ($\delta\sigma/\sigma$) away from their SM values will be larger than 1σ (or 2σ) in a given model. These results will, of course, depend on the choice of final state fermion, as well as the machine parameters which we will take from the SLAC "Red-Book" study [A.3]. Hence we assume 1000 (6250) events of each flavor at $\sqrt{s} = 1.0$ (0.4) TeV. The results of this investigation (at 1σ) can be seen in table A.3 for the LRSM and the ALRM and in figs. A.2 and A.3 for the case of the ER5M for $\sqrt{s} = 0.4$ and

Table A.1
Z' search limits in the ER5M, LRSM, and ALRM for $n_g = 3$ and/or $N = 10$ for various hadron colliders. The Z' masses are in GeV (TeV) units for the Tevatron (SSC)

machine	$\mathcal{L}$ (pb^{-1})	model	$N = 5$ $n_g = 3$	$N = 10$ $n_g = 0$	$N = 10$ $n_g = 3$
$p\bar{p}$ (2 TeV)	10^2	ER5M	515–640	575–655	445–565
		LRSM	685	680	610
		ALRM	760	795	685
$p\bar{p}$ (3 TeV)	30	ER5M	480–655	595–675	400–565
		LRSM	710	705	615
		ALRM	810	860	700
pp (2 TeV)	10^3	ER5M	525–625	585–630	475–575
		LRSM	645	645	595
		ALRM	685	710	635
SSC	10^4	ER5M	5.35–7.20	6.35–7.20	5.05–6.35
		LRSM	7.50	7.40	6.65
		ALRM	8.05	8.45	7.15
SSC'	10^5	ER5M	8.15–10.05	9.30–9.50	7.25–9.20
		LRSM	10.45	10.40	9.50
		ALRM	11.15	11.60	10.20

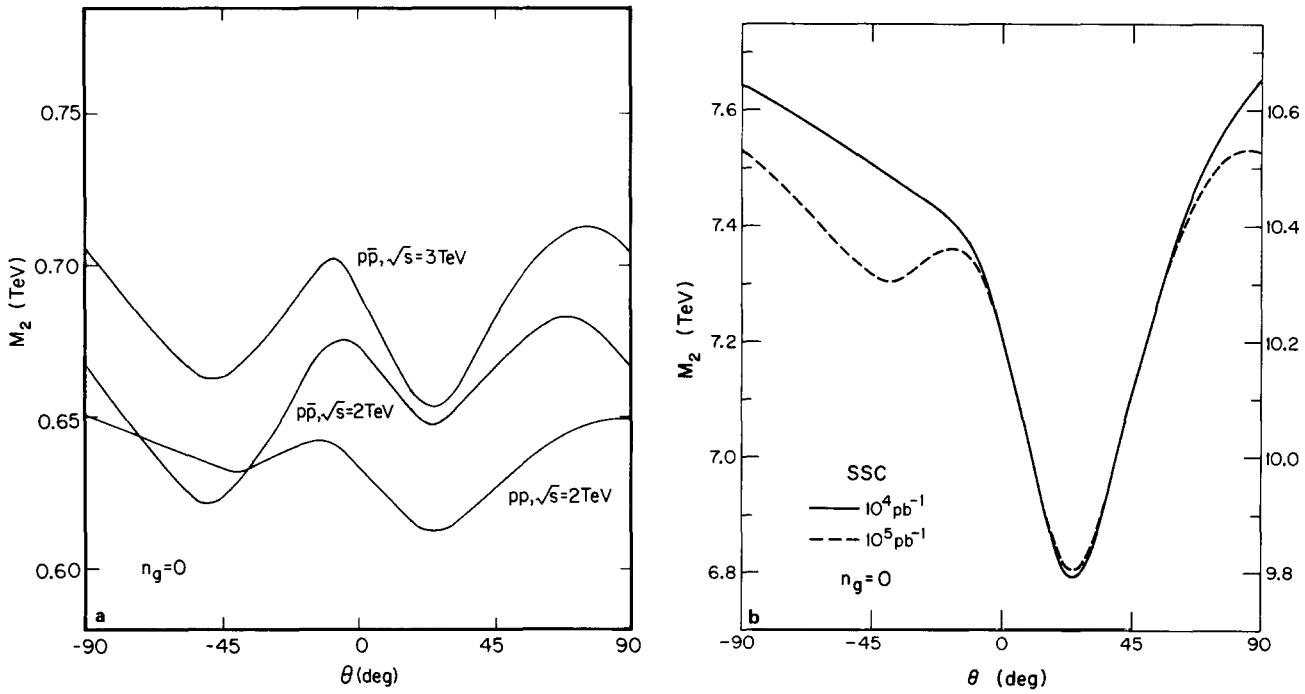

Fig. A.1. Z′ search limits for the ER5M with $N = 5$ and $n_g = 0$ as a function of θ for (a) the Tevatron and (b) the SSC. For 10^4 (10^5) pb^{-1} the left (right)-handed scale should be used.

Table A.2
Z′ search limits and A_{FB}^{ℓ} values in the LRSM and ALRM for the various hadron colliders. In calculating A_{FB}^{ℓ} we take $M_{Z'}$ (= M_2) to be 450 GeV (3 TeV) for the Tevatron (SSC). $N = 5$ events and $n_g = 0$ are assumed. Z′ masses are in units of GeV (TeV) for the Tevatron (SSC)

	$\mathscr{L}$	Z′ limit		A_{FB}^{ℓ} limit	
machine	(pb^{-1})	LRSM	ALRM	LRSM	ALRM
pp $\sqrt{s} = 2$ TeV	10^3	695	760	0.123	−0.230
p$\bar{p}$ $\sqrt{s} = 2$ TeV	10^2	750	865	0.205	−0.351
p$\bar{p}$ $\sqrt{s} = 3$ TeV	30	810	970	0.199	−0.344
SSC	10^4	8.30	9.40	0.103	−0.205
SSC′	10^5	11.35	12.55	0.103	−0.205

Table A.3
Indirect search limits on the Z′ mass (in TeV) in the LRSM and ALRM using δA_{FB}, δA_{LR}, and $\delta\sigma/\sigma$ at the 1σ level assuming $\sqrt{s} = 0.4$ or 1 TeV at an e^+e^- collider

	ALRM			LRSM		
	δA_{FB}	δA_{LR}	$\delta\sigma/\sigma$	δA_{FB}	δA_{LR}	$\delta\sigma/\sigma$
			$\sqrt{s} = 0.4$ TeV			
μ	1.15	1.60	3.32	1.35	0.88	1.32
b	1.55	1.40	0.75	1.50	2.28	0.70
c	1.05	1.10	2.18	1.35	1.90	1.65
			$\sqrt{s} = 1.0$ TeV			
μ	2.05	2.75	5.32	2.35	1.60	2.15
b	2.10	2.40	1.62	2.60	3.75	1.66
c	2.60	2.70	3.53	2.40	3.10	2.64

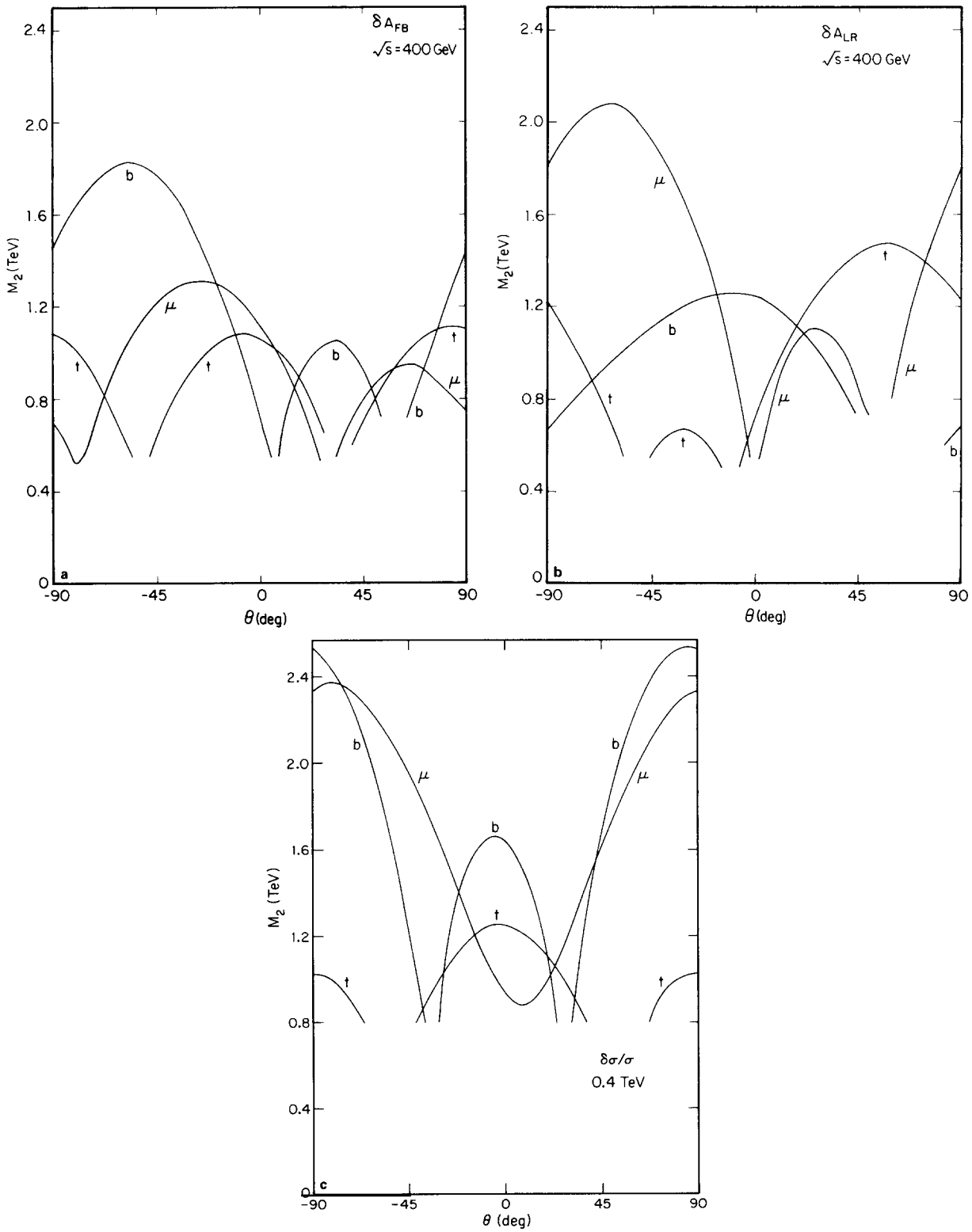

Fig. A.2. 1σ limits on the Z' mass (M_2) as a function of θ from (a) δA_{FB}; (b) δA_{LR}; and (c) $\delta\sigma/\sigma$ for $\sqrt{s} = 0.4$ TeV.

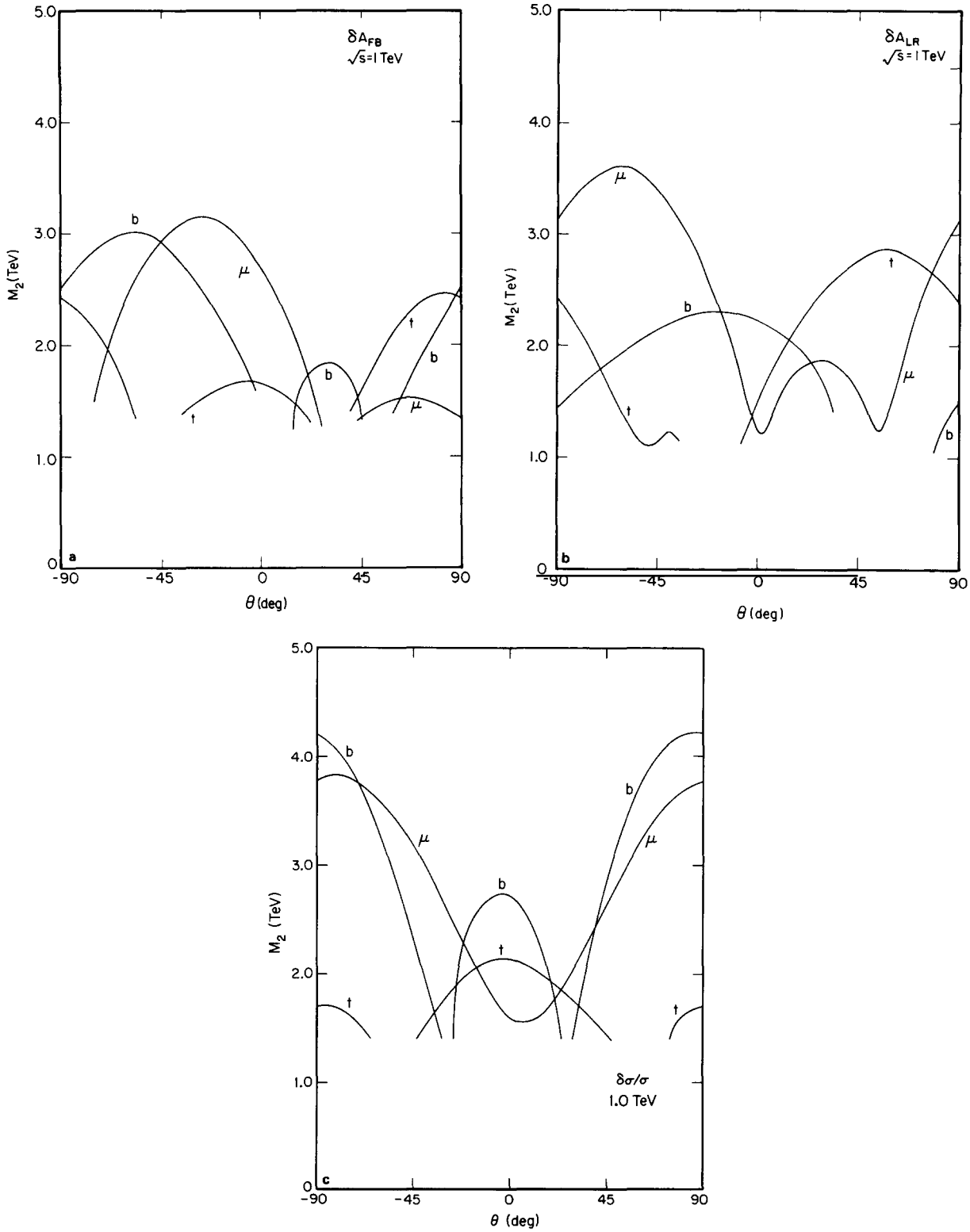

Fig. A.3. Same as fig. A.2 but for $\sqrt{s} = 1$ TeV.

1 TeV respectively. In the ER5M case it is interesting to note that, as θ varies, the final state fermion providing the strongest limit and the quantity doing so also changes. In general we see that a Z′ is detectable for values of M_2 in the range 2–6 $\sqrt{s}$ depending on the choice of model or model parameters (i.e., θ). Note that, in general, $\delta\sigma/\sigma$ provides the strongest limits. Higher limits also result in the cases of either the LRSM or the ALRM, as they did in the case of hadron colliders, due to the stronger couplings in such models.

It is clear that the study of search limits for Z′ bosons at hadron or e^+e^- colliders will continue to be an active area in the years ahead.

W_R production at machines has already been discussed to some extent in section 2 so that we merely report here the results of a recent analysis [A.2] setting search limits for W_R^+h ($W_R^{-(-)}h$) production at various hadron colliders. Table A.4 shows these search limits for 10 events of the kind $g + u \to W_R^+ h$ or $g + \bar{u} \to W_R^- \bar{h}$; to a good approximation these limits depend only on the sum of the W_R and h masses (M_R and M_h respectively). Noting that if $M_R \simeq M_h$ and remembering that $M_R \gtrsim 210$ GeV it is clear that there is very little room to search for W_R at the Tevatron. The only hope will be if $M_R \gg M_h$, otherwise the SSC will be necessary to obtain any reasonable limits.

$W_R^\pm$ may also be produced in e^+e^- either in pairs ($e^+e^- \to W_R^+W_R^-$) or singly via the $\gamma e^\pm \to W_R^\pm S^c$ subprocess. The former process has not yet been analyzed due to the rather large number of s-channel (3) and t-channel (2) exchanges which contribute. Single $W_R^\pm$ production has, however, been briefly considered [A.4]. Neglecting the light S^c mass, the above subprocess cross section is

$$\frac{d\sigma}{d\hat{t}} = \frac{\pi\alpha^2}{2x_w\hat{s}^2}\left(\frac{2M_R^2 - \hat{u}}{\hat{s}} + \frac{2(M_R^4 - \hat{s}\hat{u})}{(\hat{s}+\hat{u})^2} + \frac{2(\hat{u} - M_R^2)}{\hat{s}+\hat{u}} - \frac{2M_R^4}{\hat{s}(\hat{u}+\hat{s})}\right). \tag{A.1}$$

Then, making use of the effective photon approximation, eq. (A.1) can be folded with the γ distribution in the $e^\pm$ and integrated to obtain the total cross section shown in fig. A.4. The corresponding p_T distributions for the W_R are shown in fig. A.5. Note that in the region below the pair-production threshold ($M_R > \sqrt{s}/2$), single $W_R^\pm$ production has a rather small cross-section and, assuming a 30 fb^{-1} luminosity we obtain 20 $W_R^\pm$ events for $M_R = 0.70$ (1.3) TeV at a $\sqrt{s} = 1$ (2) TeV e^+e^- collider. Thus single $W_R^\pm$ production may not offer too much opportunity for the study of $W_R^\pm$ properties. A final conclusion must, however, await an analysis of $W_R^+W_R^-$ production.

A.2. Z′ properties: can models be distinguished?

Once a Z′ is discovered at a hadron or e^+e^- collider can we determine its couplings? In our more limited E_6 context, can we distinguish the ER5M, the LR5M, and the ALRM models from each other?

Table A.4

Search limits for $W_R^{\pm\,(-)}h$ production in the ALRM at hadron colliders

machine	$\mathscr{L}$ (pb^{-1})	$M_R + M_h$ search limit
$p\bar{p}$ $\sqrt{s} = 2$ TeV	10^2	375–400 GeV
$p\bar{p}$ $\sqrt{s} = 3$ TeV	30	405–440 GeV
pp $\sqrt{s} = 2$ TeV	10^3	500–525 GeV
SSC	10^4	4.8–5.6 TeV
SSC′	10^5	6.2–7.4 TeV

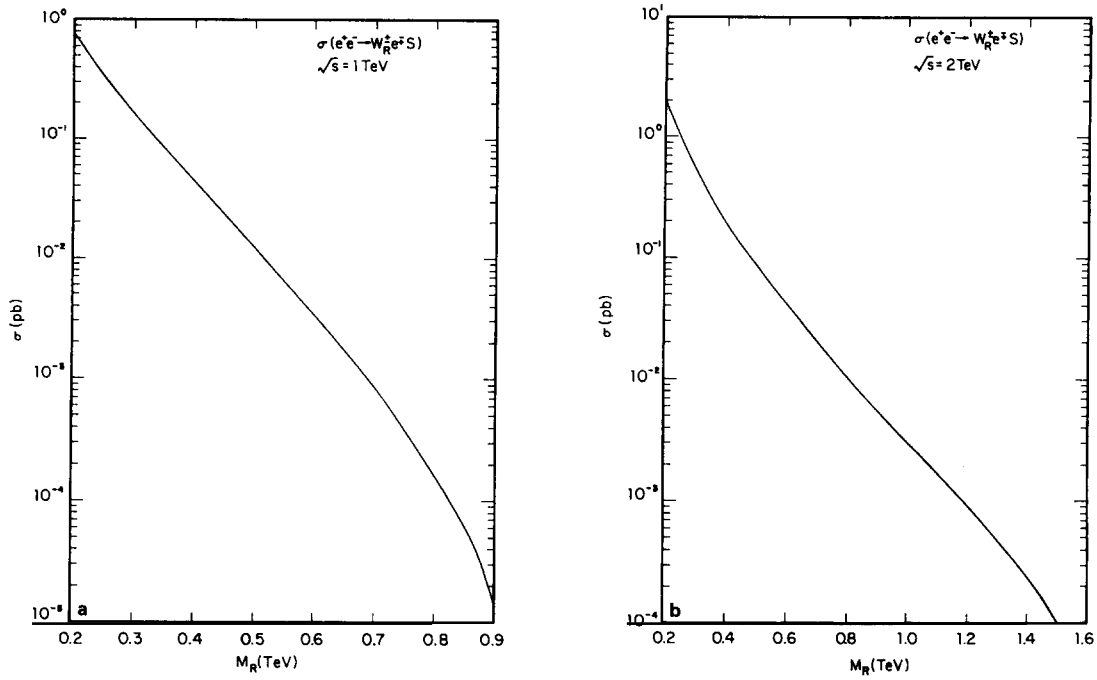

Fig. A.4. Single W_R production cross section as a function of M_R for (a) $\sqrt{s} = 1$ TeV and (b) $\sqrt{s} = 2$ TeV in the ALRM.

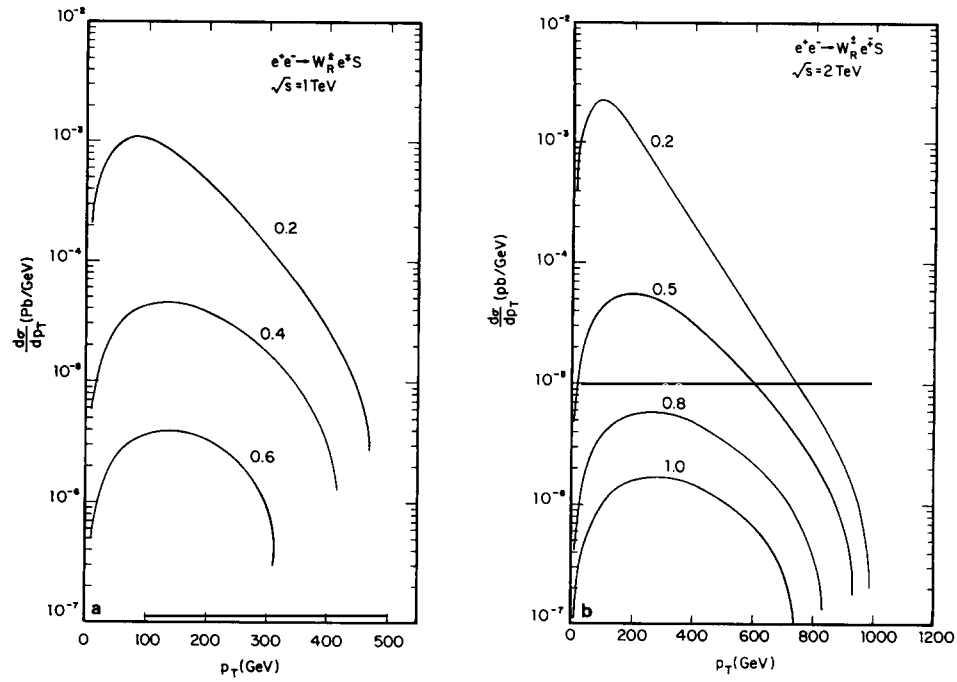

Fig. A.5. p_T distribution for single W_R production in the ALRM for different M_R values assuming (a) $\sqrt{s} = 1$ TeV for (b) $\sqrt{s} = 2$ TeV.

Can θ be uniquely determined, modulo the $\theta \to \theta + 180°$ ambiguity always present in the absence of Z–Z′ mixing? The situation at hadron and e^+e^- colliders is quite different.

At hadron colliders, the only Z′ properties that are measurable are the relative branching fractions into color-singlet final states, A_{FB}^{ℓ}, and to some extent the Z′ total width (Γ). The last quantity cannot be measured with high accuracy at hadron colliders due to the large energy resolution of such machines. Only color-singlet final states are observable since colored objects can be produced with very large rates via normal QCD-type processes and the Z′ decay to such objects will be virtually invisible against these backgrounds. If $n_g = 0$, this limits us to the decay $Z' \to \ell^+\ell^-$ only. It is obvious that without a precise value of Γ in this situation (Γ_0), it will be impossible to clearly distinguish between the various models even if A_{FB}^{ℓ} is also precisely known. The reasons for this are that a measurement of the leptonic branching fraction, however precise, cannot be used to discriminate between models without an accurate knowledge of Γ_0, and as can be seen in fig. A.6 and table A.1, we can always find a θ value such that $A_{FB}^{\ell}(\text{ALRM}) = A_{FB}^{\ell}(\text{ER5M})$. However, since A_{FB}^{ℓ} is positive for the LRSM and negative for the other two models, the LRSM can be easily distinguished. Thus A_{FB}^{ℓ}, if measured with sufficient accuracy, will separate the LRSM from the other two models under consideration, but will not distinguish between the ALRM and the ER5M.

For $n_g = 3$ at hadron colliders the situation improves somewhat since there are now additional color-singlet final states into which Z′ can decay with significant rates as shown in fig. 7 and table A.5. Although the total width in this case (Γ_3) is still only poorly determined, there are now several relative branching fractions which are measurable. Supplemented by the measurement of A_{FB}^{ℓ}, these can be used to separate the various models and determine θ (almost) uniquely, at least in principle. The problems with this approach are that the decay modes of these exotic fermions are very dependent on their assumed quantum numbers (as easily seen from section 3) and that many exotics have similar

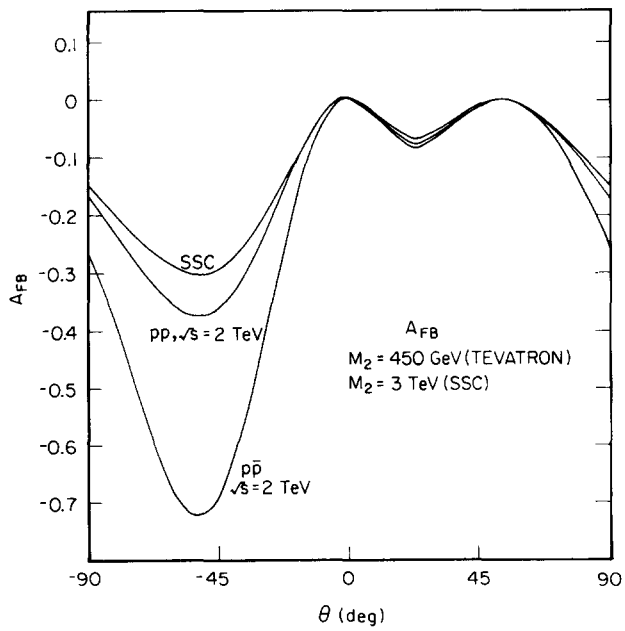

Fig. A.6. A_{FB}^{ℓ} as a function of θ in the ER5M for the Tevatron and SSC with $M_2 = 450$ GeV and 3 TeV respectively.

Table A.5
Comparison of the Z′ branching fraction (in %) and e^+e^- asymmetries for $n_g = 3$ (0) in the LRSM and ALRM

		LRSM	ALRM
asymmetry/mode	A_{LR}	0.290	0.504
	A_{FB}^{μ}	0.063	0.191
	A_{FB}^{u}	0.206	−0.358
	A_{FB}^{d}	0.211	−0.227
B	e	1.27 (2.46)	3.29 (9.04)
	u	5.62 (10.91)	5.62 (15.43)
	d	9.84 (19.20)	0.75 (2.06)
	ν_L	0.45 (0.87)	2.48 (6.80)
	ν_R	5.04	0
	h	1.20	10.29
	E	4.96	2.93
	N_L	2.48	0.45
	S_R	0	5.04
	N_R	2.48	2.48

decay patterns making their identification and separation difficult. In addition, to take phase space effects into account (fig. 7 and table A.5 assume massless exotics) one needs a relatively reliable determination of the masses of these exotics by reconstruction of their final states. For many decay patterns, however, missing energy will be present in the exotic decay signatures making it unlikely that their masses can be accurately determined. Thus, unless we are very careful or lucky, it may be hard to do too much more in the $n_g = 3$ case when we did for $n_g = 0$.

The situation at e^+e^- colliders is, of course, completely different since on the Z′ resonance there is virtually no background and, independently of the choice $n_g = 0$ or 3, there is a unique set of tests for the ER5M. In all such models, in the absence of QCD corrections, one finds

$$A_{FB}^{u} = 0\,, \qquad A_{FB}^{\mu} = -A_{FB}^{d}\,, \qquad \Gamma(Z' \to d\bar{d}) = 3\Gamma(Z' \to e^+e^-)\,, \tag{A.2}$$

and, if $n_g = 3$ (with E and h degenerate)

$$\Gamma(Z' \to h\bar{h}) = 3\Gamma(Z' \to E^+E^-)\,. \tag{A.2′}$$

Figure A.7 shows A_{FB}^{μ} (and A_{LR}) in the ER5M while table A.5 shows the branching fractions and asymmetries for the LRSM and the ALRM. The corresponding branching fractions for the ER5M are shown in fig. 7. It is immediately clear that in neither the ALRM nor the LRSM is either of the conditions (A.2) or (A.2′) satisfied. In addition, the table shows that the ALRM and the LRSM can also be clearly distinguished based on measurements of the above quantities (as well as others). If the ER5M holds is there enough information available to determine the value of θ (up to the $\theta \to \theta + 180°$ ambiguity)? The answer here may be somewhat dependent on n_g.

First, note that the predictions for A_{FB}^{μ} and A_{LR} in the ER5M are approximately symmetric about the angles $\theta_0 = \frac{1}{2}\cos^{-1}(\sqrt{3/8})$ and $\theta = \theta_0 - 90°$ and thus, e.g., $\theta = \theta_0 \pm x$ (for any x) are essentially indistinguishable as far as these quantities are concerned. Hence a double two-fold ambiguity (at least) exists no matter how well these quantities are measured. If $n_g = 0$, fig. 7 shows that the branching

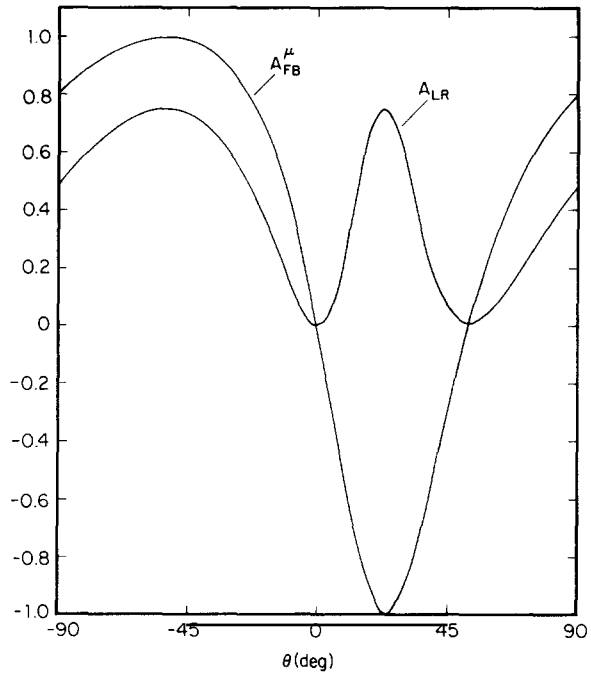

Fig. A.7. A_{FB}^{μ} and A_{LR} as a function of θ for a Z′ in the ER5M in e^+e^- annihilation.

fractions for all fermion final states show this same uncertainty and are thus not useful in removing the two-fold ambiguity. However, the total width for $n_g = 0$ (Γ_0) does *not* show this symmetry, as can be seen in fig. 7, so one might imagine that it can be used to resolve this dilemma. However, if additional final states are accessible in Z′ decay (e.g., W^+W^-, ZH, SUSY partners) it may not be so easy to use this information unless one can accurately determine the total Z′ width to ordinary fermions by separately measuring the widths to these additional channels and subtracting them from Γ_0. As we will see below, the production of a pair of Z′ bosons can allow for a determination of θ independently of the value of n_g.

If exotic fermions can appear ($n_g = 3$) as Z′ final states then the situation improves greatly as it does in the case of hadron colliders. The reason is that, as fig. 7 shows, exotic fermion final state branching fractions do not show any symmetry about θ_0. Thus, once the exotic fermion masses are accurately taken into account, measurement of the various branching fractions and asymmetries can be used to determine θ uniquely up to the $\theta \to \theta + 180°$ ambiguity. One should remember that in the $n_g = 3$ case, the total fermionic width of the Z′ (Γ_3) is independent of θ in the limit of massless final state particles.

A.3. 2Z′ production at e^+e^- and hadron colliders

Once a Z′ is discovered at an e^+e^- or hadron collider, the production of a pair of Z′ bosons [A.5], if kinematically accessible, may be quite revealing as far as couplings of the Z′ are concerned. The process $f\bar{f} \to 2Z'$ has the cross section (where N_c is the number of colors of the fermion f)

$$\frac{d\sigma}{dt} = \frac{\pi\alpha^2}{16N_c x_w^2(1-x_w)^2 s^2}\left[\frac{t}{u} + \frac{u}{t} + \frac{4sM_2^2}{ut} - M_2^4\left(\frac{1}{t^2} + \frac{1}{u^2}\right)\right]\left[(v_f^2 + a_f^2)^2 + 4v_f^2 a_f^2\right]. \tag{A.3}$$

Since the couplings appear quartically in (A.3) one might imagine, e.g., that 2Z′ production in the ER5M may be extremely sensitive to the value of θ; this is, in fact, the case as we will see below. For the $n_g = 0$ case, it turns out that Z′ pair production may be the only way to resolve the ambiguities in the value of the parameter θ.

Figure A.8 shows σ for 2Z′ production in e^+e^- for model χ ($\theta = -90°$) as a function of $\sqrt{s}$ for different values of M_2. Figure A.9 shows the strong θ dependence of σ for a fixed value of M_2 at the $\sqrt{s}$ value which maximizes σ. The *ratio* of σ's for two different θ values is, however, independent of $\sqrt{s}$ and M_2 so that fig. A.9 can be used to rescale all e^+e^- model χ cross sections to those for any other θ value. Note that as θ varies, σ can vary by as much as a factor of 25 (!) displaying the very strong θ sensitivity expected. Is 2Z′ production observable in e^+e^- annihilation? Clearly if M_2 is much larger than $\simeq$300 GeV (for $\sqrt{s} = 1$ TeV) the event rate is too small after one selects a particular trigger final state (such as $\ell^+\ell^-$ + two jets peaking at M_2). If $M_2 = 250$ GeV and $\sigma \simeq 100$ fb then model χ ($n_g = 0$) predicts $\simeq$500 ev/yr for a luminosity of 30 fb^{-1}. Clearly, for most other θ values or if $n_g = 3$ this event rate will be much smaller, e.g., $\theta = 0$, $n_g = 3$ leads to only $\simeq$8 ev/yr in this channel. The major background for this process from $\gamma\gamma \to q\bar{q}$ can be completely avoided by using cuts on the lepton pair as well as jet pair invariant masses. It seems plausible that such events should be observable at e^+e^- machines and would provide a sensitive θ probe if M_2 is not too large. Note that in the LRSM or the ALRM cases the production rate for 2Z′ final states is different than that of model χ since their couplings are quite distinct. We find that for the ALRM (LRSM) the cross-section is $\simeq$2.5 times larger ($\simeq$3.0 times smaller) than that for model χ.

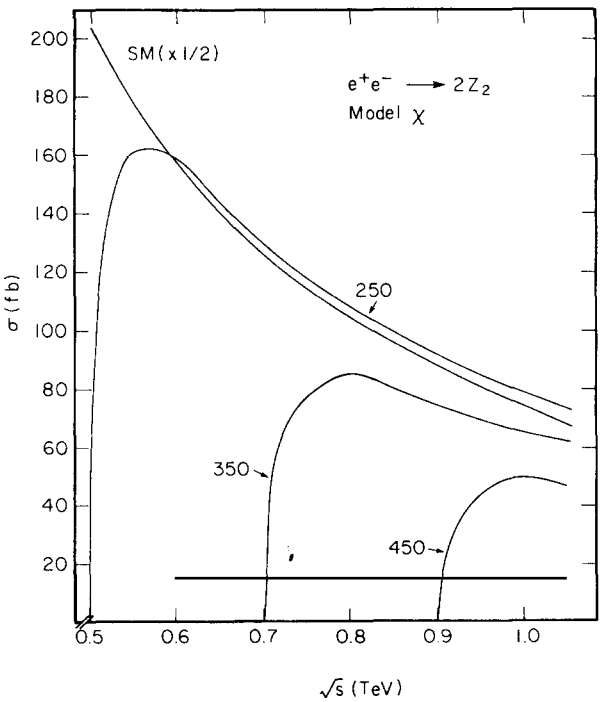

Fig. A.8. Cross sections for $e^+e^- \to 2Z_2$ as a function of $\sqrt{s}$ for different M_2 values in model χ. The SM $e^+e^- \to 2Z$ cross section is shown for comparison.

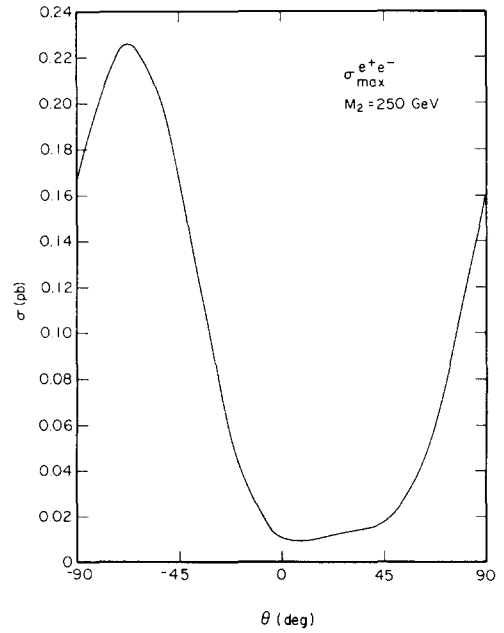

Fig. A.9. θ dependence of the $e^+e^- \to 2Z'$ cross section for $\sqrt{s} =$ 1 TeV and $M_2 = 250$ GeV.

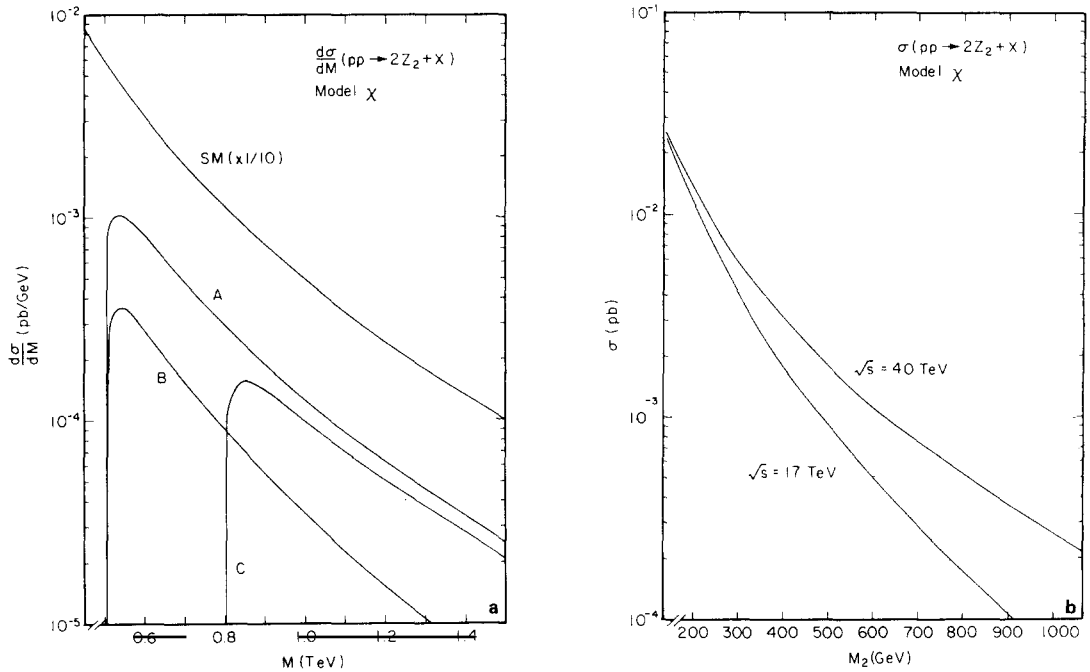

Fig. A.10. (a) Invariant mass distribution and (b) total cross section for $2Z_2$ production at SSC and LHC in model χ. (A) $\sqrt{s} = 40$ TeV, $M_2 = 250$ GeV; (B) $\sqrt{s} = 17$ TeV, $M_2 = 250$ GeV; (C) $\sqrt{s} = 40$ TeV, $M_2 = 400$ GeV.

At hadron colliders, $2Z'$ production is somewhat less interesting as we will see. Figure A.10 shows $d\sigma/dM$ and σ for different M_2 values at the LHC and SSC for model χ. Figure A.11 shows the θ dependence of $d\sigma/dM$ for $M = 0.54$ TeV and $M_2 = 250$ GeV at the SSC and can be used to rescale model χ cross-sections to those for any θ value (in the scaling approximation) for any value of M_2 just as fig. A.9 did in the e^+e^- case. Note that the θ sensitivity is much lower in the hadronic case differing only by a factor of $\simeq$10 instead of 25. The major difficulty with hadron colliders is that even at SSC energies the $2Z'$ production rate is quite small even for relatively light Z' bosons. If the signal is again $\ell^+\ell^-$ + two jets peaking at the Z' mass we obtain only 16 events/yr for model χ at the SSC assuming $n_g = 0$ and $M_2 = 250$ GeV. For larger M_2 values, $n_g = 3$, or other θ values the event rate quoted above could drop by more than an order of magnitude. It thus seems that unless M_2 is quite light and its couplings are reasonably large, the $2Z'$ production rate at random colliders will probably be too small to be useful as a further probe of Z' couplings.

A.4. The process $e^+e^- \to e^+e^-Z'$

The process $e^+e^- \to e^+e^-Z'$ [A.6] also shows some sensitivity to θ and allows us to probe $Z'e^+e^-$ couplings off-resonance. In the effective photon approximation, this process proceeds via $\gamma e^\pm \to e^\pm Z'$ for which the differential cross section is

$$\frac{d\sigma}{d\hat{t}} = \frac{\pi\alpha^2}{32x_w(1-x_w)s^2}\left(\frac{-\hat{u}}{\hat{s}} + \frac{\hat{s}}{-\hat{u}} - \frac{2M_2^2\hat{t}}{\hat{s}\hat{u}}\right)(v_e^2 + a_e^2)\,. \tag{A.4}$$

Figure A.12 shows σ as a function of $\sqrt{s}$ for different M_2 values within model χ ($\theta = -90°$) while fig.

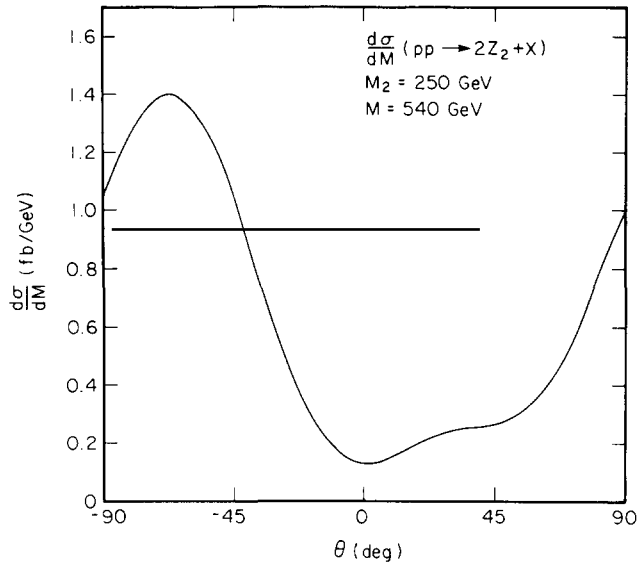

Fig. A.11. θ dependence of $d\sigma/dM$ at the SSC for $M_2 = 250$ GeV and $M = 540$ GeV.

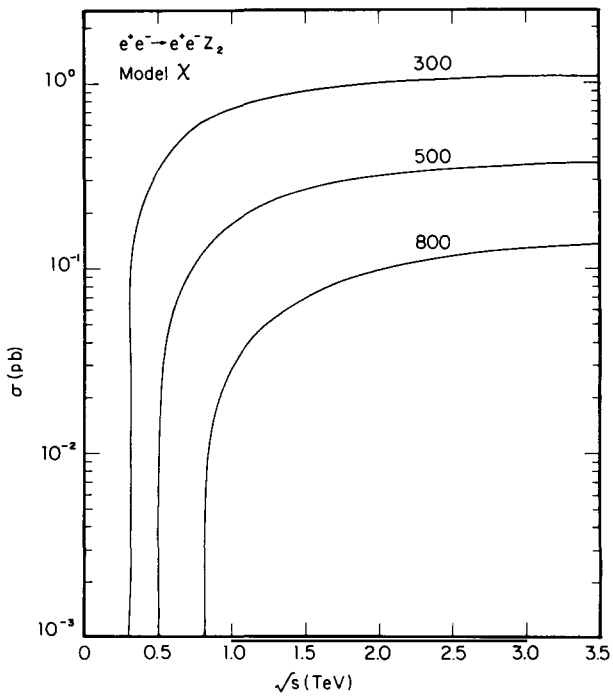

Fig. A.12. Cross section for $e^+e^- \to e^+e^-Z_2$ as a function of $\sqrt{s}$ for different M_2 values in GeV for model χ.

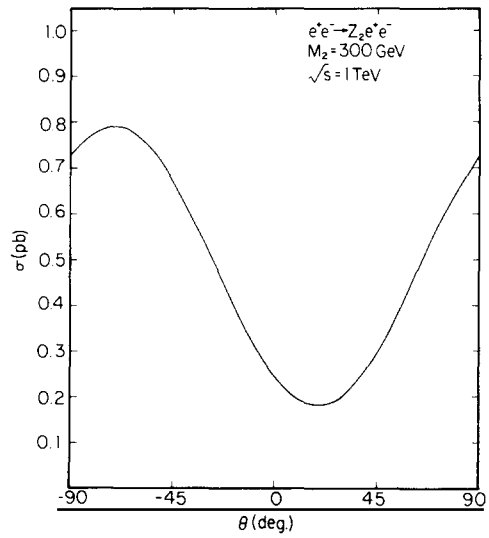

Fig. A.13. Cross section for $e^+e^- \to e^+e^-Z_2$ at $\sqrt{s} = 1$ TeV for $M_2 = 300$ GeV as a function of θ.

A.13 can be used to rescale model χ results to those for any other θ value. Note that above the threshold region, cross-sections stay relatively constant in the 100–1000 fb range for model χ. The θ dependence is much weaker here than in the 2Z′ production case with only a factor of 4 between the maximum and minimum values of σ. Also note that σ displays the same symmetry about θ_0 as do the branching fractions for the ordinary fermions. Figures A.14 show the M_2 dependence for fixed $\sqrt{s}$ for several ER5M while figs. A.15 show the corresponding Z′ p_T distribution.

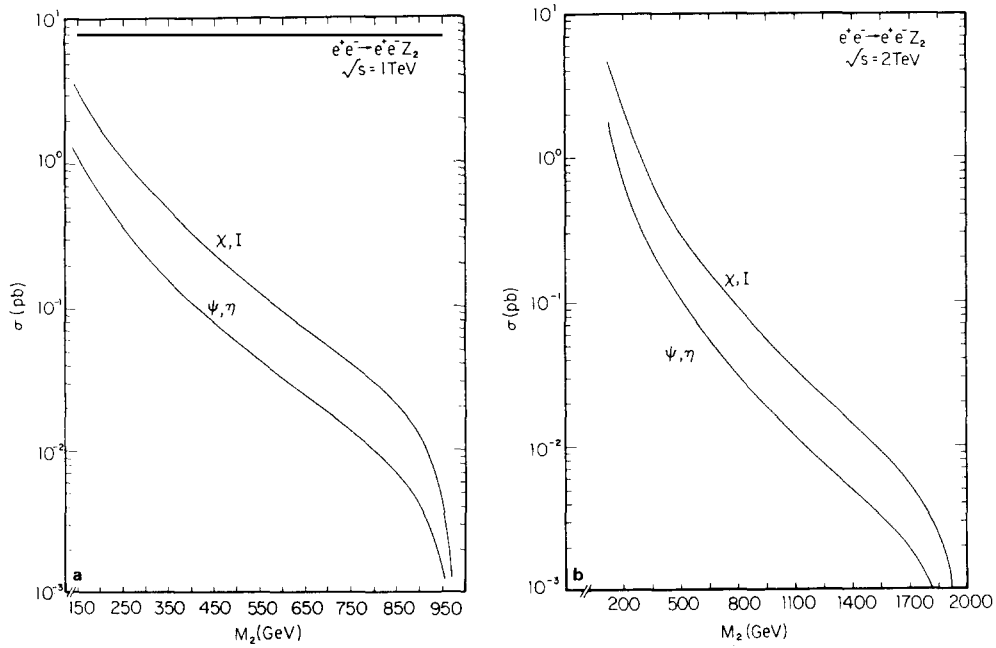

Fig. A.14. Cross section for $e^+e^- \to e^+e^-Z_2$ at (a) $\sqrt{s} = 1$ TeV and (b) $\sqrt{s} = 2$ TeV for several ER5M.

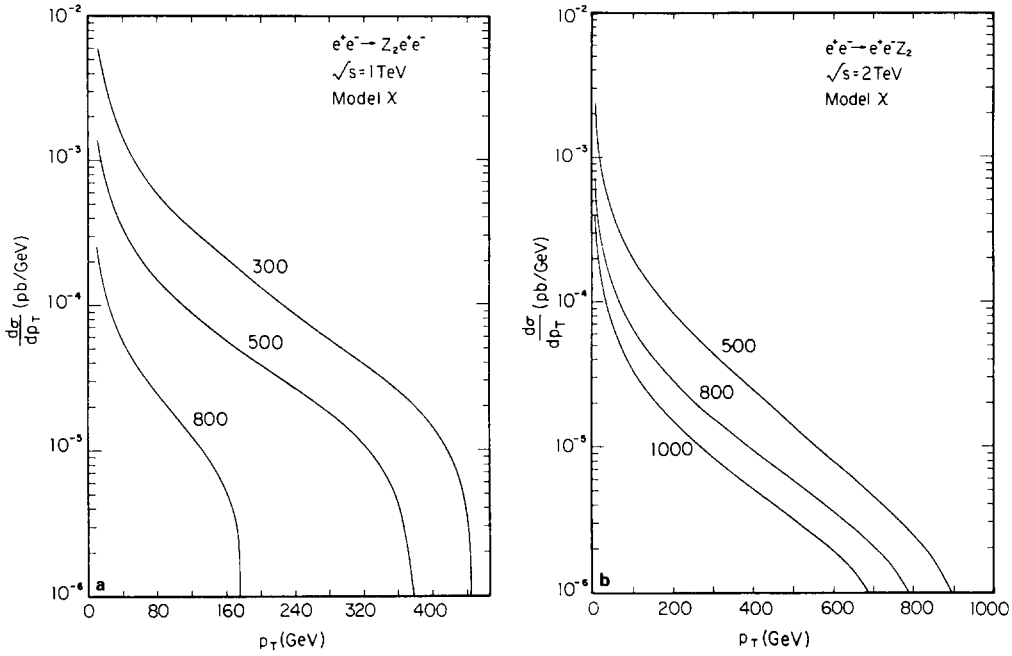

Fig. A.15. p_T distribution of the Z_2 for different M_2 values in GeV with (a) $\sqrt{s} = 1$ TeV and (b) $\sqrt{s} = 2$ TeV.

The Z′ should be observable as a peak in either the $e^+e^- \to e^+e^- + \ell^+\ell^-$ or $e^+e^- \to e^+e^-$ + two-jet channels with the size of the peak dependent on the relevant Z′ branching fractions. The relevant backgrounds from $\gamma\gamma \to \ell^+\ell^-$ and $q\bar{q}$ are easily estimated and, as in the Z′ case, are peaked at low p_T. Integrating over the Z′ peak one can compare signal to background: for model χ with $n_g = 0$ as $\sqrt{s} = 1$ TeV, we find $\sigma \cdot B \simeq 44$ (10) fb with a background of 2.8 (1.0) fb for the $\ell^+\ell^-$ mode assuming $M_2 = 300$ (500) GeV. For the two-jet mode, we find $\sigma \cdot B \simeq 484$ (110) fb with a background of 4.2 (1.5) fb. It thus appears that, at least for the optimistic case of model χ with $n_g = 0$, the $e^+e^- \to e^+e^-Z'$ process should be observable above background. It should be remembered, however, that for $n_g = 3$ and other values of θ these production cross-sections will be reduced by another factor of order 20–30. If integrated luminosities in the 30 fb^{-1} range or greater can be achieved, this process may yet be observable.

References

[1.1] S.L. Glashow, Nucl. Phys. 22 (1961) 579;
S. Weinberg, Phys. Rev. Lett. 19 (1967) 1264;
A. Salam, in: Proc. 8th Nobel Symp., ed. N. Svartholm (Almqvist and Wiksell, Stockholm and Wiley, New York, 1968) p. 367.

[1.2] D.J. Gross and F. Wilczek, Phys. Rev. D 8 (1973) 3633; D 9 (1974) 980;
H.D. Politzer, Phys. Rep. 14 (1974) 129.

[1.3] W.J. Marciano, talk given at SLAC Summer Institute Topical Conf. (August 1987).

[1.4] J.L. Rosner, lectures presented at the Lake Louise Winter Institute (Lake Louise, Canada, February 1987).

[1.5] W. Marciano, in: Proc. APS Division of Particles and Fields Meeting (Salt Lake City, UT, January 1987), eds C. DeTar and J.S. Ball (World Scientific, Singapore, 1987);
H. Georgi, H. Quinn and S. Weinberg, Phys. Rev. Lett. 33 (1974) 451.

[1.6] J. Wess and B. Zumino, Nucl. Phys. B 70 (1974) 39; Phys. Lett. B 49 (1974) 52;
H. Haber and G. Kane, Phys. Rep. 117 (1985) 75.

[1.7] H. Georgi, in: Proc. APS Division of Particles and Fields Meeting (Williamsburg, VA) ed. C.E. Carlson (AIP, New York, 1975) p. 575;
H. Fritzsch and P. Minkowski, Ann. Phys. (NY) 93 (1975) 193;
R. Marshak and R. Mohapatra, Phys. Lett. B 91 (1980) 222;
R.N. Mohapatra and J.C. Pati, Phys. Rev. D 11 (1975) 566;
G. Senjanovic and R.N. Mohapatra, Phys. Rev. D 12 (1975) 1502;
A. DeRújula, H. Georgi and S.L. Glashow, Ann. Phys. (NY) 109 (1977) 242, 258.
[1.8] F. Gürsey, P. Ramond and P. Sikivie, Phys. Lett. B 60 (1976) 177;
Y. Achiman and B. Stech, Phys. Lett. B 77 (1978) 389;
J.A. Harvey, Nucl. Phys. B 163 (1979) 254;
Q. Shafi, Phys. Lett. B 79 (1979) 301;
F. Gürsey and M. Serdaroglu, Lett. Nuovo Cimento 21 (1978) 28; 65A (1981) 337;
M.J. Bowick and P. Ramond, Phys. Lett. B 103 (1981) 338;
R. Barbieri, D.V. Nanopoulos and A. Masiero, Phys. Lett. B 104 (1981) 194;
P.H. Frampton and T.W. Kephart, Phys. Rev. D 25 (1982) 1459;
R.W. Robinett and J.L. Rosner, Phys. Rev. D 26 (1982) 2396;
R.W. Robinett, Phys. Rev. D 26 (1982) 2388;
R. Slansky, Phys. Rep. 79 (1981) 1.
[1.9] L.L. Chau, Phys. Rep. 95 (1983) 1;
G. Kane and M. Peskin, Nucl. Phys. B 195 (1982) 29;
P. Avery et al., Phys. Rev. Lett. 53 (1984) 1309.
[1.10] M.B. Green and J.H. Schwarz, Phys. Lett. B 149 (1984) 117;
M.B. Green, J.H. Schwarz and E. Witten, Superstring Theory (Cambridge Univ. Press, Cambridge, 1987).
[1.11] D. Gross, J. Harvey, E. Martinec and R. Rohm, Phys. Rev. Lett. 54 (1985) 502;
Nucl. Phys. B 256 (1985) 253; B 267 (1986) 75;
P. Candelas, G. Horowitz, A. Strominger and E. Witten, Nucl. Phys. B 258 (1985) 46;
E. Witten, Nucl. Phys. B 258 (1985) 75; Phys. Lett. B 149 (1984) 351.
[1.12] E. Calabi, in: Algebraic Geometry and Topology (Princeton Univ. Press, Princeton, 1957) p. 78;
S.T. Yau, Proc. Natl. Acad. Sci. USA 74 (1977) 1798.
[1.13] M. Dine, V. Kaplunovsky, M. Mangano, C. Nappi and N. Seiberg, Nucl. Phys. B 259 (1985) 519;
J.D. Breit, B.A. Ovrut and G.C. Segre, Phys. Lett. B 158 (1985) 33;
F. del Aguila, G. Blair, M. Daniel and G.G. Ross, Nucl. Phys. B 287 (1986) 413;
S. Cecotti, J.P. Derendiger, S. Ferrara, L. Girardello and M. Roncadelli, Phys. Lett. B 156 (1985) 318.
[1.14] E.W. Kolb, D. Seckel and M.S. Turner, Nature 314 (1985) 415; talk presented at the 9th Johns Hopkins Workshop on Current Problems in Particle Physics (Florence, Italy, 1985).
[1.15] Y. Hosotani, Phys. Lett. B 129 (1983) 193.
[1.16] J.P. Derendinger, L.E. Ibañez and H.P. Nilles, Phys. Lett. B 155 (1985) 65; Nucl. Phys. B 267 (1986) 265;
F. del Aguila, G. Blair, M. Daniel and G.G. Ross, Nucl. Phys. B 272 (1986) 413;
J. Ellis, K. Enqvst, D.V. Nanopoulos and F. Zwirner, Mod. Phys. Lett. A 1 (1986) 57;
P.K. Mohapatra, Phys. Lett. B 174 (1986) 51;
P. Kalyniak and M.K. Sundaresan, Phys. Lett. B 167 (1986) 320.
[1.17] J. Ellis, lectures presented at the Cargèse Summer School on Particle Physics (August 1987), CERN report CERN/TH.4840/87 (1987).
[1.18] C. Hull and E. Witten, Phys. Lett. B 160 (1985) 398;
C. Hull, Phys. Lett. B 167 (1986) 51; B 178 (1986) 357.
[1.19] D. Bailin, A. Love and S. Thomas, Phys. Lett. B 176 (1986) 81; B 178 (1986) 15;
B.R. Greene, K.H. Kirklin and P.J. Miron, Nucl. Phys. B 274 (1986) 574.
[1.20] K.S. Narain, Phys. Lett. B 169 (1986) 41.
[1.21] I. Frenkel and V.G. Kac, Inv. Math. 62 (1980) 23;
P. Goddard and D. Olive, talk given at the Workshop on Vertex Operators in Mathematics and Physics (Berkeley, CA, 1983).
[1.22] L. Dixon, J. Harvey, C. Vafa and E. Witten, Nucl. Phys. B 261 (1987) 678; B 274 (1986) 285;
K.S. Narain, M.H. Sarmadi and C. Vafa, Nucl. Phys. B 288 (1987) 551;
H. Kawai, D.C. Lewellen and S.H.H. Tye, Phys. Rev. Lett. 57 (1986) 1832; Nucl. Phys. B 288 (1987) 1;
I. Antoniadis, C. Bachas and C. Kounnas, Nucl. Phys. B 289 (1987) 87;
L.E. Ibañez, lectures given at the XVII GIFT Seminar on "Cuerdas y Supercuerdas" (El Escorial, Spain, June 1987), CERN Report CERN-TH. 4769/87 (1987);
B.A. Campbell, J. Ellis and D.V. Nanopoulos, Phys. Lett. B 181 (1986) 283.
[1.23] L.E. Ibañez, J.E. Kim, H.P. Nilles and F. Quevedo, Phys. Lett. B 191 (1987) 282;
I. Antoniadis, J. Ellis, E. Floratos, D.V. Nanopoulos and T. Tomaras, Phys. Lett. B 191 (1987) 96;
B.A. Campbell, J. Ellis and D.V. Nanopoulos, Phys. Lett. B 181 (1986) 283.

[1.24] B. Campbell, J. Ellis, M.K. Gaillard, D.V. Nanopoulos and K.A. Olive, Phys. Lett. B 180 (1986) 77;
B.A. Campbell, K.A. Olive and D.B. Reiss, Nucl. Phys. B 296 (1988) 129.
[1.25] E. Ma, Phys. Rev. Lett. 60 (1988) 1363.

[2.1] V. Barger, W.Y. Keung and E. Ma, Phys. Rev. Lett. 44 (1980) 1169; Phys. Rev. D 22 (1980) 727;
V. Barger, E. Ma and K. Whisnant, Phys. Rev. Lett. 46 (1981) 1501;
V. Barger, K. Whisnant and W.Y. Keung, Phys. Rev. D 25 (1982) 291;
T.G. Rizzo and G. Senjanovic, Phys. Rev. Lett. 46 (1981) 1315;
Phys. Rev. D 24 (1981) 704; D 25 (1982) 235.
[2.2] F. del Aguila and A. Mendez, Nucl. Phys. B 189 (1981) 212;
A. Masiero, Phys. Lett. B 93 (1981) 295;
N.G. Deshpande and D. Iskander, Phys. Rev. Lett. 42 (1979) 20; Phys. Lett. B 87 (1979) 383;
J.D. Bjorken, Phys. Rev. D 19 (1979) 335;
E.H. de Groot and D. Schildknecht, Z. Phys. C 10 (1981) 55.
[2.3] E.H. de Groot, G.J. Gounaris and D. Schildknecht, Phys. Lett. B 85 (1979) 339; Z. Phys. C 5 (1980) 127;
G. Fogleman and T. Rizzo, Phys. Lett. B 113 (1982) 240;
R.N. Mohapatra and D.P. Sidhu, Phys. Rev. D 18 (1978) 856;
C.N. Leung and J.L. Rosner, Phys. Rev. D 29 (1982) 2132;
T.G. Rizzo, Phys. Rev. D 25 (1982) 1237.
[2.4] J.L. Rosner, Comments Nucl. Part. Phys. 15 (1986) 195;
D. London and J.L. Rosner, Phys. Rev. D 34 (1986) 1530;
P. Langacker, R.W. Robinett and J.L. Rosner, Phys. Rev. D 30 (1984) 1470.
[2.5] R.N. Mohapatra, Unification and Supersymmetry (Springer, New York, 1986) and references therein;
Q. Shafi and Ch. Wetterich, Phys. Lett. B 73 (1978) 65;
V. Elias, J.C. Pati and A. Salam, Phys. Lett. B 73 (1978) 451.
[2.6] V. Barger and K. Whisnant, Phys. Rev. D 36 (1987) 3429.
[2.7] J. Ellis and R. Peccei, CERN Yellow Report CERN-86-02, Vols. 1 and 2 (1986).
[2.8] J. Ellis, K. Enqvist, D.V. Nanopoulos and F. Zwirner, Nucl. Phys. B 276 (1986) 14;
E. Cremmer, S. Ferrara, C. Kounnas and D.V. Nanopoulos, Phys. Lett. B 133 (1983) 61;
J. Ellis, C. Kounnas and D.V. Nanopoulos, Nucl. Phys. B 247 (1984) 373;
J. Ellis, C. Gomez and D.V. Nanopoulos, Phys. Lett. B 171 (1986) 203.
[2.9] V. Barger, N.G. Deshpande and K. Whisnant, Phys. Rev. D 35 (1987) 1005;
See also G. Lazarides, C. Panagiotakopoulos and Q. Shafi, Z. Phys. C 34 (1987) 553.
[2.10] UA1 Collab., G. Arnison et al., Phys. Lett. B 166 (1980) 484;
UA2 Collab., R. Ansari et al., Phys. Lett. B 186 (1987) 440.
[2.11] L.S. Durkin and P. Langacker, Phys. Lett. B 166 (1986) 436;
V. Barger, N.G. Deshpande and K. Whisnant, Phys. Rev. Lett. 56 (1986) 30;
J.L. Hewett, T.G. Rizzo and J.A. Robinson, Phys. Rev. D 33 (1986) 1476; D 34 (1986) 2179;
D. London and J.L. Rosner, Phys. Rev. D 34 (1986) 1530;
E. Cohen, J. Ellis, K. Enqvist and D.V. Nanopoulos, Phys. Lett. B 165 (1985) 76;
J. Ellis, K. Enqvist, D.V. Nanopoulos and S. Sarkar, Phys. Lett. B 167 (1986) 457;
J. Ellis, K. Enqvist, D.V. Nanopoulos and F. Zwirner, Mod. Phys. Lett. A 1 (1986) 57.
[2.12] S.M. Barr, Phys. Rev. Lett. 55 (1985) 2278;
T. Matsuoka, H. Mino, D. Suematsu and S. Watanabe, Prog. Theor. Phys. 76 (1986) 915;
F. del Aguila, G.A. Blair, M. Daniel and G.G. Ross, Nucl. Phys. B 283 (1987) 50; B 272 (1986) 413;
F. del Aguila, J.A. Gonzalez and M. Quiros, Phys. Lett. B 197 (1987) 89; Erratum B 200 (1988) 587;
J.F. Gunion, L. Roszkowski and H.E. Haber, Phys. Lett. B 189 (1987) 409;
J. Whitaker and N. Deshpande, Univ. of Oregon report OITS-373 (1987);
N.I. Polyakov, Moscow ITEP report ITEP-19-1987;
J. Bordes, Phys. Lett. B 190 (1987) 97.
[2.13] U. Amaldi et al., Phys. Rev. D 36 (1987) 1385.
[2.14] G. Costa et al., Nucl. Phys. B 297 (1988) 244.
[2.15] M. Veltman, Nucl. Phys. B 123 (1987) 89;
R. Barbieri and L. Maiani, Nucl. Phys. B 224 (1983) 32.
[2.16] N. Cabibbo, Phys. Rev. Lett. 10 (1963) 531;
M. Kobayashi and M. Maskawa, Prog. Theor. Phys. 49 (1973) 652.
[2.17] W.J. Marciano and A. Sirlin, Phys. Rev. D 35 (1987) 1672.

[2.18] UA1 Collab., C. Albajar et al., Phys. Lett. B 198 (1987) 271;
UA2 Collab., R. Ansari et al., Phys. Lett. B 195 (1987) 613.
[2.19] V. Barger, N.G. Deshpande, J.L. Rosner and K. Whisnant, Phys. Rev. D 35 (1987) 2893.
[2.20] J. Ellis, P.J. Franzini and F. Zwirner, Phys. Lett. B 202 (1988) 417.
[2.21] Y. Kizukuri, Phys. Lett. B 193 (1987) 339;
F. del Aguila, M. Quiros and F. Zwirner, Nucl. Phys. B 284 (1987) 530.
[2.22] F. del Aguila, L. Ametller, R. Field and L. Garrido, Phys. Lett. B 201 (1988) 375;
V. Barger and K. Whisnant, Phys. Rev. D 36 (1987) 3429;
R.W. Robinett, Phys. Rev. D 34 (1986) 182;
S. Nandi, Phys. Lett. B 188 (1987) 159;
P. Kalyniak and M.K. Sundaresan, Phys. Rev. D 35 (1987) 751;
R. Najimia and S. Wakaizumi, Phys. Lett. B 184 (1987) 410;
C. Dib and F. Gilman, Phys. Rev. D 36 (1987) 1337;
F. del Aguila, M. Quiros and F. Zwirner, Nucl. Phys. B 284 (1987) 530;
S. Nandi and T.G. Rizzo, Phys. Rev. D 37 (1988) 52;
N.G. Deshpande, J.F. Gunion and F. Zwirner, in: Proc. Workshop on Experiments, Detectors and Experimental Areas for the Supercollider (Univ. of California, Berkeley, July 1987);
R. Najima, Prog. Theor. Phys. 77 (1987) 926;
C. Ahn, M.E. Peskin, B.W. Lynn and S. Selipsky, Nucl. Phys. B 309 (1988) 221;
M. Cvetic and B.W. Lynn, Phys. Rev. D 35 (1987) 51.
[2.23] T.G. Rizzo, Phys. Lett. B 192 (1987) 125.
[2.24] S. Nandi, Phys. Lett. B 197 (1987) 144.
[2.25] S. Nandi, Phys. Lett. B 181 (1986) 375;
T.G. Rizzo, Phys. Rev. D 34 (1986) 1438;
R.W. Robinett, Phys. Rev. D 34 (1986) 182;
H. Baer, D.A. Dicus, M. Drees and X. Tata, Phys. Rev. D 36 (1987) 1363;
J.F. Gunion, L. Roszkowski and H. Haber, Phys. Lett. B 189 (1987) 409;
V. Barger and K. Whisnant, Phys. Rev. D 36 (1987) 3429; Int. J. Mod. Phys. A 3 (1988) 1907.
[2.26] N.G. Deshpande and J. Trampetic, Phys. Lett. B 206 (1988) 665.
[2.27] D. Chang, W.-Y. Keung and S.-C. Lee, Fermilab Report, Pub-87/148-T (1987).
[2.28] F. Csikor, E. Lendvai and G. Pocsik, Int. J. Mod. Phys. A 3 (1988) 2959; Mod. Phys. Lett. A 4 (1989) 661;
D. London, G. Belanger and J.N. Ng, Phys. Rev. Lett. 58 (1987) 6; Phys. Rev. D 34 (1986) 2867;
G. Belanger and S. Godfrey, Phys. Rev. D 35 (1987) 378;
V.D. Angelopoulos et al., Phys. Lett. B 176 (1986) 203;
J.P. Ader, S. Narison and J.C. Wallet, Phys. Lett. B 176 (1986) 215;
P.J. Franzini and F.J. Gilman, Phys. Rev. D 35 (1985) 855;
M. Cvetic and B.W. Lynn, Phys. Rev. D 35 (1987) 51;
T.G. Rizzo, Phys. Rev. D 34 (1986) 2699;
N.D. Tracas and P.M. Zerwas, in: Proc. La Thuile/CERN Accelerator Workshop (La Thuile, Italy, 1987), ed. J.H. Mulvey, CERN Report 87-07.
[2.29] G. Belanger and S. Godfrey, Phys. Rev. D 34 (1986) 1309.
[2.30] J.L. Hewett and T.G. Rizzo, Z. Phys. C 36 (1987) 209.
[2.31] B.W. Lynn, F.M. Renard and C. Verzengassi, Nucl. Phys. B 304 (1988) 438;
B.W. Lynn, R.G. Stuart and M. Cvetic, SLAC-PUB-4624 (1988);
D. London, G. Belanger and J.N. Ng, Phys. Rev. Lett. 58 (1987) 6;
G. Belanger and S. Godfrey, Phys. Rev. D 35 (1987) 378; D 34 (1986) 1309;
V. Barger and K. Whisnant, Phys. Rev. D 36 (1987) 979;
P.J. Franzini and F.J. Gilman, Phys. Rev. D 35 (1985) 855;
P. Langacker, W.J. Marciano and A. Sirlin, Phys. Rev. D 36 (1987) 2191;
C. Verzegnassi, Phys. Lett. B 202 (1988) 411.
[2.32] T.G. Rizzo, Phys. Rev. D 37 (1988) 1232.
[2.33] UA1 Collab., C. Albajar et al., Z. Phys. C 37 (1988) 505.
[2.34] V. Barger, N.G. Deshpande and K. Whisnant, Phys. Rev. Lett. 57 (1986) 2109;
T.G. Rizzo, Phys. Rev. D 34 (1986) 3516;
V.D. Angelopoulos, Phys. Lett. B 180 (1986) 353.
[2.35] M. Davier et al., in: Proc. ECFA Workshop on LEP 200 (Aachen, FRG, 1986), eds A. Böhm and W. Hoogland.
[2.36] T.G. Rizzo, Phys. Rev. D 36 (1987) 713.
[2.37] W. Alles, Ch. Boyer and A.J. Buras, Nucl. Phys. B 119 (1975) 125.
[2.38] S. Nandi and T.G. Rizzo, Phys. Rev. D 37 (1988) 52.

[2.39] S. Capstick and S. Godfrey, Phys. Rev. D 35 (1987) 3351;
V.D. Angelopoulos, J. Ellis, D.V. Nanopoulos and N.D. Tracas, Phys. Lett. B 176 (1986) 203;
F. Cornet and R. Rückl, Phys. Lett. B 184 (1987) 263; in: Proc. La Thuile/CERN Accelerator Workshop 1987 (La Thuille, Italy, 1987), CERN Report 87-07 (Geneva, Switzerland).
[2.40] G. Altarelli, G. Martinelli, B. Mele and R. Rückl, Nucl. Phys. B 262 (1985) 204;
E. Gabriella, Mod. Phys. Lett. A 1 (1986) 465;
R.J. Cashmore et al., Phys. Rep. 122 (1985) 275.
[2.41] B. Adeva, F. Del Aguila, D. Nanopoulos, M. Quiros and F. Zwirner, in: Proc. 1986 Summer Study on the Physics of the Superconducting Super Collider (Snowmass, CO, 1986), eds R. Donaldson and J.N. Marx;
M.J. Duncan and M. Ruiz-Altaba, in: Proc. 1986 Summer Study on the Physics of the Superconducting Super Collider (Snowmass, CO, 1986), eds R. Donaldson and J.N. Marx;
M.J. Duncan and P. Langacker, Nucl. Phys. B 277 (1986) 285;
V. Barger, N.G. Deshpande, J.L. Rosner and K. Whisnant, Phys. Rev. D 35 (1987) 166;
F. del Aguila, M. Quiros and F. Zwirner, Nucl. Phys. B 287 (1987) 419; B 284 (1987) 530;
L.S. Durkin and P. Langacker, Phys. Lett. B 166 (1986) 436;
J. Ellis, talk given at the ICFA Seminar on Future Perspectives in High Energy Physics (BNL, October 1987); CERN report CERN-TH.4888/87 (1987);
P. Chiapetta and J.-Ph. Guillet, Nucl. Phys. B 293 (1987) 541.
[2.42] J.L. Rosner, in: Proc. 1986 Summer Study on the Physics of the Superconducting Super Collider (Snowmass, CO, 1986), eds R. Donaldson and J.N. Marx; Phys. Rev. D 35 (1987) 2244; Phys. Rev. Lett. 35 (1987) 2244;
V. Barger and K. Whisnant, Phys. Rev. D 36 (1987) 979.
[2.43] N.G. Deshpande, J.F. Gunion and F. Zwirner, in: Proc. Workshop on Experiments, Detectors and Experimental Areas for the Supercollider (Univ. of California, Berkeley, 1987).
[2.44] M.J. Duncan and P. Langacker, Nucl. Phys. B 277 (1986) 285.
[2.45] S. Godfrey and W.J. Marciano, talk presented at the BNL Neutrino Workshop (Upton, NY, February 1987);
D. London, G. Belanger and J.N. Ng, Mod. Phys. Lett. A 2 (1987) 343.
[2.46] D.H. White et al., LAMPF Cherenkov Detector Proposal #1015 (January 1986).
[2.47] S. Capstick and S. Godfrey, Phys. Rev. D 37 (1988) 2466.
[2.48] E. Ma, Phys. Rev. D 36 (1987) 274; Mod. Phys. Lett. A 3 (1988) 319;
K.S. Babu, X-G. He and E. Ma, Phys. Rev. D 36 (1987) 878;
E. Ma and D. Ng, Phys. Rev. D 39 (1989) 1986.
[2.49] J.F. Gunion et al., in: Proc. Workshop from Colliders to Supercolliders (Madison, WI, May 1987); Int. J. Mod. Phys. A 2 (1987) 1199;
E. Ma, Mod. Phys. Lett. A 3 (1988) 319;
V. Barger and K. Whisnant, Int. J. Mod. Phys. A 3 (1988) 897;
J. Liu, Carnegie Mellon Univ, report CMU-HEP87-29 (1987).
[2.50] G. Beall, M. Bander and A. Soni, Phys. Rev. Lett. 48 (1982) 848.
[2.51] J. Carr et al., Phys. Rev. Lett. 51 (1983) 627;
D.P. Stoker et al., Phys. Rev. Lett. 54 (1985) 1887.
[2.52] T.G. Rizzo, Phys. Lett. B 206 (1988) 133.
[2.53] D. London and J.L. Rosner, Phys. Rev. D 34 (1986) 1530;
J.L. Rosner, Comments Nucl. Part. Phys. 15 (1986) 195.
[2.54] T.G. Rizzo, Ames Lab Reports IS-J-2823, IS-J-2821 (1987); Phys. Rev. D 38 (1988) 71.
[2.55] S. Godfrey, Phys. Lett. B 195 (1987) 78.
[2.56] T.G. Rizzo, Ames Lab Report (1988), Phys. Rev. D 39 (1989) 3490.

[3.1] M. Drees and X. Tata, Phys. Rev. Lett. 59 (1987) 528.
[3.2] T.G. Rizzo, Phys. Rev. D 34 (1986) 1438.
[3.3] V. Barger et al., Phys. Rev. D 33 (1986) 1912.
[3.4] J.L. Rosner, Comments Nucl. Part. Phys. 15 (1986) 195;
P.M. Fishbane, R.E. Norton and M.J. Rivard, Phys. Rev. D 33 (1986) 2632.
[3.5] S. Kalara and R.N. Mohapatra, Phys. Rev. D 35 (1987) 3143; Z. Phys. C 37 (1988) 395;
K. Ito, Univ. of Tokyo Reports UT-480, 483 (1986); Phys. Lett. B 184 (1987) 331.
[3.6] L. Wolfenstein, Phys. Rev. Lett. 51 (1983) 1943.
[3.7] T.P. Cheng and L.-F. Li, Phys. Rev. Lett. 55 (1985) 2249;
P.H. Frampton and C. Jarlskog, Phys. Lett. B 154 (1985) 421;
S.P. Rosen, Phys. Rev. D 31 (1984) 208.
[3.8] H. Fritzsch, Phys. Lett. B 70 (1977) 436.
[3.9] T.G. Rizzo, Phys. Rev. D 35 (1987) 1677.

[3.10] J.L. Hewett and T.G. Rizzo, Phys. Rev. D 34 (1986) 2790.
[3.11] G. Eilam and T.G. Rizzo, Phys. Lett. B 188 (1987) 91.
[3.12] U. Bellgardt et al., Nucl. Phys. B 299 (1988) 1.
[3.13] ARGUS Collab., Phys. Lett. B 185 (1987) 288.
[3.14] CLEO Collab., Phys. Rev. D 35 (1987) 3533.
[3.15] V. Barger, N.G. Deshpande and K. Hagiwara, Phys. Rev. D 36 (1987) 3541.
[3.16] V.D. Angelopoulos et al., Nucl. Phys. B 292 (1987) 59.
[3.17] T. Kamae, Plenary talk presented at 24th Intern. Conf. on High Energy Physics (Munich, Germany, August 1988).
[3.18] T.G. Rizzo, Phys. Rev. D 34 (1986) 2163;
F.J. Gilman and S.H. Rhie, Phys. Rev. D 32 (1985) 324;
J.L. Rosner, Nucl. Phys. B 248 (1984) 503.
[3.19] JADE Collab., W. Bartel et al., Z. Phys. C 36 (1987) 15.
[3.20] UA1 Collab., talk presented at Intern. Europhysics Conf. on High Energy Physics (Uppsala, Sweden, June 1987).
[3.21] UA1 Collab., A. Honma, in: Proc. 23rd Intern. Conf. on High Energy Physics (Berkeley, CA, 1986) ed. S. Loken (World Scientific, Singapore).
[3.22] T.G. Rizzo, Phys. Rev. D 35 (1987) 3519.
[3.23] J.L. Hewett and T.G. Rizzo, Phys. Rev. D 36 (1987) 3367.
[3.24] N.G. Deshpande, G. Eilam, V. Barger and F. Halzen, Phys. Rev. Lett. 54 (1985) 1757.
[3.25] T.G. Rizzo, Mod. Phys. Lett. A 2 (1987) 505;
A. Datta, M. Drees, R.M. Godbole and X.R. Tata, Phys. Rev. D 37 (1988) 1876;
A. Datta and R.M. Godbole, Phys. Rev. D 37 (1988) 225.
[3.26] D. Duke and J. Owens, Phys. Rev. D 30 (1984) 49.
[3.27] E. Eichten, I. Hinchliffe, K. Lane and C. Quigg, Rev. Mod. Phys. 56 (1984) 579.
[3.28] UA1 Collab., G. Arnison et al., talk presented at Annual Meeting of APS Division of Particles and Fields (Eugene, OR, 1985);
UA2 Collab., J.A. Appel et al., Z. Phys. C 30 (1986) 1.
[3.29] T.G. Rizzo, Phys. Rev. D 34 (1986) 892.
[3.30] D. London, G. Belanger and J.N. Ng, TRIUMF Report TRI-PP-87-48 (1987).
[3.31] R.W. Robinett, Phys. Rev. D 34 (1986) 182.
[3.32] M. Drees and X. Tata, Phys. Lett. B 196 (1987) 65.
[3.33] M. Drees, Nucl. Phys. B 298 (1988) 333.
[3.34] E. Farhi and L. Susskind, Phys. Rep. 74 (1981) 277.
[3.35] Rare K and B Decays Subgroup Summary Report, 1988 DPF Snowmass Summer Study on High Energy Physics in the 1990's (Snowmass, CO, July 1988).
[3.36] G. Belanger et al., 1988 DPF Snowmass Summer Study on High Energy Physics in the 1990s (Snowmass, CO, July, 1988).
[3.37] M.K. Gaillard and D.V. Nanopoulos, 1986 Summer Study on the Physics of the SSC (Snowmass, CO, 1986), eds R. Donaldson and J.N. Marx.
[3.38] B.A. Campbell, J. Ellis, K. Enqvist, M.K. Gaillard and D.V. Nanopoulos, Int. J. Mod. Phys. A 2 (1987) 831.
[3.39] Particle Data Group, Phys. Lett. B 204 (1988) 1.
[3.40] A. Jodido et al., Phys. Rev. D 34 (1986) 1967; D 37 (1988) 237.
[3.41] T.G. Rizzo, Phys. Rev. D 34 (1986) 2076.
[3.42] T.G. Rizzo, Phys. Rev. D 33 (1986) 3329.
[3.43] I. Vendrumin, Padua Report DFPDS/88 (1988).
[3.44] J.P. Leveille, Nucl. Phys. B 137 (1978) 63.
[3.45] J. Maalampi and M. Roos, Helsinki Report HU-TFT-88-17 (1988), and references therein.
[3.46] T.G. Rizzo, Phys. Rev. D 34 (1986) 2160.
[3.47] R.D. Bolton et al., Phys. Rev. Lett. 56 (1986) 2461.
[3.48] R. Decker, Z. Phys. C 35 (1987) 537.
[3.49] A. Ray-Mukhopadhyaya and A. Raychaudhuri, Phys. Rev. D 37 (1988) 807;
B. Mukhopadhyaya, A. Ray and A. Raychaudhuri, Phys. Lett. B 186 (1987) 147; B 190 (1987) 93;
A. Raychaudhuri, ICTP Report IC/87/184 (1987).
[3.50] R.W. Robinett, Phys. Rev. D 33 (1986) 1908.
[3.51] J. Maalampi and M. Roos, Phys. Lett. B 188 (1987) 487; B 176 (1986) 396.
[3.52] G.G. Branco and L. Lavoura, Nucl. Phys. B 278 (1986) 738.
[3.53] J. Pulido, Z. Phys. C 36 (1987) 131.
[3.54] P. Langacker and D. London, Phys. Rev. D 38 (1988) 886.
[3.55] D.A. Morris, Phys. Rev. D 37 (1988) 2012;
J.A. Grifols, J. Sola and A. Mendez, Phys. Rev. Lett. 57 (1986) 2348.
[3.56] A. Barroso and J. Maalampi, Phys. Lett. B 187 (1987) 85;
S.M. Barr and A. Masiero, Phys. Rev. Lett. 58 (1987) 187.

[3.57] N.G. Deshpande, G. Eilam, P. Lo, J. Trampetic and P. Singer, Phys. Rev. Lett. 59 (1987) 183;
S. Bertonlini, S. Borzumati and A. Masiero, Phys. Rev. Lett. 59 (1987) 180.
[3.58] N.G. Deshpande, K. Panose and J. Trampetic, Phys. Lett. B 214 (1988) 467.
[3.59] CLEO Collab., Cornell Univ. Report CLNS-88/862 (1988).
[3.60] H. Dreiner, Mod. Phys. Lett. A 3 (1988) 867.
[3.61] A. Masiero, D.V. Nanopoulos and A.I. Sanda, Phys. Rev. Lett. 57 (1986) 663.
[3.62] J. Liu, Z. Phys. C 37 (1987) 139.
[3.63] E. Ma, Mod. Phys. Lett. A 3 (1988) 319.
[3.64] G.K. Leontaris and J.D. Vergados, Z. Phys. C 41 (1989) 623.
[3.65] J. Maalampi, A. Pietila and I. Vilja, Mod. Phys. Lett. A 3 (1988) 373.
[3.66] G.K. Leontaris, N.D. Tracas and J.D. Vergados, Phys. Lett. B 193 (1987) 335.
[3.67] K. Wilson, Phys. Rev. 179 (1969) 1499.
[3.68] J.L. Hewett and T.G. Rizzo, Z. Phys. C 34 (1987) 49.
[3.69] T.G. Rizzo, Phys. Rev. D 40 (1989) 754.
[3.70] T.G. Rizzo, Phys. Rev. D 34 (1986) 2699.
[3.71] J.L. Hewett and T.G. Rizzo, Z. Phys. C 36 (1987) 209.
[3.72] T.G. Rizzo, Phys. Rev. D 34 (1986) 1438.
[3.73] F. del Aguila, E. Laerman and P. Zerwas, Nucl. Phys. B 297 (1988) 1.
[3.74] D. Schaile and P.M. Zerwas, in: Proc. La Thuile/CERN Accelerator Workshop (La Thuile, Italy, 1987), ed. J.H. Mulvay, CERN Report 87-07 (1987).
[3.75] J.L. Hewett and S. Pakvasa, Phys. Lett. B (in press).
[3.76] G. Couture and J.N. Ng, Phys. Rev. D 35 (1987) 70.
[3.77] H. Dreiner et al., Mod. Phys. Lett. A 3 (1988) 443.
[3.78] V. Barger and K. Hagiwara, Phys. Rev. D 37 (1988) 3320.
[3.79] R.W. Robinett, Phys. Lett. B 197 (1987) 531.
[3.80] V. Barger, K. Hagiwara and K. Igi, Phys. Rev. D 38 (1988) 2149.
[3.81] W. Buchmuller, R. Ruckl and D. Wyler, Phys. Lett. B 191 (1987) 442.
R. Ruckl, in: Proc. 1987 DESY Workshop on HERA Physics (Hamburg, Germany, October 1987).
[3.82] J.F. Gunion and E. Ma, Phys. Lett. B 195 (1987) 257.
[3.83] N. Harnew, in: Proc. 1987 DESY Workshop on HERA Physics (Hamburg, Germany, October 1987).
[3.84] J. Ellis, F. Pauss et al., in: Proc. Workshop on Physics at Future Accelerators (La Thuile, Italy, 1987), ed. J.H. Mulvay, CERN Report 87-07 (1987).
[3.85] J.A. Grifols and S. Peris, Phys. Lett. B 201 (1988) 287.
[3.86] A. Dobado, M.J. Herrero and C. Munoz, Phys. Lett. B 191 (1987) 449.
[3.87] J. Freeman, talk presented at the 7th Topical Workshop on Proton–Antiproton Collider Physics (Fermilab, June 1988).
[3.88] R.W. Robinett, Phys. Rev. D 37 (1988) 1321.
[3.89] T.G. Rizzo, Z. Phys. C (in press).
[3.90] J.L. Hewett, Phys. Lett. B 196 (1987) 223;
T.G. Rizzo, Phys. Lett. B 188 (1987) 95.
[3.91] A. Ali et al., in: Proc. 1987 DESY Workshop on HERA Physics, DESY Report DESY-88-119 (1988).
[3.92] V. Barger and W.-Y. Keung, Phys. Rev. D 34 (1986) 2902.
V. Barger et al., Mod. Phys. Lett. A 2 (1987) 437.
[3.93] S. Godfrey, J.L. Hewett and T.G. Rizzo, Phys. Rev. D 37 (1988) 643.
[3.94] V. Barger et al., 1986 Summer Study on the Physics of the SSC (Snowmass, CO, 1986), eds R. Donaldson and J.N. Marx.
[3.95] T.G. Rizzo, Phys. Lett. B 181 (1986) 385.
[3.96] E. Eichten et al., Phys. Rev. D 34 (1986) 1547.
[3.97] J.L. Hewett and S. Pakvasa, Phys. Rev. D 37 (1988) 3165.
[3.98] V. Barger, T. Han, K. Hagiwara and D. Zeppenfeld, Phys. Lett. B 220 (1989) 464.
[3.99] E.N. Argyres, C.G. Papadopoulos and S. Vlassopoulos, Phys. Lett. B 202 (1988) 425.
[3.100] R. Ruckl and P. Zerwas, in: Proc. La Thuile/CERN Accelerator Workshop (La Thuile, Italy 1987), ed. J.H. Mulvay, CERN Report 87-07 (1987).
[3.101] R.W. Robinett, Phys. Rev. D 37 (1988) 84.
[3.102] W. Buchmuller and D. Wyler, Phys. Lett. B 177 (1986) 377.
[3.103] I. Bigi et al., Phys. Lett. B 181 (1986) 157.
[3.104] V. Barger et al., Phys. Rev. D 35 (1987) 3366;
K. Hikasa, in: Proc. 5th INFN–Eloisatron Project Workshop on New Aspects of VHE PP Physics (Erice, Italy, June 1987).
[3.105] J.L. Hewett and T.G. Rizzo, Phys. Rev. D 35 (1987) 2194.
[3.106] J.L. Hewett and T.G. Rizzo, Ames Lab Report IS-J-3037 (1988), Z. Phys. C, to be published.
[3.107] R.W. Robinett, Phys. Rev. D 36 (1987) 719.

[3.108] V. Barger, R.J.N. Phillips and K. Whisnant, Phys. Rev. Lett. 57 (1986) 48.
[3.109] V. Barger and R.J.N. Phillips, Collider Physics (Addison-Wesley, Reading, 1987).
[3.110] M. Gell-Mann, P. Ramond and R. Slansky, in: Supergravity, eds D.Z. Freedman and P. Van Nieuwenhuizen (North-Holland, Amsterdam, 1979) p. 315.
[3.111] G.C. Branco and C.Q. Geng, Phys. Rev. Lett. 58 (1987) 969.
[3.112] E. Ma, Phys. Rev. Lett. 58 (1987) 1047; 59 (1987) 607; Phys. Rev. Lett. 60 (1988) 1363.
[3.113] P-Y. Xue, Zaragoza Univ. Report, DFTUZ-87-15 (1987).
[3.114] K. Enqvist and J. Maalampi, Phys. Lett. B 180 (1986) 347.
[3.115] J.A. Grifols and J. Sola, Phys. Lett. B 182 (1986) 53.
[3.116] G.C. Branco et al., Phys. Rev. D 36 (1987) 928.
[3.117] M. Doi et al., Phys. Rev. D 37 (1988) 1923.
[3.118] J.W.F. Valle, Phys. Lett. B 186 (1987) 73.
[3.119] H. Fritzsch, Phys. Lett. B 70 (1977) 436; B 73 (1978) 317; B 166 (1988) 423.
[3.120] E. Witten, Nucl. Phys. B 268 (1986) 79.
[3.121] C.H. Albright, Phys. Lett. B 178 (1986) 219;
A.L. Kagan and C.H. Albright, Phys. Rev. D 38 (1988) 917.
[3.122] R.N. Mohapatra and J.W.F. Valle, Phys. Rev. Lett. 34 (1986) 1642; Phys. Lett. B 177 (1986) 47;
R.N. Mohapatra, Phys. Rev. Lett. 56 (1986) 561.
[3.123] F. Gabbiani, INFN-Padua Report DFPD-20/87 (1987).
[3.124] M.V. Altaiskij, P.S. Isaev and S.G. Kovalenko, Dubna JINR Report (1988).
[3.125] S. Nandi and V. Sarkar, Phys. Rev. Lett. 56 (1986) 564.
[3.126] J. Derendinger, L. Ibañez and H.P. Nilles, Nucl. Phys. B 267 (1986) 365.
[3.127] D. London, G. Belanger and J.N. Ng, Phys. Rev. D 34 (1986) 2867.
[3.128] V. Sarkar and R.B. Mann, Univ. of Toronto report (1987).
[3.129] E. Ma, Europhys. Lett. 3 (1987) 145.
[3.130] A.V. Kyuldjiev, Nucl. Phys. B 243 (1984) 387.
[3.131] J.A. Morgan, Phys. Lett. B 102 (1981) 247.
[3.132] M.A. Stephanov, ITEP Report ITEP-88-105 (1988).
[3.133] M.B. Voloshin, Phys. Lett. B 209 (1988) 360.
[3.134] R. Barbieri and R.N. Mohapatra, Phys. Rev. Lett. 61 (1988) 27;
R. Barbieri, R.N. Mohapatra and T. Yanagida, Phys. Lett. B 213 (1988) 69.
[3.135] D. Notzold, Phys. Rev. D 38 (1988) 1658.
[3.136] J. Lattimer and J. Cooperstein, Phys. Rev. Lett. 61 (1988) 23.
[3.137] A. Aharonov, G. Alexander, I. Goldman and S. Nussinov, Phys. Rev. Lett. 60 (1988) 1789.
[3.138] M.B. Voloshin, M.I. Vyotskii and L.B. Okun, Zh. Eksp. Teor. Fiz. 91 (1986) 754 [Sov. Phys.-JETP 64 (1986) 446].
[3.139] J. Liu, Phys. Rev. D 35 (1987) 3447;
G. Branco and J. Liu, Phys. Lett. B 210 (1988) 164.
[3.140] T.G. Rizzo, Phys. Rev. D 36 (1987) 303.
[3.141] S. Sarkar and A.M. Cooper, Phys. Lett. B 173 (1986) 71.
[3.142] J. Pulido and J. Ralston, Phys. Rev. D 38 (1988) 2864.
[3.143] J. Lui, Commun. Theor. Phys. 9 (1988) 485.

[4.1] B. Campbell, J. Ellis, M.K. Gaillard, D.V. Nanopoulos and K.A. Olive, Phys. Lett. B 180 (1986) 77.
[4.2] V. Barger and K. Whisnant, Int. J. Mod. Phys. A 3 (1988) 1907.
[4.3] J.P. Derendinger, L.E. Ibañez and H.P. Nilles, Nucl. Phys. B 267 (1986) 365.
[4.4] P. Binetruy, S. Dawson, I. Hinchliffe and M. Sher, Nucl. Phys. B 273 (1986) 501.
[4.5] J. Ellis, D.V. Nanopoulos, S.T. Petcov and F. Zwirner, Nucl. Phys. B 283 (1987) 93.
[4.6] J. Ellis, K. Enqvist, D.V. Nanopoulos and F. Zwirner, Nucl. Phys. B 276 (1986) 14.
[4.7] E. Cohen, J. Ellis, K. Enqvist and D.V. Nanopoulos, Phys. Lett. B 165 (1985) 76.
[4.8] L.E. Ibañez and J. Mas, Nucl. Phys. B 286 (1987) 107.
[4.9] J.F. Gunion, L. Roszkowski and H.E. Haber, Phys. Rev. D 38 (1988) 105; Phys. Lett. B 189 (1987) 409.
[4.10] H.E. Haber and M. Sher, Phys. Rev. D 35 (1987) 2206.
[4.11] M. Drees, Phys. Rev. D 35 (1987) 2910.
[4.12] J. Gunion and H.E. Haber, Nucl. Phys. B 272 (1986) 1; B 278 (1986) 449.
[4.13] D. London, G. Belanger and J.N. Ng, TRIUMF Report TRI-PP-87-49 (1987).
[4.14] R.W. Robinett, Phys. Rev. D 34 (1986) 182.
[4.15] B.W. Lee, C. Quigg and H.B. Thacker, Phys. Rev. Lett. 38 (1977) 883; Phys. Rev. D 16 (1977) 1519.

[4.16] H. Baer, D. Dicus, M. Drees and X. Tata, Phys. Rev. D 36 (1987) 1363.
[4.17] J.F. Gunion, H.E. Haber, G. Kane and S. Dawson, A Higgs hunters guide, Univ. of California–Davis Report, UCD-89-4 (1989).
[4.18] J. Ellis and R. Peccei, eds, Physics at LEP, Yellow Report 86-02 (CERN, Geneva, 1986).
[4.19] S. Nandi, Phys. Lett. B 181 (1986) 375.
[4.20] J.F. Gunion et al., Nucl. Phys. B 294 (1987) 621.
[4.21] D. Dicus, C. Kao, J.L. Hewett and T.G. Rizzo, Phys. Rev. D 40 (1989) 787.
[4.22] R.N. Cahn and S. Dawson, Phys. Lett. B 136 (1984) 196.
[4.23] F. Wilczek, Phys. Rev. Lett. 39 (1977) 1304;
L. Bergstrom and P. Poutraines, Phys. Lett. B 182 (1986) 83;
G. Gamberini, G.F. Guidice and G. Ridolfi, Nucl. Phys. B 292 (1987) 237;
R.W. Robinett, Phys. Rev. D 33 (1985) 736.
[4.24] T.G. Rizzo, Phys. Lett. B 191 (1987) 187.
[4.25] T.G. Rizzo, Mod. Phys. Lett. (in press).
[4.26] D.A. Dicus, K.J. Kallianpur and S.S.D. Willenbrock, Phys. Lett. B 200 (1988) 187.
[4.27] E. Ma, Phys. Rev. Lett. 57 (1986) 287.
[4.28] J.A. Grifols and A. Mendez, Phys. Rev. D 22 (1980) 1725.
[4.29] T.G. Rizzo, Phys. Rev. D 39 (1989) 728.

[5.1] P. Binétruy, S. Dawson, I. Hinchliffe and M. Sher, Nucl. Phys. B 273 (1986) 501.
[5.2] P. Binétruy, S. Dawson and I. Hinchliffe, Phys. Lett. B 179 (1986) 262;
P. Binétruy and M.K. Gaillard, Phys. Lett. B 168 (1986) 347.
[5.3] S. Dawson, presented at XXIII Intern. Conf. on High Energy Physics (Berkeley, CA, 1986);
P. Binétruy and M.K. Gaillard, Phys. Rev. D 34 (1986) 3609.
[5.4] P. Binétruy, S. Dawson and I. Hinchliffe, Phys. Rev. D 35 (1987) 2215;
P. Binétruy, S. Dawson, M.K. Gaillard and I. Hinchliffe, Phys. Lett. B 192 (1987) 377; Phys. Rev. D 37 (1988) 2633.
[5.5] G.D. Coughlan, G. German, G.C. Ross and G. Segre, Phys. Lett. B 198 (1987) 467;
G.D. Coughlan, Int. J. Mod. Phys. A 4 (1989) 411.
[5.6] G.D. Coughlan and G. German, Phsys. Lett. B 186 (1987) 356.
M.C. Bento and G.G. Ross, Nucl. Phys. B 292 (1987) 400.
[5.7] G.C. Ross, Phys. Lett. B 200 (1988) 441.
[5.8] J. Breit, B. Ovrut and G. Segre, Phys. Lett. B 162 (1985) 303;
P. Binétruy and M.K. Gaillard, Phys. Lett. B 168 (1986) 347.
[5.9] M. Mangano, Z. Phys. C 28 (1985) 613;
E. Witten, Phys. Lett. B 155 (1985) 151.
[5.10] S. Ferrara, I. Girardello and H.P. Nilles, Phys. Lett. B 125 (1983) 457;
M. Dine, R. Rohm, N. Seiberg and E. Witten, Phys. Lett. B 156 (1985) 55.
[5.11] E. Cohen, J. Ellis, C. Gomez and D.V. Nanopoulos, Phys. Lett. B 160 (1985) 62.
[5.12] J.-P. Derendinger, L.E. Ibañez and H.P. Nilles, Phys. Lett. B 155 (1985) 65.
[5.13] E. Witten, Nucl. Phys. B 268 (1986) 79;
M. Dine, N. Seiberg, X-G. Wen and E. Witten, Nucl. Phys. B 289 (1987) 319; B 278 (1986) 769.
[5.14] L.E. Ibañez and J. Mas, Nucl. Phys. B 286 (1987) 107;
L.E. Ibañez, talk given at the NATO Workshop on Super Field Theories (Vancouver, July 1986).
[5.15] J. Ellis, lectures presented at the 28th Scottish Universities Summer School in Physics (Edinburgh, Scotland, 1985);
J. Ellis, D.V. Nanopoulos, M. Quiros and F. Zwirner, Phys. Lett. B 180 (1986) 83;
J. Ellis, A.B. Lahanas, D.V. Nanopoulos, M. Quiros and F. Zwirner, Phys. Lett. B 188 (1987) 408.
[5.16] Y.J. Ahn, J.D. Breit and G. Segre, Nucl. Phys. B 273 (1986) 175;
M. Quiros, Phys. Lett. B 196 (1987) 461; B 173 (1986) 265.
[5.17] L.E. Ibañez and H.P. Nilles, Phys. Lett. B 169 (1986) 354.
[5.18] M. Drees, Nucl. Phys. B 298 (1988) 333.
[5.19] G.G. Ross, talk given at the 1987 Intern. Symp. on Lepton and Photon Interactions at High Energies (DESY, Hamburg, 1987);
B.R. Greene, K.H. Kirklin, P.J. Miron and G.G. Ross, Nucl. Phys. B 278 (1986) 667; B 292 (1987) 606; Phys. Lett. B 180 (1986) 69; B 192 (1987) 111;
G.G. Ross, talk given at the XXIII Intern. Conf. on High Energy Physics (Berkeley, CA, July 1986); talk given at the 8th Workshop on Grand Unification (Syracuse, NY, April 1987).
[5.20] S.-T. Yau, in: Argonne Symp. on Anomalies, Geometry and Topology (World Scientific, Singapore, 1985).
[5.21] K. Choi and J.E. Kim, Phys. Lett. B 165 (1985) 71;
N. Dragon, U. Ellwanger and M.G. Schmidt, Phys. Lett. B 154 (1985) 373; Nucl. Phys. B 255 (1985) 549.

[5.22] L.E. Ibañez and G.G. Ross, Phys. Lett. B 110 (1982) 45;
L. Alvarez-Gaumé, M. Claudson and M.B. Wise, Nucl. Phys. B 207 (1982) 96;
C.R. Nappi and B.A. Ovrut, Phys. Lett. B 113 (1982) 175;
M. Dine and W. Fischler, Phys. Lett. B 110 (1982) 227;
K. Inoue, A. Kakuto, H. Kamatsu and S. Takeshita, Prog. Theor. Phys. 68 (1982) 927;
J. Ellis, K. Enqvist, D.V. Nanopoulos, and F. Zwirner, Mod. Phys. Lett. A 1 (1986) 57.
[5.23] K. Enqvist, D.V. Nanopoulos and M. Quiros, Phys. Lett. B 169 (1986) 343.
[5.24] D.V. Nanopoulos and S. Weinberg, Phys. Rev. D 20 (1979) 2484.
[5.25] K. Enqvist, D.V. Nanopoulos, S. Kalara and K. Olive, Phys. Lett. B 193 (1987) 41.
[5.26] J. Ellis, K. Enqvist, D.V. Nanopoulos and K. Olive, Phys. Lett. B 188 (1987) 415; Nucl. Phys. B 297 (1988) 103.
[5.27] I. Affleck and M. Dine, Nucl. Phys. B 249 (1985) 361.
[5.28] M. Drees, Phys. Lett. B 181 (1986) 279.
[5.29] K. Yamamoto, Kyoto Univ. report NEAP-39 (1987).
[5.30] G. Costa, F. Feruglio and F. Gabbiani, Nucl. Phys. B 286 (1987) 325.
[5.31] F. Gabbiani, Nuovo Cimento 99A (1988) 285; 98A (1987) 223.
[5.32] Q. Shafi, talk given at Intern. Workshop on Superstrings, Composite Structures, and Cosmology (Univ. of Maryland, College Park, MD, March 1987).
[5.33] G.'t Hooft, Phys. Rev. Lett. 37 (1976) 8;
R. Jackiw and C. Rebbi, Phys. Rev. Lett. 37 (1976) 177;
C. Allan, R. Dashen and D. Gross, Phys. Lett. B 63 (1976) 334.
[5.34] R. Peccei and H. Quinn, Phys. Rev. Lett. 38 (1977) 1440; Phys. Rev. D16 (1977) 1791;
F. Wilczek, Phys. Rev. Lett. 40 (1978) 279;
S. Weinberg, Phys. Rev. Lett. 40 (1978) 223.
[5.35] D. Dicus et al., Phys. Rev. D 18 (1978) 1829;
D. Dearborn, D. Schramm and G. Steigman, Phys. Rev. Lett. 56 (1986) 26.
[5.36] J. Preskill, M. Wise and F. Wilczek, Phys. Lett. B 120 (1983) 127;
L. Abbott and P. Sikivie, Phys. Lett. B 120 (1983) 133;
M. Dine and W. Fischler, Phys. Lett. B 120 (1983) 137.
[5.37] M. Dine, W. Fischler and M. Srednicki, Phys. Lett. B 104 (1981) 199;
J.E. Kim, Phys. Rev. Lett. 43 (1979) 103;
M.A. Shifman, V.I. Vainstein and V.I. Zakharov, Nucl. Phys. B 166 (1986) 493;
A.P. Zhitnitskii, Sov. J. Nucl. Phys. 31 (1980) 260.
[5.38] G. Lazarides, C. Panagiotakopoulos and Q. Shafi, Phys. Rev. Lett. 56 (1986) 432;
E. Witten, Phys. Lett. B 149 (1984) 351; B 153 (1985) 243;
K. Choi and J.E. Kim, Phys. Lett. B 154 (1985) 393; B 165 (1985) 71;
M. Dine and N. Seiberg, Nucl. Phys. B 273 (1986) 109.
[5.39] P. Candelas et al., Nucl. Phys. B 258 (1985) 46;
E. Witten, Phys. Lett. B 155 (1985) 151;
M. Dine et al., Phys. Lett. B 156 (1985) 55;
[5.40] S.M. Barr, K. Choi and J.E. Kim, Nucl. Phys. B 283 (1987) 591;
P. Sikivie, Phys. Rev. Lett. 48 (1982) 1156;
Ya.B. Zel'dovich, I.Y. Kobzarev and L.B. Okun, Zh. Eksp. Teor. Fiz. 67 (1974) 3.
[5.41] F. Gabbiani, Int. J. Mod. Phys. A 3 (1988) 397; Nuovo Cimento 100A (1988) 167.
[5.42] J.E. Kim, Phys. Rev. Lett. 43 (1979) 103;
M.A. Shifman, A.I. Vainshtein and V.I. Zakharov, Nucl. Phys. B 166 (1986) 493.
[5.43] A. Guth, Phys. Rev. D 23 (1981) 347;
A.D. Linde, Phys. Lett. B 108 (1982) 389;
A. Albrecht and P. Steinhardt, Phys. Rev. Lett. 48 (1982) 1220.
[5.44] B.A. Campbell et al., Phys. Lett. B 173 (1986) 270;
D.V. Nanopoulos and K.A. Olive, in: Proc. Snowmass 1986 Workshop on the SSC (Snowmass, CO, 1986);
K.A. Olive, in: Proc. Theoretical Workshop on Cosmology and Particle Physics: Quarks and Galaxies (LBL, 1986).
[5.45] G. Steigman, C. Sarazin, H. Quintono and J. Faulkner, Astrophys. J. 83 (1978) 1050;
W.H. Press and D.N. Spergel, Astrophys. J. 296 (1985) 679.
[5.46] J. Silk, K.A. Olive and M. Srednicki, Phys. Rev. Lett. 55 (1985) 257;
M. Srednicki, K.A. Olive and J. Silk, Nucl. Phys. B 279 (1987) 804;
T.K. Gaisser, G. Steigman and S. Tilav, Phys. Rev. D 34 (1986) 2206;
J. Hagelin, K.-W. Ng and K.A. Olive, Phys. Lett. B 180 (1986) 375.
[5.47] J. Ellis, K. Enqvist, D.V. Nanopoulos and S. Sarkar, Phys. Lett. B 167 (1986) 457.

[5.48] K. Davidson and T.D. Kinman, Astrophys. J. Suppl. 58 (1985) 321;
R.T. Rood, T.M. Bania and T.L. Wilson, Astrophys. J. 280 (1984) 629.
[5.49] J. Preskill, Phys. Rev. Lett. 43 (1979) 1365;
Ya.B. Zeldovich and M. Khlopov, Phys. Lett. B 79 (1978) 329.
[5.50] Q. Shafi and C. Wetterich, Phys. Lett. B 129 (1983) 387; B 152 (1985) 51.
[5.51] G. Lazarides, C. Panagiotakopoulos and Q. Shafi, Phys. Rev. Lett. 56 (1986) 432.
[5.52] E. Witten, Nucl. Phys. B 249 (1985) 557.
[5.53] G. Lazarides, C. Panagiotakopoulos and Q. Shafi, Phys. Rev. Lett. 56 (1986) 557; Nucl. Phys. B 307 (1988) 937.
[5.54] R.N. Mohapatra and J.W.F. Valle, Phys. Lett. B 186 (1987) 303.
[5.55] J.R. Cuddell, F. Halzen, X.G. He and S. Pakvasa, Phys. Lett. B 196 (1987) 227.
[5.56] G. Altarelli et al., Nucl. Phys. B 308 (1988) 724.
[5.57] H. Albrecht et al., Phys. Lett. B 192 (1987) 245.
[5.58] S. Glashow and E. Jenkins, Phys. Lett. B 196 (1987) 223;
F. Hoogeveen and C.N. Leung, Phys. Rev. D 37 (1988) 3340.
[5.59] I.I. Bigi and A.I. Sanda, Phys. Lett. B 194 (1987) 307;
J. Maalampi and M. Roos, Phys. Lett. B 188 (1987) 487; B 195 (1987) 489;
A. Datta, E.A. Paschos and U. Türke, Phys. Lett. B 196 (1987) 376;
J.B. Bjorken and I. Dunietz, Phys. Rev. D 36 (1987) 2109.
[5.60] AMY Collab., H. Sagawa et al., Phys. Rev. Lett. 60 (1988) 93;
VENUS Collab., H. Yoshida et al., Phys. Lett. B 198 (1987) 570;
TOPAZ Collab., I. Adachi et al., Phys. Rev. Lett. 60 (1988) 97.
[5.61] N. Nakamura, I. Umemura and K. Yamamoto, Prog. Theor. Phys. 79 (1988) 502.
[5.62] M. Carena and C. Wagner, Phys. Lett. B 186 (1987) 361.
[5.63] E. Cohen et al., Phys. Lett. B 165 (1985) 76.
[5.64] R.R. Volkas, A.J. Davies and G.C. Joshi, Univ. of Melbourne report UM-P-87/91 (1987).
[5.65] J. Pulido, Phys. Lett. B 181 (1986) 288.
[5.66] J. Pulido, Lisbon CFMC report IFM-9/87; Z. Phys. C 36 (1987) 131.
[5.67] M. Drees, K. Enqvist and D.V. Nanopoulos, Phys. Lett. B 189 (1987) 321.
[5.68] M. Drees, K. Enqvist and D.V. Nanopoulos, Nucl. Phys. B 294 (1987) 1.
[5.69] J. Pulido, Nucl. Phys. B 269 (1986) 119.
[5.70] F. del Aguila, J.A. Gonzalez and M. Quiros, Phys. Lett. B 201 (1988) 315; Nucl. Phys. B 307 (1988) 571.
[5.71] J. McDonald, Liverpool Univ. DAMP report LTH-177-Rev. (1987).

[A.1] J.L. Hewett and T.G. Rizzo, Int. J. Mod. Phys. (in press).
[A.2] J.L. Hewett and T.G. Rizzo, 1988 DPF Snowmass Summer Study on High Energy Physics in the 1990s (Snowmass, CO, 1988).
[A.3] C. Ahn et al., SLAC "Red-Book" Report, SAC-Report-329 (1988).
[A.4] T.G. Rizzo, Ames Lab Report IS-J-3239 (1988).
[A.5] T.G. Rizzo, Ames Lab Report IS-J-3092 (1988).
[A.6] T.G. Rizzo, Ames Lab Report IS-J-3091 (1988).